T.R.

GEBZE TECHNICAL UNIVERSITY

GRADUATE SCHOOL OF NATURAL AND APPLIED SCIENCES

CORRELATION AMONG CAE AND TEST RESULTS FOR FULL VEHICLE NVH MODEL

UĞUR ÜRESİN

A THESIS SUBMITTED FOR THE DEGREE OF

MASTER OF SCIENCE

DEPARTMENT OF MECHANICAL ENGINEERING

GEBZE

2017

T.R.

GEBZE TECHNICAL UNIVERSITY

GRADUATE SCHOOL OF NATURAL AND APPLIED SCIENCES

CORRELATION AMONG CAE AND TEST RESULTS FOR FULL VEHICLE NVH MODEL

UĞUR ÜRESİN

A THESIS SUBMITTED FOR THE DEGREE OF

MASTER OF SCIENCE

DEPARTMENT OF MECHANICAL ENGINEERING

THESIS SUPERVISOR

ASSOC. PROF. DR. AHMET ZAFER ŞENALP

GEBZE

2017

T.C.

GEBZE TEKNİK ÜNİVERSİTESİ

FEN BİLİMLERİ ENSTİTÜSÜ

TAM MODELLENMİŞ BİR ARACIN TİTREŞİM VE GÜRÜLTÜ PERFORMANSI İÇİN CAE VE TEST KORELASYONU ÇALIŞMASI

UĞUR ÜRESİN

YÜKSEK LİSANS TEZİ

MAKİNE MÜHENDİSLİĞİ ANABİLİM DALI

DANIŞMANI

DOÇ. DR. AHMET ZAFER ŞENALP

GEBZE

2017

GEBZE TEKNİK ÜNİVERSİTESİ	YÜKSEK LİSANS JÜRİ ONAY FORMU

GTÜ Fen Bilimleri Enstitüsü Yönetim Kurulu'nun 24/05/2017 tarih ve 2017/28 sayılı kararıyla oluşturulan jüri tarafından 30/05/2017 tarihinde tez savunma sınavı yapılan Uğur ÜRESİN'in tez çalışması Makine Mühendisliği Anabilim Dalında YÜKSEK LİSANS tezi olarak kabul edilmiştir.

JÜRİ

ÜYE
(TEZ DANIŞMANI) : Doç. Dr. Ahmet Zafer ŞENALP

ÜYE : Doç. Dr. İlyas KANDEMİR

ÜYE : Y. Doç. Dr. Polat ŞENDUR

ONAY

Gebze Teknik Üniversitesi Fen Bilimleri Enstitüsü Yönetim Kurulu'nun ...../...../..... tarih ve ...../..... sayılı kararı.

İMZA/MÜHÜR

Doç. Dr. Arif Çağdaş AYDINOĞLU
Gebze Teknik Üniversitesi
Fen Bilimleri Enstitüsü Müdürü

SUMMARY

In automotive industry, NVH (Noise Vibrations Harshness) is one of the important parameters in terms of the comfort of a vehicle and the quality perceived by the customer. For attributes like NVH, advanced numerical methods such as finite element analysis (FEA) and computer aided engineering (CAE) software are used.

In this study, CAE and test correlation of a heavy commercial vehicle were examined in terms of vibration transfer path analysis and internal noise transfer path analysis.

First, all three-dimensional modelled body, chassis, engine and internal and external trim parts of the vehicle were transformed into finite element models. Also an air model for the vehicle cabin was created for noise transfer function analysis. Then, modal analysis was performed for each subsystem separately. For each subsystem, modal results from NASTRAN are combined with related FE models to transform them into modal models. With combining modal models together, the full vehicle model was constructed to perform vibrational transfer function (VTF) and noise transfer function (NTF) analysis. Physical tests were carried out on the prototype vehicle to validate the results of the CAE analyses carried out during this entire process. In the physical tests, impacts are given by modal hammer and the accelerations from different points of the prototype vehicle were obtained and the data was processed by the LMS Lab View program.

As a result, the correlation between the results obtained by CAE and the physical tests were examined and the main parameters affecting the correlation were investigated in NVH perspective.

Key Words: Vehicle NVH Correlation, NVH CAE, NVH Test, Transfer Path Analysis, Vehicle Development, Validation.

ÖZET

Otomotiv endüstrisinde NVH (Ing. Noise, Vibration, Harshness) kavramı bir aracın konforu ve müşterinin algıladığı kalite açısından en önemli parametrelerden biridir. NVH gibi araç özellikleri için, sonlu elemanlar analizi (FEA) yöntemi gibi nümerik analiz yöntemleri ve bilgisayar destekli mühendislik (CAE) yazılımları kullanılır.

Bu çalışmada, ağır ticari bir aracın CAE ile fiziksel test arasındaki korelasyonu, titreşim iletim fonksiyonu (VTF) analizi ve kabin iç gürültü iletim fonksyionu (NTF) analizi açısından incelenmiştir.

Öncelikle, aracın üç boyutlu olarak modellenmiş altsistemleri (gövde, şasi, motor ve aktarma parçaları) ile iç ve dış trim parçaları birer sonlu elemanlar modeline dönüştürüldü. NTF analizi için hava modeli oluşturuldu ve kabin ile birleştirildi. NASTRAN programı ile her alt sistem modeli için ayrı ayrı modal analiz yapıldı. Kurum içinde geliştirilmiş bir yazılımla, her bir alt sistemin FEA modeli ile ilgili modele ait modal sonuçlar birleştirilerek alt sistem modal modelleri oluşturuldu. Yine aynı yazılımla, tüm modal modeller bir araya getirildi ve sınır şartları (lastik-yol teması vb.) tanımlanarak tam araç modal modeli oluşturuldu. Yine kurum içinde geliştirilmiş bir yazılımla tam araç model modeline NTF ve VTF analizleri yapıldı. Daha sonra araç prototopi üzerinde modal çekiç ile transfer yolu analizleri yapıldı. Modal çekiç ile aracın belli noktalarına verilen kuvvet girdilerine karşılık yine aracın belli noktalarına yerleştirilen ivmemetreler ile ivme değerleri okundu. Veriler LMS Lab View programı ile işlendi.

Sonuç olarak, CAE ve fiziksel test yoluyla elde edilen sonuçların korelasyonu incelenerek, korelasyonu etkileyen CAE parametreleri araştırıldı.

Anahtar Kelimeler: CAE ve Test Korelasyonu, Titreşim ve Gürültü Analizi, İletim Yolu Analizi, Araç Geliştirme, Doğrulama.

ACKNOWLEDGEMENTS

I would like to express my gratitude to Assoc. Prof. Ahmet Zafer Şenalp for his supervision and guidance during all phases of this study.

I would like to express my sincere thanks to my colleague Umut Özcan who motivated me to do this work and support me with his deep technical knowledge, to my colleague Baran Gümüş who helped me through VSIGN software and physical tests. Without their support, it wouldn't be possible to complete this study.

Finally, I would like to express my deep gratitude to my lovely parents. Without their unconditional support I wouldn't have become the person who I am today.

TABLE of CONTENTS

	Page
SUMMARY	v
ÖZET	vi
ACKNOWLEDMENTS	vii
TABLE of CONTENTS	viii
LIST of ABBREVIATIONS and ACRONYMS	xi
LIST of FIGURES	xiii
LIST of TABLES	xxi
1. INTRODUCTION	1
1.1. Literature Review	3
1.2. Purpose of The Study	8
1.3. Outline	10
2. THEORY AND BACKGORUND	11
2.1. Theory of Mechanical Vibrations	11
2.1.1. Undamped Free Vibration	11
2.1.2. Forced Vibration	16
2.1.3. Viscous Damping	16
2.1.3.1. Underdamped Case ($\xi < 1$)	19
2.1.3.2. Overdamped Case ($\xi > 1$)	20
2.1.3.3. Critically Damped Case ($\xi = 1$)	21
2.1.4. Mechanical (Structural) Damping	21
2.1.4.1. Internal and External Damping	21
2.1.4.2. Distributed and Localized Damping	22
2.1.4.3. Modeling Structural Damping	23
2.1.5. Modal Analysis	24
2.1.6. Frequency Response Function (FRF)	25
2.2. Theory of Acoustics	26
2.2.1. Fundamental Concepts of Acoustics	27

2.2.2. Speed and Frequency 28
2.2.3. Sound Waves 30
2.2.4. Acoustic Measurement 32
2.2.4.1. Frequency Analysis 32
2.2.4.2. Random Noise 35
2.2.4.3. Levels and Decibels 36
2.2.4.4. Acoustic Impedance 37
2.2.5. Physiology of Hearing 37
2.3. Vehicle NVH Theory 40
2.3.1. Structure-borne and Air-Borne Noise 41
2.3.2. Noise Sources and Transfer Path 41
2.3.3. Engine Radiated Noise and Engine Order 42
3. ANALYSIS VIA CAE 44
3.1. Finite Element Model Creation 45
3.1.1. Element Types 47
3.1.2. Meshing and Quality Criteria 49
3.1.2.1. Aspect Ratio 50
3.1.2.2. Skewness 51
3.1.2.3. Warpage 52
3.1.2.4. Taper 52
3.1.2.5. Jacobian Ratio 53
3.1.2.6. Twist Angle 53
3.1.2.7. Element Size 54
3.1.3. Connection Types 54
3.1.3.1. Adhesive Line Connection 54
3.1.3.2. Spot Weld Connection 55
3.1.3.3. Seam Line Connection 56
3.1.3.4. Bolt Connection 57
3.1.4. Rigidizing 57
3.1.5. Non-Structural Mass (NSM) 58
3.2. Vehicle FE Model Creation 58

3.3. FE Display Model Creation 63
3.4. Modal Analysis and Modal Model Creation 65
3.5. Boundary Conditions 67
3.6. Transfer Path Analysis via CAE Model 68
3.6.1. Vibrational Transfer Function (VTF) Analysis via CAE 70
3.6.2. Noise Transfer Function (NTF) Analysis via CAE 78
4. ANALYSIS VIA MODAL HAMMER TEST 81
4.1. Noise and Vibration Measurement and Instrumentation 82
4.1.1. Noise Measurement and Instrumentation 82
4.1.1.1. Noise Classification 82
4.1.1.2. Noise Measurement 82
4.1.1.3. Microphones 83
4.1.1.4. Pre-amplifiers 86
4.1.2. Vibration Measurement and Instrumentation 87
4.1.2.1. Vibration Transducers 87
4.1.2.2. Modal Hammer 93
4.1.2.3. Modal Exciter (Shaker) 94
4.1.2.4. Data Acquisition Device 94
4.2. Transfer Path Analysis on Prototype Vehicle 95
4.2.1. Vibration Transfer Function (VTF) via Hammer Test 96
4.2.2. Noise Transfer Function (NTF) via Hammer Test 111
5. CORRELATION AMONG CAE AND TEST RESULTS 112
5.1. VTF Correlation Results 113
5.2. NTF Correlation Results 173
6. DISCUSSION 177
7. CONCLUSION 181

REFERENCES 183
BIOGRAPHY 188

LIST of ABBREVIATIONS and ACRONYMS

Abbreviations and Acronyms		**Explanations**
dB	:	Decibel
E	:	Young Modulus
F	:	Force
Hz	:	Hertz
m	:	Meter
s	:	Second
δ	:	Displacement
Ω	:	Ohm
ω_n	:	Natural frequency
AC	:	Alternative Current
ATV	:	Acoustic Transfer Vector
BEM	:	Boundary Element Method
CAD	:	Computer Aided Design
CAE	:	Computer Aided Engineering
DC	:	Direct Current
DOE	:	Design of Experiment
DOF	:	Degree of Freedom
EO	:	Engine Order
FE	:	Finite Elements
FEA	:	Finite Elements Analysis
FEM	:	Finite Elements Method
FRF	:	Frequency Response Function
LFSS	:	Low Frequency Sound Source
MDOF	:	Multi Degree of Freedom
NTF	:	Noise Transfer Function
NVH	:	Noise Vibration Harshness
RPM	:	Revolution Per Minute

RMS	:	Root Mean Square
TPA	:	Transfer Path Analysis
SDOF	:	Single Degree of Freedom
SPL	:	Sound Pressure Level
WOT	:	Wide Open Throttle
VTF	:	Vibration Transfer Function

LIST of FIGURES

Figure No:		Page
2.1:	Undamped spring-mass system undergoing free vibrations.	12
2.2:	Free body diagram of undamped spring-mass system.	13
2.3:	Response of undamped spring-mass oscillator (k=m=1 choosen).	16
2.4:	Viscous damping element.	17
2.5:	Damped spring-mass-dashpot system undergoing free vibrations.	18
2.6:	Free body diagram of spring-mass-dashpot system.	18
2.7:	Underdamped responses for SDOF spring-mass-dashpot system.	20
2.8:	Frequency response function (FRF) model.	25
2.9:	Various wave phenomena.	28
2.10:	Wavelength and frequency distribution.	29
2.11:	Sound wave.	30
2.12:	Tuning fork and sound propagation.	31
2.13:	General sound pressure levels.	37
2.14:	The structure of human ear.	39
2.15:	Vibration of the ear drum.	39
2.16:	Engine noise radiation.	42
3.1:	Discretization.	44
3.2:	Elements and nodes.	45
3.3:	Pre-processing stages in ANSA.	46
3.4:	Shell element classification.	48
3.5:	Solid element classification.	49
3.6:	Aspect ratio criteria for tria and quad shell elements.	50
3.7:	Aspect ratio criteria for common solid elements.	51
3.8:	Skewness (skew angle) criteria for tria and quad shell elements.	51
3.9:	Warpage criterion for quad elements.	52
3.10:	Taper criterion for quad elements.	53
3.11:	Twist criteria for solid elements.	54
3.12:	Adhesive line connection.	55

3.13:	Two members connected by spotwelds.	55
3.14:	Spotweld connection.	56
3.15:	Seam line connection.	56
3.16:	Bolt connection.	57
3.17:	FEM and rigidized model of wiper system.	58
3.18:	Cabin finite element model.	61
3.19:	Chassis finite element model.	61
3.20:	Engine finite element model.	61
3.21:	Cabin display model.	64
3.22:	Chassis display model.	64
3.23:	VSIGN GUI.	65
3.24:	RBE2 connetions (BC's) for front cabin-chassis attachments.	67
3.25:	RBE2 connetion (BC) for left chassis-front axle attachment.	68
3.26:	Vibrational transfer path 1.	71
3.27:	Vibrational transfer path 2.	71
3.28:	Vibrational transfer path 2 (continuation).	72
3.29:	Vibrational transfer path 3,4,5,6.	72
3.30:	Vibrational transfer path 7,8,9,10,11.	73
3.31:	Vibrational transfer path 12.	73
3.32:	Front axle air suspension.	74
3.33:	Vibrational transfer path 13 and 14.	75
3.34:	Vibrational transfer path 15.	76
3.35:	Vibrational transfer path 16 and 17.	77
3.36:	Vibrational transfer path 18.	77
3.37:	Vibrational transfer path 19.	78
3.38:	Structure model for coupling.	79
3.39:	Seat and bed cushon model for coupling.	80
3.40:	Fluid cavity model for coupling.	80
4.1:	A sound level meter.	83
4.2:	Free-field, pressure and random response of microphones	86
4.3:	Brüel & Kjaer type 4188 1/2-inch microphone.	86

4.4:	CCLD Microphone Preamplifier Type 2671, Brüel & Kjær	87
4.5:	Proximity probe principle.	88
4.6:	Velocity transducer principle.	89
4.7:	Piezoelectric accelerometer principle.	91
4.8:	Triaxial DeltaTron accelerometer type 4529-B, Brüel & Kjær.	93
4.9:	ICP impact hammer model 086C41, imi sensors.	94
4.10:	A typical modal exciter (Brüel & Kjær,type 4824).	94
4.11:	LMS SCADAS Recorder01 data acquisition device.	95
4.12:	Front axle region (passenger side) of the prototype vehicle.	97
4.13:	Impact points on front axle for transfer path 1 and 2.	97
4.14:	Impact on X direction for transfer path 3.	98
4.15:	Impact on Y direction for transfer path 3.	98
4.16:	Impact on Z direction for transfer path 3.	99
4.17:	Impact on X direction for transfer path 4.	99
4.18:	Impact on Y direction for transfer path 4.	99
4.19:	Impact on Z direction for transfer path 4.	100
4.20:	Impact on X direction for transfer path 5.	100
4.21:	Impact on Y direction for transfer path 5.	100
4.22:	Impact on Z direction for transfer path 5.	101
4.23:	Impact on X direction for transfer path 6.	101
4.24:	Impact on Y direction for transfer path 6.	101
4.25:	Impact on Z direction for transfer path 6.	102
4.26:	Impacts for transfer path 7.	102
4.27:	Impacts for transfer path 9.	103
4.28:	Impacts for transfer path 10.	103
4.29:	Impacts for transfer path 12.	104
4.30:	Impact on X direction for transfer path 13.	105
4.31:	Impact on Y direction for transfer path 13.	105
4.32:	Impact on Z direction for transfer path 13.	105
4.33:	Impacts for transfer path 15.	106
4.34:	Steering wheel hub and the accelerometer.	107

4.35:	Passenger seat pedestal and the accelerometer.	107
4.36:	Cablift and the accelerometer.	107
4.37:	Cabin ARB (anti-roll bar).	108
4.38:	Impact on X direction for transfer path 16.	108
4.39:	Impact on Y direction for transfer path 16.	109
4.40:	Impact on Z direction for transfer path 16.	109
4.41:	Impact on X direction for transfer path 17.	110
4.42:	Impact on Y direction for transfer path 17.	110
4.43:	Impact on Z direction for transfer path 17.	110
4.44:	Impacts for transfer path 18 and 19.	111
4.45:	NTF test microphones in vehicle cabin.	112
5.1:	VTF correlation for transferpath1 response1.	114
5.2:	VTF correlation for transferpath1 response2.	114
5.3:	VTF correlation for transferpath1 response3.	115
5.4:	VTF correlation for transferpath1 response4.	115
5.5:	VTF correlation for transferpath1 response5.	116
5.6:	VTF correlation for transferpath1 response6.	116
5.7:	VTF correlation for transferpath1 response7.	117
5.8:	VTF correlation for transferpath2 response1.	117
5.9:	VTF correlation for transferpath2 response2.	118
5.10:	VTF correlation for transferpath2 response3.	118
5.11:	VTF correlation for transferpath2 response4.	119
5.12:	VTF correlation for transferpath2 response5.	119
5.13:	VTF correlation for transferpath2 response6.	120
5.14:	VTF correlation for transferpath2 response7.	120
5.15:	VTF correlation for transferpath3 response1.	121
5.16:	VTF correlation for transferpath3 response2.	121
5.17:	VTF correlation for transferpath3 response3.	122
5.18:	VTF correlation for transferpath3 response4.	122
5.19:	VTF correlation for transferpath3 response5.	123
5.20:	VTF correlation for transferpath3 response6.	123

5.21: VTF correlation for transferpath3 response7. 124
5.22: VTF correlation for transferpath4 response1. 124
5.23: VTF correlation for transferpath4 response2. 125
5.24: VTF correlation for transferpath4 response3. 125
5.25: VTF correlation for transferpath4 response4. 126
5.26: VTF correlation for transferpath4 response5. 126
5.27: VTF correlation for transferpath4 response6. 127
5.28: VTF correlation for transferpath4 response7. 127
5.29: VTF correlation for transferpath5 response1. 128
5.30: VTF correlation for transferpath5 response2. 128
5.31: VTF correlation for transferpath5 response3. 129
5.32: VTF correlation for transferpath5 response4. 129
5.33: VTF correlation for transferpath5 response5. 130
5.34: VTF correlation for transferpath5 response6. 130
5.35: VTF correlation for transferpath5 response7. 131
5.36: VTF correlation for transferpath6 response1. 131
5.37: VTF correlation for transferpath6 response2. 132
5.38: VTF correlation for transferpath6 response3. 132
5.39: VTF correlation for transferpath6 response4. 133
5.40: VTF correlation for transferpath6 response5. 133
5.41: VTF correlation for transferpath6 response6. 134
5.42: VTF correlation for transferpath6 response7. 134
5.43: VTF correlation for transferpath7 response1. 135
5.44: VTF correlation for transferpath7 response2. 135
5.45: VTF correlation for transferpath7 response3. 136
5.46: VTF correlation for transferpath7 response4. 136
5.47: VTF correlation for transferpath7 response5. 137
5.48: VTF correlation for transferpath7 response6. 137
5.49: VTF correlation for transferpath7 response7. 138
5.50: VTF correlation for transferpath8 response1. 138
5.51: VTF correlation for transferpath8 response2. 139

5.52: VTF correlation for transferpath8 response3. 139
5.53: VTF correlation for transferpath8 response4. 140
5.54: VTF correlation for transferpath8 response5. 140
5.55: VTF correlation for transferpath8 response6. 141
5.56: VTF correlation for transferpath8 response7. 141
5.57: VTF correlation for transferpath9 response1. 142
5.58: VTF correlation for transferpath9 response2. 142
5.59: VTF correlation for transferpath9 response3. 143
5.60: VTF correlation for transferpath9 response4. 143
5.61: VTF correlation for transferpath9 response5. 144
5.62: VTF correlation for transferpath9 response6. 144
5.63: VTF correlation for transferpath9 response7. 145
5.64: VTF correlation for transferpath10 response1. 145
5.65: VTF correlation for transferpath10 response2. 146
5.66: VTF correlation for transferpath10 response3. 146
5.67: VTF correlation for transferpath10 response4. 147
5.68: VTF correlation for transferpath10 response5. 147
5.69: VTF correlation for transferpath10 response6. 148
5.70: VTF correlation for transferpath10 response7. 148
5.71: VTF correlation for transferpath11 response1. 149
5.72: VTF correlation for transferpath11 response2. 149
5.73: VTF correlation for transferpath11 response3. 150
5.74: VTF correlation for transferpath11 response4. 150
5.75: VTF correlation for transferpath11 response5. 151
5.76: VTF correlation for transferpath11 response6. 151
5.77: VTF correlation for transferpath11 response7. 152
5.78: VTF correlation for transferpath12 response1. 152
5.79: VTF correlation for transferpath13 response1. 153
5.80: VTF correlation for transferpath13 response2. 153
5.81: VTF correlation for transferpath13 response3. 154
5.82: VTF correlation for transferpath13 response4. 154

5.83: VTF correlation for transferpath13 response5. 155
5.84: VTF correlation for transferpath13 response6. 155
5.85: VTF correlation for transferpath13 response7. 156
5.86: VTF correlation for transferpath14 response1. 156
5.87: VTF correlation for transferpath14 response2. 157
5.88: VTF correlation for transferpath14 response3. 157
5.89: VTF correlation for transferpath14 response4. 158
5.90: VTF correlation for transferpath14 response5. 158
5.91: VTF correlation for transferpath14 response6. 159
5.92: VTF correlation for transferpath14 response7. 159
5.93: VTF correlation for transferpath15 response1. 160
5.94: VTF correlation for transferpath16 response1. 160
5.95: VTF correlation for transferpath16 response2. 161
5.96: VTF correlation for transferpath16 response3. 161
5.97: VTF correlation for transferpath16 response4. 162
5.98: VTF correlation for transferpath16 response5. 162
5.99: VTF correlation for transferpath16 response6. 163
5.100: VTF correlation for transferpath17 response1. 163
5.101: VTF correlation for transferpath17 response2. 164
5.102: VTF correlation for transferpath17 response3. 164
5.103: VTF correlation for transferpath17 response4. 165
5.104: VTF correlation for transferpath17 response5. 165
5.105: VTF correlation for transferpath17 response6. 166
5.106: VTF correlation for transferpath18 response1. 166
5.107: VTF correlation for transferpath18 response2. 167
5.108: VTF correlation for transferpath18 response3. 167
5.109: VTF correlation for transferpath18 response4. 168
5.110: VTF correlation for transferpath18 response5. 168
5.111: VTF correlation for transferpath18 response6. 169
5.112: VTF correlation for transferpath18 response7. 169
5.113: VTF correlation for transferpath19 response1. 170

5.114: VTF correlation for transferpath19 response2. 170
5.115: VTF correlation for transferpath19 response3. 171
5.116: VTF correlation for transferpath19 response4. 171
5.117: VTF correlation for transferpath19 response5. 172
5.118: VTF correlation for transferpath19 response6. 172
5.119: VTF correlation for transferpath19 response7. 173
5.120: NTF correlation for transferpath16 response left passenger ear. 174
5.121: NTF correlation for transferpath16 response right passenger ear. 174
5.122: NTF correlation for transferpath17 response left passenger ear. 175
5.123: NTF correlation for transferpath17 response right passenger ear. 175
6.1: Iterations to correlate amplitude levels at a specific frequency. 178
6.2: Inverse peaks problem at a specific frequency. 179
6.3: Iterations to change direction of a peak at a certain frequency. 180

LIST of TABLES

Table No:		Page
2.1:	Frequency response function (FRF) names.	26
2.2:	Frequency response function (FRF) names (2).	26
2.3:	Propagation speed of sound in various medium.	30
2.4:	Standardized nominal 1/3 octave and octave centre (red) frequencies (Hz).	34
3.1:	Number of elements for specific subsytem FE models.	59
3.2:	Number of nodes for specific subsytem FE models.	60
3.3:	Modelling strategy for major trim parts.	62
3.4:	Defined transfer paths.	64

1. INTRODUCTION

Today, due to globalization and increased competition, it has become more difficult for automotive manufacturers to capture success than ever. In the 21st century, customers expect better quality, more advanced features and better performance from a new vehicle. Having a large number of products in the market due to globalization has made it a necessity to meet customer expectations in the sense that it is the reason for preference for automotive manufacturers [1].

In the automotive industry, customer expectations can be listed primarily as attractive exterior and interior design, safety, good ride control, low fuel consumption, durability, entertainment tools and comfort. It is very essential to meet customer expectations not only for passenger vehicles but also for medium and heavy commercial vehicles to compete in the market. In this sense, automotive manufacturers have begun to follow long product development processes to meet customer demands.

The product development process generally begins with market research and benchmarking. At this point, the expectations of the customer are clearly identified. The targets that are appropriate to the company's financial resources and intellectual capital are set.

The engineering footprint of the product development process begins after determining the appropriate targets for the market and company resources. As mentioned earlier, there are expectations of customers such as attractive exterior and interior design, safety, good ride control, low fuel consumption, durability, entertainment tools and comfort, and each engineering team carries out design studies in order to meet these expectations.

The optimum designs in the vehicle may vary for engineering teams working in the product development process. Even beyond a possibility, this is inevitable. For example, a design that causes weight increase in the vehicle may be a pretty good sense of safety, while fuel consumption is quite inefficient. Similarly, a design that shows the car visually good can have undesired consequences for NVH.

NVH (Noise Vibrations and Harshness) is one of the most important parameter in terms of the comfort of a vehicle and the high quality of the customer's perception. In a customer of view, it is easy to compare two vehicles in terms of NVH. Because, regardless of technical knowledge, a customer may feel disturbed by the vibration and hear the noise of the vehicle caused by the vibrating panels. In this sense, it can be said that the quality of NVH is very important for the reason that a vehicle is preferred by the customer on the market. This whole process should be followed not only for passenger cars but also for medium and heavy commercial vehicles as mentioned before.

In the automotive industry, the latest technologies and computerized systems are used in all vehicle development processes, including NVH. In the process of mature design, engineers work to reach the optimal level of engineering, with the help of CAE, in order to reach the specified targets for vehicle programs.

With the help of methods such as finite elements analysis (FEA) and the help of CAE, the vehicle can be designed to reach the specified targets. At the same time, the CAE process is very important in terms of anticipating the problems that may arise in manufacturing and taking action for resolution or making design changes. The solution of a problem that may arise in the manufacturing process can be much more expensive and longer than a solution in the CAE process.

As with many other engineering approaches, CAE is an engineering method that reaches its conclusion under certain assumptions and approaches. Therefore, during the product development process, the final designs with CAE are produced as prototypes and validated by tests. At this point it is very important that the CAE results correlate with the test results. Low correlation can be a sign of problems, and therefore additional spending and a prolonged period of time.

CAE and test correlation for a heavy commercial vehicle is also important in terms of NVH perspective. In a heavy commercial vehicle, there are many sources that can cause noise in the cabin. These resources can be classified as airborne and structure-borne. Structure-borne noise which is primarily caused by the powertrain excitations. The excitation coming from the powertrain may cause any part of the body subsystem to vibrate and consequently a change in the sound pressure level

(SPL). In the low frequency range of 50-200 Hz, undesirable booming noise may occur in the passenger cabin.

In this study, correlation between CAE and physical tests are identified for a full NVH model of a heavy commercial vehicle based on noise and vibration transfer path analyzes.

1.1. Literature Review

Academic studies on vehicle NVH analyzes, mainly performed in the last 15 years, is examined. In this section, the examined academic studies are given in chronological order.

CAE models are mathematical models with a visual representation. The increase in the number of elements in a CAE model means that the time for the iterations also increases. In addition, there is a critical number of elements for computers with limited processing capabilities. Because after a certain number of elements, the CAE model grows excessively and computers can not perform analyzes.

Gurgoze suggested that a mathematical model should be as simple as possible and as complex as necessary. Gurgoze generated a formulation of how to roughly determine the fundamental frequency and first mode shape of a beam or bar to which springs and point masses are connected [2].

In literature, Finite Elements Method (FEM) and Boundary Elements Method (BEM) are generally used in order to make vibro-acoustic analysis.

Many researchers have conducted and discussed the vibro-acoustic response of a vehicle using methods such as strongly coupled structure-fluid interaction or unconformed structure-fluid interaction [3]-[5].

Suzuki et al. used BEM in order to overcome the noise issues inside a vehicle cabin [3]. They proposed a new formulation for complex boundary conditions to solve practical sound problems in a vehicle cabinet.

Pal and Hagiwara's used FEM for the coupled structure-fluid problems. They investigated the correlation between vibration of cabin walls and the SPL at the position of the passenger ear [4].

For coupled systems, Freymann et al. investigated fluid-structure interaction in order to predict the SPL. FE and BE models of the chassis frame of the vehicle were created and used in order to perform the vibro-acoustic analysis [6].

In similar coupling study, Kim and Lee studied the structural acoustical response of a vehicle cabin in terms of the structural-acoustic modal coupling coefficients. Furthermore, they also investigated the contribution of the structural panels to the interior noise levels [7].

According to Ewins, experimental modal analysis is obtaining a mathematical model from measured data performed in order to identify the dynamical characteristic of a structure [8].

Mohanty et al. investigated structure borne noise reduction in a vehicle using numerical methods. They used FEM and BEM to characterize the acoustic field of a vehicle interior [9].

In a serie of studies, Marburg et al. investigated the optimized design parameters based on vibro-acoustic analysis and also investigated the vibro-acoustic response of the noise level inside the vehicle cabin [10]-[12].

Apart from FEM and BEM, Acoustic Transfer Vector (ATV) which enables the contribution analyses to identify the problem sources, is one of the phenomena frequently encountered in literature studies.

In a study, Herrin et al. investigated an engine model which is separated into various different components. The objective of this study, which is based on the contribution analysis, is to understand to how contribute sound radiating components to the overall SPL [13].

For NVH-issues remaining in late vehicle development stages, Plunt discussed the use of experimental Transfer Path Analysis (TPA) to find optimized solutions [14].

Liu et al. generated a vibro-acoustic model in order to predict the noise inside the vehicles. In the study, both FEM and BEM models were used for the vibro-

acoustic analysis. In addition they used ADAMs software in order to determine interaction forces in the vehicle [15].

Plunt discussed several practical cases to demonstrate how TPA, FE models and experiments can support each other efficiently in order to find optimal and quality balanced solutions to complex NVH issues in the last stages of the development process [16].

G.Kamci et al. performed an investigation for the interior noise level of the passenger cabin both comparing the results of the coupled and uncoupled analysis with the obtained experimental results [5].

Slave et al. used CAE models verified by experimental measurements to determine the vibration modes of a truck cabin. A significant reduction in vibration amplitude in the CAE analysis was observed to eliminate the cab yaw motion from the vibration mode of the front axle cylinder as a result of adding a lateral link between the front of the cabin and the first cross member of the chassis [17].

Shariyat and Djamshidi developed an effective procedure to reduce motor-induced vibrations which is based on NVH analysis results of a full vehicle model, adding rigidity and strength constraints to the account. The NVH analysis results of the entire vehicle were used in the optimization procedure to eliminate the transmitted vibration. A procedure was developed to reduce the most of the accelerations transmitted to the midpoint of the driver's seat track. A DOE-based response surface methodology (RSM) was adopted to detect the optimal solution. The natural frequencies of the body, suspension and other subsystems were taken into account when detecting the optimal solution [18].

Wolff et al. were performed panel acoustic additive analysis. They used specially designed audio probes that can measure sound pressure and particle velocity at the same time. During driving, the panel measured particle velocity data to perform acoustic contribution analysis and air-borne transfer paths from the sources to the listening positions from the sources [19].

Han, Guo, Yu and Zhu introduced new two parameters, which were “acoustic contribution sum” and “total sound field contribution” to analyze the interior sound field characterized with multiple field points sound pressure peaks, and to determine the integrated acoustic contributions of automotive body panels. Hence,

with these two parameters, current PACA method was improved by solving the problem of multiple peak sound pressure reduction [20].

In another study, Binxing et al. used various calculation methods, such as FEM, BEM and Statistical Energy Analysis (SEA) to determine the acoustic characteristics of the vehicle. In the high frequency range, they used SEA method to conduct the analysis [21].

Yuksel et al. investigated the structure-borne noise which is caused by the vibrating cabin panels. They used methodologies FEM was used for the structural analysis of the vehicle, BEM was integrated with the results obtained from FEM for the acoustic analysis of the cabin to predict cabin interior SPL of a commercial vehicle. Also they performed Panel Acoustic Contribution Analysis (PACA) to determine the contribution of each panel to the interior noise level [22].

Mansinh et al. (2011) used different diagnostic techniques like Transfer Path Analysis (TPA), Modal Contribution Analysis (MCA) and Panel Acoustic Contribution Analysis (PACA) in order to arrive at First Time Right optimization. The study determined the component and system level weak points as a part of performance optimization [23].

According to Guan and Gruber, to build up a FEM Model for NVH analysis the assembly process and load case definition play an significant role. Both steps are very complex and the possibility to make mistakes is very high. After initial analysis the results has to be interpreted to understand the NVH behavior and investigate optimization potential. Diagnostic tools could be used to determine modal or panel participation factors or perform transfer path analysis (TPA). Then components or subsystems could be optimized using numerical optimization tools. For this step often super elements are used to reduce calculation time without losing too much of accuracy. As a full vehicle often contains of many single super elements the handling is also an important point. A basic precondition for optimization is that the analysis model has to be of good quality to achieve more accurate optimization results [24].

Abreu and Moura (2012), used techniques as mechanical vibration analysis, operational modal analysis and operational deflection shape to determine the root cause of increased levels of vibration felt at idle speed in a vehicle prototype. Study

demonstrated the methodology used to identify the cause of the different behaviors between vehicles and improvements made in the body according to the results of the numerical experimental confrontation [25].

Xie et al. (2013), proposed the test and simulation integrated TPA and optimization method to reduce vibration of a subsytem (the steering) in idle. First the contributors to the steering wheel vibration were studied, including the vibrational excitation sources, the transmission paths, and the steering wheel itself. Then a series of improvements were perforned. Results showed that the steering Wheel vibration in idle condition drops over %70 [26].

Britto et al. (2013) represented a case study on low frequency NVH performance evaluation and refinement for heavy commercial vehicle (HCV) truck using mixed Test-CAE methodology. They claimed that it is important to set competitive overall vehicle level NVH targets and cascade it down to system and sub-system targets in order to achieve better NVH performance. Test-CAE correlation was carried out to validate Finite Element (FE) modeling procedure and methodology. The methodology helped to optimize the design efficiently to achieve the full vehicle level NVH targets. An attempt has been made to achieve overall vehicle level NVH targets with minimal test measurements [27].

Akei et al. (2014) described a vibration estimation and transfer path analysis (TPA) using a engine multibody dynamic (MBD) model and measured frequency response functions (FRtF). The MBD model of the engine was built and the forces entering the main frame of an agricultural machine were predicted. The accuracy of prediction is confirmed when compared with the results obtained from the conventional TPA method. The contribution of each transfer path was analyzed and the vibration levels of the operator position were estimated using the measured FRFs and the simulated input forces. As a consequence, the vibrations of the operator position and the input forces estimated accurately [28].

Lu and Ma (2015), deals with the development phase of a prototype engine in which a specific testing activity was carried out to improve the overall NVH behavior of the powertrain. A case study was described in order to explain the optimization process in detail. In the study, first, NVH targets of the engine were set with aid of benchmark tests on existing competitive products. Then series of baseline tests,

such as 1M SPL test and noise source identification were performed on the engine. The results indicated that an obvious breathing vibration mode exist near the intake manifold, which radiates high level noise. A correlation validation was performed to find out the main reason that caused the vibration of intake manifold in order to achieve the NVH targets, and then its structure was optimized through CAE analysis to change its modal frequencies. As a result, the NVH performance of the engine was significantly improved after the optimization work [29].

According to Fard and Liu (2015), the development and application of the vehicle advanced CAE allowed the vehicle designers to significantly reduce the weight and improve the structural performance of the body. They modeled the members and panels of the automotive body in white (BIW) and approximated using shell and beam elements. They used Guyan reduction method in order to obtain joints properties from the original detailed CAE model. They created the automotive seat concept model and added to the concept BIW model. A good correlation was reached in low frequency range [30].

1.2. Purpose of The Study

As mentioned before, the product development process in the automotive industry is a long process that requires high capital and massive knowledge. Increasing competition and globalization necessitate the use of advanced CAE technologies in the product development process. In this process, product designs made with the help of CAE are validated by physical tests.

CAE is a process that is realized with certain assumptions, as in all other engineering methodologies. Therefore, it is a common but undesirable fact that test results differ from CAE results. Since it can cause additional time and resource usage, it is very important that the correlation between CAE and Test is high. One time true design will prevent these losses and provide the opportunity to see possible faults before production and take action.

In this study, modifications that could be made in the CAE for high CAE and test correlation in terms of NVH is investigated and improvements that could be

made in the interior of a heavy commercial vehicle is also investigated. In addition, understand to how contribute sound radiating components to the overall SPL is another purpose of this study.

In the studies investigated in the literature survey, it has been founded that the correlation studies are generally made on simple beams, plates or simplified vehicle models. Most of the work done on the vehicle model were perfomed on a quarter or half vehicle model. However, in this study, a complete NVH model was used, which was prepared with all trimmings of a complex vehicle model of a truck. The correlation study was performed on the FE model obtained by identical modeling of the prototype vehicle. Also, unlike other studies, modal model approach is used instead of direct FEM and BEM methods in this study. The modal model was created by using an in-house software (VSIGN) to reduce the DOF from millions to a few thousand DOF.

Two paramaters were choosen as critical. One of the parameters is that FE modelling technique. An optimized FE modelling criteria was used for the full vehicle model. The other parameter is about stiffness of bushings and mounts. Especially for bushings, a wide range of tolerance can be mentioned due to manufacturing. So, bushing stiffnesses are quite important and critical in order to obtain high correlation. In addition, bushing stiffnesses are also important for the vehicle dynamics team. Since engineers in vehicle dynamics team use rigid ADAMS model, bushing stiffnesses must be identified accurately. At this point, it can be mentioned that this study is also helpful for vehicle dynamics team.

In the CAE phase, all analyzes were performed using different computer software based on finite element analysis. In order to create FE model, all three-dimensional modeled body, chassis, engine, transmission parts and internal and external trim parts of the vehicle were transformed into a finite element model with the aid of the ANSA software. Then, the air model for the vehicle cabin was created with the aid of the ANSA software. The coupling of the generated air model was performed with the aid of the SFE AKUSMOD software. Modal analysis was performed with the help of the NASTRAN software and the results were analyzed in the METAPOST software. Modal results from NASTRAN are combined with FE models and transformed into modal model with the help of VSIGN software. Then

modal approach is used for TPA analysis model with the help of MOTRAN which is the solver of the VSIGN. TPA results were examined using the Envision and PiRate software. Physical tests were carried out on the prototype of the vehicle to validate the results of the CAE analyzes carried out during this entire process. The physical tests were performed with modal hammer; the results were obtained with Lab View program.

1.3. Outline

This thesis first introduces product development process for vehicles. Then the literature review is presented. On the basis of the literature survey, recommendations for the improvement which can be made which might be implemented with the new techniques in order to satisfy the correlation.

The second chapter presents the theory and the background of this study. First, theory of mechanical vibrations is presented. Second, theory of acoustics is presented. Third, theory of NVH is presented briefly.

In the third chapter, the subsystems of the heavy commercial vehicle is presented. Process of building a CAE model in order to perform NVH analyses is an another subject of this chapter. Finally, the results of NVH analyzes are presented in this section.

In the forth chapter, NVH-Test results and its procedure are presented. In addition, test methods and improving techniques are discussed.

In the fifth chapter is the chapter that is presented correlation results among CAE and physical test. In addition, studies to improve the correlation are presented in this chapter.

The sixth chapter is the discussion chapter. The correlation results are discussed in this chapter. Interpretations on correlation based on frequency and transfer paths are presented here.

Last but not least, the seventh chapter is the conclusion part of this study. In this chapter, the results of this study are given and at the same time recommendations are given for future researchers.

2. THEORY AND BACKGROUND

In this section, theory of mechanical vibrations and theory of acoustics is presented. Additionally, NVH theory and its applications is also presented.

2.1. Theory of Mechanical Vibrations

Vibration is a mechanical phenomenon whereby oscillations occur about an equilibrium point. The vibration word comes from the vibrationem in Latin (shaking or brandishing). The oscillations may be periodic, such as the motion of a pendulum—or random, such as the movement of a tire on a bumpy road.

Vibration can be desirable: for example, the motion of a tuning fork, the reed in a woodwind instrument or harmonica, a mobile phone, or the cone of a loudspeaker.

In many cases, however, vibration is undesirable, wasting energy and creating unwanted sound. For example, the vibrational motions of engines, electric motors, or any mechanical device in operation are typically unwanted. Such vibrations could be caused by imbalances in the rotating parts, uneven friction, or the meshing of gear teeth. Careful designs usually minimize unwanted vibrations.

The studies of sound and vibration are closely related. Sound, or pressure waves, are generated by vibrating structures (e.g. vocal cords); these pressure waves can also induce the vibration of structures (e.g. ear drum). Hence, attempts to reduce noise are often related to issues of vibration [31].

2.1.1. Undamped Free Vibration

Free vibration occurs when a mechanical system is actuated by initial input and free vibration is allowed. Examples of such vibrations pull the child back and forth on the swing, hit a fork and allow it to steal. The mechanical system vibrates at one or more natural frequencies and is immersed in immobility [31].

In a specific mass-spring system, a solid mass is hang from an extensional spring under gravity acceleration g directed along the spring direction [32].

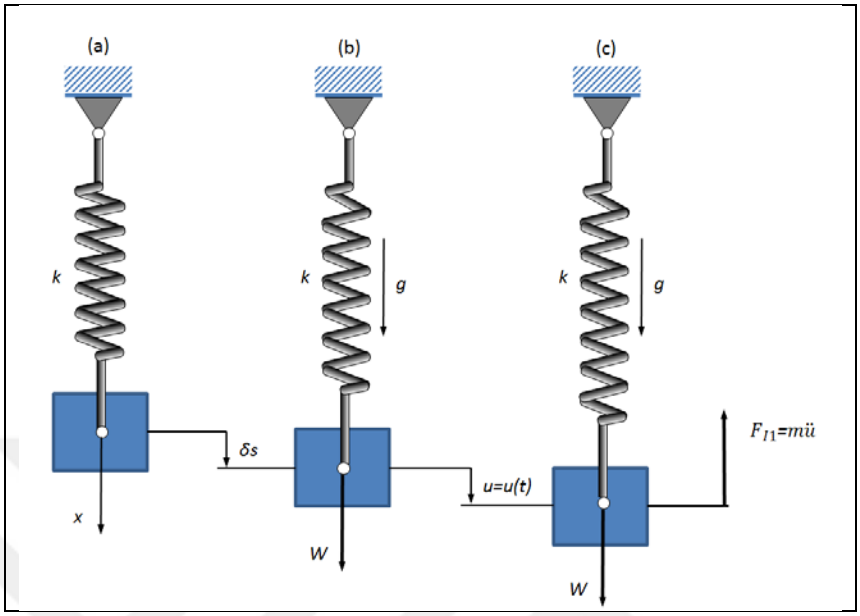

Figure 2.1: Undamped spring-mass system undergoing free vibrations.

The only force is the weight force in the mass-spring system and it is calculated by equation 2.1

$$W = mg \tag{2.1}$$

The static deflection of the mass

$$\delta s = \frac{W}{k} = \frac{mg}{k} \tag{2.2}$$

And the initial conditions (ICs as abbrevation) for the system can be defined as

$$u(0) = u_0 \tag{2.3}$$

$$\dot{u}(0) = v_0 \tag{2.4}$$

By releasing the mass and applying no force for t > 0, the oscillator is set in motion, and a free vibrations response occurs.

Let u(t) be the deviation from the static equilibrium position so that the total deflection is $\delta s + u(t)$ as shown in Figure 2.1(c).

The function u(t) is called the dynamic response. For this system, u = u(t) is the only degree of freedom (DOF).

By removing the spring and replacing it the spring force $Fs = k(\delta s + u(t))$ is illustrated in Figure 2.2. Except from spring force, weight of mass $W = mg$ which is independent of time, and the internia force $\ddot{u} = \ddot{u}(t)$ are added.

The sketch shown in the Figure 2.2 is called a Dynamic Free Body Diagram (DFBD).

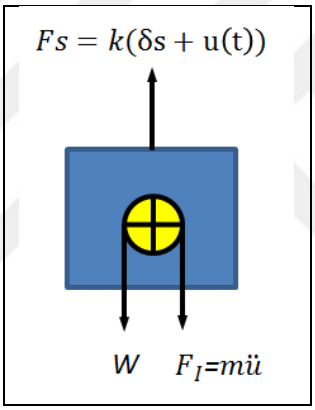

Figure 2.2: Free body diagram of undamped spring-mass system.

By applying equations of equilibrium in the x direction $m\ddot{u} = W - k(\delta s + u) = mg - k\delta s - ku$ and by canceling $mg - k\delta s = 0$, the equation becomes:

$$m\ddot{u} + ku = 0 \tag{2.5}$$

This is the equation of motion (EOM) of the undamped, free, single DOF, spring-mass system shown in Figure 2.1. It is a second order, linear Ordinary Differential Equation (ODE) in u(t).

Note that the static deflection δs is disappeared from this EOM, in fact the mass is oscillate about that position.

By dividing the equation (2.5) through by m and launch the term ω_n called natural frequency or resonant frequency:

$$\ddot{u} + \omega_n^2 = 0 \tag{2.6}$$

in which

$$\omega_n = +\sqrt{\frac{k}{m}} \tag{2.7}$$

The unit of natural frequency is radians per second (rad/s).

In order to express the response in terms of complex exponentials Let $u(t) = Ce^{\lambda t}$, where C ≠ 0 and λ are generally complex.

Since $\ddot{u} = \lambda^2 Ce^{\lambda t}$, substitution into (2.6) requires

$$(\lambda^2 + \omega_n^2)Ce^{\lambda t} = 0 \tag{2.8}$$

Since C ≠ 0 (if C = 0, the solution is null) and the exponential never vanishes, the term $\lambda^2 + \omega_n^2$ must be zero. This gives the characteristic equation

$$(\lambda^2 + \omega_n^2) = 0 \tag{2.9}$$

and the roots become:

$$\lambda_{1,2} = \pm i\omega_n \tag{2.10}$$

in which $i = \sqrt{-1}$ denotes the imaginary unit. Because both $e^{i\omega_n t}$ and $e^{-i\omega_n t}$ satisfy the linear ODE (2.5), so does any linear combination of them. Finally, general solution in terms of complex exponentials is found as

$$u(t) = C_1 e^{i\omega_n t} + C_2 e^{-i\omega_n t} \tag{2.11}$$

in which C_1 and C_2 are generally complex numbers.

In order to express the response in terms of trigonometric functions, Euler's relation for the complex exponentials is used

$$e^{\pm i\theta} = \cos\theta \pm i \sin\theta \tag{2.12}$$

and the solution (2.11) becomes:

$$u(t) = (C_1 + C_2)\cos\omega_n t + i(C_1 - C_2)\sin\omega_n t \tag{2.13}$$

In order to simplify the linkage of this expression to the initial conditions, the constants $A_1 = (C_1 + C_2)$ and $A_2 = i(C_1 - C_2)$ are defined. Then, expression of the response in terms of trigonometric functions becomes:

$$u(t) = A_1\cos\omega_n t + A_2\sin\omega_n t \tag{2.14}$$

Here A_1 and A_2 are real constants that can be directly determined from the initial conditions (2.3) and (2.4). By replacing them into (2.14) yields

$$u(t) = u_0 \cos\omega_n t + \frac{V_0}{\omega_n}\sin\omega_n t \tag{2.15}$$

This expression is the free vibration response of an undamped SDOF system in terms of trigonometric functions and initial conditions. Although (2.15) holds only for free vibrations, the solution will be reused as the homogeneous portion of the response of a forced SDOF oscillator. Another common expression of (2.15) is phased response (also called phase-shifted response) form

$$u(t) = U\cos(\omega_n t - \alpha) \tag{2.16}$$

Here the amplitude U and the phase angle α are linked to the initial conditions (2.15) by

$$U = \sqrt{u_0^2 + \left(\frac{v_0}{\omega_n}\right)} \tag{2.17}$$

$$\tan\alpha = \frac{v_0}{\omega_n u_0} \tag{2.18}$$

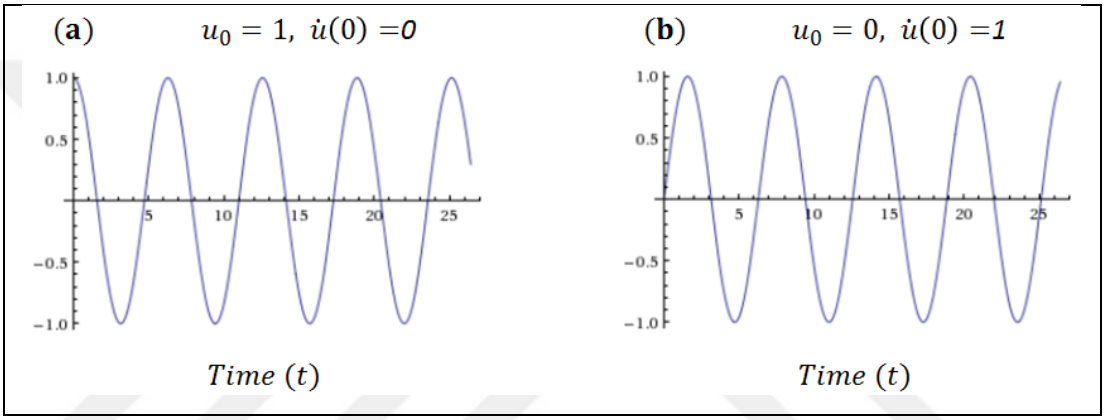

Figure 2.3: Response of undamped spring-mass oscillator (k=m=1 choosen) a)unit initial displacement without initial velocity, b)unit inital velocity without initial displacement.

2.1.2. Forced Vibration

Forced vibration occurs when a time-varying disturbance (load, displacement, or velocity) is applied to a mechanical system. Discomfort may be periodic and steady state input or a random input. Periodic input can be a harmonic or non-harmonic. Examples of such vibrations include a washing machine vibrating due to an imbalance, vehicle vibrations caused by an engine or a bumpy road, or vibrations of a building during an earthquake. In linear systems, the frequency of the steady-state vibration response due to the application of a periodic, harmonic input is

equal to the applied force or frequency of movement, and the magnitude of the response depends on the actual mechanical system [31].

2.1.3. Viscous Damping

When mechanical systems vibrate in a fluid medium such as water, oil, gas, and air, the resistance presented by the fluid to the moving body causes the energy to dissipate. The amount of energy dissipated depends on several factors such as the size and shape of the vibrating body, the viscosity of the fluid, the frequency of vibration, and the velocity of the vibrating body. The damping force is proportional to the velocity of the vibrating body in viscous damping [33].

A basic viscous damping element is shown in Figure 2.4.

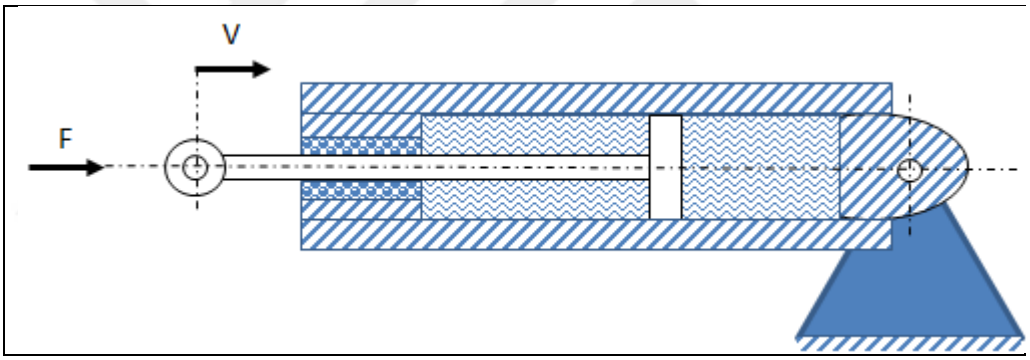

Figure 2.4: Viscous damping element.

The response plots of Figure 2.3 convey the idea that, once an undamped SDOF oscillator is set in motion, that motion will continue for all times $t > 0$ without any change in amplitude. On the other hand, all mechanical systems exhibit some damping, which dissipates energy and causes the motion eventually to be consumed away. In this section, the case of a SDOF oscillator under the simplest damping model: viscous damping, which is linearly proportional to the velocity is considered.

The model includes a dashpot element of viscosity $c \geq 0$, as illustrated in Figure 2.5(a).

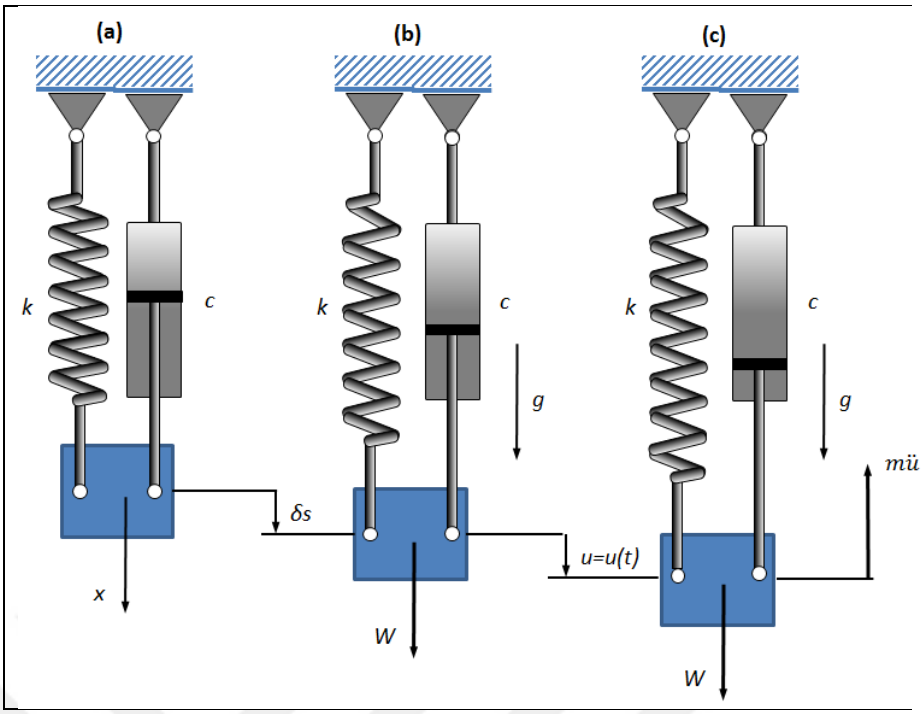

Figure 2.5: Damped spring-mass-dashpot system undergoing free vibrations.

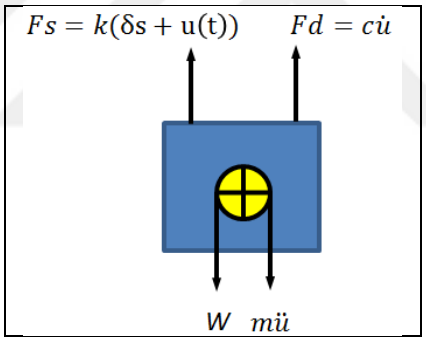

Figure 2.6: Free body diagram of spring-mass-dashpot system.

From the Dynamic Free Body Diagram (DFBD) shown in Figure 2.5, the physical form of the EOM is

$$m\ddot{u} + c\dot{u} + ku = 0 \qquad (2.19)$$

Divide the equations (2.19) through by m and denote

$$c = 2\xi\omega_n m \tag{2.20}$$

$$\xi = \frac{c}{2\omega_n m} = \frac{c}{2\sqrt{km}} \tag{2.21}$$

Here ω_n is the undamped circular natural frequency (or fundamental frequency) introduced in the previous section, while $\xi = \frac{c}{2\omega_n m} = \frac{c}{2\sqrt{km}}$ is the viscous damping factor or damping ratio, also called damping coefficient.

Finally, convert the equation (2.19) to the canonical form of the equation of motion:

$$\ddot{u} + 2\xi\omega_n\dot{u} + \omega_n^2 u = 0 \tag{2.22}$$

This is a linear, second-order ordinary differential equation (ODE) with constant coefficients. The only difference with respect to the undamped case is the presence of the velocity term $2\xi\omega_n\dot{u}$.

As usual in solving ODEs with the canonical form (2.22), assume a complex exponential solution

$$u(t) = Ce^{\lambda t} \tag{2.23}$$

where C and λ are generally complex values to be determined. Inserting into (2.22), the characteristic equation (2.24) is obtained:

$$\lambda^2 + 2\xi\omega_n\lambda + \omega_n^2 = 0 \tag{2.24}$$

which is quadratic in λ. Roots of the equation (2.24) are given by

$$\lambda_{1,2} = -\xi\omega_n \pm \omega_n\sqrt{\xi^2 - 1} \tag{2.25}$$

It should be noted that for the undamped case: ξ=0, the roots reduce to $\pm i\omega_n$, as found previously. The magnitude of the damping factor ξ compared to unity can be used to segregate three cases.

2.1.3.1. Underdamped Case (ξ < 1)

In this case, the damping is called subcritical. The roots $\lambda_{1,2}$ in (2.25) are complex conjugate. The motion is oscillatory with decreasing amplitude. This is the most common case in typical structures, and thus the most pratically important one.

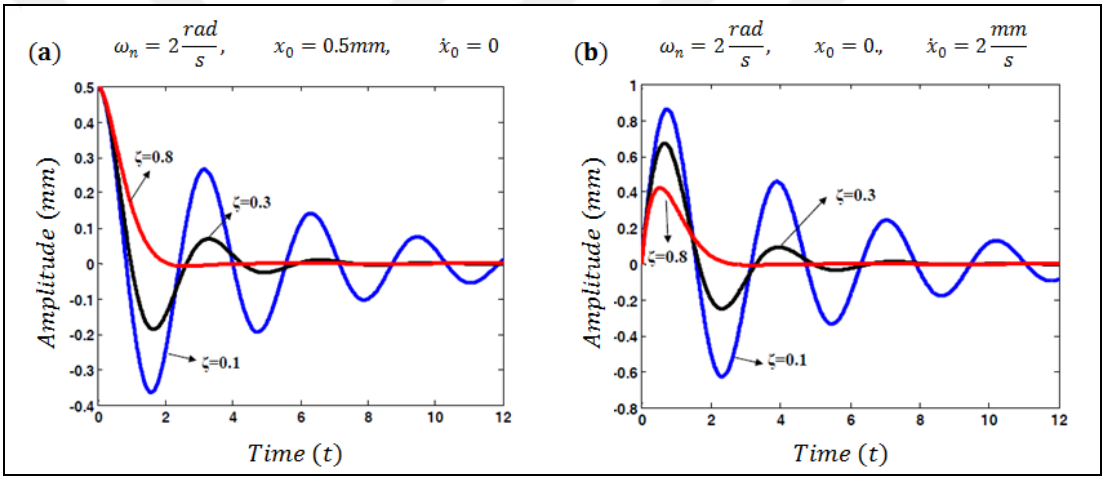

Figure 2.7: Underdamped responses for SDOF spring-mass-dashpot system a)with initial displacement without initial velocity, b)with inital velocity without initial displacement.

2.1.3.2. Overdamped Case (ξ > 1)

In this case, the damping is called overcritical. The roots $\lambda_{1,2}$ in (2.25) are negative and coalesce. The motion is non-oscillatory. Its amplitude decays monotonically except possibly for one zero crossing.

2.1.3.3. Critically Damped Case (ξ = 1)

In this case, the damping is called critical. The roots roots $\lambda_{1,2}$ in (2.25) are negative real and coalesce. The motion is non-oscillatory. Its amplitude decays monotonically except possibly for one zero crossing. Since the response produces the most rapid decay toward the static posiiton, critical damping is of interest in the design of devices such as instruments and suspensions.

2.1.4. Mechanical (Structural) Damping

Damping is an impact within or upon an oscillatory system that has the effect of reducing, restricting or preventing its oscillations. In physical systems, damping is composed by processes that dissipate the energy stored in the oscillation. Examples include viscous drag in mechanical systems, resistance in electronic oscillators, and absorption and scattering of light in optical oscillators. Damping not based on energy loss can be important in other oscillating systems such as those that occur in biological systems. Up to now, the previous works on SR for a fractional linear oscillator, the damping coefficient is mainly considered as a fractional friction. However, a viscous damping does exist in an oscillator, such as in an integral-order linear oscillator and in a Duffing oscillator [34]-[36].

In structural systems, damping is more complex, appearing in various forms. They can generally be categorized as into internal versus external, and ditributed versus localized [32].

2.1.4.1. Internal and External Damping

Internal damping is due to the structural material itself. Types of sources: microstructural defects, relative movements of crystal grains, eddy currents in ferromagnetic media, molecular shifts in metals and molecular chain movements of polymers. The macroscopic effect is the production of a hysteresis loop in the stress-strain graphs. The hysteresis loop represents energy distributed per unit

volume and stress cycle per unit of material. Such damping is closely related to cyclic movements such as vibration.

External damping comes from border effects. The structural damping produced by frictional friction has an important shape: stick and slip contact or impact. This can be between structural components such as joints or between a structural surface and nonstructural solid environments such as soil. This form is usually modeled by the Coulomb damping, which describes the energy consumption of the dry-friction.

Another form of external damping is fluid damping. When a material is immersed in a fluid such as air or water and there is a relative movement between the structure and the fluid, a drag force appears. This force causes energy dissipation through internal fluid mechanisms such as viscosity, convection or turbulence. This distribution is collectively known as fluid damping. A well-known example is a vehicle shock absorber: a liquid (liquid or air) is forced through a small opening by a piston [32]

2.1.4.2. Distributed and Localized Damping

The entire damping eventually comes from friction effects, but it can happen at different times. If the effects are scattered over volumes or surfaces at macro scales, distribution without damping can be mentioned. But sometimes the engineer uses damping devices designed to create useful effects. For example: shock absorbers, airbags, parachutes, motion absorbers for buildings or bridges in seismic or hurricane areas, active piezoelectric shock absorbers for gaps.

These devices are often modeled as point forces or moments and can be idealized as lumped objects as they are used to generate localized damping. This distinction appears primarily at the modeling level, since all motion-pulsing devices eventually operate as a consequence of a certain type of internal energy conversion at the molecular level [32].

2.1.4.3. Modeling Structural Damping

In structures containing joints, for example, Coulomb (dry friction) damping is often dominant; This model is not partly linear because the damping force depends on the speed sign. Fluid damping tends to be highly nonlinear because the friction at the relative velocity between the solid and the liquid is not linear in the interacting flow turbulence. Another modeling complication is that friction is dependent on manufacturing or construction details that are not easy to predict; e.g., welded connections to bolted connections.

To compensate for these complications is that the damping factor of most buildings, especially metallic ones, is light in the sense that the damping factor ξ is smaller than one. In addition, damping is generally useful for safety in the sense of mitigating resonance effects. This gives structural engineers a bit of a jump-off to simplify dynamic analysis as follows:

- A basic damping model such as linear viscous damping is not a concern.
- Mode overlap can be applied because EOM is linear. Hence, frequencies and mode shapes for an undamped system can be reused if additional assumptions are made, such as modal damping or Rayleigh damping.

If precise modeling of damping effects is important for safety and performance, it should be emphasized that these simplifications are not recommended. This occurs in the following scenarios:

- Damping is very important in function or operation. Consider a shock absorber, for example. Tipper devices can be modeled more accurately using the data of the manufacturer, for example without dry friction.
- The damping system can disturb the stability by feeding it into the place without removing the energy. This can occur in active control systems and aerostats [32].

2.1.5. Modal Analysis

Modal analysis is the process of determining the parameters (natural frequency, vibration mode, internal damping) needed to create a mathematical model that shows the dynamic behavior of a vibrating system.

It is important for design to be able to calculate the natural frequencies and damping values of the structures. The most fundamental problem of vibration engineering is to determine the natural frequencies of dynamic systems and avoid resonance at these frequencies by making design changes or making them difficult. Resonance analysis is simple, such as a shaft, and complicated structures such as airplanes; It forms the basis of vibration analyzes carried out for dynamic systems such as mechanics and bridges, such as washing machines.

Vibrating structures can be modeled as single- and multi-degree-of-freedom systems. In addition, in a linear vibration theory, a multi-degree of freedom system can be expressed as the sum of several single degree of freedom systems [45].

While natural frequencies can be analytically determined for simple structures, complex modal analysis is usually performed using experimental modal analysis or computer aided analysis software.

For a cantilever beam subjected to free vibration, and the system is considered as continuous system in which the beam mass is considered as distributed along with the stiffness of the shaft, the equation of motion can be written as (Meirovitch, 1967),

$$\frac{d^2}{dx^2}\left(EI(x)\frac{d^2Y(x)}{dx^2}\right) = \omega^2 m(x)Y(X) \tag{2.26}$$

Where, E is the young modulus of beam material, I is the moment of inertia of the beam cross-section, $Y(x)$ is displacement in y direction at distance x from fixed end, ω is the circular natural frequency, m is the mass per unit length, m = ρA(x) , ρ is the material density, x is the distance measured from the fixed end.

2.1.6. Frequency Response Function (FRF)

The frequency response function is a particular tool in order to perform vibrational analysis and testing. A frequency response function (FRF) is a transmission function stated in the frequency domain. Frequency response functions are complex functions that include real and imaginary components. It can also be represented in terms of magnitude and phase. A frequency response function can be generated from measured data or analytical functions. A frequency response function refers to a function of an applied kinematic response frequency. Response can be given in terms of displacement, speed or acceleration. Also, the response parameter may appear in the denominator or denominator of the transfer function [37].

The solution of a vibration problem can be expressed as the relationship between an input and its output. Here input is force, output is vibration [38].

If the force and the vibration are expressed at the frequency base (amplitude and phase), the relation is calculated by equation 2.27 and 2.28.

$$\mathrm{X}(\omega) = \mathrm{H}(\omega) * \mathrm{F}(\omega) \tag{2.27}$$

$$\mathrm{H}(\omega) = \frac{X(\omega)}{F(\omega)} \tag{2.28}$$

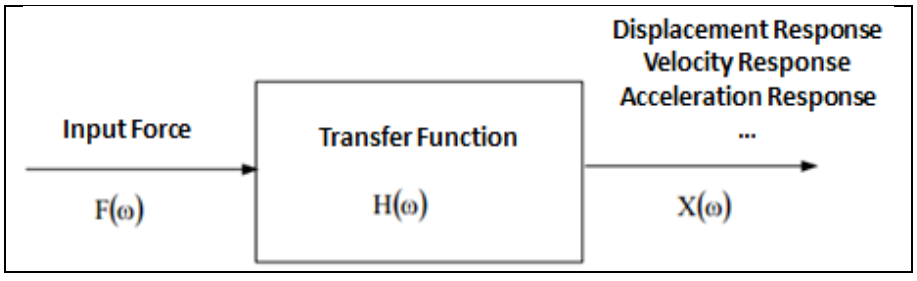

Figure 2.8: Frequency response function (FRF) model.

$F(\omega)$ is the input force as a function of the angular frequency ω. $\mathrm{H}(\omega)$ is called frequency response function and includes both amplitude and phase

components. $X(\omega)$ is the displacement response function. Similarly, transfer functions can be developed for the velocity and acceleration responses.

Each function is a complex function, which can also be expressed in terms of magnitude and phase. Hence, Each function is a spectral function. There are many types of spectral functions. For simplicity, consider each to be a Fourier transform.

$$|\mathrm{H}(\omega)| = \left|\frac{X(\omega)}{F(\omega)}\right| = \frac{1}{k}\frac{1}{\sqrt{(1-r^2)^2 + (2\xi r)^2}} \tag{2.29}$$

$$\mathrm{r} = \frac{f}{f_n} = \frac{\omega}{\omega_n} \tag{2.30}$$

There are six basic transfer functions as shown in Tables 2.1 and 2.2.

Table 2.1: Frequency response function (FRF) names.

Dimension	**Displacement/Force**	**Velocity/Force**	**Acceleration/Force**
Name	Compliance Admittance Receptance	Mobility	Accelerance Inertance

Table 2.2: Frequency response function (FRF) names.

Dimension	**Force/Displacement**	**Force/Velocity**	**Force/Acceleration**
Name	Dynamic Stiffness	Mechanical Impedance	Apparent Mass Dynamic Mass

2.2. Theory of Acoustics

Acoustics is a branch of science related with sound, that is, wave motion in liquids, gases and solids, and the effects of the wave motion. Therefore, the scope of acoustics ranges from fundamental physical acoustics to bioacoustics, psychoacoustics and music, and includes technical fields such as transducer technology, sound recording and reproduction, design of concert halls and theatres, and noise control [38].

2.2.1. Fundamental Concepts of Acoustics

One of the characteristics of fluids, that is, gases and liquids, is that there are no restrictions on deformation. Fluids have no ability to transmit shearing forces. Hence, fluids react against a change of shape only due to inertia. Besides, fluids react against a change in its volume with a change of the pressure. Sound waves can be expressed as convulsive oscillation disturbances propagating in a fluid. Waves contain liquid molecules that move back and forth in the direction of propagation (without net flow) in the presence of changes in pressure, density and temperature.

The sound pressure change, the difference between the instantaneous value of the total pressure and the static pressure is what people hear. It is easier to measure the sound pressure than the intensity and temperature fluctuations, for example. Notice that the sound waves are longitudinal waves, the bending waves on a beam or the waves on an extended string are transverse waves that move back and forth in a direction perpendicular to the direction of propagation of the particles.

In most cases, the oscillation changes transmitted by the fluid are extremely small. Considering the air changes corresponding to a sound pressure level of 120 dB, which is a very high sound pressure level close to the pain threshold, it is likely to get an idea of the magnitude ordering of these changes.

Sound waves that are spreading in different directions interact. Waves are reflected by a hard surface and are absorbed more or less by a soft surface; they are scattered by small obstacles. Due to the breakage, only a partial shadow occurs behind the screen, and if the environment is not homogeneous, for example due to temperature gradients, the waves break and change direction as they propagate.

The speed with which sound waves propagate in fluids is independent of the frequency. Other waves that have an acoustical relevance depend on the frequency content of the wave form, for example, the bending waves in the plates and beams.

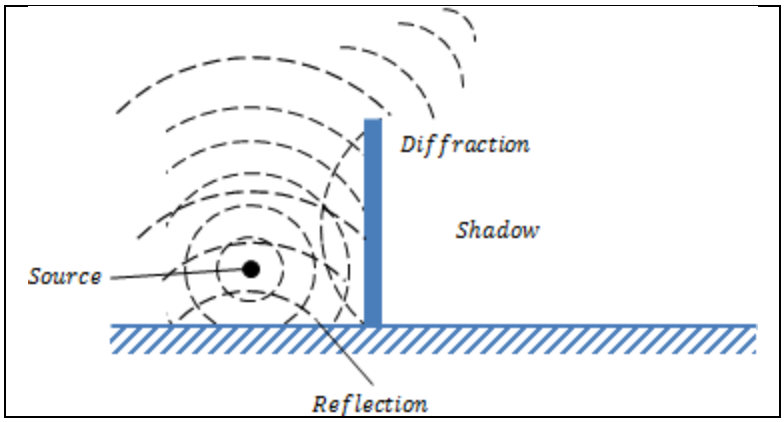

Figure 2.9: Various wave phenomena.

A mathematical description of the wave motion in a fluid can be obtained by first combining the equations expressing the fact that mass is preserved and secondly the equations expressing the fact that the local longitudinal force caused by a difference in local pressure is balanced by the inertia of the medium. In addition, the sound is almost an adiabatic, meaning there is no heat flow.

Observation that many acoustic phenomena include perturbations that are several orders of magnitude smaller than the equilibrium values of the environment makes it possible to simplify the description of mathematics by ignoring high-order terms. The result is a linearized wave equation. This is the second-order partial differential equation expressed in terms of the sound pressure p,

$$\frac{\partial^2 p}{\partial x^2} + \frac{\partial^2 p}{\partial y^2} + \frac{\partial^2 p}{\partial z^2} = \frac{1}{c^2}\frac{\partial^2 p}{\partial t^2} \tag{2.31}$$

in a Cartesian (x, y, z) coordinate system. Here t is the time and c is the speed of sound [38].

2.2.2. Speed and Frequency

The sound propagation rate is related to some characteristics of the atmosphere and the environment. The most important of the environmental properties is the kinetic energy of the molecules it touches in the environment

where it propagates, which means that the speed of sound propagation affects the temperature of the environment in which it is located.

Therefore, the relationship between the frequency or period of a wave and the wavelength depends on the propagation velocity c.

$$c = \frac{\lambda}{T} = \lambda \mathrm{f} \tag{2.32}$$

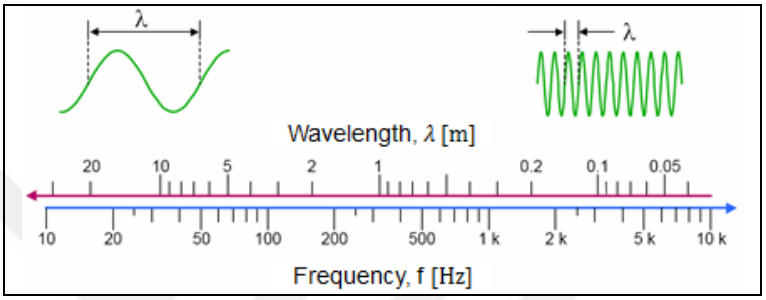

Figure 2.10: Wavelength and frequency distribution.

As mentioned earlier, the speed of sound propagation is also related to ambient temperature. The propagation velocity of the sound in the air can be calculated by the equation (2.33) by assuming that the air is the ideal gas.

$$c = 20{,}05\sqrt{T_k}\ \ [m/s] \tag{2.33}$$

T_k is the temperature of the air in Kelvin.

According to equation (2.34),

$$T_k = 273{,}2 + T_{Celsius} \tag{2.34}$$

the propagation speed at 21 degrees is found 344 m/s.

In the same way, the propagation speed of sound in the air can also be calculated by the equation (2.35).

$$c \cong 331{,}4 + 0{,}6T_c \left[\frac{m}{s^2}\right] \quad (2.35)$$

Table 2.3: Propagation speed of sound in various medium.

Material	Speed of Sound
Rubber	60 m/s
Air at 40°C	355 m/s
Air at 20°C	343 m/s
Lead	1210 m/s
Gold	3240 m/s
Glass	4540 m/s
Copper	4600 m/s
Aluminum	6320

2.2.3. Sound Waves

Rarefaction, the reduction of the density of an item is the opposite of compression. There are also rarefaction waves in nature such as compression that can circulate in waves (eg sound waves). A general rarefaction wave is the area of low relative pressure after a shock wave [40].

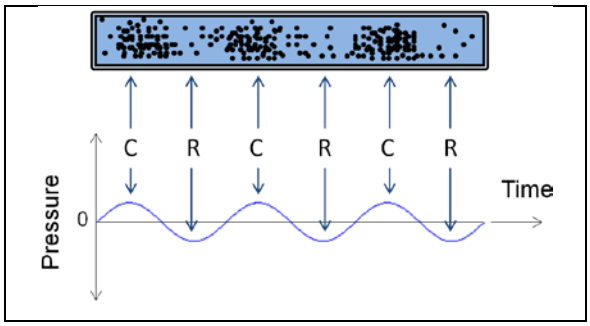

Figure 2.11: Sound wave.

In the Figure 2.11, pressure change of a sound wave is shown. R stands for rarefaction and C stands for compression.

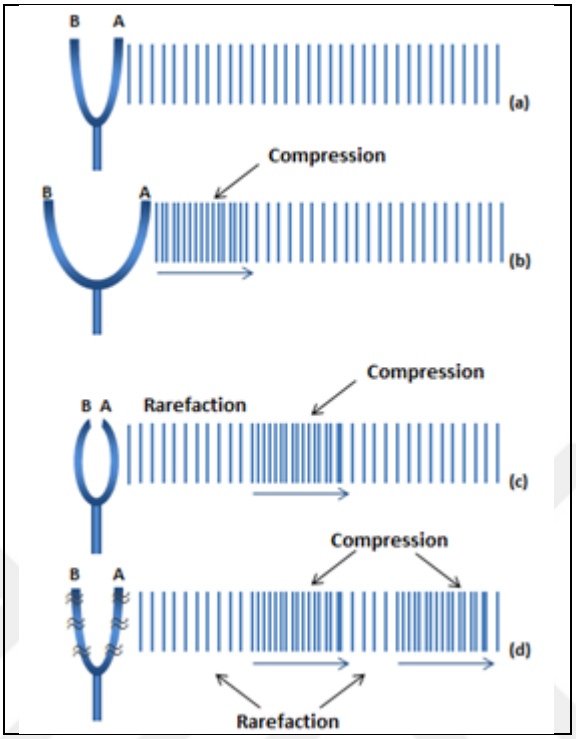

Figure 2.12: Tuning fork and sound propagation.

Sound waves are classified as longitudinal waves. The vibrational motion of a tuning fork can be examined to understand how the sound waves are spreading. A tuning fork and the sound propagation is shown in Figure 2.12.

As the A side of the tuning fork moves towards the right, it compresses the air near the particles and brings it into a compression chamber as shown in Figure 2.11(b). Due to the vibration of air layers, this compression travels as a disturbance. When the prong A returns to its original position, the pressure on the right is reduced and a rarefaction occurs. This rarefaction advances as a disturbance like compression. As the tuning fork continues to vibrate, the alternating pressure and the waves of rarefaction are spread in the air as shown in Figure 2.11(d). The direction of motion of sound waves is the same as the direction of movement of air particles. For this reason, they are classified as longitudinal waves. As a result, longitudinal waves are advancing in compression and rarefaction [40].

2.2.4. Acoustic Measurement

The most important criterion of sound is rms sound pressure, which is defined by equation 2.36.

$$p_{rms} = \sqrt{\overline{p^2(t)}} = \left(\lim_{T \to \infty} \frac{1}{T} \int_0^T p^2(t) dt \right)^{1/2} \tag{2.36}$$

In statistics and its practice, the root mean square (RMS or rms) is defined as the square root of mean square (the arithmetic mean of the squares of a set of numbers). The RMS is also known as the quadratic mean and is a specific case of the generalized mean with exponent 2. RMS can also be defined as an integral of the squares of the instantaneous values during a cycle for a continuously varying function [41].

2.2.4.1. Frequency Analysis

Single frequency sound is useful for analyzing acoustic events, but practically speaking sounds have 'broadband' characteristics, which means that most of them cover the broadband frequency range. If the sound is more stable or less steady, it will be more practical to analyze it in the frequency domain than to look at the sound pressure as a function of time.

Frequency (or spectral) analysis of a signal involves decomposition of the signal into its spectral components. This analysis can be performed via digital analyzers using discrete Fourier transforms ('FFT analyzers'). In addition, the signal can be passed through a number of contiguous analogue or digital bandpass filters with different centre frequencies, a ‘filter bank.’ Filters can show the same bandwidth or display a constant relative bandwidth, which means a certain percentage of the bandwidth's center frequency. On a logarithmic frequency scale, the constant relative bandwidth corresponds to a uniform resolution. Such a scale is better aligned with the subjective range of musical sounds from a linear scale, and

so frequencies are often represented on a logarithmic scale in acoustics and frequency analysis is often performed with constant percentage filters. In acoustics, octave band filters and a third octave band filter are the most common filters [30].

An octave is a 2: 1 frequency ratio, which is a basic unit in music scales. Thus, the lower limit frequency of an octave band is half the upper frequency limit, and the center frequency is the geometric mean shown in the equations 2.37,

$$f_1 = f_c/\sqrt{2} \tag{2.37a}$$

$$f_u = \sqrt{2}f_c \tag{2.37b}$$

$$f_c = \sqrt{f_1 f_u} \tag{2.37c}$$

where f_c is the centre frequency. Similary, a one-third octave band is a band for which $f_u = 2^{1/3}f_1$, and

$$f_1 = f_c/2^{1/6} \tag{2.38a}$$

$$f_u = 2^{1/6}f_c \tag{2.38b}$$

$$f_c = \sqrt{f_1 f_u} \tag{2.38c}$$

The corresponding standardised nominal centre frequencies of octave and one-third octave band filters is given in table 2.4. Because the human ear may respond to frequencies in the range from 20 Hz to 20 kHz, that is, a range of three decades, ten octaves or thirty one-third octaves [38].

Table 2.4: Standardized nominal 1/3 octave and octave centre (red) frequencies (Hz).

20	25	31.5	40	50	63	80	100
125	160	200	250	315	400	500	630
800	1000	1250	1600	2000	2500	3150	4000
5000	6300	8000	10000	12500	16000	20000	

One of the important characteristics of the average square value of the signal is that it can be divided into frequency bands. This means that if a signal is analyzed on a third octave band, the sum of the mean squared values of the filtered signals equals the mean square value of the unfiltered signal. The reason for this is that the products of different frequency components are mean zero, so that all the cross terms disappear. This can be demonstrated by analyzing a sum of two pure tones with different frequencies,

$$\begin{aligned}\overline{(A\sin\omega_1 t + B\sin\omega_2 t)^2} &= A^2\overline{\sin^2\omega_1 t} + B^2\overline{\sin^2\omega_2 t} \\ &\quad + 2AB\overline{\sin\omega_1 t + \sin\omega_2 t} \\ &= (A^2 + B^2)/2\end{aligned} \tag{2.39}$$

It should be noted that the mean square root values of the two signals are added unless ω 1 = ω2.

Thus,

$$p_{rms}^2 = \sum_i p_{rms_i}^2 \tag{2.40}$$

where p_{rms_i} is the rms values of the output of the i'th filter. Equation (2.40) is known as Parseval's formula [38].

2.2.4.2. Random Noise

Many sound generators produce noise instead of pure sound. While pure tones and other periodic signals are deterministic, noise is a stochastic or random phenomenon. Constant noise (or stationary noise) is a stochastic sign with time-invariant statistical properties.

White noise, a term analogous to white light, is a constant noise with a fixed power spectral density, that is, a constant hertz average characteristic value. An example of this is the sound of a vacuum cleaner. When the white noise is passed through a bandpass filter, the average squared of the output signal is proportional to the bandwidth of the filter. When the white noise is analyzed with fixed percentage filters, the average square of the output is proportional to the center frequency of the filter. For example, if the white noise is analyzed by a set of octave band filters, the mean square values of the output signals of two adjacent filters differ by two factors.

Pink noise is stationary noise with fixed square root coef- ficient in continuous-width bands (eg octave bands). This means that lower frequencies are emphasized compared to white noise. It is observed that the average square value of a certain pink voice signal in the octave bands is three times greater than the noise mean square value in the third octave bands.

The mean square sound pressures produced by individual sources are value added when more than one independent noise source is present at the same time. The reason for this is that independent sources produce unrelated signals, that is, signals whose product averages are equal to zero. For this reason, cross terms disappear.

$$\begin{aligned}\overline{(p_1(t)+p_2(t))^2} &= \overline{p_1^2(t)} + \overline{p_2^2(t)} + \overline{2p_1(t)p_2(t)} \\ &= \overline{p_1^2(t)} + \overline{p_2^2(t)}\end{aligned} \tag{2.41}$$

$$p_{rms,tot}^2 = \sum_i p_{rms_i}^2 \tag{2.42}$$

The similarity between Equations (2.40) and (2.42) should be noted. Since the signals generated by different mechanisms are always irrelevant, the addition of mean squared values of unrelated signals is a very practical precaution. Almost all the real-life signals are mutually unrelated.

2.2.4.3. Levels and Decibels

Since sound is perceived by the pressure change of the air that is in contact with the eardrum, it is important that the sound source is created by a sound source at a certain point rather than the sound power.

The sound pressure level is indicated by SPL or Lp.

$$L_p = 10\log_{10}\frac{p_{rms}^2}{p_{ref}^2} = 20\log_{10}\frac{p_{rms}}{p_{ref}} \tag{2.43}$$

where p_{ref} is the reference sound pressure. The reference sound pressure is 20µPa for sound in air because 20µPa is the minimum pressure required for an average adult person to hear a sound wave.

The most audible sound pressure fluctuations between 20µPa and 100Pa are quite low when compared with static air pressure (100.000 Pa). 20µP is considered to be the lowest sound level that can be heard by an average person, and is therefore referred to as the threshold of hearing. 100Pa is a very high level and causes pain, so it is called threshold of pain. (See Figure 2.12). The ratio of these two levels is more than one billion. Therefore, a linear plot of indicators in terms of Pa will lead to very large changes in the measurement results over a very wide range.

The benefit of using the Decibel scale is that it appears more clearly when the dB scale is put next to the Pa scale. The linear indicator chart with very large numbers and wide range is a simpler scale conversion starting at the threshold of hearing (0dB) and ending at the threshold of pain (130dB). What should be noted here is the addition of the word "level" to the side of the "voice press", indicating that it has a certain level according to a reference. The sound pressure level symbol

is Lp. If the ratio of the two pressures is less than 1, the dB value will be negative, and if it is greater than 1, it will be positive [42]

It should be remembered that the change in the air pressure that enables sound propagation and conduction can be demonstrated by a sinus curve for a simple harmonic sound wave and that the rms value of such a sound pressure is $\sqrt{2}/2$ times the sound pressure amplitude.

The rms value of the sound pressure produced by a harmonic sound wave coming from different frequencies at different frequencies can be found in Equation 2.40 as mentioned earlier.

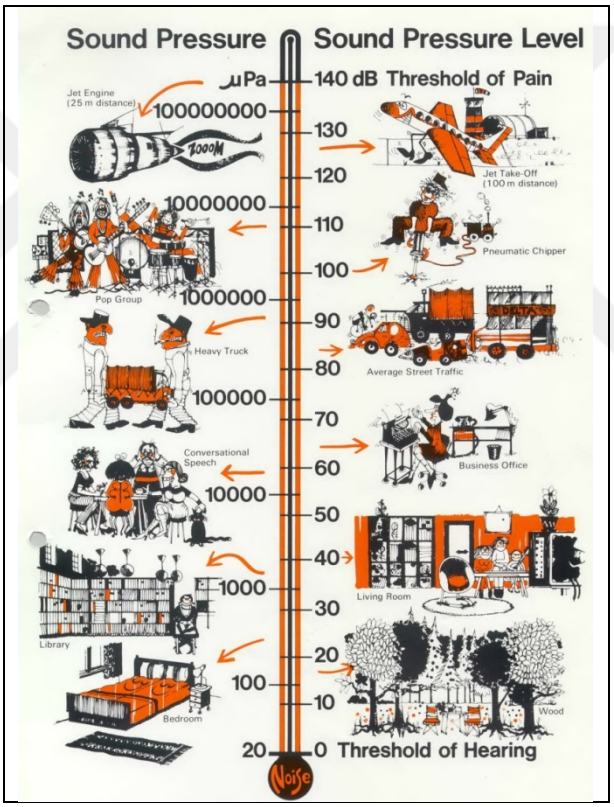

Figure 2.13: General sound pressure levels.

2.2.4.4. Acoustic Impedance

Impedance is the ratio of the complex amplitudes of the two signals representing the cause and effect. For example, the ratio of an AC voltage, a

mechanical force versus the frequency of oscillation, or the ratio of the sound pressure to the velocity of the sound pressure, over a portion of an electric circuit.

The term derives from the "inhibit" (inhibition, inhibition) action. This means that opposition to the flow of the current is a measure. The impedance is reciprocal, there is an application which is adapted from the act of confession and which shows the lack of such an opposition. It should not be forgotten that these concepts require complicated representations of harmonic signals because it is pointless to divide the instantaneous sound pressure with the instantaneous particle velocity. There is no simple way to describe the properties that correspond to a complex value of impedance without using complex representations.

Acoustic impedance is a very good measure to determine the radiation emitted from the source, especially the peripheral acoustic transmission and reflections of materials with different acoustic impedances [38].

2.2.5. Physiology of Hearing

As already mentioned, the acoustic branches have a wide frequency range depending on the field of application. However, when the human hearing field and the human voice perception field are considered, certain restrictions exist and are being investigated in psychoacoustics.

Engineering acoustics is concerned with a variety of application areas, such as infra-red, ultrasound, underwater acoustics and the like, as previously mentioned. However, in the acoustic design of environments or equipment intended for direct human use, the important parameter is that of the human ear. It is important to be knowledgeable about how the ears will be heard when dealing with the subjective perception of the acoustic as well as the acoustic signal processing. Sound waves can be thought of as continuous analog signals containing various information such as frequency, phase, amplitude and so on. Today, technology provides accurate measurement of physical quantities related to sound; However, when considering the human voice perception, it is important to have information about the psychoacoustic parameters to be explained in detail. The structure of human ear is briefly shown in Figure 2.14.

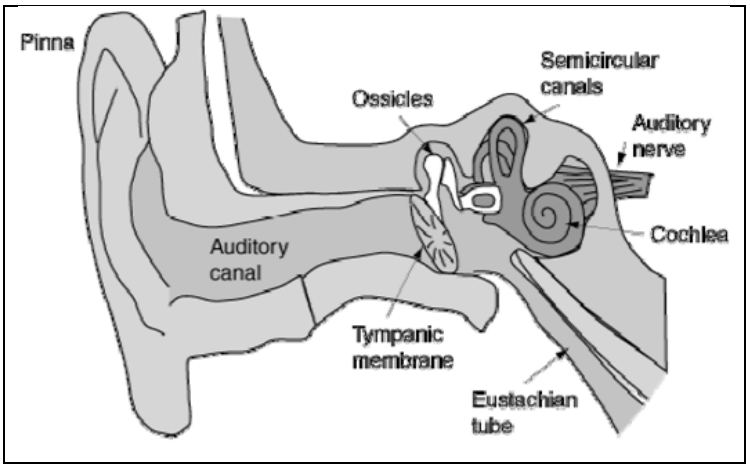

Figure 2.14: The structure of human ear.

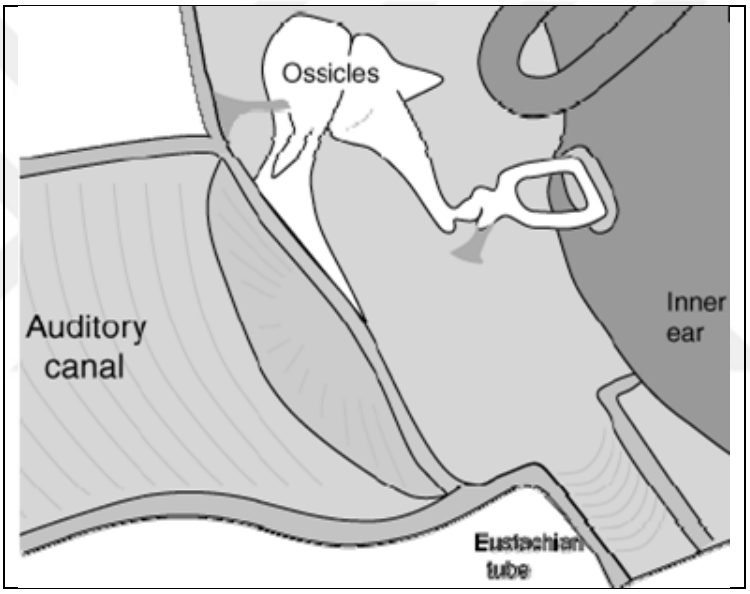

Figure 2.15: Vibration of the ear drum.

When audible audible waves approach the ears, the pinna directs the sound waves to the tympanic membrane (eardrum) through the auditory canal, which acts as a tube and has its own physical quantities such as resonance frequency [44]. For this reason, it performs a certain amplification to the frequencies roughly between 2 and 5 kHz. The ear drum receives the vibrations from the audio channel and the vibrations are transmitted to the middle ear by vibrations of the ear drum due to the difference in pressure between the outer ear and the inner ear (Figure 2.15).

2.3. Vehicle NVH Theory

In previous sections, theories of mechanical vibrations and acoustic theory were presented. In this section, basic information about NVH concept is given.

Overall vehicle NVH performance is considered to be the combination of three main sub-attributes: Powertrain NVH, Road NVH and Wind NVH. All these sub-characteristics require different design methodologies and strategies and are often developed by considering different systems and subsystems in the vehicle.

Wind NVH characteristic requires a good aerodynamic body design to provide less turbulent airflow, and a very good sealing strategy to the selection and positioning of suitable door insulation materials and strategy to appropriate side mirror design.

In the development of the powertrain NVH characteristic, the more effective parameters such as the engine block dynamic rigidity, the noise transfer functions, the sensitivity of the body parts can be mentioned.

In the development of road NVH requires the choice of appropriate dynamic hardness for suspension work and good body sealing. As can be seen, all subfeatures in vehicle NVH development are mainly influenced by different aspects. For this reason, a balance is required not only for NVH, vehicle dynamics, performance and other qualities, but also for sub NVH attributes.

The sound wave propagation from the noise source to the ears consists of two different routes, which are taken from the structure-borne and air-borne. As already mentioned, in this study only the structural noise that caused the motor vibration is addressed.

It is important to identify both build and airborne noise contribution in vehicle acoustic and vibration development work so that you can have information about which noise source is a strong contributor or which part of the body or chassis is weaker. It is also worth considering the absorption of the inner voice. This basic knowledge makes it possible to improve vehicle NVH in a way that is better in terms of quality and cost.

2.3.1. Structure-borne and Air-borne Noise

In most of the acoustic events, sound is spread by the vibrations of solid objects. In an internal combustion engine, sound is radiated by the vibrations of the engine block and this noise is transferred in air, through the dash panel and the interior space of the vehicle to the driver's or passenger's ear. This way of noise transfer is called air-borne noise.

Another way of sound radiation from the internal combustion engine, for example, is due to structure-borne excitations. Due to combustion and the free moments of inertia of the rotating objects, a certain amount of force is generated within the engine structure in a wide frequency range, which is transferred to the body panels through the engine mounts and chassis frames. This results in low frequency sound radiation from the body panels and driveline and is defined as structure-borne noise.

This better expresses the true meaning of the sound of the acoustic from the air and from the structure. The intention here is to provide a basic background for the route of transmission into the vehicle and what arises from the air and its structure. Therefore, details of the wave propagation and stress distributions that occur in the joints will not be explained.

2.3.2. Noise Sources and Transfer Path

As mentioned in the previous sections, vehicle during its operation is subjected to various excitations from either its components or the road conditions. While those excitations would be harmonic in the simplest way, they are usually random depending on the operating conditions. In this study the structure-borne noise of the vehicle is examined. Hence, the focus point will be the contribution of powertrain components and the impact of the main powerplant transfer paths.

2.3.3. Engine Radiated Noise and Engine Order

The internal combustion engine is one of the vehicle's greatest sources of excitation. Since theengine noise from both the air and the structure is scattered at different frequency ranges, the vehicle powertrain must be considered in the development of NVH, as they are contributed in different ways and require different NVH processes.

Ratiated noise from the main structure of the engine (block, cylinders, etc.) can be divided into two main categories. First, camshaft, valves, pistons, crankshaft and so on. It can be expressed as the mechanical sound produced by the motor structure in response to the motions of the components. The second is due to the motor structure given to the gas pressure profile during combustion [46].

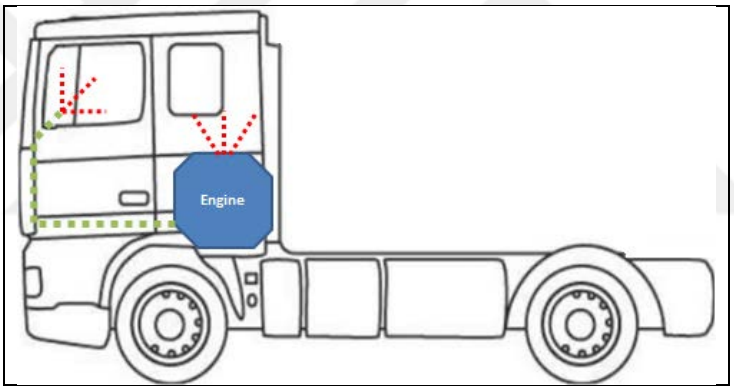

Figure 2.16: Engine noise radiation.

Air-borne noise radiation from the components are transmitted through the air to the interior of the compartment and the vehicle body, and finally to the driver and to the passenger's ear. Particularly in diesel engines, combustion characteristics give great importance to engine radiation noise. Common rail diesel engines have some parameters that affect combustion efficiency such as rail pressure, start of main injection timing, pre-ignition timing. The other very significant engine noise contribution is mostly due to the build-in excitations coming from the engine and transmission housings (mounts). Vibrations are damped to a certain level by means of rubber or hydraulic engine blocks. The rest of the force is transferred to the body

and is converted into sound pressure inside the vehicle by the excitations of the vehicle panels and the drive line components. In the Figure 2.15, the engine noise routes of structure welded and airborne are briefly shown.

Engine orders play a crucial role in defining the majority of engine-driven NVH problems. Engine orders are referenced to the crankshaft rotation speed. In the case of a four-stroke internal combustion engine with an N-cylinder, there will be N/2 times ignition per revolution. The result of the ignition pulses is the ignition torque, which can be split into sinusoids. The force due to the moment of inertia of the rotating parts also contributes significantly to the excitation of the engine.

In order tracking, it is essential to identify important orders that are relevant to the mechanics of the system being searched. For example, it is very important to know that the four-cylinder four-stroke internal combustion engine produces the most dominant arousal forces at the 2nd and multi-stage. Another important issue is to choose the order correctly, so that important orders are separated. Furthermore, the setting of the appropriate frequency resolution provides an appropriate selection of the sweep rate with a correct measurement of the peaks in important orders. That is, the optimum sweep speed should be selected to analyze the data correctly. For example, if vehicle 1 is exposed to the accelerator of wide-throttle, the RPM sweep will be so fast that it will be difficult to identify and separate the peaks in the frequency domain data. However, for example, if the second or third gear wide open throttle acceleration is selected as the measurement method, each significant peak can be perceived more accurately.

In this study, engine radiated noise is not considered but the interior sound pressure level (SPL).

3. ANALYSIS VIA CAE

Computer-aided engineering (CAE) is the broad usage of computer software to aid in engineering analysis tasks. It includes finite element analysis (FEA), computational fluid dynamics (CFD), multibody dynamics (MBD), and optimization.

CAE tools are very widely used in the automotive industry. In fact, their use has enabled the automakers to reduce product development cost and time while improving the safety, comfort, and durability of the vehicles they produce. The predictive capability of CAE tools has progressed to the point where much of the design verification is now done using computer simulations rather than physical prototype testing. CAE dependability is based upon all proper assumptions as inputs and must identify critical inputs (BJ). Even though there have been many advances in CAE, and it is widely used in the engineering field, physical testing is still a must. It is used for verification and model updating, to accurately define loads and boundary conditions and for final prototype sign-off [47].

The finite element method (FEM), or finite element analysis (FEA), is based on the concept of building a complicated geometry with simple blocks, or, dividing a complicated geometry into small and manageable pieces. This procedure is called discretization [48]. A basic discretization procedure is shown in Figure 3.1.

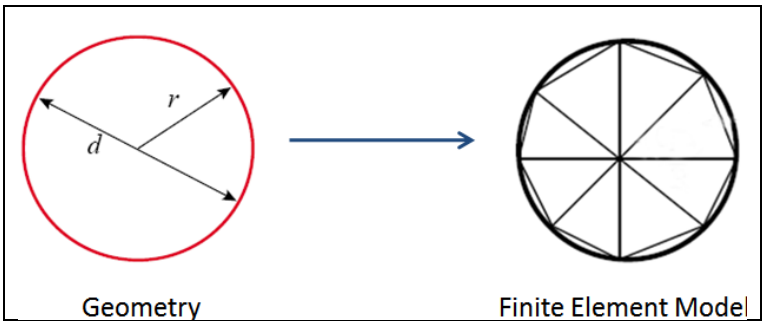

Figure 3.1: Discretization.

In FEM, a set of acceptable finite elements interconnected at points called nodes. In Figure 3.2, the finite element model consists of nine triangular elements

and each element contains three nodes. For example, element E1 contains nodes 4, 5 and 9.

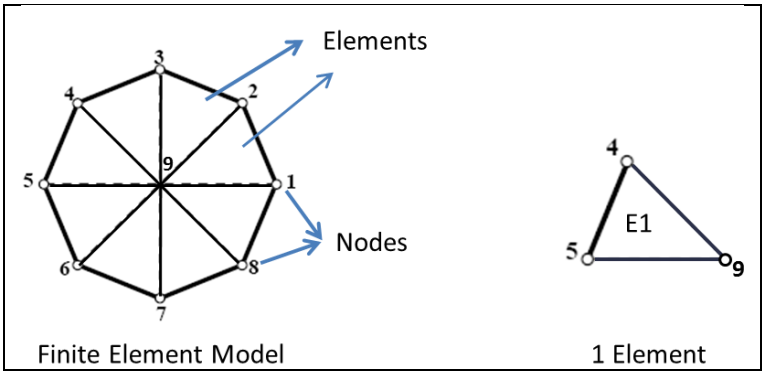

Figure 3.2: Elements and nodes.

In FEM, elements have physical properties such as Young's modulus, shear modulus, Poisson's ratio, thickness and coefficient of thermal expansion.

In this study, preprocessing was performed by using several softwares such as ANSA developed by Beta CAE Systems and SFE AKUSMOD.

3.1. Finite Element Model Creation

A heavy duty truck consist of different systems. In terms of product development, the design of each system requires a specialized engineering team for the system. These systems can be generally described as follows: Body System, Frame And Mounting System, Engine System, Suspension System, Driveline System, Brake System, Transmission System, Clutch System, Exhaust System, Fuel System, Steering System, Climate Control System, Information, Gauge and Warning Device System, Electrical Power Supply System, In-Vehicle Entertainment System, Lighting System, Electrical Distribution and Electronic Control System, Electronic Features System and Fuel Cell System.

Body in white or BIW refers to the phase in vehicle manufacturing in which a car body's sheet metal components have been welded together. BIW is termed before painting & before moving parts (closures and deck lids as well as fenders),

the engine, chassis sub-assemblies, or trim (instrument panel, windshield, seats, upholstery, entertainment systems etc.) have been assembled in the frame structure [49]. If windshield is attached to the BIW body, this is called body in prime or BIP.

In terms of NVH, all of these systems are important because the performance of NVH in a stand-alone system and the performance of the systems in the full vehicle are different. In this sense, modeling of all systems and subsystems for NVH is very important in terms of accuracy of analysis. For NVH analysis, it may be more efficient to classify these systems as Upper Body, Under Body, and Powertrain (Engine and Driveline); because the Upper Body is vital in terms of internal noise and vibration characteristics; the Powertrain is important in terms of being the source of the vibrations that occur as a result of combustion, and the Under Body is the most important transfer path in the propagation of these vibrations.

As mentioned before, the finite element models are created by using ANSA developed by Beta CAE Systems in this study. The interior air model for internal noise analysis was also created using ANSA software. Additionaly, SFE AKUSMOD software is used for air coupling, VSIGN is used to build full vehicle model (and also to analyze).

The FE modeling process from CAD parts in the ANSA software can be summarized as shown in Figure 3.3.

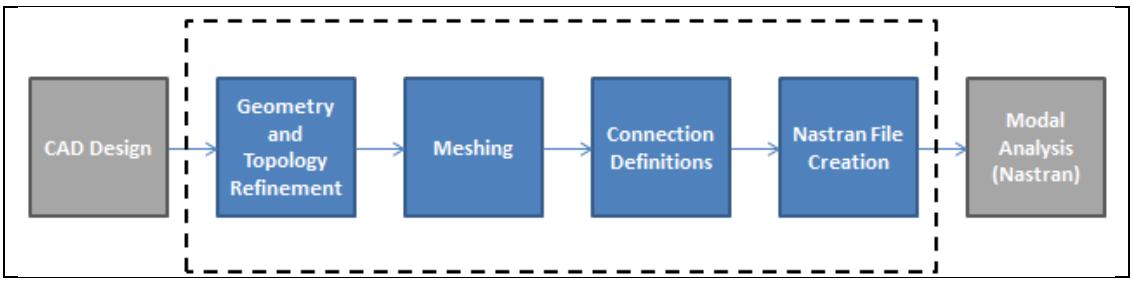

Figure 3.3: Pre-processing stages in ANSA.

In order to increase the accuracy of the finite element analysis and to provide a high correlation with the test, the modeling criteria previously determined by in-house studies is used. Due to the large size of the model, restrictions are made at

some points. For example, instead of creating a FE model that represents the geometry as a whole, only special elements are used (this process is called Rigidizing), which includes the connection points, of the center of gravity, inertia and weight information of the geometry.

In this correlation study, all measuring instruments used in the tests on the prototype vehicle were calibrated. Thus, the accuracy of the test results is provided. Since the test results were considered correct and invariant, all the iterations were done by the CAE model to ensure correlation. There are two types of iterations in this study. One of these is the modeling technique of the vehicle finite element model. The second is to change the bush and mount stiffness values (details are given in section 3.5.1). In the following sections, details of the creation of the finite element model are presented.

3.1.1. Element Types

In finite elements theory, elements can be classified as 1D, 2D and 3D elements in general. 1D elements are referred to as line elements while 2D elements are referred to as shell elements and 3D elements are referred to as solid elements [50]. In addition to this classification, some special elements can be mentioned such as spring elements and rigid link elements.

One of the most important advantages of 1D element is that it is useful when bending is the root cause of the failure especially in structures which have long members. In 1D elements, changes in material properties along the cross-section of the members are negligible [50].

2D elements are more common to use. 2D elements (or shell elements) are often used for thin, sheet structures such as body plates under bending deformation. Shell elements are much more efficient than 3D elements (or solid elements) in terms of computational duration. In shell elements, as in 1D elements, the change in material properties along the cross-sectional area is negligible.

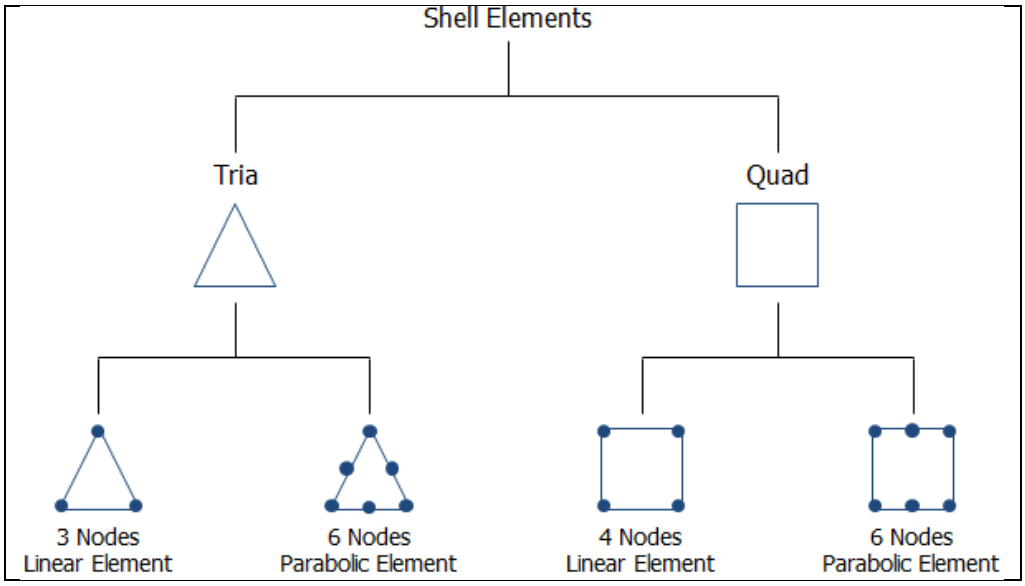

Figure 3.4: Shell element classification.

2D and 3D elements has sub-classifications according to their geometrical shapes. These sub-classifications for 2D and 3D elements are presented in Figure 3.4 and 3.5 respectively. In addition, each element is represented by an equation. Furthermore, equations can be linear or parabolic.

The simplest 2D finite element analysis can be performed with three nodes which is call triangle element. The four nodes element is called quadrilateral (quad) elements [52].

Solid elements gives most accurate stresses in each direction than shell elements. As a major disadvantage of solid elements, it may requires small and refined meshing, which increase the time needed for the solver to compute all this. In some cases, the solver may not be able to complete the analysis because of the excessive growth of the model, which is caused by solid elements. Therefore, the FE model used in combination with shell and solid elements in a hybrid way is quite common.

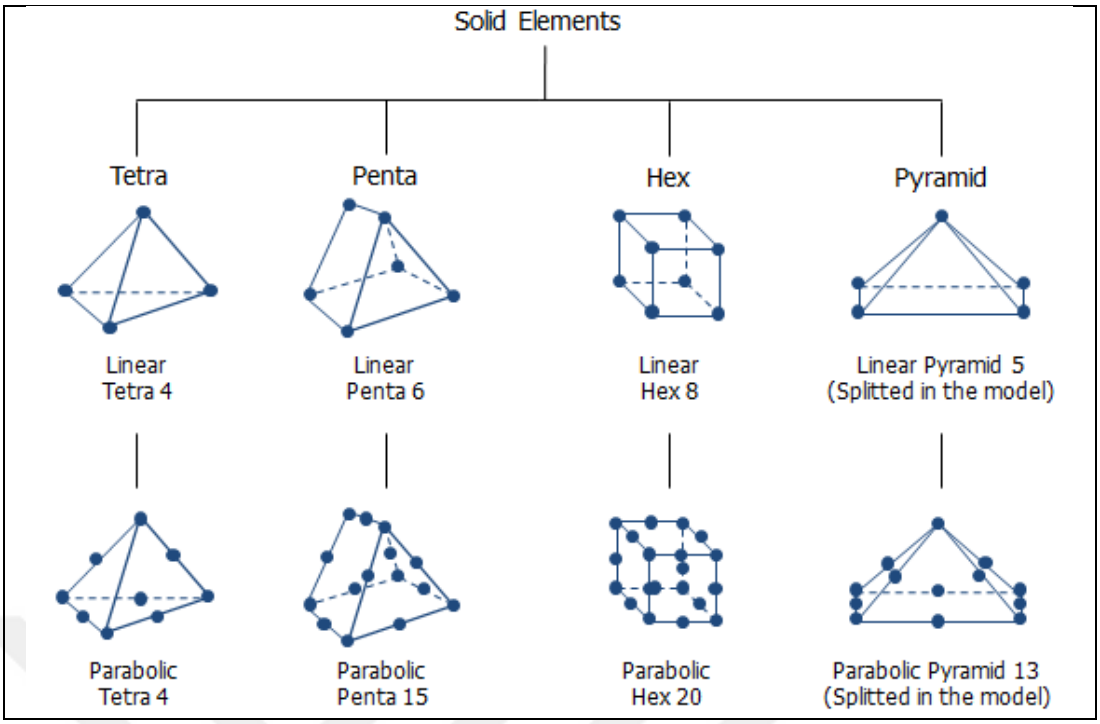

Figure 3.5: Solid element classification.

Consequently, shell elements are, in many cases, more cost-effective than solid elements. Typically, the shells are used for fine areas resulting from the tendency of the stresses to bend. However, solid elements give better stress results. Sub-modeling is an effective way to take conditions from your rough model of shell elements and transform them into more useful results using solid items. In the vehicle model, both solid and shell elements are used.

3.1.2. Meshing and Quality Criteria

Numerous mesh quality parameters are available for almost all FEA software. Most commonly used mesh quality parameters can be listed as:

- Aspect Ratio
- Skewness
- Warpage
- Taper
- Jacobian Ratio

- Twist Angle
- Element Length (Element Size)

All of these equations related to meshing and meshing quality criteria are presented in the following sections.

In this study, front and rear axle subsystems are meshed with 3 to 5 mm element sizes. Other subsystems are generally meshed with 10 mm shell elements and 3 mm solid elements.

3.1.2.1. Aspect Ratio

The aspect ratio of the shell element is defined as the ratio of the shortest edge length to the longest edge length. For example, a square has an aspect ratio of 1 with sides of the same length [51].

Aspect ratio criteria for tria and quad shell elements is shown in Figure 3.6.

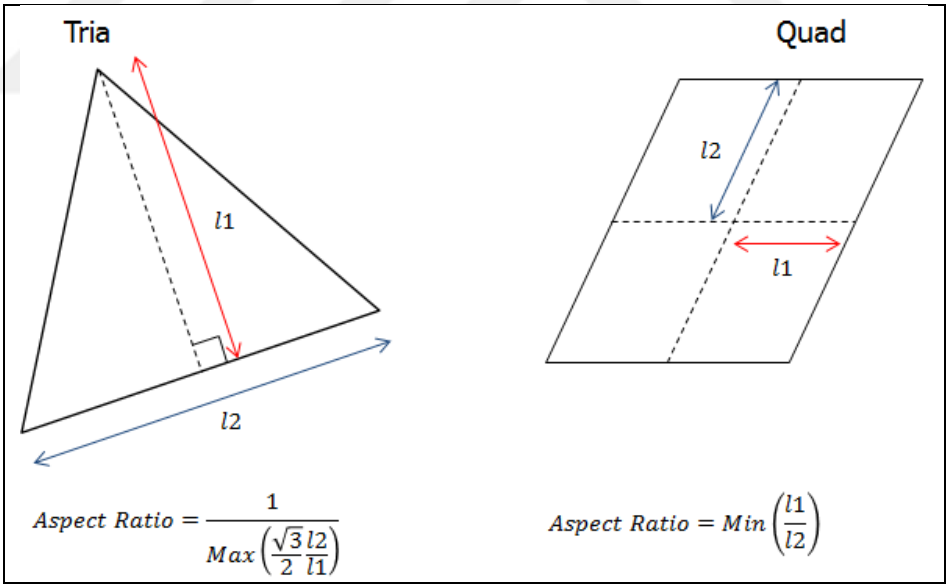

Figure 3.6: Aspect ratio criteria for tria and quad shell elements.

In solid elements the aspect ratio is defined by different equations according to the element shape. These equations are shown in Figure 3.7.

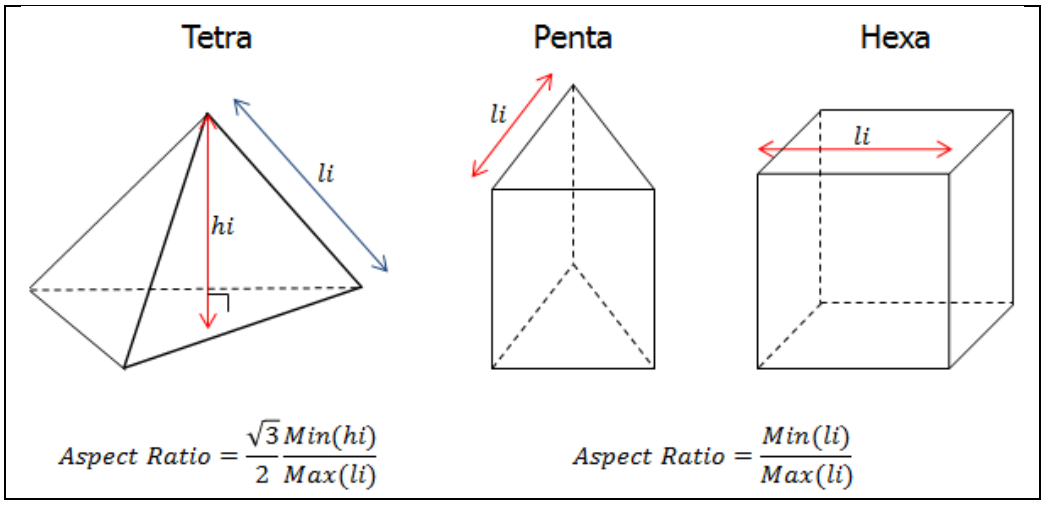

Figure 3.7: Aspect ratio criteria for common solid elements.

3.1.2.2. Skewness

The quadrants are formed at an angle by two lines passing through the midpoints of the edges. The skewness (skew angle) represents the absolute value of the difference between 90 degrees and 90 degrees. A rectangle is a slope angle of 0 because the angle between the lines is 90 degrees. For triangular and quadruple elements, the inclination angle is as follows. For the solid elements, each element calculates the slope angle for the face and sets to the minimum value [51].

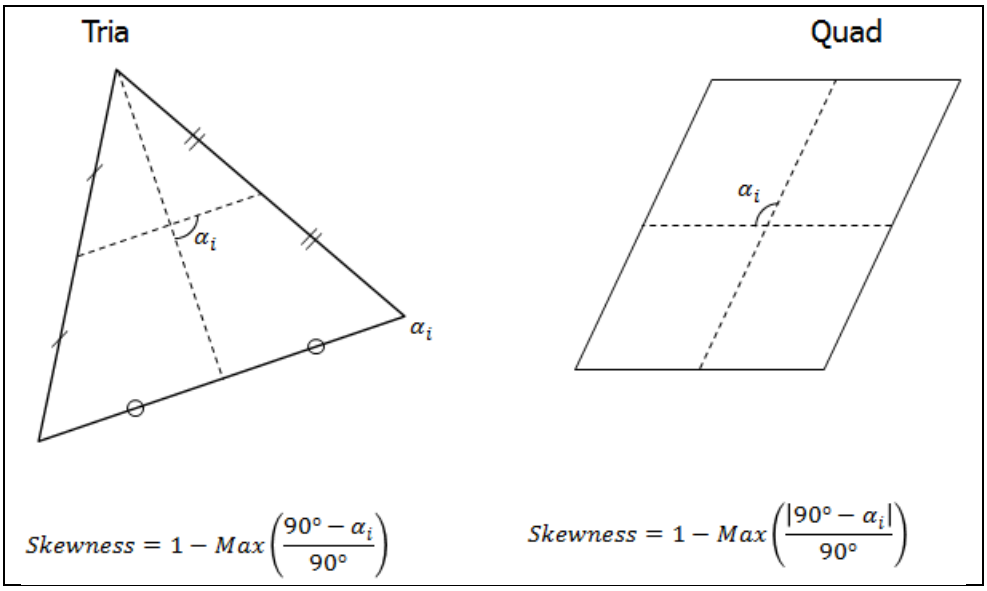

Figure 3.8: Skewness (skew angle) criteria for tria and quad shell elements.

3.1.2.3. Warpage

The warpage of quadrilateral elements is defined as the deviation from the most appropriate plane containing the element.

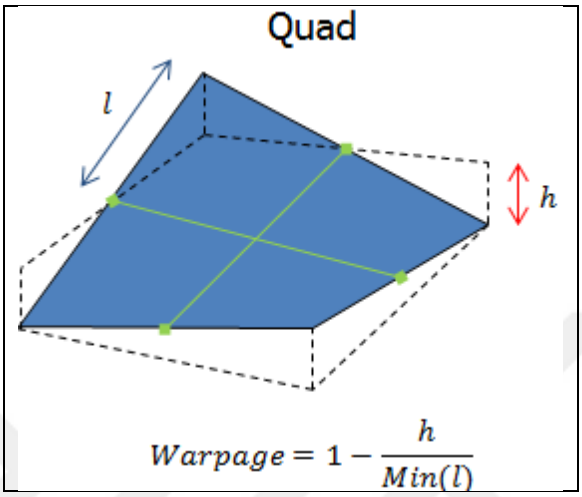

Figure 3.9: Warpage criterion for quad elements.

It is not always valid to define a 4-nodes plane. For this reason, a node of the quadruple element can be created outside a plane. Bending is a measure of how this node is distorted, and when it approaches 0, the element is more planar. For quadruple elements, it can be found in the form of collision. For a rigid body (Hexa, Wedge), calculate the curvature for each element and set the maximum value [51].

3.1.2.4. Taper

Controls the amount of deviation of the quadrilateral from the rectangular shape. The rectangular element 1 is tapered and is rectangular (closer to the triangular shape), the taper is smaller. For quadruple elements, the slope angle is found as shown. For a solid element (Hexa, Wedge), each element calculates the slope angle for the face and sets to the minimum value [51].

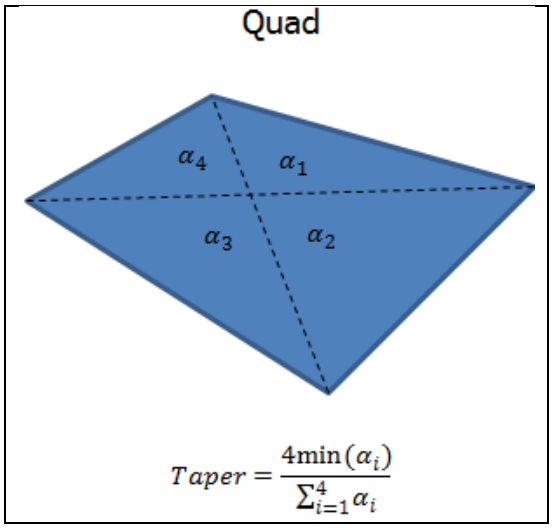

Figure 3.10: Taper criterion for quad elements.

3.1.2.5. Jacobian Ratio

Jakob calculation is generally performed at the integration points of the elements known as Gaussian points. The Jacobian Determinant is calculated at each integration point and the Jacob ratio is found by the ratio of the maximum and minimum determinant values. The Jacobian Decision of 2D elements is computed after being projected onto a plane, and the determinism of 3D elements is found by direct computation.

If the quadrilateral element is not convex, the negative Jacob ratio is obtained and the elements with negative Jakob Ratio are not solved accurately [51].

3.1.2.6. Twist Angle

Twist represents the factor which measures how much two facing element faces are twisted [51].

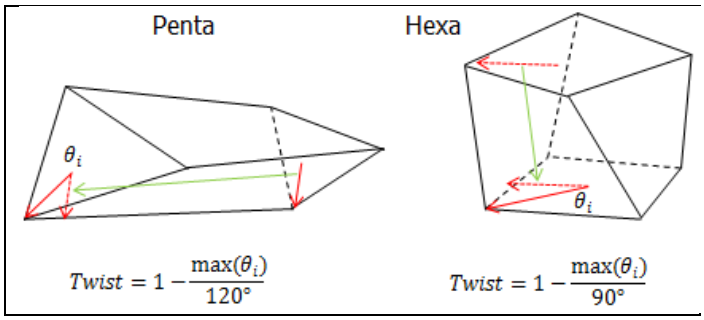

Figure 3.11: Twist criteria for solid elements.

3.1.2.7. Element Size

Element size (or mesh element size) is an evaluation criterion that effects accuracy and the computational time. As element size decreases, the computational time increases but the accuracy has a limit. At this point, there is an optimal element size in terms of accuracy and the computational time.

3.1.3. Connection Types

In the vehicle model, there are different connection types such as adhesive line, seam line, spot weld, RBE2, RBE3, CBAR and CONM2. Adhesive line, seam line and spot weld connections are the special connections. These connections consists of geometry with its physical properties and connection which is mostly RBE3. On the other hand, RBE2, RBE3 and CBAR has no geometrical property. Unlike RBE2 and RBE3 elements, the CBAR elements have material properties. For this reason, CBAR elements are used to describe the body of the bolts.

3.1.3.1. Adhesive Line Connection

In Figure 3.1, an example adhesive line connection is shown. Green and magenta squares are shell elements belong to different parts. Purple blocks represent the geometry of the adhesive. Yellow bars represent CBAR connections

and finally blue bars represent RBE3 connections. This kind of connection is called RBE3-HEXA-RBE3 type connection.

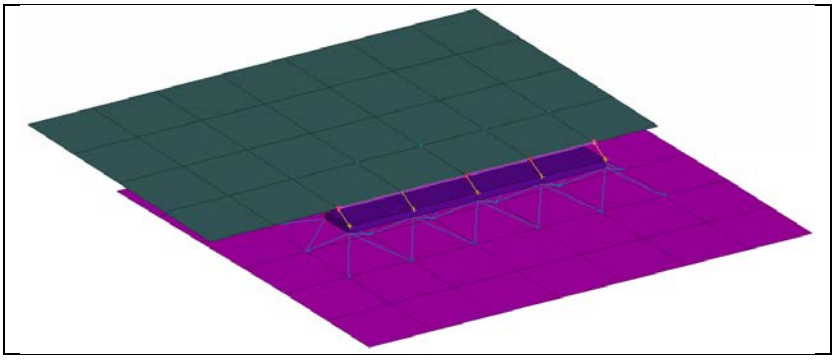

Figure 3.12: Adhesive line connection.

Mostly, bolts consist of a number of RBE2 (according to number of parts connected) and a CBAR which represents body of the bolt. As mentioned before, while RBE2 is not an elastic element, CBAR has capability to be deformed. At that point, it is suitable to model the body of bolts with CBAR instead of RBE2.

3.1.3.2. Spot Weld Connection

In Figure 3.1, two member which is connected with spot welds on different points is shown. In Figure 3.1, detailed visualization of spot weld is shown.

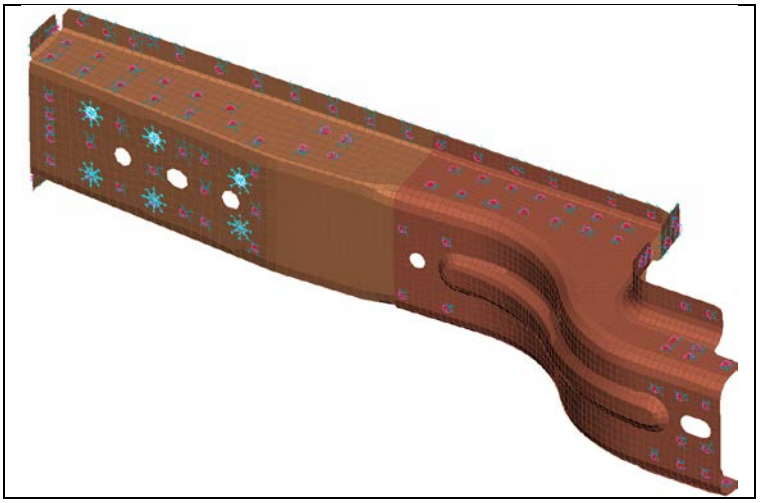

Figure 3.13: Two members connected by spotwelds.

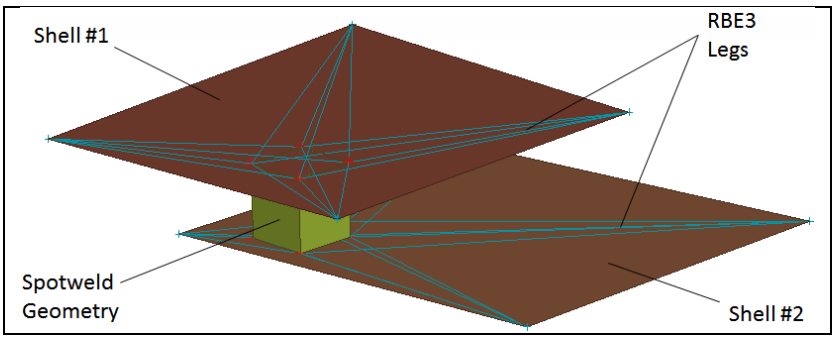

Figure 3.14: Spotweld connection.

As in the case of the adhesive connections, the spotweld type connection also has the RBE3-HEXA-RBE3 type connection.

3.1.3.3. Seam Line Connection

Seamline type connection is a type of connection used for parts joined by continuous welding. Seam line type connection is quite similar to the adhesive line connection. As in the case of the adhesive connections, the spotweld type connection also has the RBE3-HEXA-RBE3 type connection. An example seam line connection is shown in Figure 3.1.

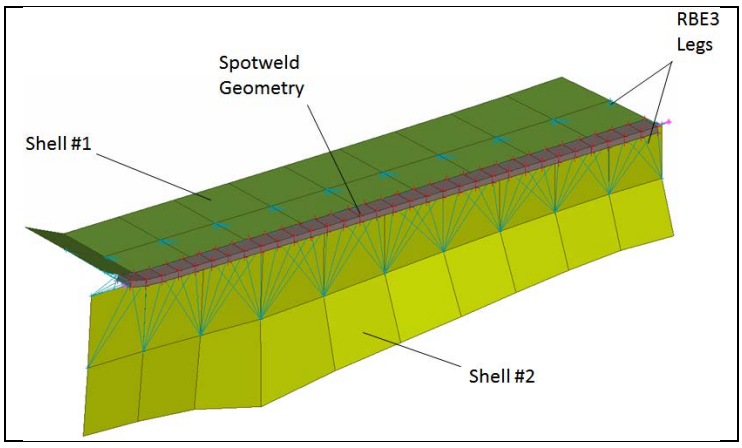

Figure 3.15: Seam line connection.

3.1.3.4. Bolt Connection

Bolts can be defined with two different method. First, holes can be connected with many nodes RBE2 elements. Second, each hole can be connected with many nodes RBE2 elements then all master nodes of RBE2 elements are connected with CBAR elements. Second method is more useful since bolts can be extended under load in reality. An example bolt connection is shown in Figure 3.1. In this Figure, yellow bar is a typical CBAR element and blue lines are many nodes RBE2 elements.

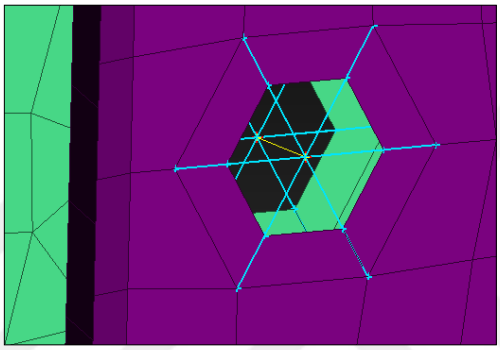

Figure 3.16: Bolt connection.

3.1.4. Rigidizing

Rigidizing is to convert a finite element model into a CONM2 and RBE3 set. The main purpose of this process is that reducing the number of elements in order to run the model.

In Figure 3.17, an example is shown. The wiper system is rigidized in order to reduce the number of elements in the full vehicle model.

Since NASTRAN can not run the model after exceeding a specific number of elements, rigidizing is inevitable for large finite element models. Furthermore, rigidizing keeps the weight and inertia data. So, there is no change in boundary conditions while rigidizing.

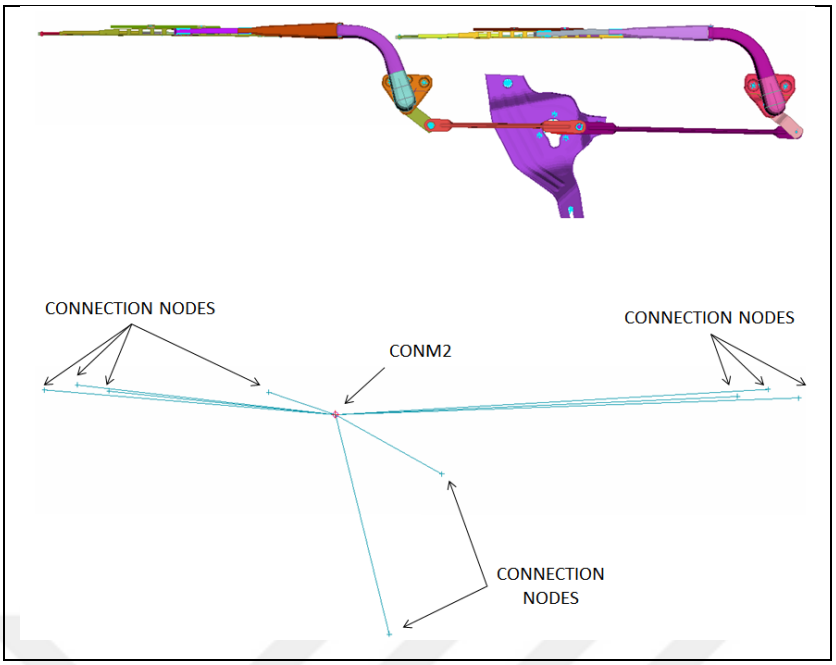

Figure 3.17: FEM and rigidized model of wiper system.

3.1.5. Non-Structural Mass (NSM)

All elements that have a mass but no specific geometry can be identified in the FE model by entering its NSM value. Thus, all the elements that do not contain geometry but must be considered mass can be added to the model and the actual weight of the model can be defined. The unit of NSM value is the mass per unit area. The body color of the vehicle model in this study, which weighs 17kg, is defined as NSM.

3.2. Vehicle FE Model Creation

In this study, full vehicle model can be classified into three major parts: Cabin, Chassis and the Powertrain (Engine and Driveline). 3D CAD models of all the parts of the vehicle were created with the CATIA program. Meshing of CAD parts was performed in the ANSA program using the meshing criteria described in the previous chapters.

In general, the cast parts are meshed as solid, while the sheet metal and plastic parts are meshed as shell. In several iterations, the element size was choosen as 10mm for shell elements. For solid elements, the element size was choosen as 5mm. The number of elements of specific FE models are given in table 3.1. Other models such as linking members are not given due to their low number of elements.

Table 3.1: Number of elements for specific subsytem FE models.

Subsystem Model	**Number Elements**	
	Shells	**Solids**
Cabin (With Trims)	1,762,161	1,528,456
Chassis (With Trims)	2,708,297	6,066,750
Engine	288,480	3,929,080
Front Axle	486,024	2,877,900
Rear Axle	1,243,523	5,179,478
Front Axle - Left Spindle	120,550	597,461
Front Axle - Right Spindle	120,550	597,461
Rear Axle – Left Spindle	243,910	1,033,594
Rear Axle – Right Spindle	247,288	1,046,203
Chassis – Front Anti Roll Bar	4,992	59,588
Cabin - Anti Roll Bar (ARB)	72,528	154,393
TOTAL	7,298,303	23,070,364

The number of nodes of specific FE models are given in table 3.2. Since the excessice numbers of nodes, the display model technique is used for component. Details about display model is given in section 3.3.

Since transmission was taken from supplier, the transmission model is a superelement model. A typical superlement model has no visual expression and elements. So, the number of elements of the transmission model is unknown. The number of elements of the tire model is aslo unknown since it comes from the manufacturer as vsign component model.

Table 3.2: Number of nodes for specific subsytem FE models.

Subsystem Model	**Number Of Nodes**
Cabin (With Trims)	1,762,161
Chassis (With Trims)	2,708,297
Engine	-
Front Axle	612,273
Rear Axle	1,215,990
Front Axle - Left Spindle	131,017
Front Axle - Right Spindle	131,017
Rear Axle – Left Spindle	235,778
Rear Axle – Right Spindle	238,830
Chassis – Front Anti Roll Bar	11,825
Cabin - Anti Roll Bar (ARB)	46,812
TOTAL	7,094,000

In order to reduce the number of elements, parts that are thought not to affect the correlation are rigidized.

Consequently, the full vehicle model consists of more than 30 million elements. Solving this huge model requires too much computational time. In order to reduce the computational time and increase the number of iterations, modal approach is used in this study.

The cabin FE model, chassis FE model and engine FE model are shown in Figure 3.18, 3.19 and 3.20 respectively.

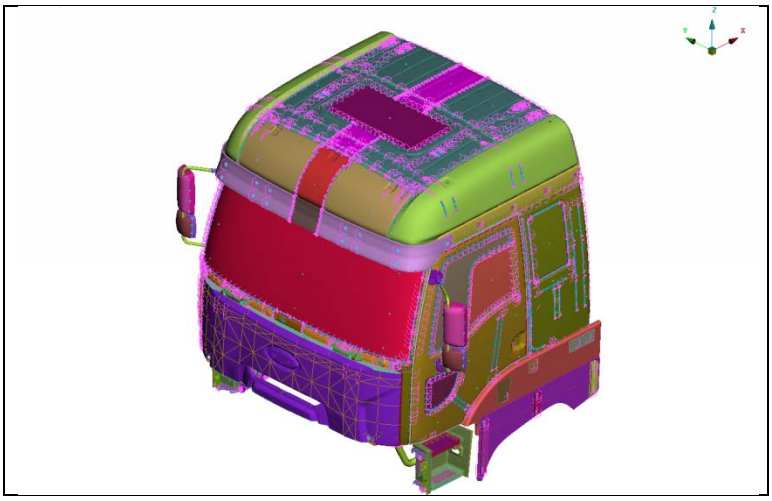

Figure 3.18: Cabin finite element model.

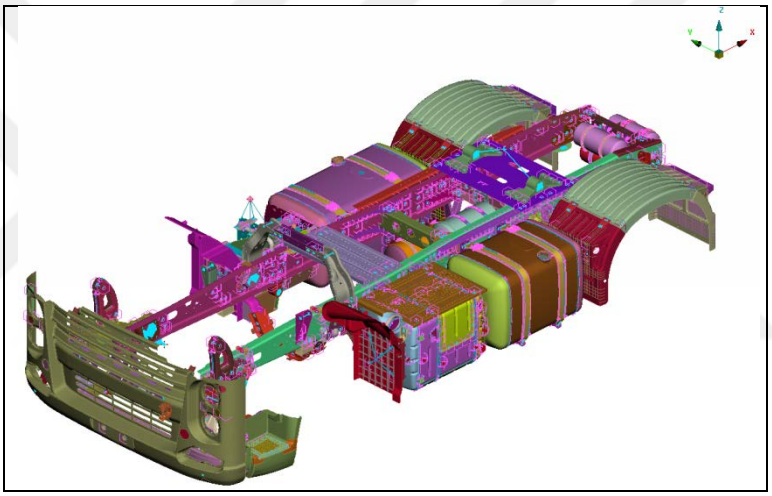

Figure 3.19: Chassis finite element model.

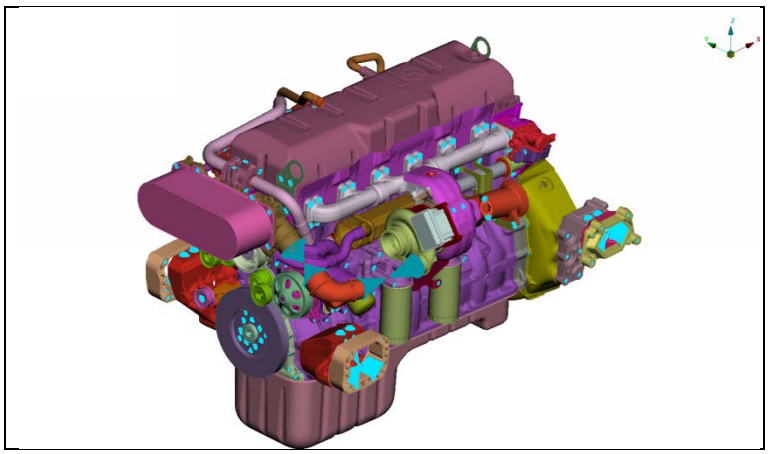

Figure 3.20: Engine finite element model.

In this study, several modelling strategies were tried in order to obtain high correlation. Finally, an optimal modelling strategy was reached. This modeling strategy is about how trim parts are modeled. The modelling technique for major trim components is given in table 3.3.

Table 3.3: Modelling strategy for major trim parts.

Trim Parts	**Modelling Strategy**
Front doors	FE
Decklid	FE
Hood	FE
Seats	FE
Instrument panel (IP) structure	FE
Fuel tank	FE
Fuel lines	Rigidized
Fuel canister	Rigidized
Heat shields	FE
Radiator & fan assembly	Rigidized
Expansion tank	Rigidized
Brake booster	Rigidized
ABS unit	Rigidized
Brake lids	Rigidized
Pedals	FE
Top mount	Rigidized
Spare wheel	Rigidized
Tools	Not modelled
Carpets	NSM
Mastic	NSM
Headliner	NSM
Sound package insulation	NSM

Table 3.3: Modelling strategy for major trim parts (continuation)

Trim Parts	Modelling Strategy
Airbags	Rigidized
Restraint systems	Rigidized
Lamp assembly	Rigidized
Horn	Rigidized
Water container	Rigidized
Wiper assembly	Rigidized
Mirrors (Glass)	Rigidized
Front fender	FE
Wheelhouse	FE
Bumper energy absorber	Rigidized
Paint	NSM
Battery	Rigidized
Wiring harnest	Rigidized
Speakers	Rigidized

3.3. FE Display Model Creation

Since the fully trimmed NVH vehicle model is made up of millions of elements, it is quite difficult to view the vehicle modes and mode shapes in the post-process. In addition, there is no need to see the all modes and mode shapes in this operation, since only the vibration and noise transfer paths are examined. Therefore, by creating display models for each subsystem (cabin, chassis etc), it is possible to see mode shapes with a computer with limited processing power.

The display modelling is a process performed with the aid of the ANSA program and is a process of creating a much simpler visualization of the model to be analyzed. It should be noted that the display model is not sent to the solver. On the contrary, the complete model is sent to the solver. However, since the solver gives the results of all grids in the full model, it is not possible to view the results.

Therefore the full model and a node list of the display model is sent the solver. The solver performs calculations on the entire vehicle model, but only gives the results of the nodes in the display model. Thus, during the post-process, the display model is displayed easily instead of the full vehicle model.

The cabin and the chassis display models are shown in the Figure 3.21 and 3.22 respectively.

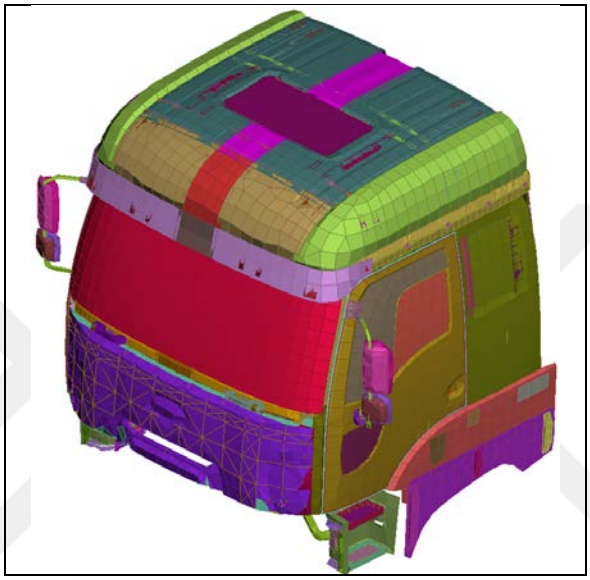

Figure 3.21: Cabin display model.

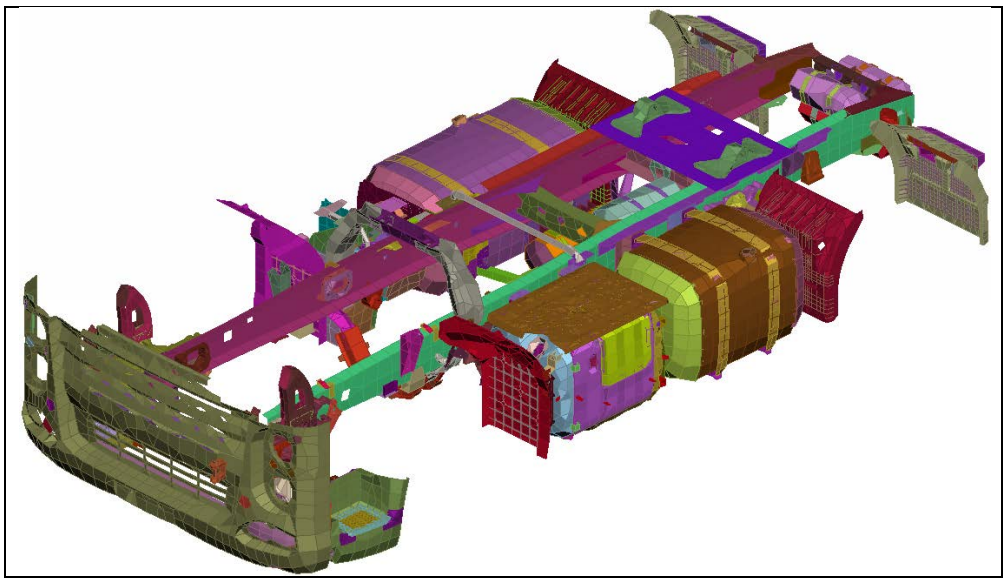

Figure 3.22: Chassis display model.

3.4. Modal Analysis and Modal Model Creation

In this study, pre-processing is performed by ANSA, SFE Akusmod and VSIGN software. Analysis is performed by using MSC NASTRAN and VSIGN software. Post-processing is performed by using Metapost, ENVISION and Pi-Rate software.

VSIGN is an in-house vehicle NVH CAE software. The VSIGN name comes from 'Vehicle System Integrated GUI for NVH'. It is useful for building and modifying vehicle NVH CAE models and also for organizing analysis results and launch plots or animations etc. In Figure 3.23, GUI of VSIGN program is shown.

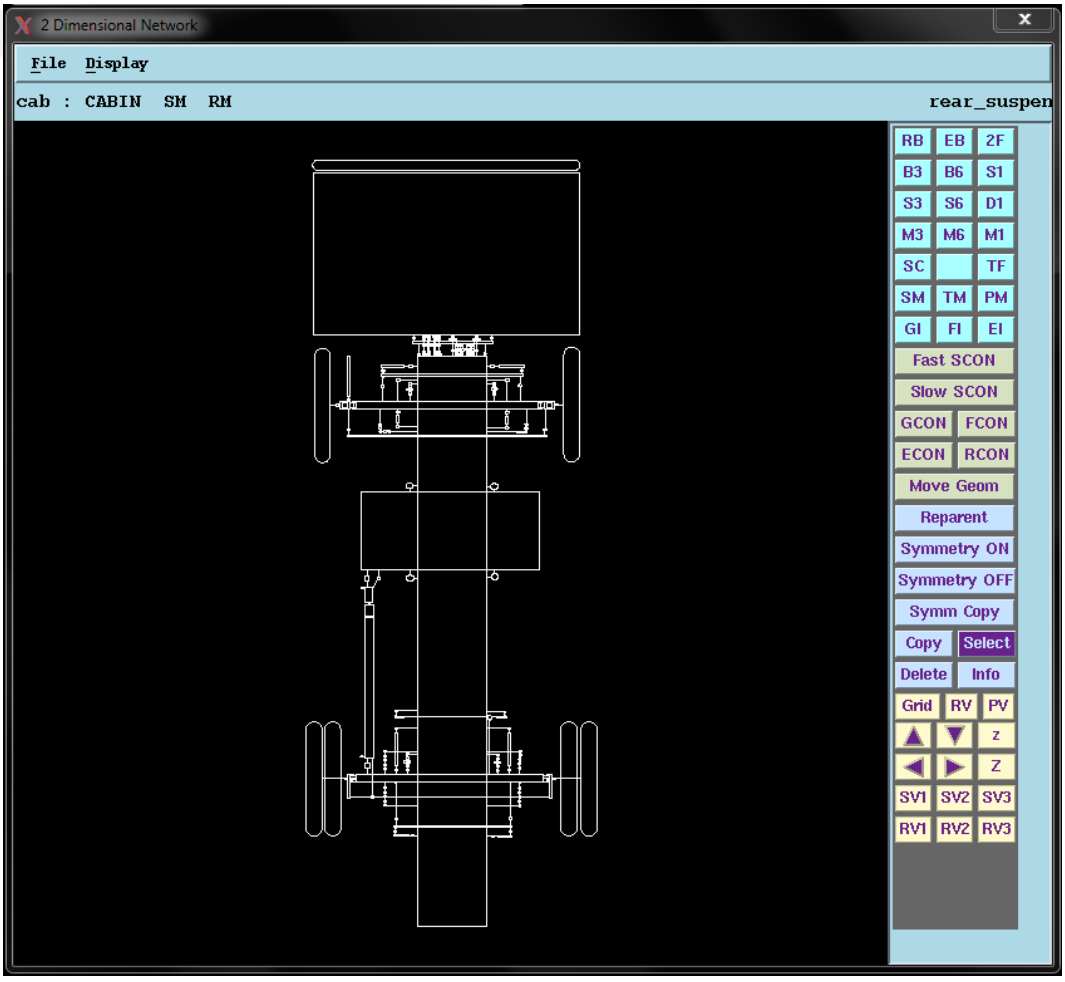

Figure 3.23: VSIGN GUI.

MOTRAN is the solver while VSIGN is the GUI. The MOTRAN name comes from 'Modal Transfer function Analysis'. MOTRAN is not a finite element program. It

takes input from a finite element solver (e.g. NASTRAN). In this study, all finite element analyzes are performed by using NASTRAN and results are processed with VSIGN in order to use in MOTRAN. NASTRAN gives op2 result files. Different op2 result files (e.g. cabin, chassis, axles) are converted into im files in VSIGN. Each im file is shown as a block in VSIGN. These modular building blocks called components. In VSIGN, blocks are connected together by constraints. MOTRAN allows variable subsystems, e.g. brakes on or off, shock stiction, transmission gear, torque converter lock, etc. [46].

MOTRAN is not a mechanism program and it has no capability to predict responses accurately when large displacements occur.

MOTRAN is very useful in order to solve for modes of complex continuous systems like a vehicle. MOTRAN converts the differential equations into algebraic equations by discretization. Typical vehicle body model is discretized into about 2 million elements which is 12 million degrees of freedom i.e. 12 million equations. These 12 million equations are formulated and solved using FEA. About 5000 modes are obtained by FEA. Technically, it can be recovered 12 million modes but it takes too much computational time.

In this study, body vehicle model FEA modes are obtained in about 1 hour. Other systems such as chassis, front and rear axles etc. are also modeled and calculated in NASTRAN. Tires and other parts are modeled in VSIGN. Combining the modes of all FEA parts is done in VSIGN. Consequently, a vehicle modal model is created and tens of millions of DOF are reduced to a few thousand in modal space. Basicaly, 1 mode equals 1 DOF and each DOF is essentially a mass-spring system.

In order to reduce the DOF from millions to thounsands, modal mass and modal stiffness matrices are assembled. The mass and stiffness matrices are diagonalized by using modal transformation. This uncouples the equations and the solution is much simpler using linear algebra. As previously mentioned, uncoupling provides that each mode is essentially a 1 DOF mass-spring system which is easy to solve. Finally, matrices are transformed back from modal to physical coordinates in order to get desired responses (e.g. FRF) [46].

In this study, as post-process, given results from VSIGN are evaluated in Envision and PiRate software. Envision is useful for visual expression of modes.

PiRate (Parameter Interface Response And Target Evaluator) is a in-house program and it is compatible with VSIGN. PiRate has capability to express post-process peaks, modal contribution, panel acoustic contribution, design sensitivity and noise path analysis.

3.5. Boundary Conditions

In this study, boundary conditions can be classified as component level boundary conditions and full vehicle boundary conditions. For coponent level bondary conditions each component is connected on their attachment points with the RBE2 elements.

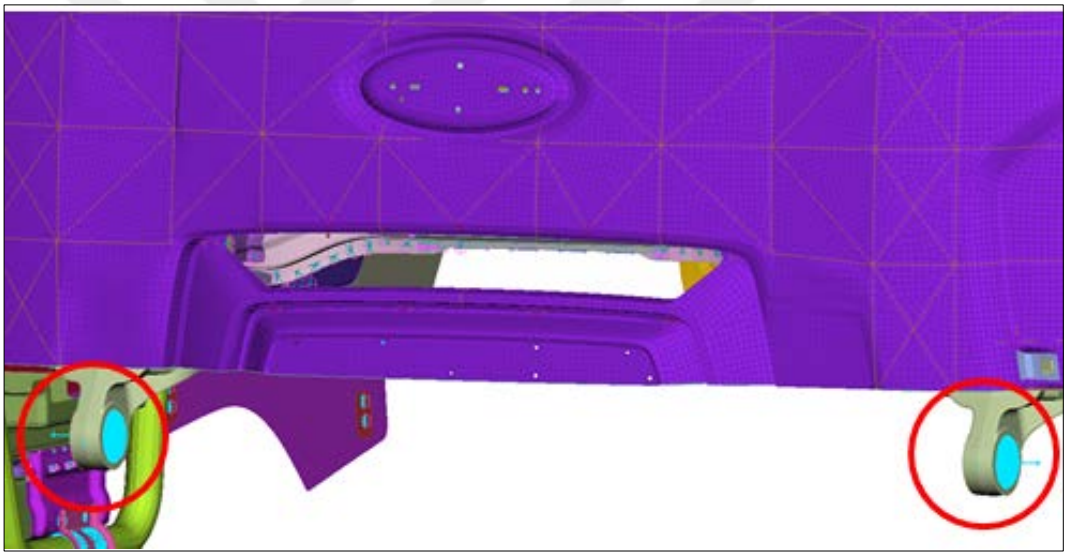

Figure 3.24: RBE2 connetions (BC's) for front cabin-chassis attachments.

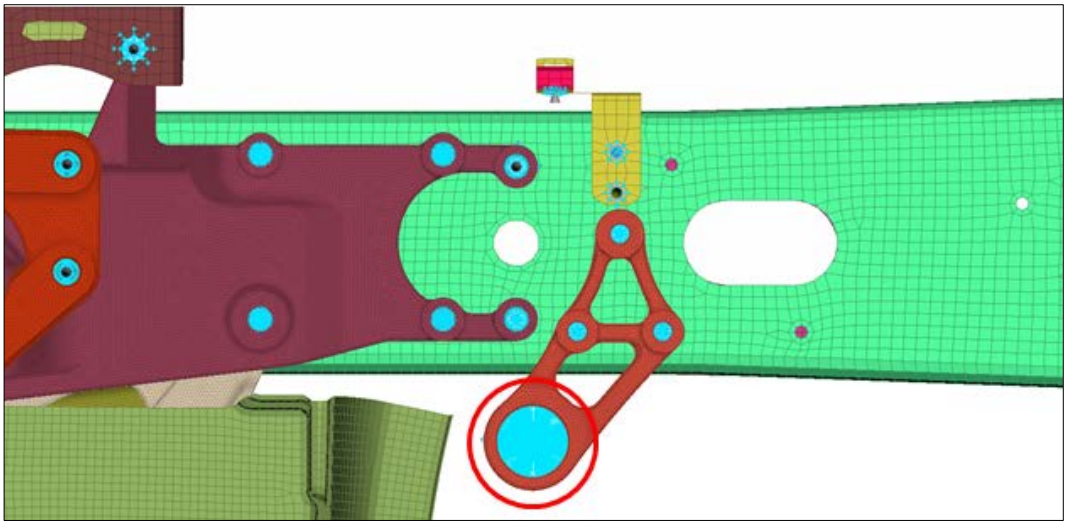

Figure 3.25: RBE2 connetion (BC) for left chassis-front axle attachment.

As an example, front cabin-chassis attachments for the cabin model and the one side of the chassis-front axle attachment for the chassis model are shown in figure 3.24 and 3.25 respectively. These connections (boundary conditions) are defined for component level modal analysis.

For full vehicle model, the only boundary condition is defined between tires and the ground.

3.6. Transfer Path Analysis via CAE Model

Using the modal approach with the MOTRAN software which is the solver of VSIGN, both results of the vibrational transfer path analysis and the results of the noise transfer path analysis were obtained.

The first step in performing VTF analysis with the aid of CAE is to determine the transfer paths on the prepared vehicle model. As mentioned earlier, vibration sources in the vehicle can be generally classified as powertrain loads and road loads. In this context, vibrational transfer paths must be the paths in which the vibrational energy from the engine and from the road can travel and reach the driver and the passenger.

Since CAE and test correlation are examined in this study, the reaction points were chosen as places where the acceleration meters could easily be placed on the

prototype vehicle. Because the data acquisition device used for the hammer impact test can be connected to 7 accelerometers (or 7 accelerometers and 2 microphones) at a time, no more than 7 vibration response points were identified for each defined transfer path.

Table 3.4: Defined transfer paths.

Transfer Paths	**Impact Point Subsystem**	**Response Types**
Path 1	Front axle (Passenger side)	7 Accelerations
Path 2	Front axle (Passenger side)	7 Accelerations
Path 3	Front axle (Passenger side)	7 Accelerations
Path 4	Front axle (Passenger side)	7 Accelerations
Path 5	Front axle (Passenger side)	7 Accelerations
Path 6	Front axle (Passenger side)	7 Accelerations
Path 7	Rear axle (Passenger side)	7 Accelerations
Path 8	Rear axle (Passenger side)	7 Accelerations
Path 9	Rear axle (Passenger side)	7 Accelerations
Path 10	Rear axle (Passenger side)	7 Accelerations
Path 11	Rear axle (Passenger side)	7 Accelerations
Path 12	Front axle (Passenger side)	1 Acceleration
Path 13	Rear engine mount (Driver Side)	7 Accelerations
Path 14	Front engine mount (Driver Side)	7 Accelerations
Path 15	Upper exterior step (Passenger Side)	1 Acceleration
Path 16	Front Cabin Mount (Passenger side)	6 Accelerations 2 SPL
Path 17	Rear Cabin Mount (Passenger side)	6 Accelerations 2 SPL
Path 18	Rear axle (Passenger side)	7 Accelerations
Path 19	Rear axle (Passenger side)	7 Accelerations

Totally, 19 transfer paths were defined. Generally, each transfer path includes 7 responses. Only one response was defined for transfer paths 12 and 15. 6 of these

responses are vibration responses, and 2 of them are sound pressure level (SPL) responses.

It should be noted that the results obtained from the CAE are not presented here because there are too many plots. All CAE results are presented in the correlation section together with the test results (Chapter 5).

3.5.1. Vibrational Transfer Function (VTF) Analysis via CAE

In this section, defined vibrational transfer paths (or vibrational transfer functions) are presented. 119 vibrational points and 19 impact points were defined in order to understand vibrational transfer characteristics of the vehicle. Generally, all impacts points were defined at different places. However, some transfer points used the same impact points. Transfer paths 1 and 2 and transfer paths 18 and 19 have the same impact points between themselves. Because the test data acquisition device can collect up to 7 responses at a time in one impact. Details about data acquisition are presented in chapter 4.

Vibration response points were chosen around the elements that would change the stifness between them. In other words, the vibration response points were chosen where the stiffness values changed. Critically, the reason for choosing mount stiffness as a parameter is that the mounts come with a very wide range of stiffness tolerances from the manufacturer (e.g. tolerance is ±20% for engine mount stiffnesses).

Thus, bushing and mount stiffnesses were selected as a second iteration parameter in order to correlate with the test results. (Previously, FE modeling parameters were mentioned as the first iteration parameter.)

Since the bushes and mounts are defined as bush elements and mount elements in VSIGN, each iteration is made as a change of stiffness value on VSIGN.

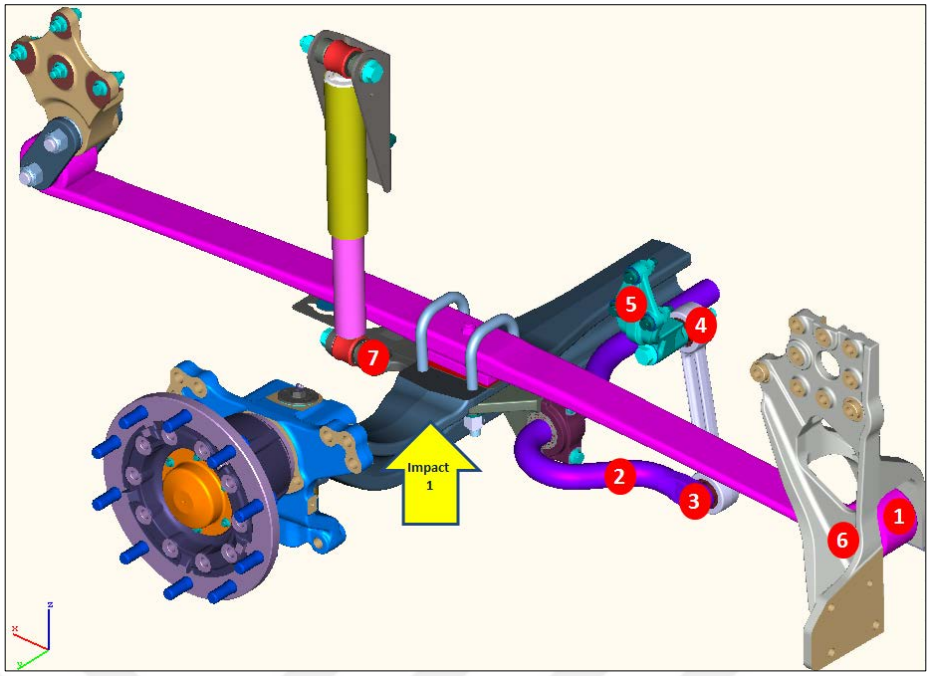

Figure 3.26: Vibrational transfer path 1.

The vibrational transfer path 1 and 2 are shown in Figure 3.26 and 3.27 respectively. The impacts for transfer path 1 and 2 were given on front axle. Vibrational responses were collected from 7 different locations.

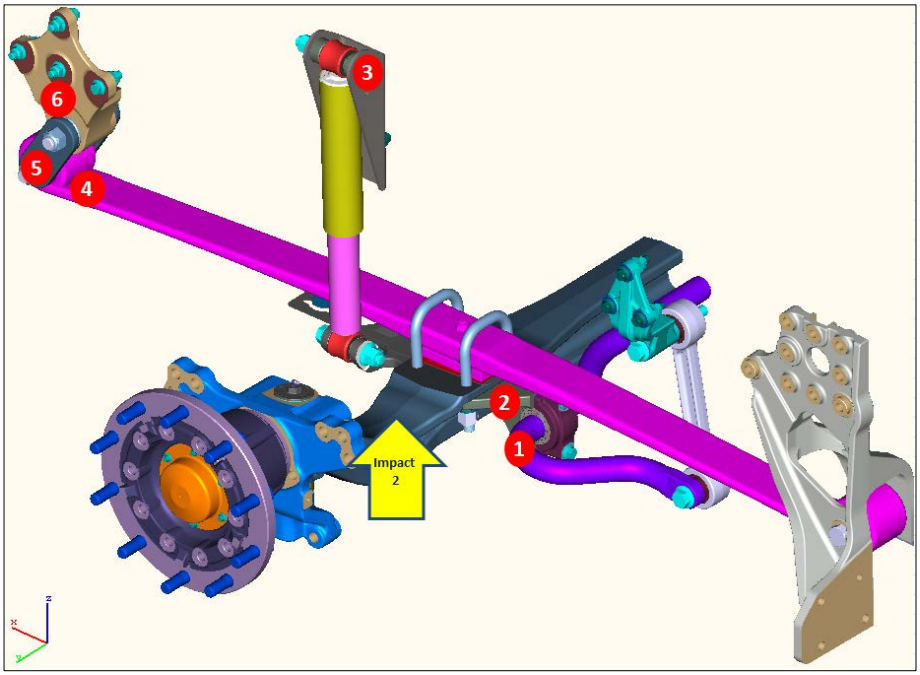

Figure 3.27: Vibrational transfer path 2.

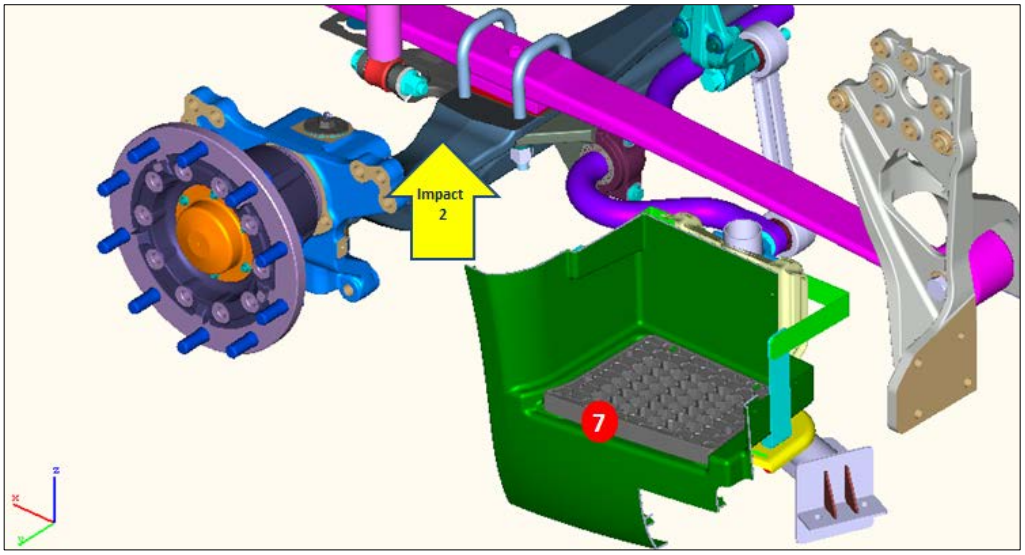

Figure 3.28: Vibrational transfer path 2 (continuation).

In vibrational transfer paths 3 to 11, all response points are same. The impacts were applied on front suspension subsystem for transfer paths between 3 and 6 (See figure 3.29).

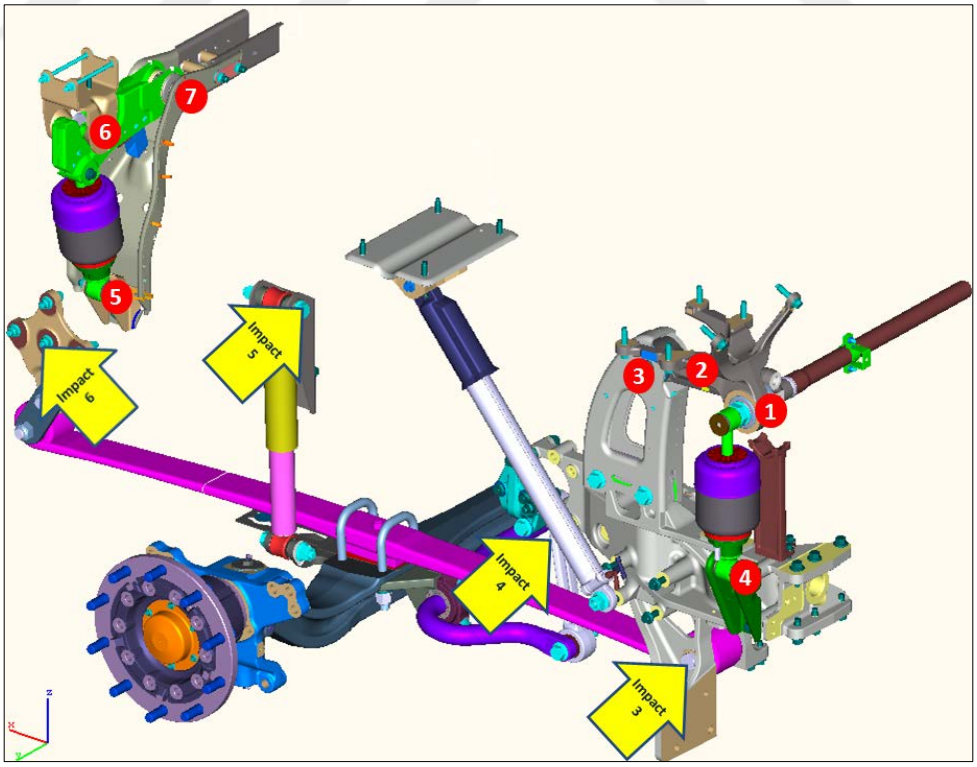

Figure 3.29: Vibrational transfer paths 3,4,5,6.

The impacts were applied on rear suspension subsystem for transfer paths between 7 and 11 (See figure 3.30).

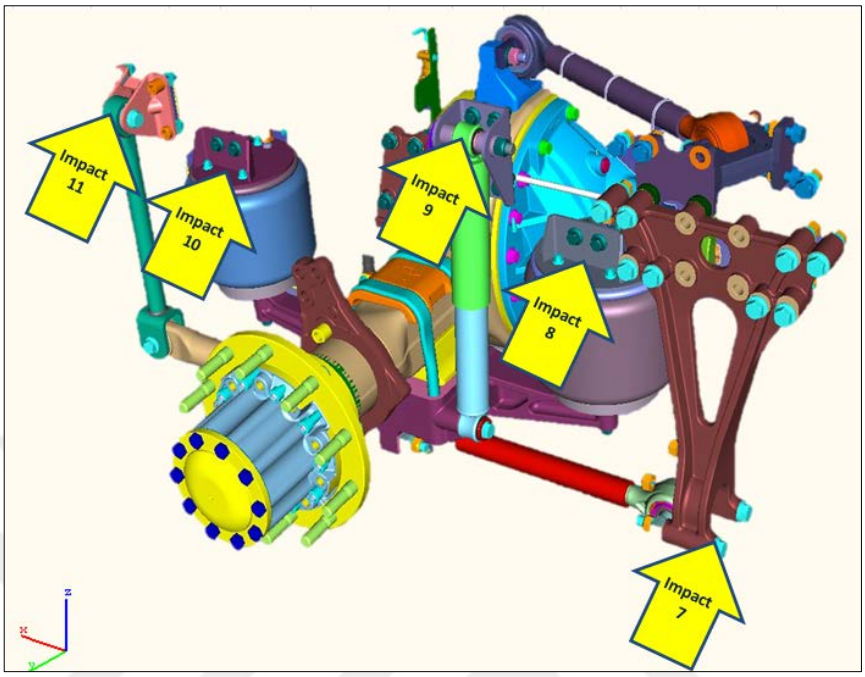

Figure 3.30: Vibrational transfer paths 7,8,9,10,11.

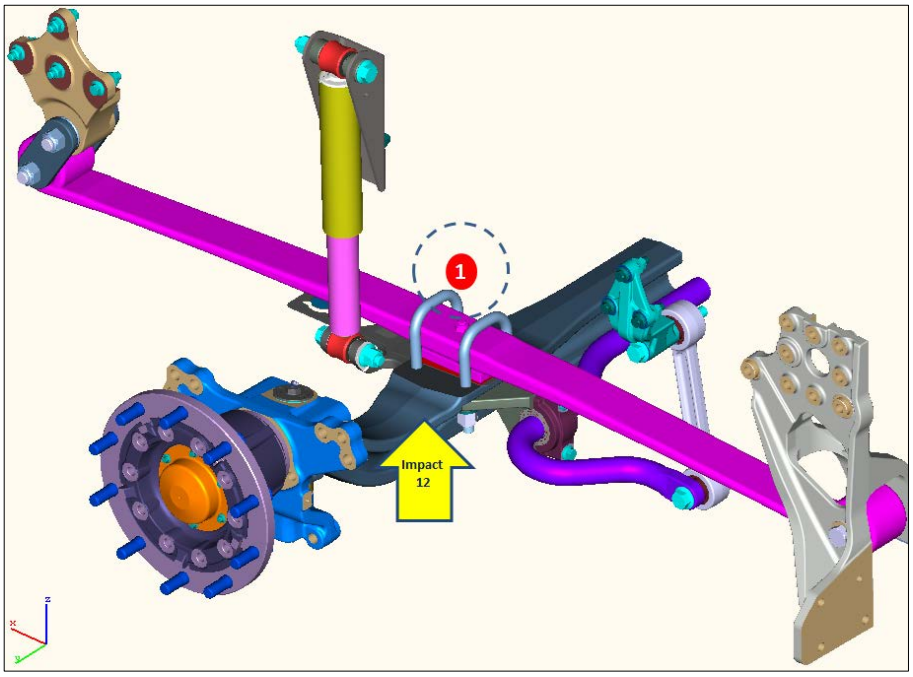

Figure 3.31: Vibrational transfer path 12.

In Figure 3.31, there is circle with dashed lines. Normally, there is an air suspension in this circle. However, this air suspension is not shown here because it is not geometrically modeled. (This air suspension is defined as spring element in VSIGN). The air suspension on the prototype vehicle is shown in Figure 3.32.

Figure 3.32: Front axle air suspansion.

Vibrations can reach the vehicle cabin from road as well as from the engine. On other vibrational transfer paths (path 13 and 14), the engine mounts were impacted to detect how vibrations from the engine reached the vehicle cabin. Since the engine mounts are normally located behind the chassis frame, it is impossible to access this region from the outside in the physical vehicle. For this reason, the connection brackets between the engine mount and the chassis frame, which are the places that the impact hammer can reach on the prototype vehicle, are selected as impact points.

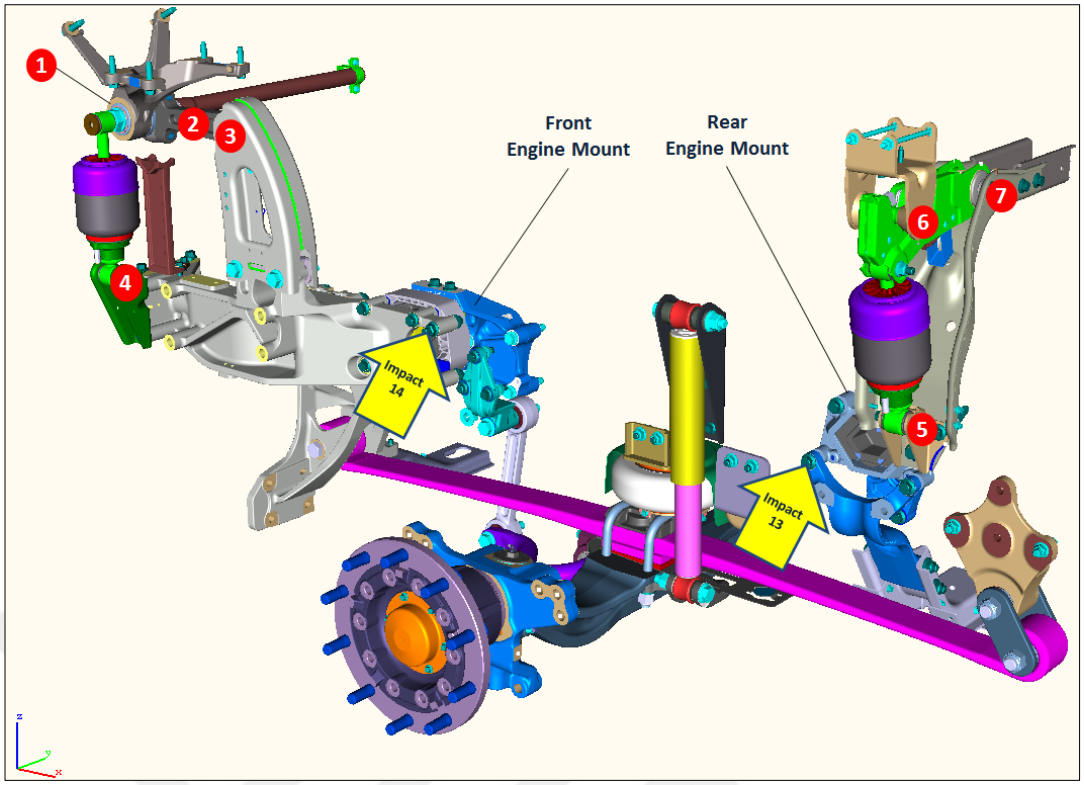

Figure 3.33: Vibrational transfer path 13 and 14.

At the same time, the engine mounts on the driver side were chosen as impact points because access is relatively easy and the driver side can be excited more easily. The engine mounts on the driver side and the vibration responses from these points are shown in Figure 3.33.

The exterior step is consists of two separate parts in prototype vehicle (and also in CAE vehicle model). Lower part of the exterior step is connected to the chassis. On the other hand, the upper part is connected to the cabin. In path 2, the lower part of the exterior step was impacted (see Fig. 3.28). In path 15, the upper part of the exterior step was impacted and the reponse was collected from very close region the impact area (see Fig. 3.34).

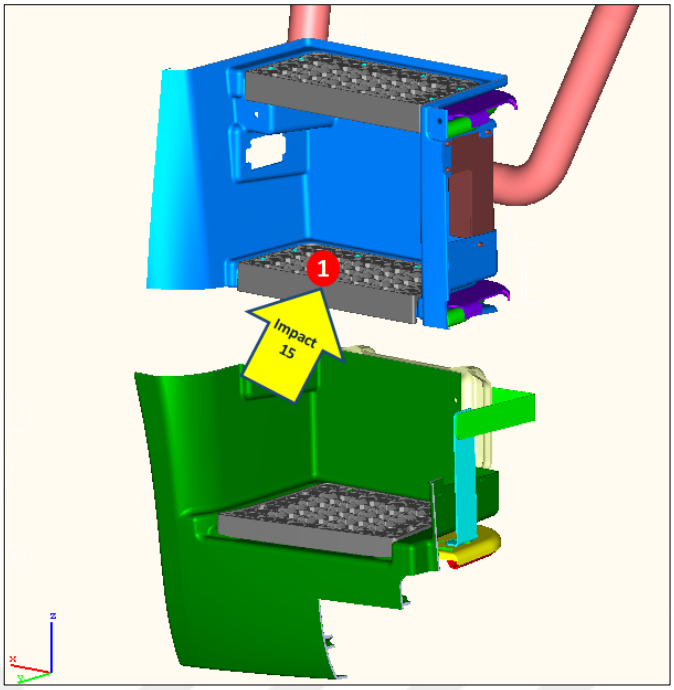

Figure 3.34: Vibrational transfer path 15.

In vibrational transfer paths 16 and 17 (see Figure 3.35), the vibrations reaching the car cabin were examined. The cabin mounts on the passenger side were impacted and vibration responses were collected from 6 different locations. These places are steering hub, driver and passenger seat connections and cab lift. In these transfer paths, sound pressure exchange (SPL) responses at the driver and passenger ear coordinates are also collected. The details of the SPL response are given in section 3.5.2.

Finally, last two transfer paths (18 and 19) are defined in the rear axle to understand how the excitations coming from the rear wheels are transmitted in the vehicle. The transfer paths 18 and 19 are shown in Figures 3.36 and 3.37 respectively. The impact points of the transfer path 18 and 19 are same.

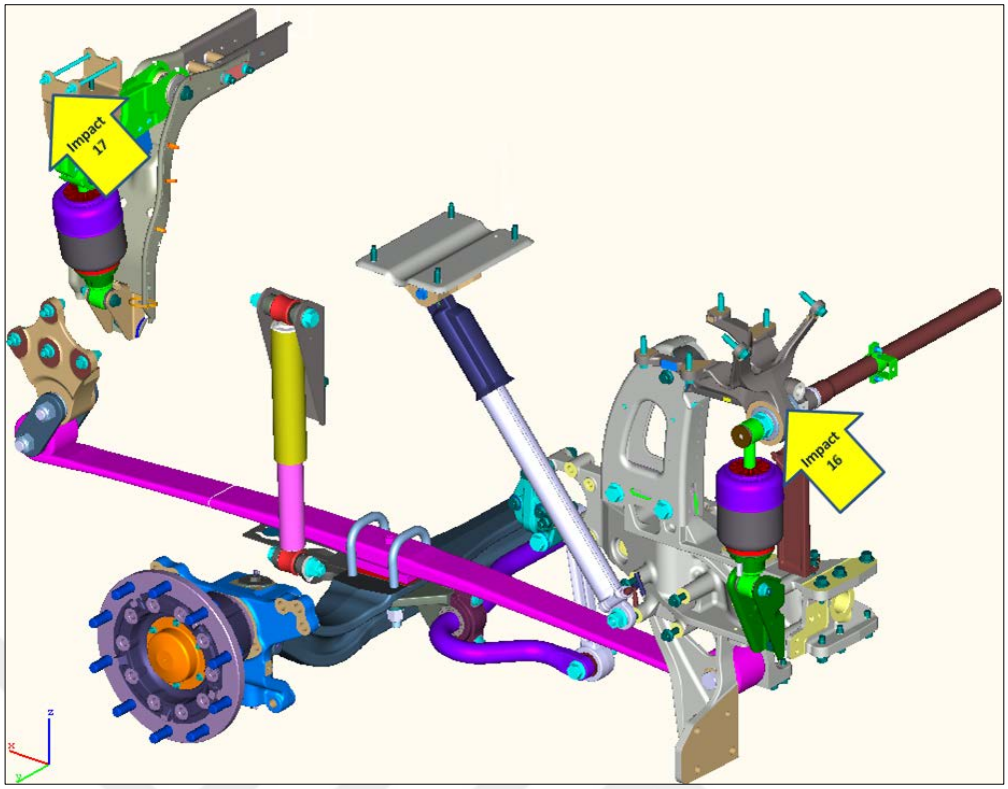

Figure 3.35: Vibrational transfer path 16 and 17.

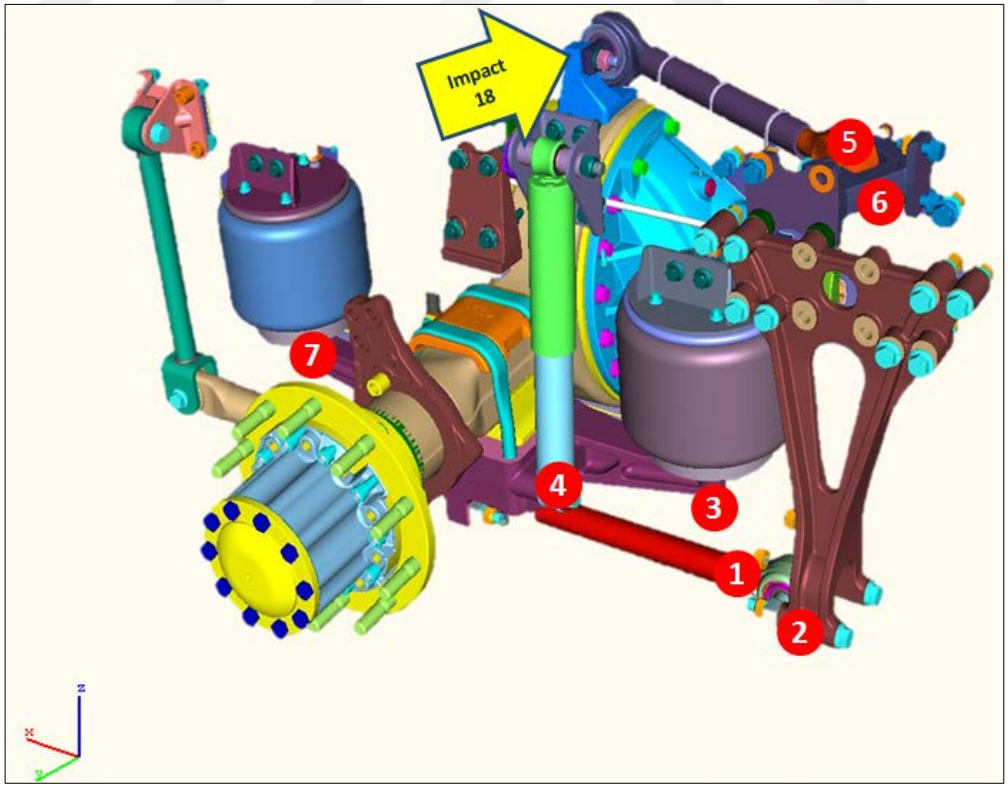

Figure 3.36: Vibrational transfer path 18.

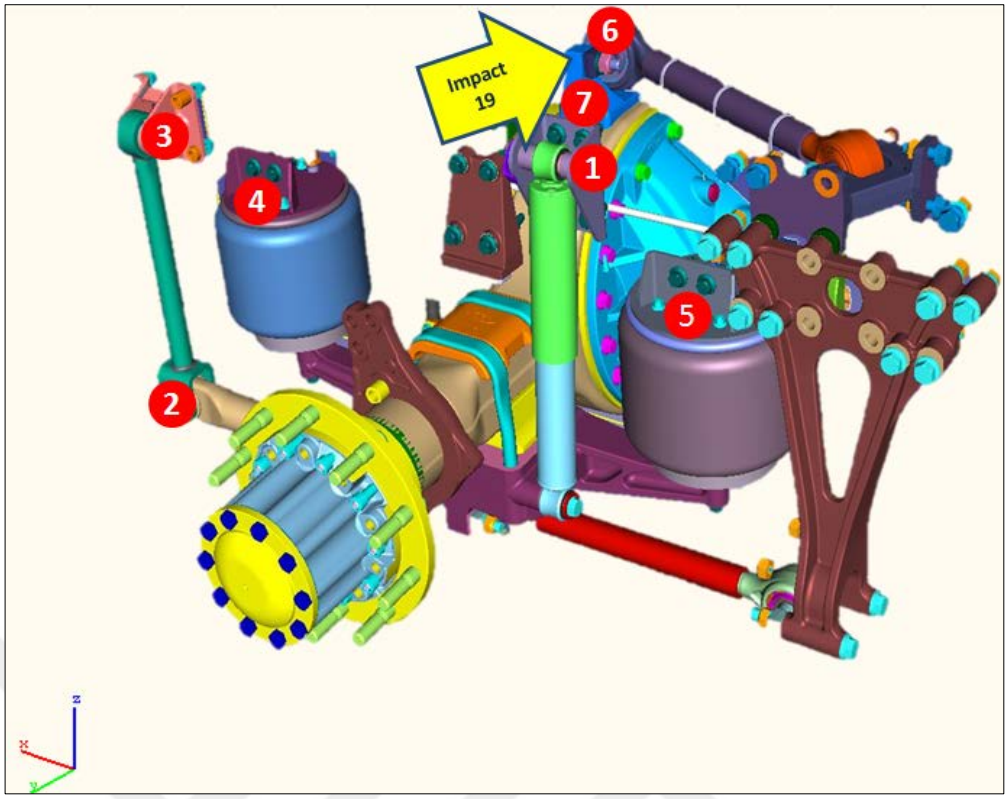

Figure 3.37: Vibrational transfer path 19.

3.5.2. Noise Transfer Function (NTF) Analysis via CAE

In order to analyze interior noise, the acoustic cavity of the vehicle cabin needs to be both defined and meshed. As for any FE analysis it is important to create an accurate and realistic model. In order to determine the sound pressure level (SPL) in the vehicle cabin, the interior (volume) should be meshed such that the vibration from the structure can be transferred to the cavity across the outer envelope of the cavity mesh. Cavity mesh (volume mesh) was created directly from the structural finite element model in ANSA software. Cavity model shown in the Figure 3.40.

First, all interior trims removed the cabin model (See Figure 3.38). Then, all holes that has a diameter bigger than 60mm are closed by shell elements in order to prevent cavity leakage. By adding seat and bed cushon models (See Figure 3.39) are added to cabin model, the air generation model is prepared.

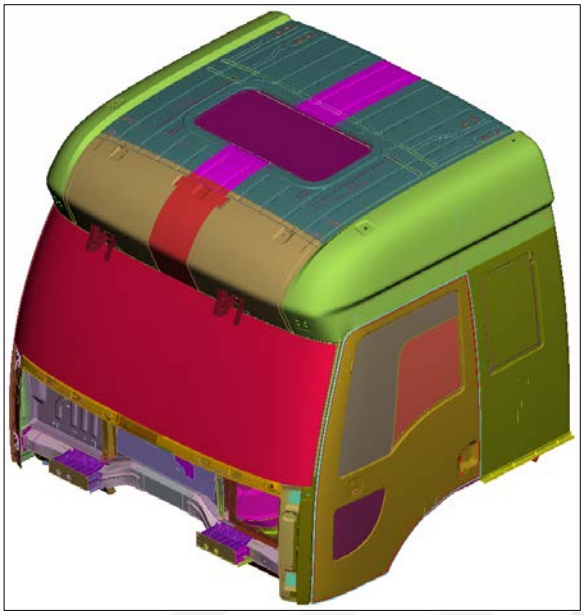

Figure 3.38: Structure model for coupling.

Only the BIP, doors and sunroof models are available in the structural model for coupling.

Finally, cavity model is created in ANSA software. When the Cavity model is prepared, the ear coordinates of the driver and the passenger are defined. Thus, when the cavity is analyzed, only the points corresponding to the ear coordinates are obtained and the analysis is completed faster. The ear coordinates are selected to be about 20 mm out of the seat head in the -x direction, and the points should be symmetrical relative to the vehicle position. The cavity model consist of solid models with 60mm element size.

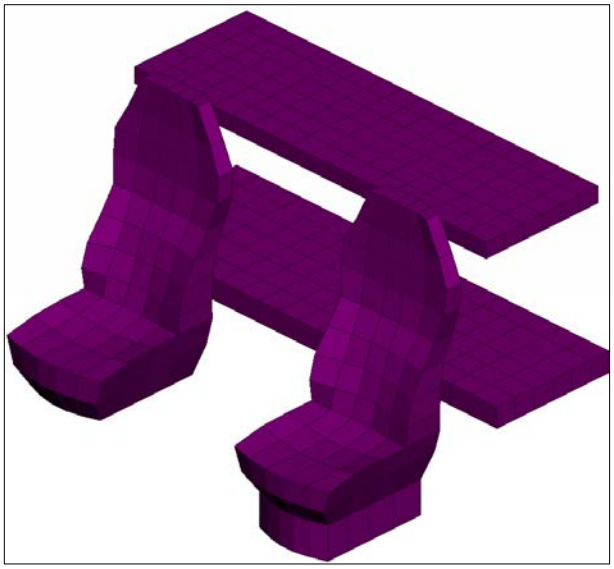

Figure 3.39: Seat and bed cushon model for coupling.

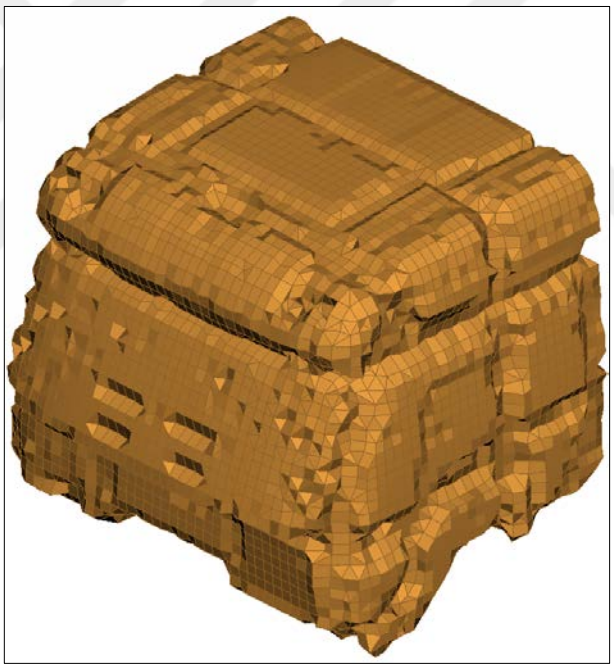

Figure 3.40: Fluid cavity model for coupling.

Fluid model consist of volume elements. There are 33266 hexa elements, 2928 tetra elements and 1624 penta elements in the fluid model. In total, the fluid model has 37818 solid elements.

Material property of fluid model is defined with 0.001223 g/cm^3 density value and 0.1417 bulk value.

4. ANALYSIS VIA MODAL HAMMER TEST

As mentioned earlier, testing is a common method used to validate CAE analyzes performed in the product development process. This section provides information on the NVH tests, test equipment, and testing performed in this study.

4.1. Noise and Vibration Measurement and Instrumentation

In this section, the equipment used to perform the NVH tests is introduced in general terms. In addition, measurement techniques used in the NVH tests conducted under this study is presented.

People are delicate to vibrations. Prior to any instruments got to be distinctly accessible, all vibration examination was performed by tuning in and feeling. This strategy is still utilized by the individuals who don't have instruments. People have some inherent sensors in their skin and their ears. These organic transducers served a survival capacity and still do. The human ear is incredibly touchy to the littlest pressure change. The pressure sensors in human skin can recognize consistent pressure, and furthermore wavering vibration.

Frequency analysis is indispensable so as to distinguish the sources of vehicle vibration and noise problems. People are outfitted with a frequency analyser. Human brain and ear are extremely sensitive frequency analyzer. The frequencies that the human ear perceives are between 20 Hz and 20 kHz (20 000 Hz). However, the borders stated here are extreme values measured in young people with extremely sensitive ears. The ears of most people are not that sensitive.

For most people 30 Hz is hardly audible but it can absolutely be felt with the pressure sensors in the fingertips. But the pressure sensors in the fingertips are able to detect low frequency (less than 100 Hz) vibrations. For higher frequencies, the tones should be considered since a great majority of mechanical vibrations are perceptible to the human ear [1].

Although humans have improved vibration and noise detection capabilities, it is necessary to use instruments to objectively evaluate vibration and noise.

Quantitative evaluation is inevitable, in particular for design direction and benchmarking between designs. As a result, advanced vibration and sound measuring instruments are essential to the product development process and NVH engineers.

4.1.1. Noise Measurement and Instrumentation

In this section, the classification of sound in the perspective of NVH and the measurement techniques and measuring instruments of these sounds are presented.

4.1.1.1. Noise Classification

In vehicle NVH application sounds (noise) are classified according to their sources. In general, the noise in a car can be sorted as follows: aerodynamic noise, air intake noise (intake noise), background noise, belt noise, booming noise, brake wire brush noise, door shut noise, engine combustion noise, engine noise, gear noise, pass by noise (the sound heard from the outside of the vehicle), exhaust noise, fan noise, road noise and tyre noise.

Booming noise is a typical annoying acoustic problem in passenger cars, vans and commercial vehicle cabs. The situation arises when a single narrow band dominates the interior noise of a motor vehicle. The frequency band is usually somewhere in the range 50-200 Hz, a range where the half wave length of acoustical pressure waves is similar to interior dimensions of the vehicle. The compartment acts as a resonator and amplifies the transmitted sound in the receiver frequency band in which the standing pressure waves are established.

4.1.1.2. Noise Measurement

A typical sound meter is designed and used to measure sound pressure. These days, these gadgets can be anything from straightforward gadgets with simple

channels and identifiers and a moving coil meter to advanced computerized analysers. A block diagram of a simple sound level meter is shown in Figure 4.1.

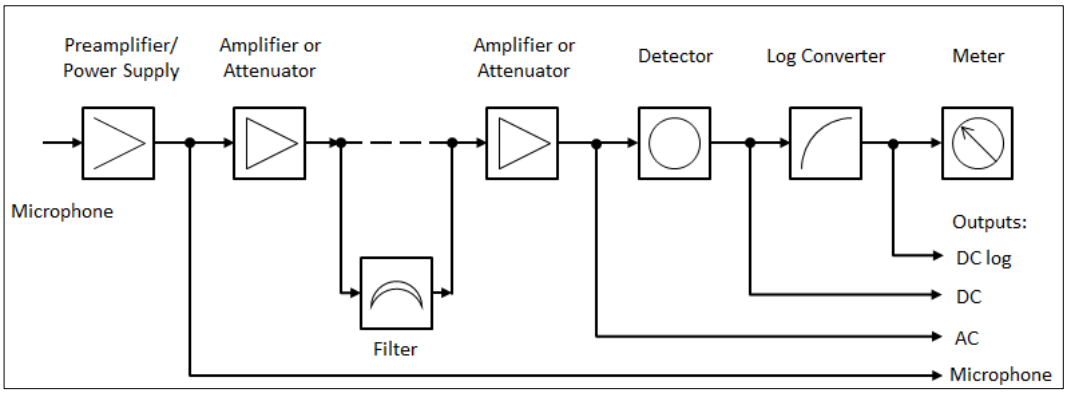

Figure 4.1: A sound level meter.

Basically, a microphone allows sound to be measured by converting the sound pressure to an electrical signal and amplifying it by various filters [38].

4.1.1.3. Microphones

A microphone is an electroacoustic device that translates mechanical vibrations caused by sound waves into electrical signals. The microphone is a complement to the loudspeaker as it gives the signal voltage to the sound waves. With the aid of the speakers, the electrical signals are converted into sound. Because of this translation feature, microphone and speaker are called transducers. Transducer means converter.

There are many physical principles for generating electrical signals from vibrations in a sound wave. These include the principles of change of connection resistance, piezo electric, electromagnetism and magnetostriction. Today, the principles in practice are piezo-electric, electromagnetic, electro-static and capacitive principles.

Condenser microphones are commly used in order to measure sound (noise). Condenser microphones measure sound more accurately than other kind of

microphones. The diaphragms of the condenser microphones are extremely thin, and extremely strectched.

The diaphram of a condenser microphone is both very thin and highly stretched. In the housing of the microphone cartridge, the other part of the condenser is located very close to the diaphragm and is the back plate. The capacitor is electrically charged to an external voltage on the back plate or to the specifications of the diaphragm or back plate. The capacitance changes when the diaphragm moves in response to the sound pressure. As a result, it generates an electric voltage which is proportional to the instantaneous sound pressure [38].

The section, which is mounted on the head of a microphone and converts an acoustic energy into electrical energy, is called an element (or capsule). Each type of microphones is referred to by the name of the element it uses. There are microphones with five types of elements [54].

- Dynamic Microphone
- Condenser Microphone
- Ribbon Microphone
- Crystal or Ceramic Microphones
- Carbon Microphone

It should be noted that other microphone classifications are also available in different sources.

Studio microphones are manufactured in two diaphragm types: Dynamic (Coil) and Condenser (Capacitive)

Dynamic microphones have a membrane attached to the bobbin and wrapped around a permanent magnet. The sound waves that touch the membrane cause the coil to move around the permanent magnet and generate an electrical signal at the coil ends. Dynamic microphones which are not influenced by the shock due to their construction are used while taking live scenes. The most popular types of microphones in the marketplace are dynamic microphones.

Dynamic microphones have some unique features. The tall is short and the structures are sturdy and light. The use of dynamic microphones without auxiliary

voltage source is expanding. Although it has a powerful output, its suitability is not sensitive to the frequency of the sound. Dynamic microphones are not expensive. Dynamic microphones are used for thick sounds when recording audio. Compared to condenser microphones, they are more resistant to sound intensity. For this reason it is placed close to the sound sources and is easily used in high volume sound sources [55].

Among the condenser microphones, there are two plates with dielectric and moving conductors, which are dielectric plates. Three of them form the capacitor. When the sound waves strike, the plate moves and changes the capacity of the condenser. If voltage is connected to the capacitor terminals, the capacity will change due to the current. This change creates a vibration. These vibrations are converted into sound signals. Condenser microphones can not turn a sound into an electrical signal if there is no working voltage from the outside. This voltage is 48 volts, called the concealed power (Phantom Power). In advanced sound recording systems, this microphone is preamplified by the microphone preamble it is connected to.

Sensitivity of a microphone to detect sounds from a single direction or from different directions is called a pickup pattern. The graph of the pick-up pattern is called the polar pattern. There are three different pickup patterns in the microphones [55].

- Omnidirectional (All directions)
- Unidirectional
- Bidirectional (dual direction)

Omnidirectional microphones reflect very little changes between the microphone and the source. These types of microphones are very little affected by small bursts of sound, wind and hand grips. These microphones are cheap at the same time. But they can not distinguish unwanted voices and are difficult to use in noisy environments. It also creates a feedback problem in environments where there are many reflective surfaces.

On the other hand, one-way microphones can distinguish unwanted sounds. It creates less environmental sense, and there is no risk of feedback when there are too many reflective surfaces.

The frequency response of any device operating in a frequency range is the output range of 3 dB of the 0 dB reference line as shown in Figure 4.2.

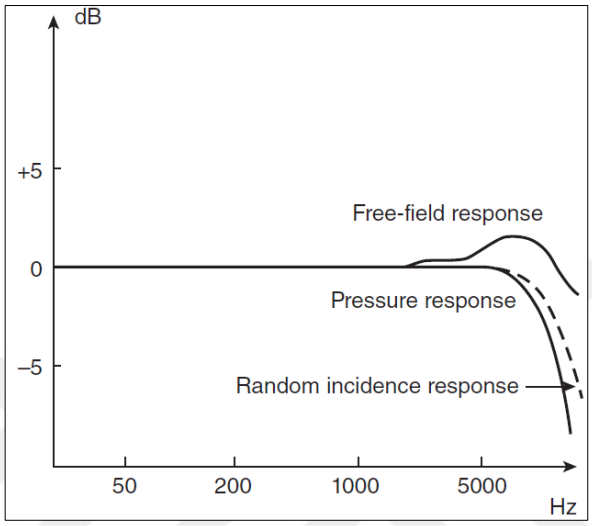

Figure 4.2: Free-field, pressure and random response of microphones.

In this study, one dimensional Brüel & Kjaer type 4188 1/2-inch condenser microphones (See Figure 4.3.) are used in order to obtain sound pressure levels in driver and passenger ear positions.

Figure 4.3: Brüel & Kjaer type 4188 1/2-inch microphone.

4.1.1.4. Pre-amplifiers

A pre-amplifier is an electronic amplifier that separates a small electronic signal for reprocessing or amplification. The pre-amplifiers is usually placed close to the sound source to reduce distortion and noise in the signal [55].

In this study, Brüel & Kjaer type 2671 CCLD microphone preamplifier (See Figure 4.4.) is used in order to obtain sound pressure levels in driver and passenger ear positions.

Figure 4.4: CCLD Microphone Preamplifier Type 2671, Brüel & Kjær.

4.1.2. Vibration Measurement and Instrumentation

Ears, hand and watch/timer can be subjectively used to sense vibrations. Most of us, however, want a hard number that we can compare to. Transducers, along with a readout instrument, can provide this number.

Ears and hands can be used to detect vibrations subjectively. In engineering, however, a hard number is necessary in order to perform comparison. The transducers can provide this number with a data acquisition instrument.

In this section, equipment used in vibration measurement and vibration measurement techniques are introduced. In addition, the vibration measurement instruments used in this study are presented in this section.

4.1.2.1. Vibration Transducers

One of the sensors that are frequently used in industrial control and automation applications is the proximity sensor. As can be understood from the

standpoint of proximity, proximity is the sensor that sees the presence or proximity of an object. The proximity sensor works by checking for changes in the electromagnetic or electrostatic field. More specifically, the proximity sensor utilizes the eddy current principle.

The proximity probe detects the change in void and, therefore, measures the relative distance or displacement between the probe and the surface finish. The practical maximum frequency perceived by proximity probes is about 1500 Hz. Minimum frequency is 0 Hz - static displacement can be measured [1].

The maximum distances the sensors can control must be known. For example, a sensor with a maximum distance of 2 cm can see the object near 2 cm and send a signal accordingly. However, this sensor may not be able to see objects 2 cm away. Some sensors have pots where the maximum distance can be set.

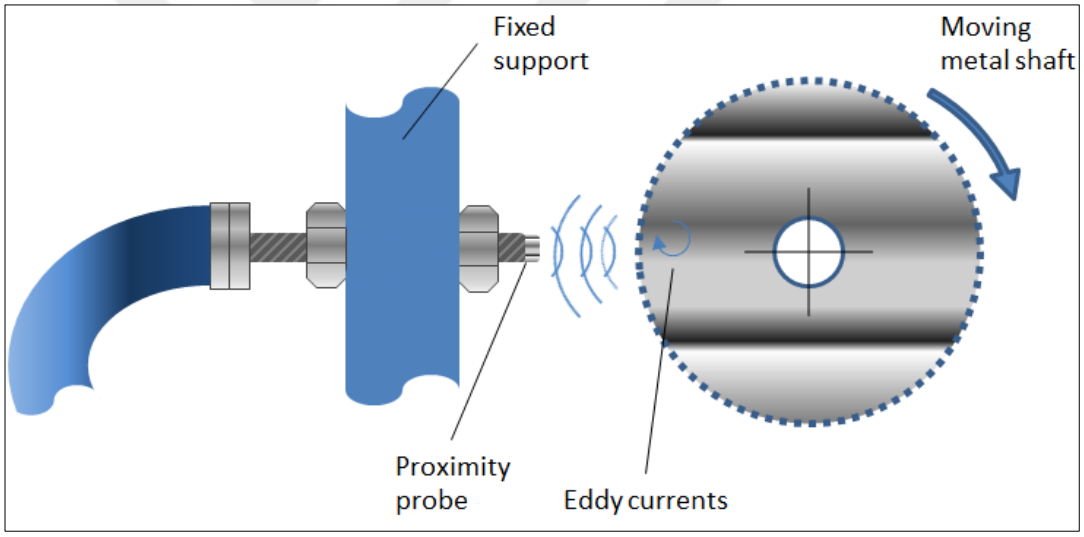

Figure 4.5: Proximity probe principle.

Different types of proximity sensors are used according to the target object's characteristic. An inductive proximity sensor can be used for a metal object. Capacitive or photoelectric sensors can be used for metal, plastics, etc. objects. Proximity sensors are available in many different features with the emerging technology. In general three types of vibration transducers can be listed as displacement transducers, velocity transducers and acceleration transducers. One

of the most common type of displacement transducers is the proximity probe (see Figure 4.5).

Proximity sensors, which are usually in a 3-pin structure, have two DC (+ and -) terminals and a signal terminal on the other end. The logic gives 1 or 0, depending on whether the signaling object is present or absent.

The use of proximity sensors in industrial automation applications is quite common. A moving cismin can be used to check that it has reached the target, or it can be used to check if it is in the position it should be before starting a moving cismin move. It can be used in different areas according to the needs of control applications.

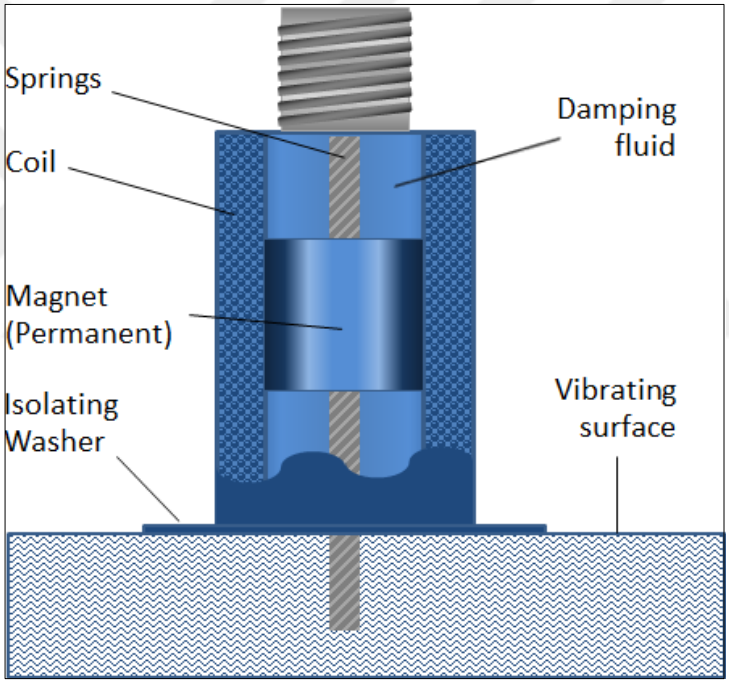

Figure 4.6: Velocity transducer principle.

Velocity transducers are simply the adaptation of a coil in a speaker. Velocity transducers are created by hanging a inner mass (which is a permanent magnet feature) with springs. The cavity in which the inner mass is located is filled with a fluid that is subject to damping which is usually oil [1]. As shown in Figure 4.6, an outer box wire col is installed.

During operation, while the inner mass is suspended on the springs, the cover is held by the vibrating object and moves with the vibrating object. The relative movement between the coil and the permanent magnet produces a voltage that is proportional to the velocity of movement, so it is a voltage reception.

Design of velocity transducers are generally quite heavy and large but also robust. Natural frequencies of a velocity transducer is considered in their design. Generally, lower natural frequencies than their exictation frequency range (generally 10-1000 Hz) are desirable.

It is not applicable to use velocity transducers in lightweight structures. Their remarkable masses cause the system to load up to its own weight and change the vibrational behavior of the structure. Multiaxial transducers are vacant. They are usually located on their base - a tripod is provided which can be adjusted for use on sloped or rough surfaces [1].

Acceleration transducer (or accelerometer) is a device that measures the acceleration applied to a structure. Coordinate acceleration (reference acceleration) need not be known in the measurement of the applied acceleration. Instead, the accelerometer looks at the applied forces on the reference axis to the test mass in it, originating from the mass. For example, if the accelerometer shows a value of 9.81 m / s^2 on a flat surface in a region close to sea level on the world, the value it will show on a free falling object or in free space will be 0 m / s^2.

Accelerometers are used in many fields of application in industry and scientific studies. High-sensitivity accelerometers are one of the most important components used in tunnels, airplanes, ships and submarines navigation systems. Besides, it detects the vibration in the rotating machines and observes the limits within which the vibration takes place. Today, tablet computers and digital cameras are used in the introduction of anti-vibration systems, in image clarification and in the activation of user-sensitive systems.

The most common acceleration transducer type is the piezoelectric accelerometer (See Figure 4.7).

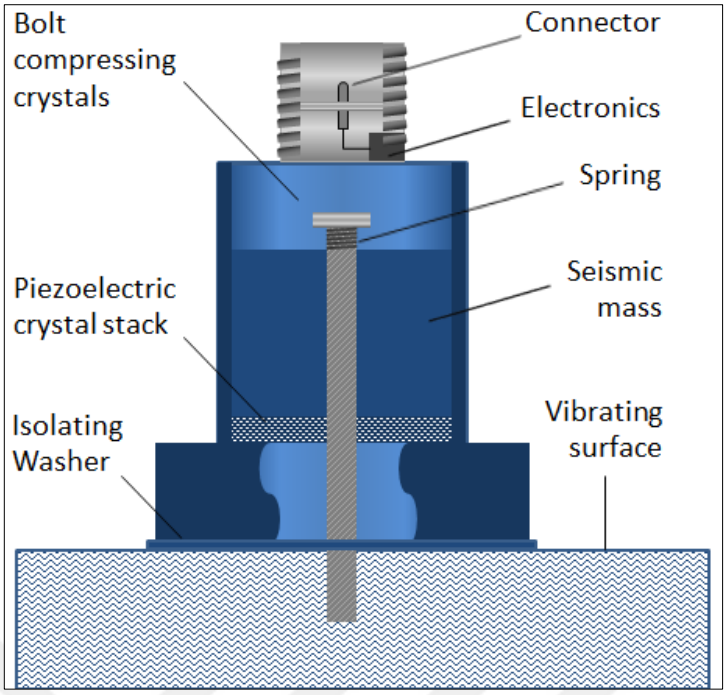

Figure 4.7: Piezoelectric accelerometer principle.

The piezoelectric accelerometer includes a quartz crystal (or barium titanate - a manufactured quartz) on top with a mass bolt. During the operation, case of the accelerometer is held against the vibrating object and the mass is inclined to remain constant in space. In piezoelectric accelerometers, the effective element is piezoelectric material. One side of the piezoelectric material is attached to the fixed body. The central mass is held on the other side of the material. When the force depended to the acceleration is applied, the piezoelectric material changes shape and an electrical output is generated. The produced load is proportional to the applied force and therefore to the acceleration. The signal generated by using the signal shaping circuits and amplifiersis converted to voltage.

The accelerometer self-generates the signal output bu the signal has high impedance and can not be used by most analyzers. The output impedance of the accelerometer must be coherent to the impedance of the data acquisition device. The output signal of the accelerometer must be converted by a special electronics into a low impedance signal. This electronic circuit might be integrated with the accelerometer or may be outside the accelerometer [1].

An accelerometer can not only measure structural accelerations but also measure gravity. Hence, accelerometry does not have to be accelerating or slowing down in order to be able to take measurements. Accelerometers measure the specific gravity or g-force per unit mass or weight. The accelerometer is the only transducer that can accurately detect pressure wave vibrations at high frequencies.

Most accelerometers can not show the value of their measurements, but they provide information to other devices. Accelerometers have a working frequency, which limits how rapid they will respond to an acceleration change.

Single and multiple axis accelerometer models are available, which measure the magnitude and direction of the magnitude of the vector as a vector magnitude and can be used in the measurement of orientation (because the direction of the weight changes) and acceleration measurement, vibration, narrowing, and falling.

Another type is capacitive accelerometers. There is a capacitive effect between two parallel plates close to each other and a capacitance value appears. In this type of accelerometers, capacitive transmission principle is used. If an acceleration is applied, the distance between the fixed electrode and the moving electrode will change and the capacity value will be changed. As a result, an acceleration related output value will be obtained.

Like velocity transducers, natural frequencies of a accelerometer is considered as well in their design.

Acceleration sensors are divided into analog and digital outputs. Analog acceleration sensors give continuous voltage to the output of the voltage. The digital acceleration sensors give modulated output values according to the application area. Features to consider when selecting acceleration sensors:

- Number of axes: As is known, acceleration sensors must have more than one axis to control the movement. 2 and 3 axis are widely used in the market.
- Sensitivity: Depending on the importance of measurement, low sensitivity or high acceleration sensors can be preferred. Accelerating acceleration sensors can give a lot of reaction even with a small change in acceleration.

- Bandwidth: In order to detect acceleration changes in a slow moving system, the bandwidth should be 50 Hz and 100 Hz at high speed.
- Impedance: The impedance of the output element of the applied system must match the applied acceleration [56].

One of the Brüel & Kjær brand accelerometers used in this study is shown in Figure 4.8.

Figure 4.8: Triaxial DeltaTron accelerometer type 4529-B, Brüel & Kjær.

4.1.2.2. Modal Hammer

Modal hammer is a test instrument which applies a force pulse to excite a structure. It is primarily used in Modal Laboratory when an assessment of the range of frequency of the structural modes is made.

Impact hammer is used to determine impact forces on vehicle chassis, engine block and various medium and small sized parts. The reaction forces of the surfaces induced by Impact hammer can be calculated with the help of accelerometers. The frequency response functions of the surfaces and structures tested can be obtained using multichannel FFT analysis capable measurement systems. Impact hammer has three impact tips, aluminum, plastic and rubber, which can be changed according to pulse width, amplitude and bandwidth. The modal hammer used in this study is shown in Figure 4.9.

Figure 4.9: ICP impact hammer model 086C41, imi sensors.

4.1.2.3. Modal Exciter (Shaker)

Modal exciter was not used in this study and only general information is given in this heading.

A shaker is a device used in vibration testing in order to excite the structure either for durability testing or modal testing (see Fig. 4.10). The natural frequencies and modes of the excited components can be determined using such shakers.

Figure 4.10: A typical modal exciter (Brüel & Kjær,type 4824).

4.1.2.4. Data Acquisition Device

Data acquisition devices are used to perform FFT analysis. A typical data acquisition device collects the acceleration and force data from accelerometers and the impact hammer, and also calculates the frequency response of the surface.

In this study, LMS SCADAS Recorder01 was used for data acquisition and it is shown in Figure 4.11.

Figure 4.11: LMS SCADAS Recorder01 data acquisition device.

4.2. Transfer Path Analysis on Prototype Vehicle

In Transfer Path Analysis, sources and receivers are considered as two separate subsystems. For structural transfer path analysis, these two subsystems are interconnected by a number of rigid connections called transfer paths. Depending on the design of the driveline and the driving options (front, rear and four-wheel drive), the possible transfer paths consist of elements such as engine, gearbox, gearbox and exhaust connections. In the case of air-way transfer, the engine intake manifold, exhaust pipes and vibrating panes constitute transfer paths.

The Transfer Path Analysis method takes the Frequency Response Function (FRF) between the receiver and inputs (force and volumetric velocities) applied at various energy source points, and combines the inputs from these operational conditions. In operational conditions, the sound pressure level in receivers can be specified by the superposition of partial results.

The vibro-acoustic transfer function is most commonly measured by excitation with impact or shaking. (In this study, the stimulus with the impact attractor was used). Acoustic transfer function is obtained by using volumetric velocity source. Operational inputs are determined by calculating experimental data, analytical simulation or indirectly. There are therefore three types of data groups. These are operational data (forces, volumetric velocities, accelerations and pressures), frequency response functions, and complex dynamic stiffness data at connection points.

Operational data should be collected from many points depending on the number of channels of the measuring system. Since it is not so easy to synchronize the different measurements with each other, it is important to associate the measurements with a reference measurement channel.

For all transfer paths, the source / receiver transfer functions need to be identified. The corresponding acceleration FRFs can be measured using a hammer or shaker from the transfer paths on the sides of the receivers. In order to measure the acoustic FRF, the volumetric velocity source must be used. Vibro-acoustic FRF (between force and pressure) can be measured directly using a hammer or shaker, or reversibly by means of a volumetric speed source. During the measurement of these FRFs, it should be considered that the source side is separated by the receiver. Performing operational measurements at the points where the receivers are located will also be appropriate in terms of verifying the total contribution of the receivers to the system on all transfer paths [16].

4.2.1. Vibration Transfer Function (VTF) via Hammer Test

In this study, VTF analysis was performed with the acceleration values obtained from the accelerometer placed at certain points of the vehicle, by giving impacts with modal hammer at certain points of the prototype vehicle. In this section, the impact points and the accelerometer points are introduced.

The data acquisition device has 24 channels. The triaxial accelerometer has 3 outputs (cartesian coordinates). Since one channel goes to the modal hammer, maximum 7 accelerometers can be connected to the data acquisition device in a batch. In this study, there are different batches according to the impact area and accelerometer areas. Due to symmetry of the vehicle, only one side of the subsystems were tested.

In chapter 3, 19 different transfer paths were introduced. Since it is a correlation study, same transfer paths were evaluated on the prototype vehicle. This section provides an overview of how impacts are placed and how accelerometers are positioned.

Figure 4.12: Front axle region (passenger side) of the prototype vehicle.

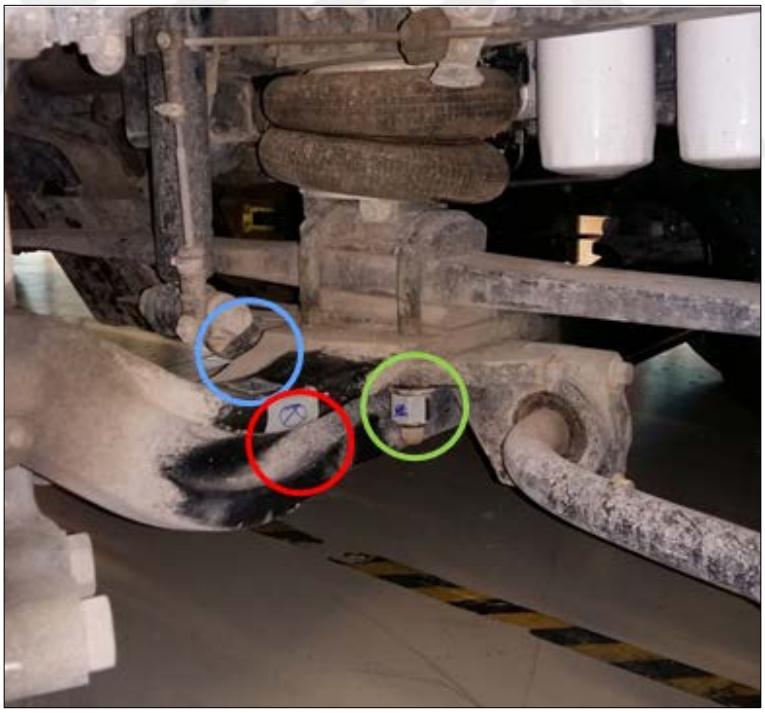

Figure 4.13: Impact points on front axle for transfer path 1 and 2.

It is possible to impact in 3 directions (x, y, z) on a single impact point (grid) selected in the CAE. However, in the prototype vehicle, it is almost impossible to make an impact in three directions from a single point due to both access problems

and the geometry of the surface of the parts. Therefore, when impact is applied to a point with the impact hammer, the closest points around the selected point where the desired impact (x, y, z) can be imparted smoothly are selected. Three different impact points for x, y and z directions are given for transfer paths, in Figures from 4.14 to 4.32.

Figure 4.14: Impact on X direction for transfer path 3.

Figure 4.15: Impact on Y direction for transfer path 3.

Figure 4.16: Impact on Z direction for transfer path 3.

Figure 4.17: Impact on X direction for transfer path 4.

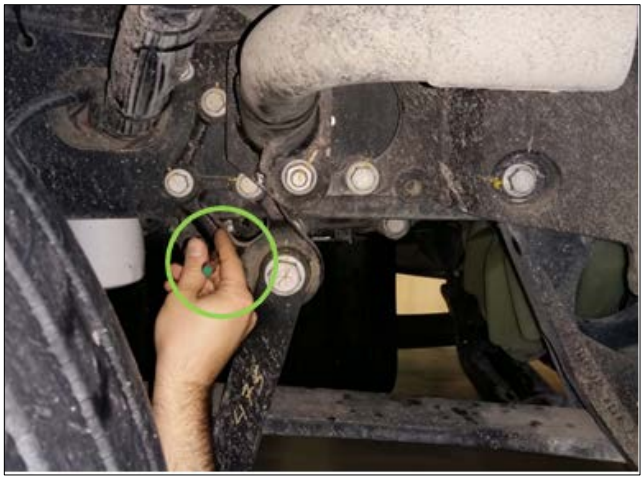

Figure 4.18: Impact on Y direction for transfer path 4.

Figure 4.19: Impact on Z direction for transfer path 4.

Figure 4.20: Impact on X direction for transfer path 5.

Figure 4.21: Impact on Y direction for transfer path 5.

Figure 4.22: Impact on Z direction for transfer path 5.

Figure 4.23: Impact on X direction for transfer path 6.

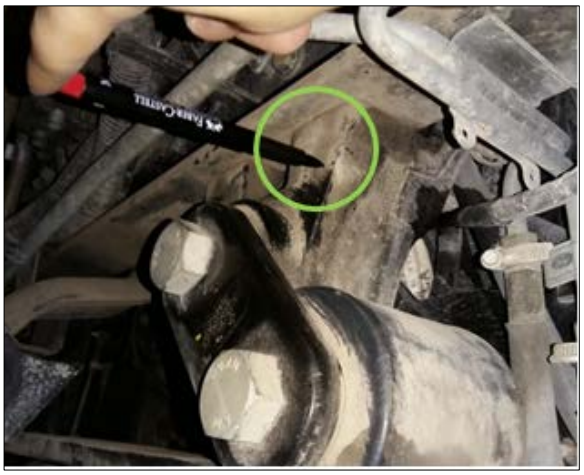

Figure 4.24: Impact on Y direction for transfer path 6.

Figure 4.25: Impact on Z direction for transfer path 6.

In transfer path 7, the impacts were given as shown in Figure 4.26. The red and blue circles represent the impacts on X and Z directions respectively and the green arrow represent the impact on Z direction.

Figure 4.26: Impacts for transfer path 7.

In the transfer path 9, impacts were given on the shock absorber as shown in Figure 4.27. The green and blue circles represent the impacts on Y and Z directions respectively and the red arrow represent the impact on X direction. In the transfer

path 11, impacts were given on the rear shock absorber as similar with the transfer path 9.

Figure 4.27: Impacts for transfer path 9.

In transfer paths 8 and 10, the impact were given on the brackets that connect the air suspensions on rear axle with the chassis frame. The impacts for transfer path 10 were given as shown in Figure 4.28. The red, green and blue circles represent the impacts on X, Y and Z directions respectively.

Figure 4.28: Impacts for transfer path 10.

In transfer path 12, there is an air suspension. Since geometry of the air suspension, the impacts were given in the same way as impact (see. Figure 4.29).

Figure 4.29: Impacts for transfer path 12.

As mentioned earlier, the engine mounts remain behind the chassis frame, so they can not be reached on the prototype vehicle. For this reason, the impacts to be given to the engine mounts are given from the points where the engine mounts are connected to the chassis frame. In the transfer path 13, the X, Y, and Z impacts on the rear engine mount are shown in Figure 4.30, 4.31 and 4.32 respectively.

Figure 4.30: Impact on X direction for transfer path 13.

Figure 4.31: Impact on Y direction for transfer path 13.

Figure 4.32: Impact on Z direction for transfer path 13.

In transfer path 15, the upper part of the exterior step (connected to the cabin) was excited.

Exterior step consists of plastic parts, cast steps and metal skeleton. In order to avoid mode of the plastic parts, the accelerometer was placed in the casting section of exterior step. Again for the same reason, impact was given to the metal skeleton of the exterior step. The impacts are shown in Figure 4.33. (X, Y and Z impacts are represented with red, green and blue circles respectively).

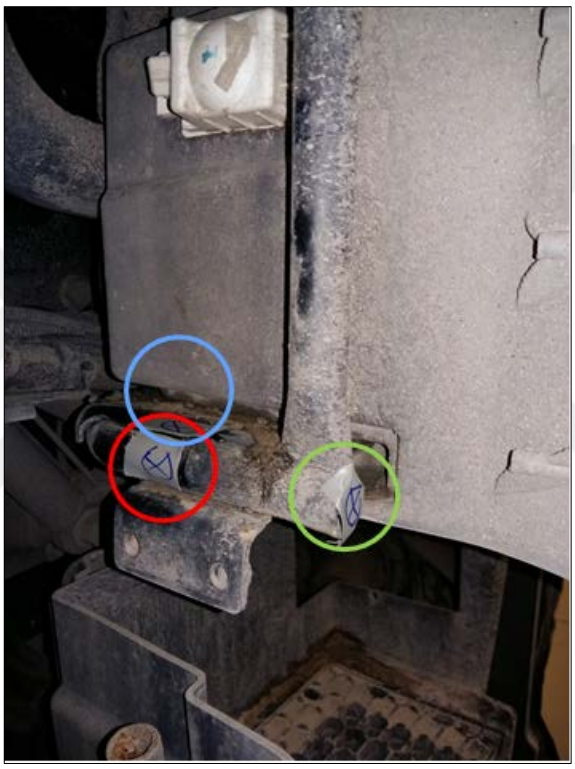

Figure 4.33: Impacts for transfer path 15.

As mentioned before, in vibrational transfer paths 16 and 17 (see Figure 3.26), the vibrations reaching the car cabin were examined. The vibration responses were collected from 6 different locations. These places are steering hub, driver and passenger seat connections and cab lift. These places and the accelerometers are shown in Figure 4.34, 4.35 and 4.36 respectively.

Figure 4.34: Steering wheel hub and the accelerometer.

Figure 4.35: Passenger seat pedestal and the accelerometer.

Figure 4.36: Cablift and the accelerometer.

In transfer path 16 and 17, the impacts were given on the front and the rear cabin air suspensions respectively. The front cabin air suspension is connected via the cabin ARB (anti-roll bar) and it is shown in Figure 4.37.

Figure 4.37: Cabin ARB (anti-roll bar).

In the transfer path 16, the X, Y, and Z impacts on the cabin ARB (anti-roll bar) are shown in Figure 4.38, 4.39 and 4.40 respectively.

Figure 4.38: Impact on X direction for transfer path 16.

Figure 4.39: Impact on Y direction for transfer path 16.

Figure 4.40: Impact on Z direction for transfer path 16.

In the transfer path 17, the X, Y, and Z impacts on the rear cabin air suspension bracket are shown in Figure 4.41, 4.42 and 4.43 respectively.

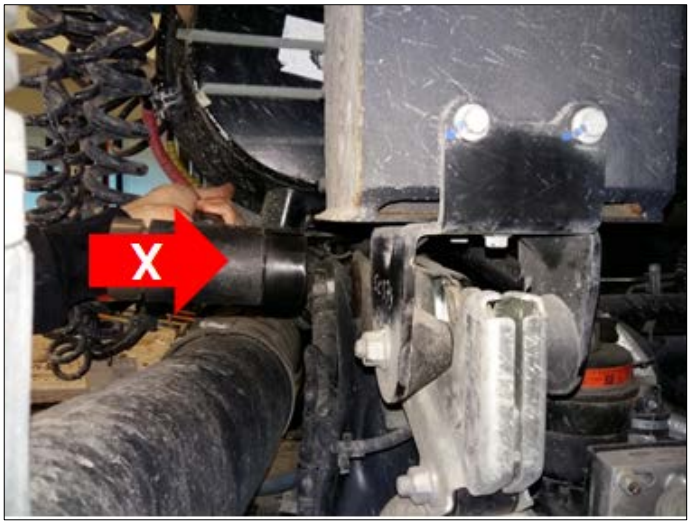

Figure 4.41: Impact on X direction for transfer path 17.

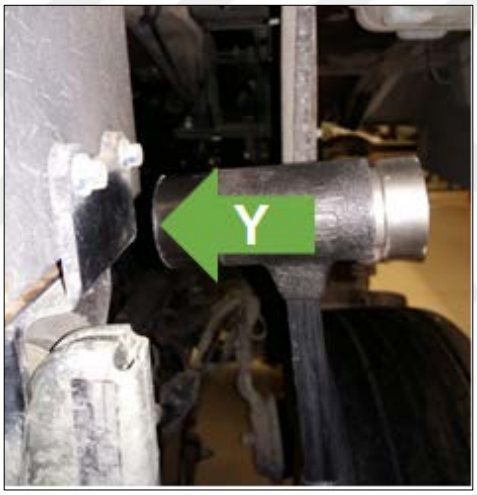

Figure 4.42: Impact on Y direction for transfer path 17.

Figure 4.43: Impact on Z direction for transfer path 17

Finally, the impacts on the V-arm bushing for transfer path 18 and 19 are shown in Figure 4.44.

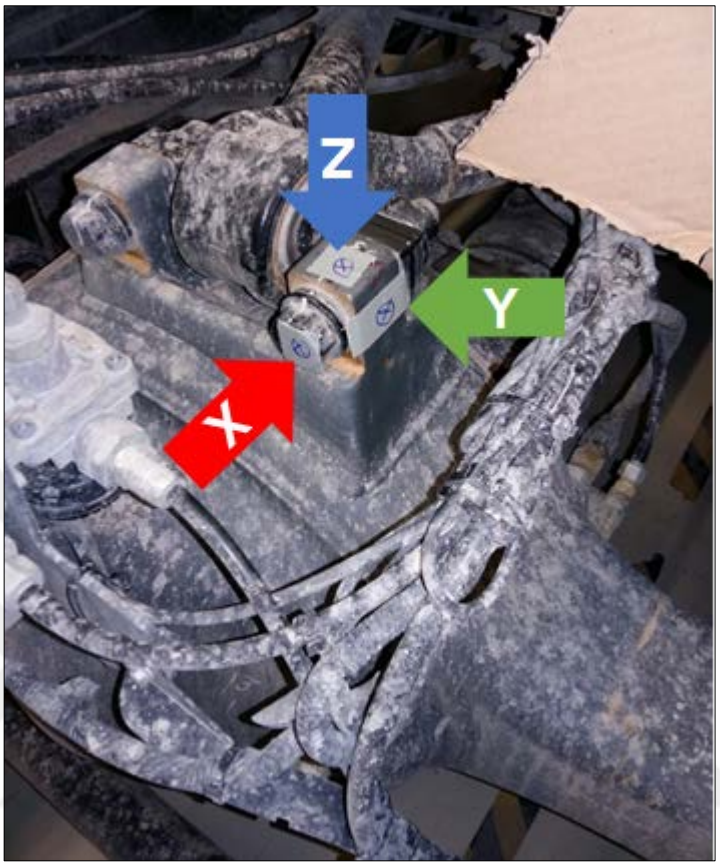

Figure 4.44: Impacts for transfer path 18 and 19.

4.2.2. Noise Transfer Function (NTF) via Hammer Test

A transfer function between two points, which defines how noise (pressure) at a point will respond to a vibratory input (force) at a given second point, as a function of frequency. In the vehicle NTF measurements, the noise is usually measured at the driver's and passenger ear positions with input(s) provided at the engine mount and suspension body attachment points. Units of Pascal/Newton are often used.

As mentioned in section 4.2.1, the cabin mounts on the passenger side were impacted and sound pressure level (SPL) responses at the driver and passenger ear

coordinates were collected. Microphones were placed in the cabin in order to corresponding to the driver's left ear and the passenger’s right ear (see Figure 4.45).

Figure 4.45: NTF test microphones in vehicle cabin.

During the noise measurement, all environmental sounds (e.g. sound from air conditioning) were blocked in order to obtain accurate measurement.

The cabin mounts on the passenger side were impacted and sound pressure level (SPL) responses at the driver and passenger ear coordinates were collected.

5. CORRELATION AMONG CAE AND TEST RESULTS

In this section, the results of the last iteration from the iterations made to ensure the correlation between the CAE and the test are given. The RMS values of the three-way acceleration results obtained in the test with both CAE and modal hammer were used. RMS values are used because of the large number of transfer paths and because the vehicle model is too large and complex. Again for the same reason, the results are logarithmic.

In graphs, the vertical axis shows the amplitude value (rms of accelerations) and the vertical axis shows the frequency value. Due to the company's privacy policy, the values on the graph's vertical axis are hidden.

5.1. VTF Correlation Results

In this section, VTF correlations are given for each response of 19 transfer paths previously described. Because of the large number of responses, all impact states (x, y, and z) for a response are shown together in a graph. The dashed lines show the test results and the continuous lines show the CAE results. The red, green, and blue colors represent impacts in the x, y, and z directions, respectively.

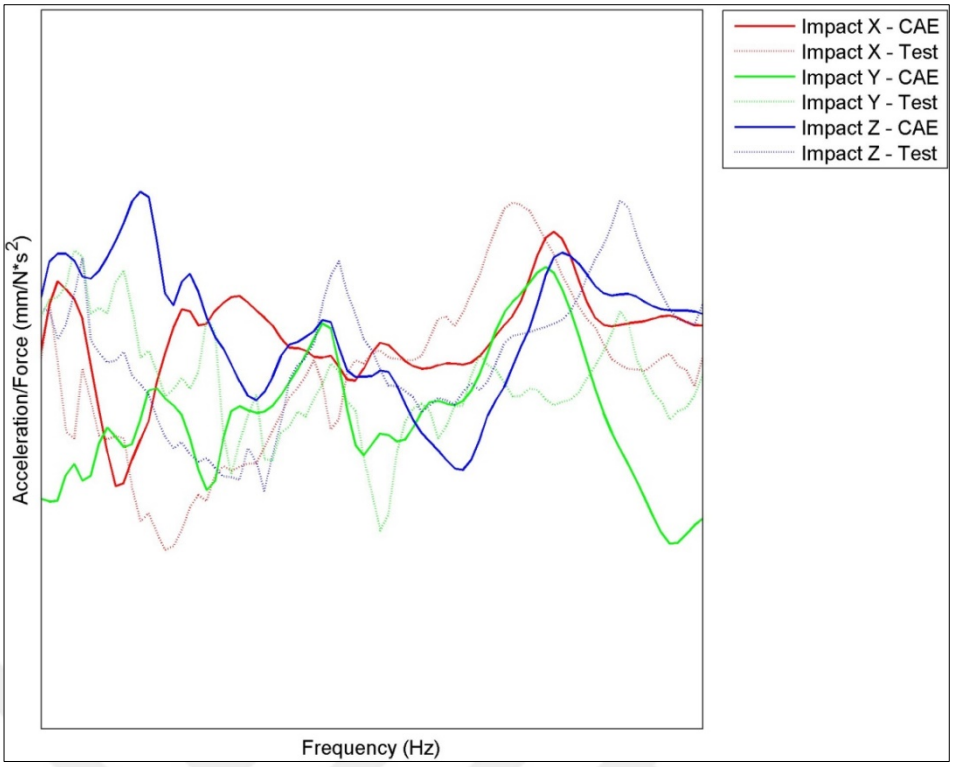

Figure 5.1: VTF correlation for transferpath1 response1.

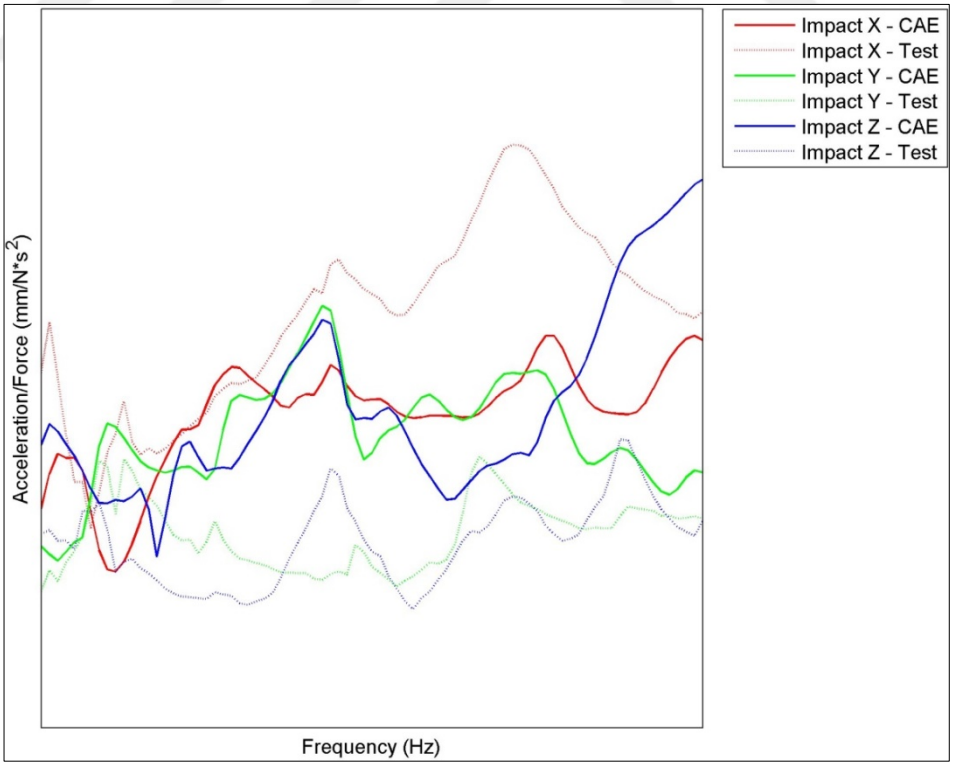

Figure 5.2: VTF correlation for transferpath1 response2.

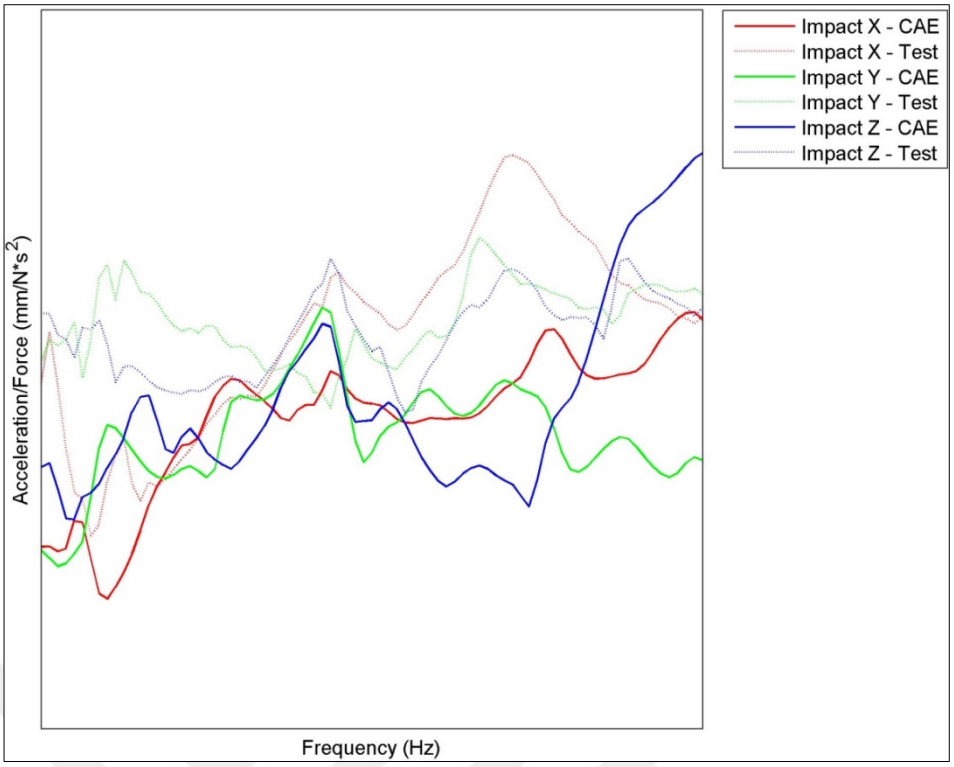

Figure 5.3: VTF correlation for transferpath1 response3.

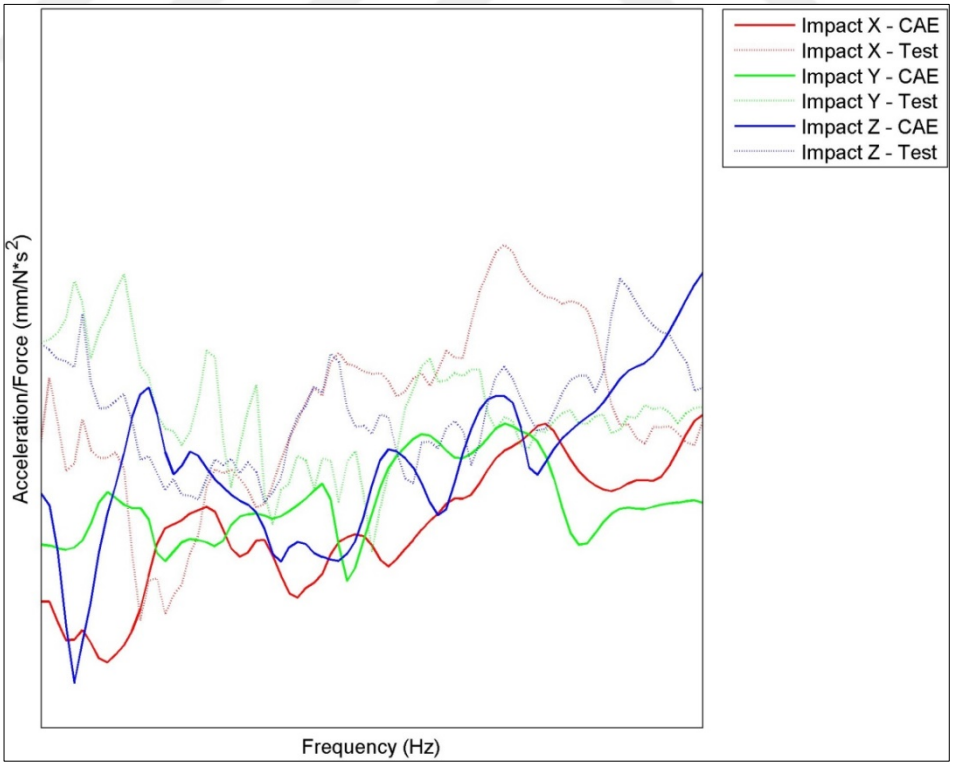

Figure 5.4: VTF correlation for transferpath1 response4.

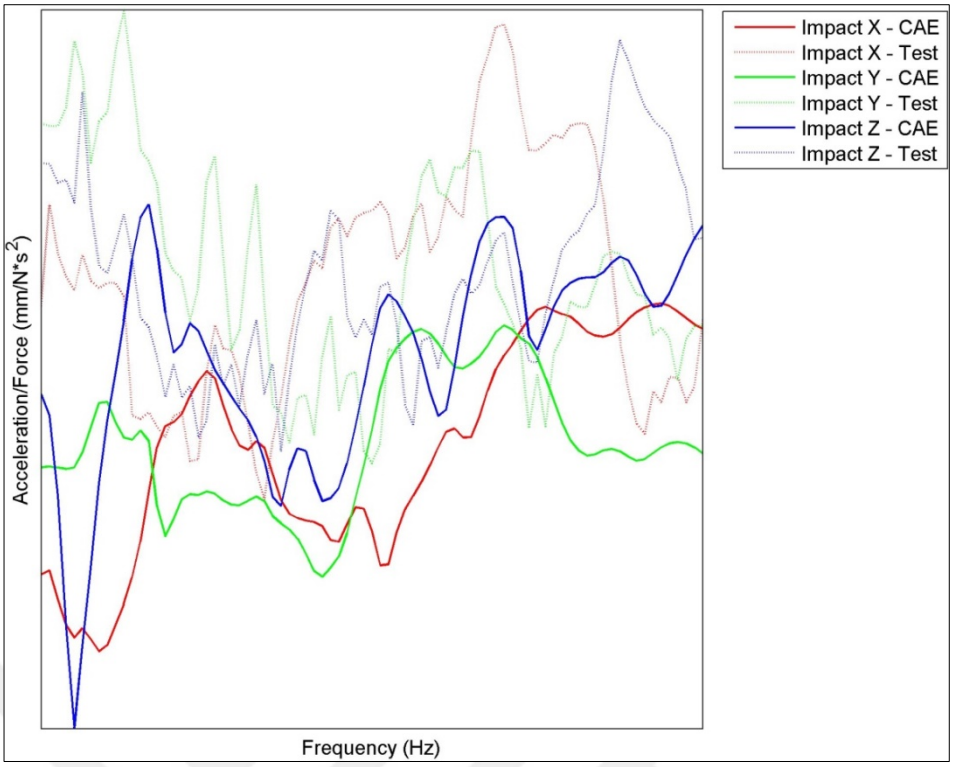

Figure 5.5: VTF correlation for transferpath1 response5.

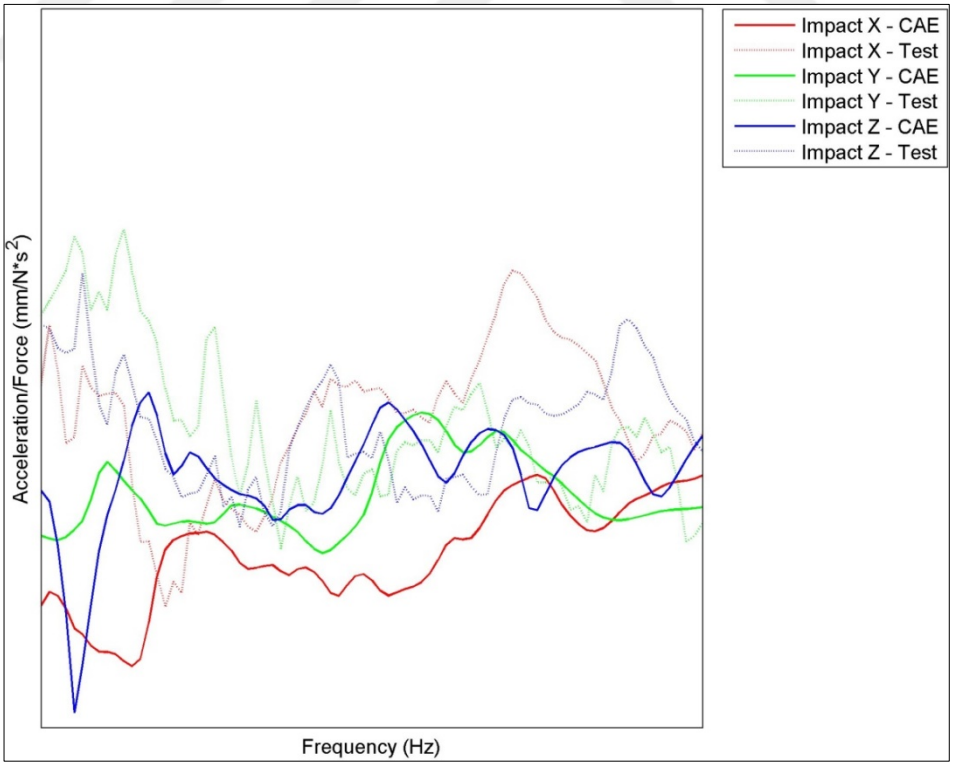

Figure 5.6: VTF correlation for transferpath1 response6.

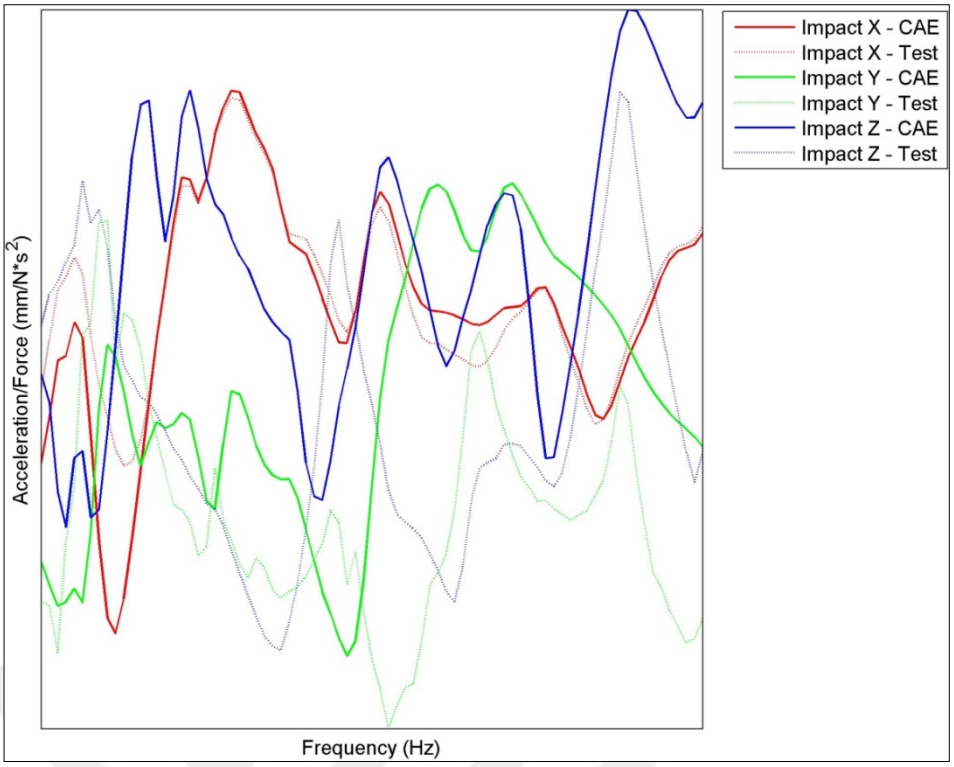

Figure 5.7: VTF correlation for transferpath1 response7.

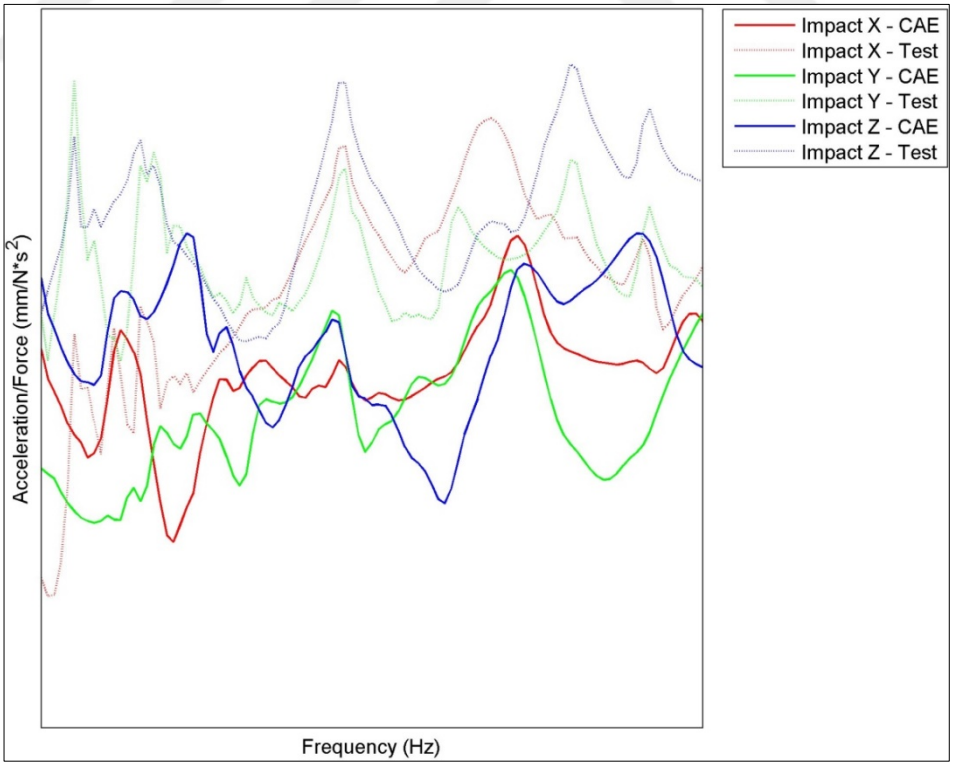

Figure 5.8: VTF correlation for transferpath2 response1.

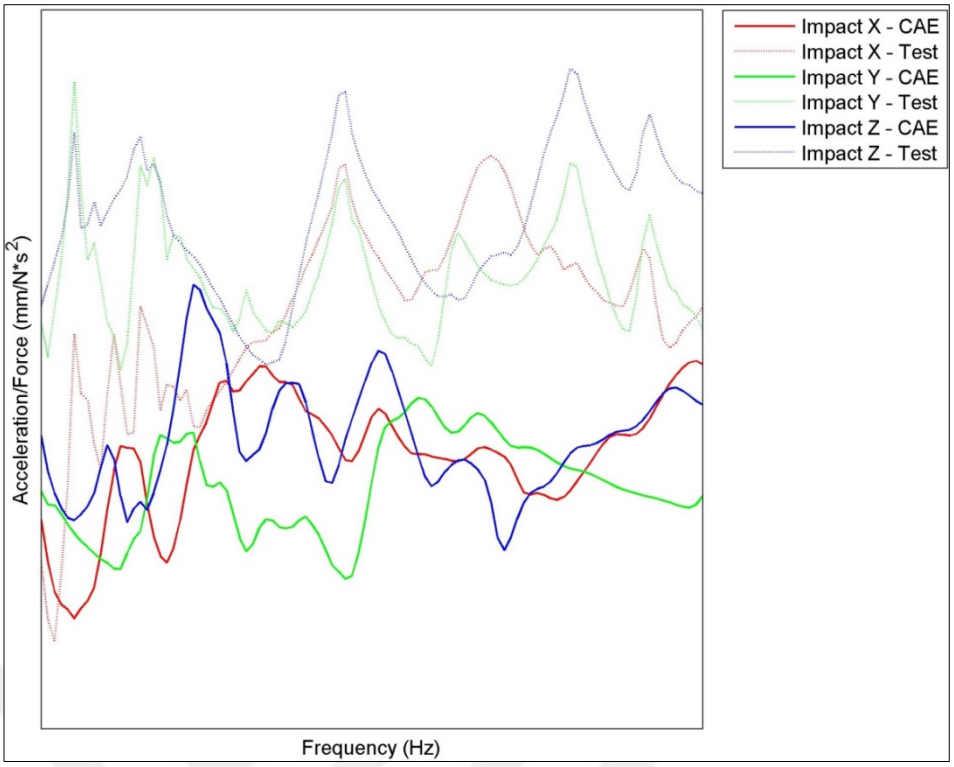

Figure 5.9: VTF correlation for transferpath2 response2.

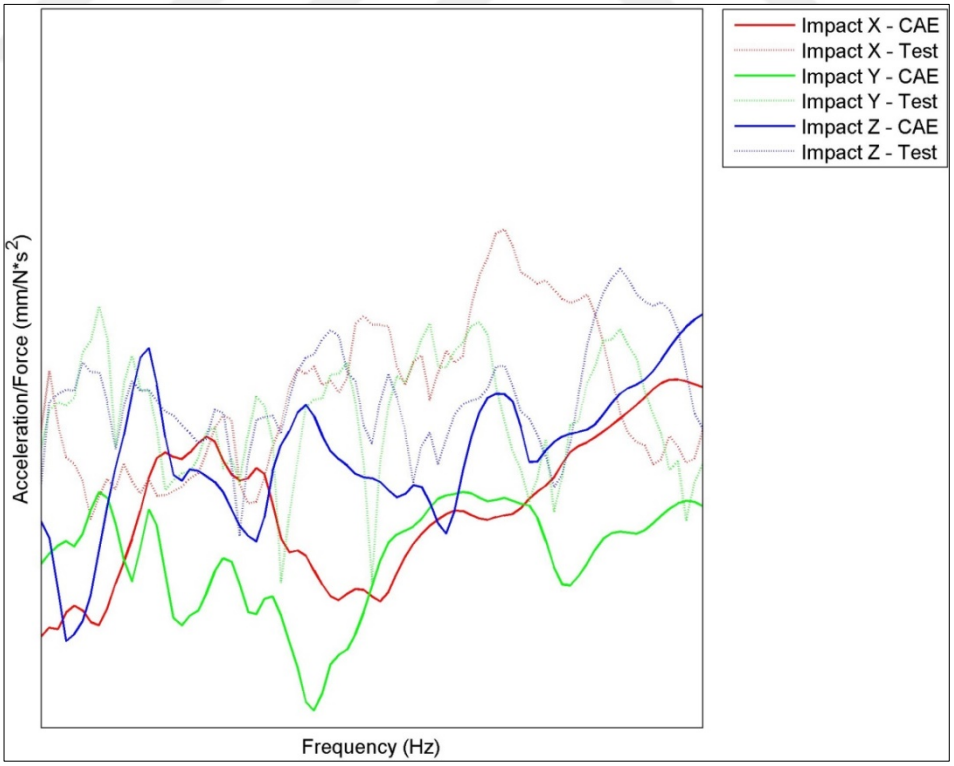

Figure 5.10: VTF correlation for transferpath2 response3.

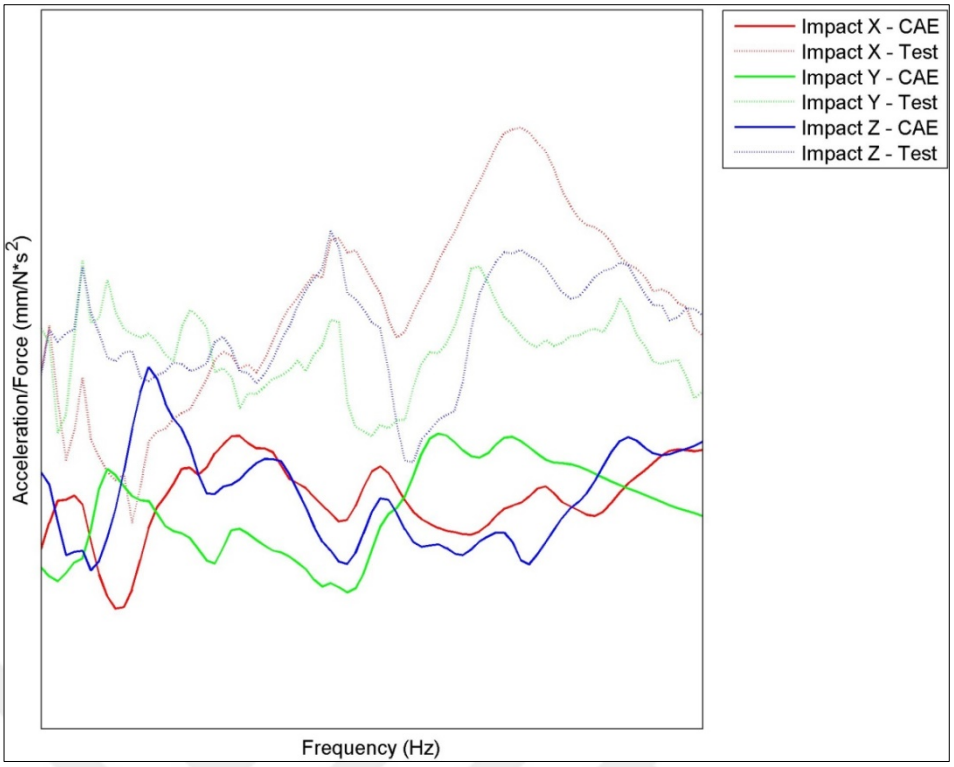

Figure 5.11: VTF correlation for transferpath2 response4.

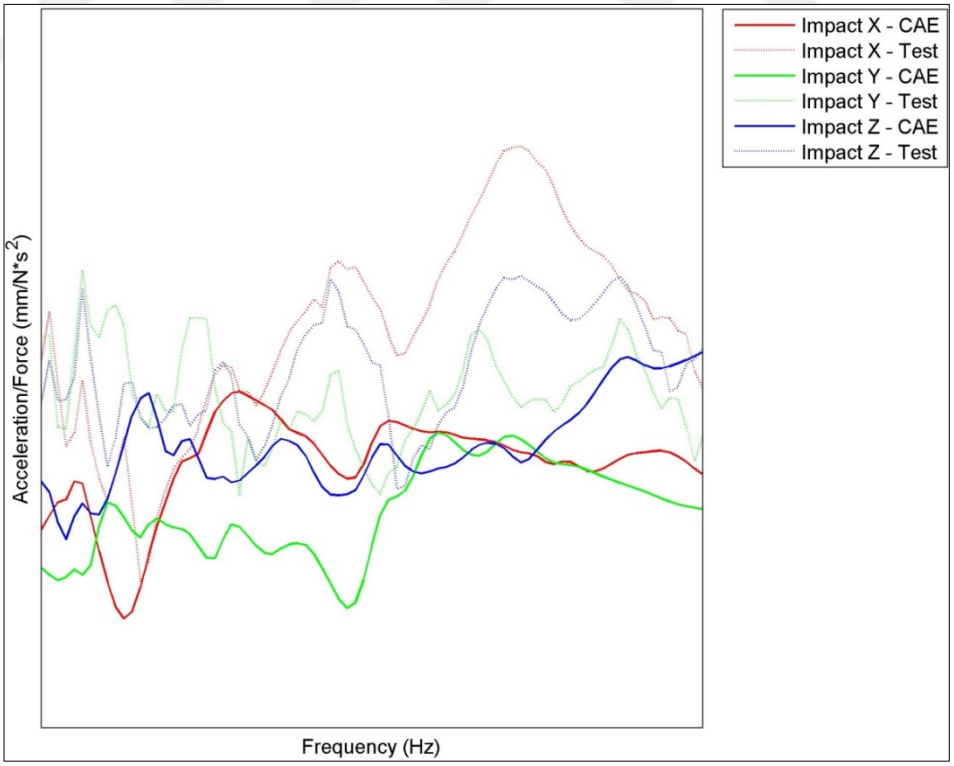

Figure 5.12: VTF correlation for transferpath2 response5.

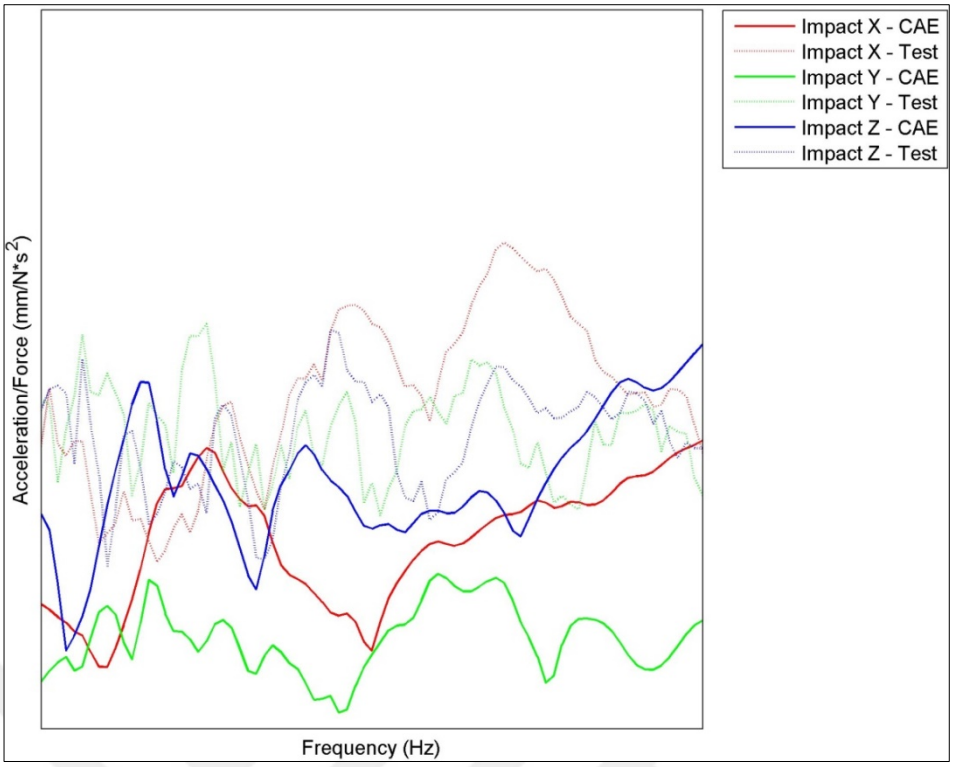

Figure 5.13: VTF correlation for transferpath2 response6.

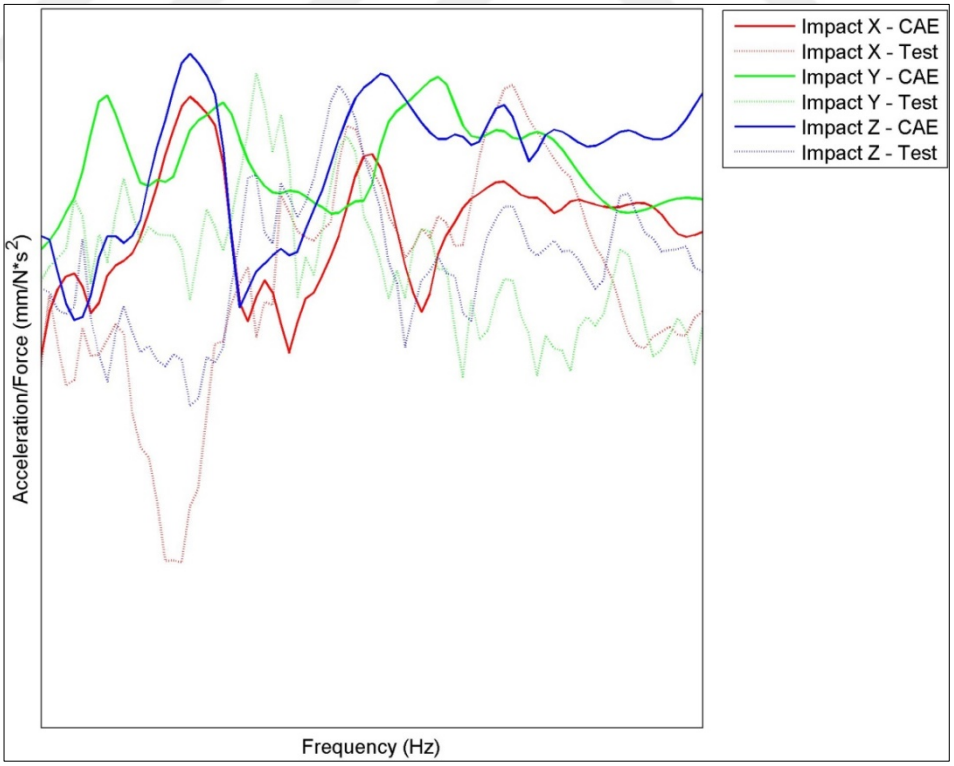

Figure 5.14: VTF correlation for transferpath2 response7.

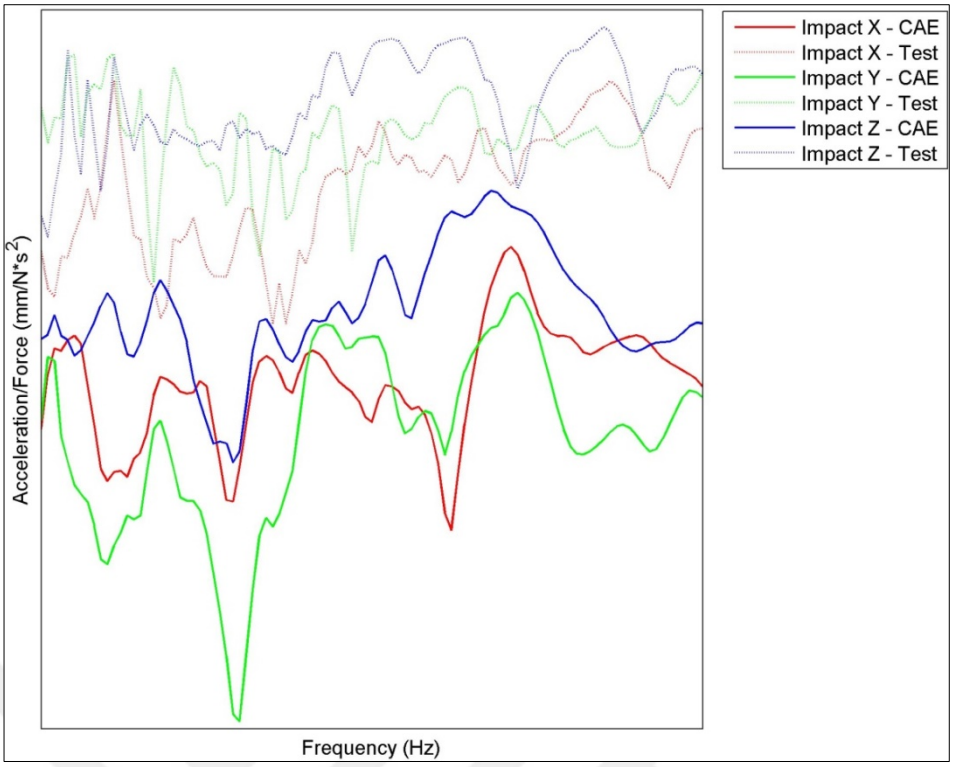

Figure 5.15: VTF correlation for transferpath3 response1.

Figure 5.16: VTF correlation for transferpath3 response2.

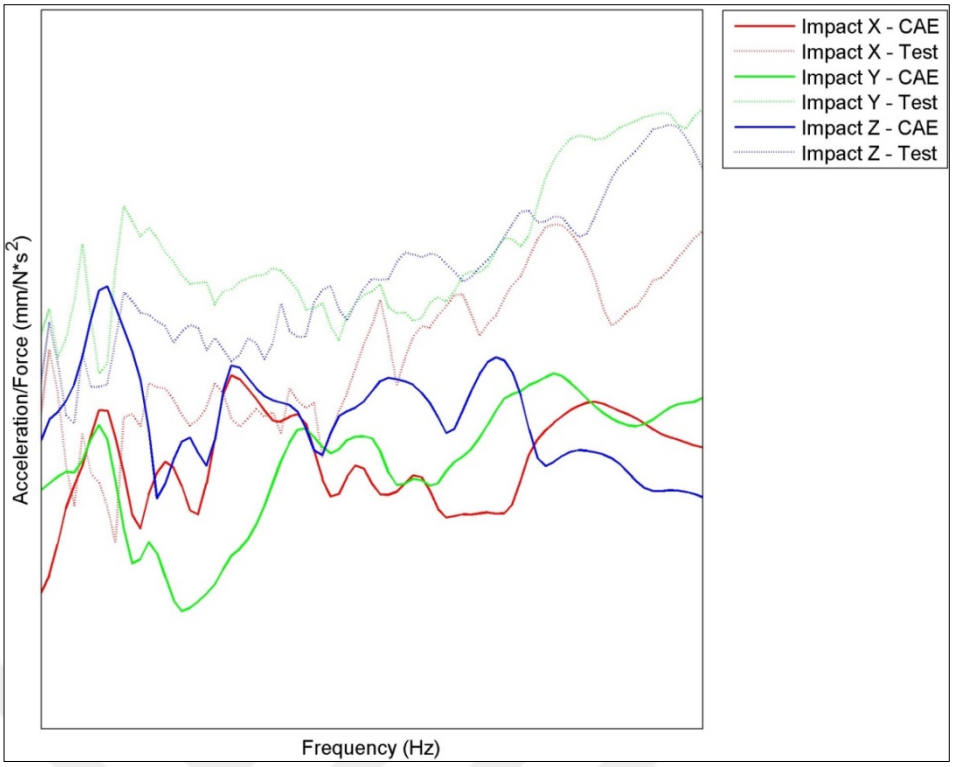

Figure 5.17: VTF correlation for transferpath3 response3.

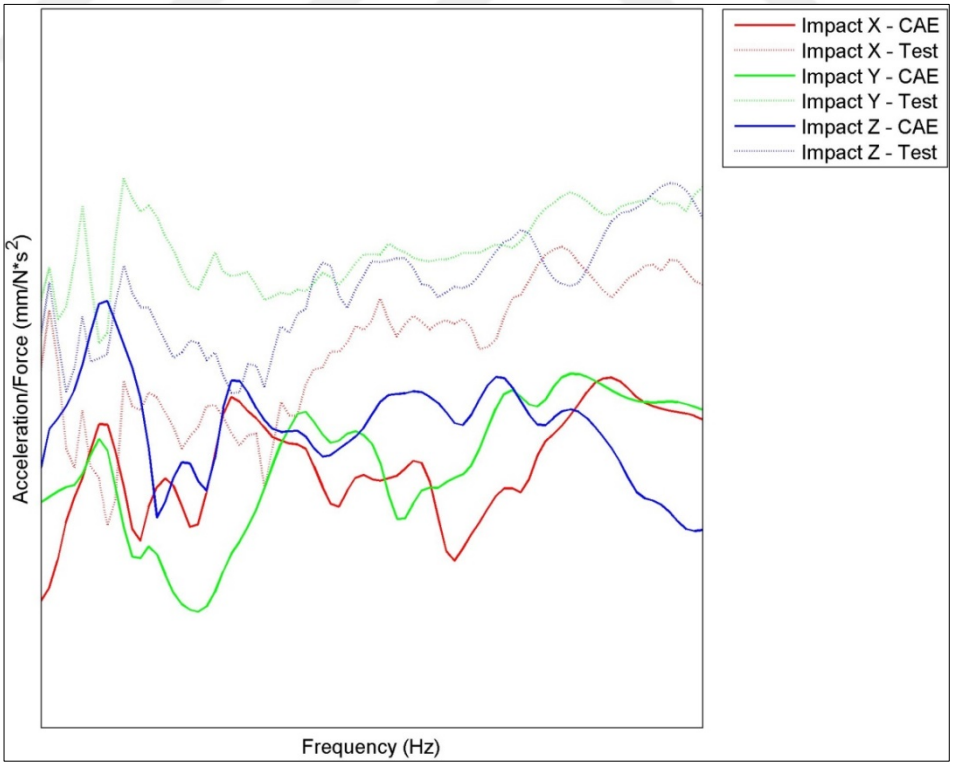

Figure 5.18: VTF correlation for transferpath3 response4.

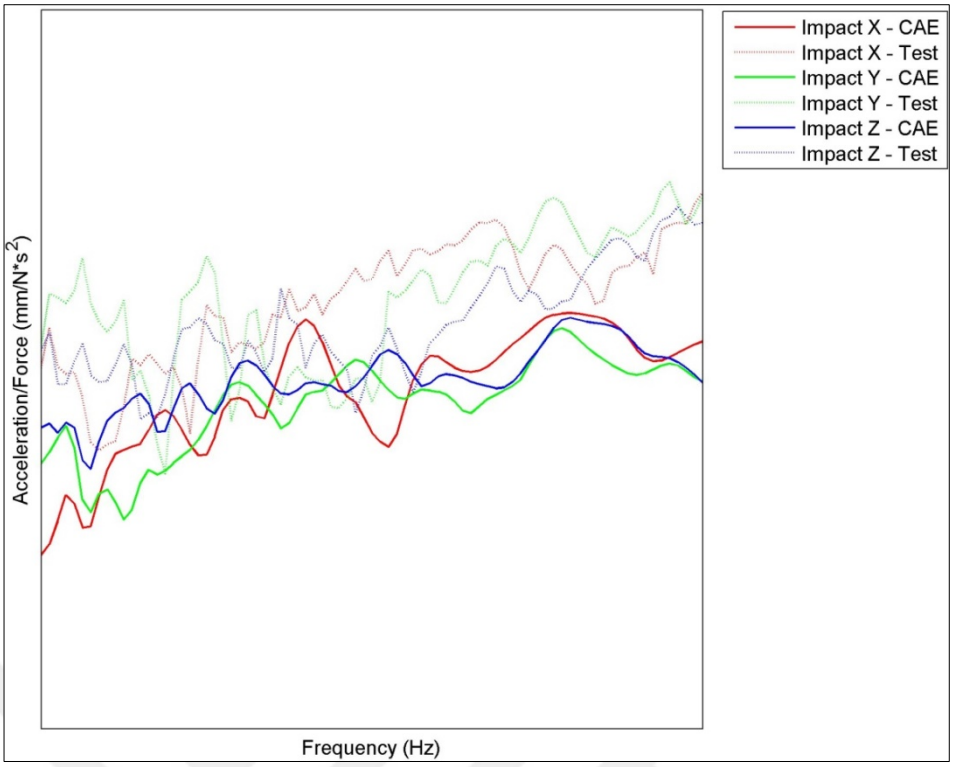

Figure 5.19: VTF correlation for transferpath3 response5.

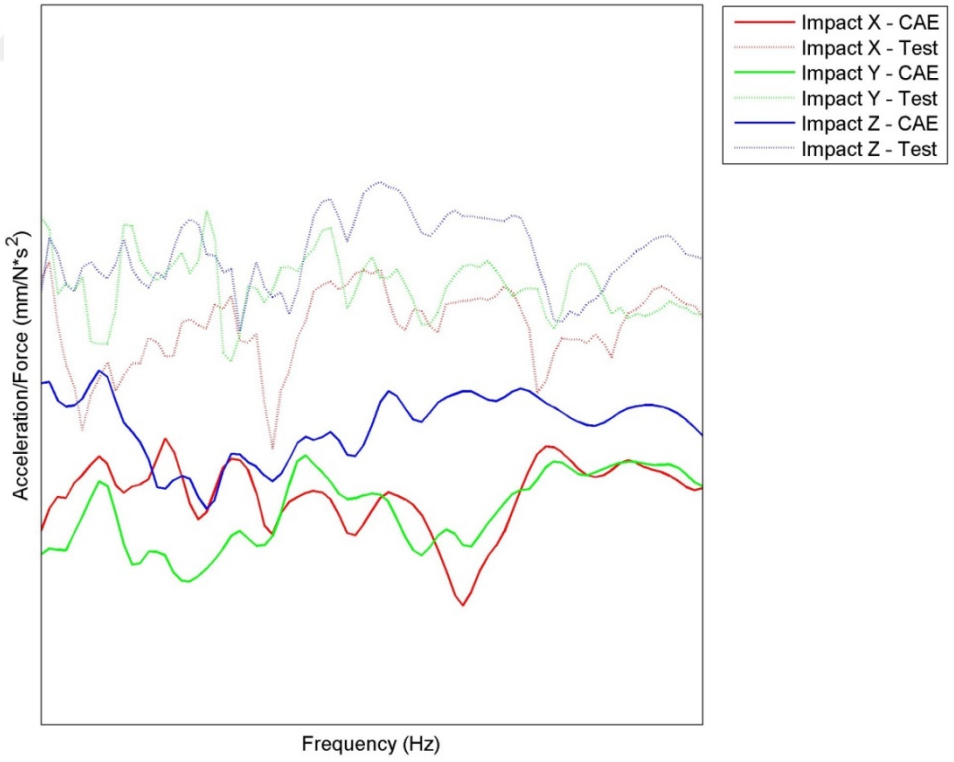

Figure 5.20: VTF correlation for transferpath3 response6.

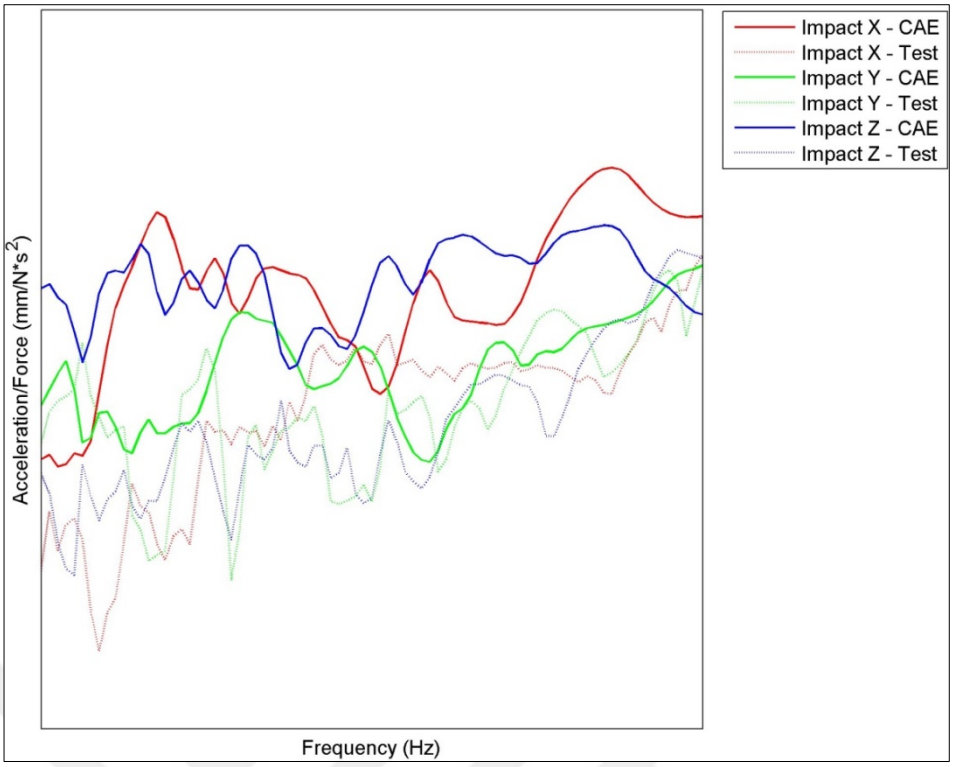

Figure 5.21: VTF correlation for transferpath3 response7.

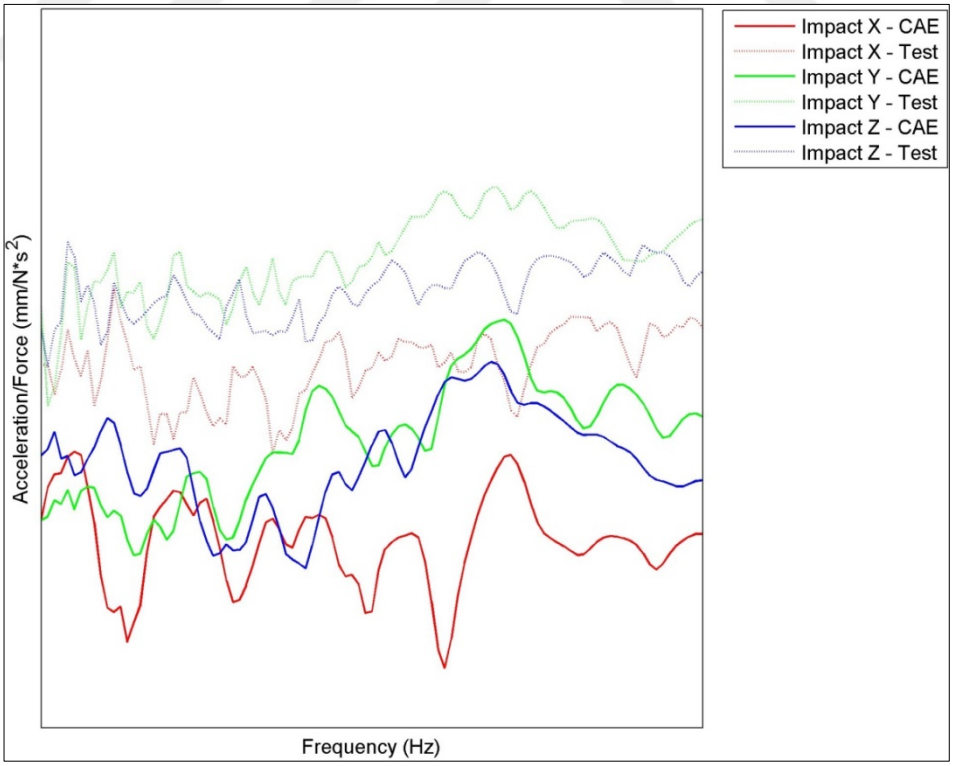

Figure 5.22: VTF correlation for transferpath4 response1.

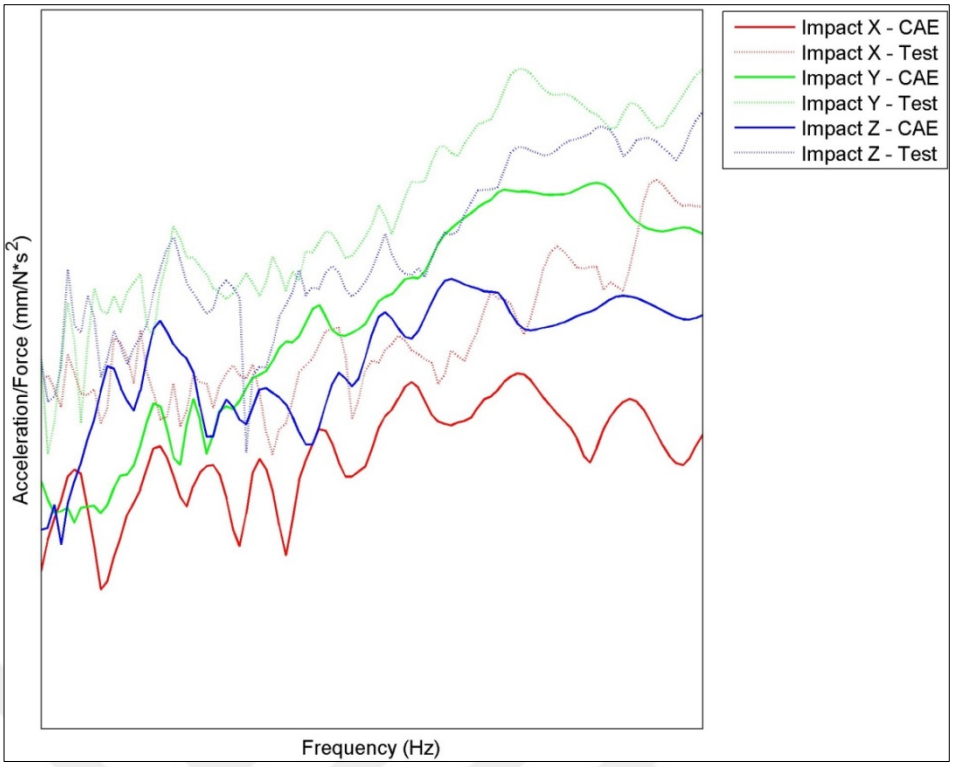

Figure 5.23: VTF correlation for transferpath4 response2.

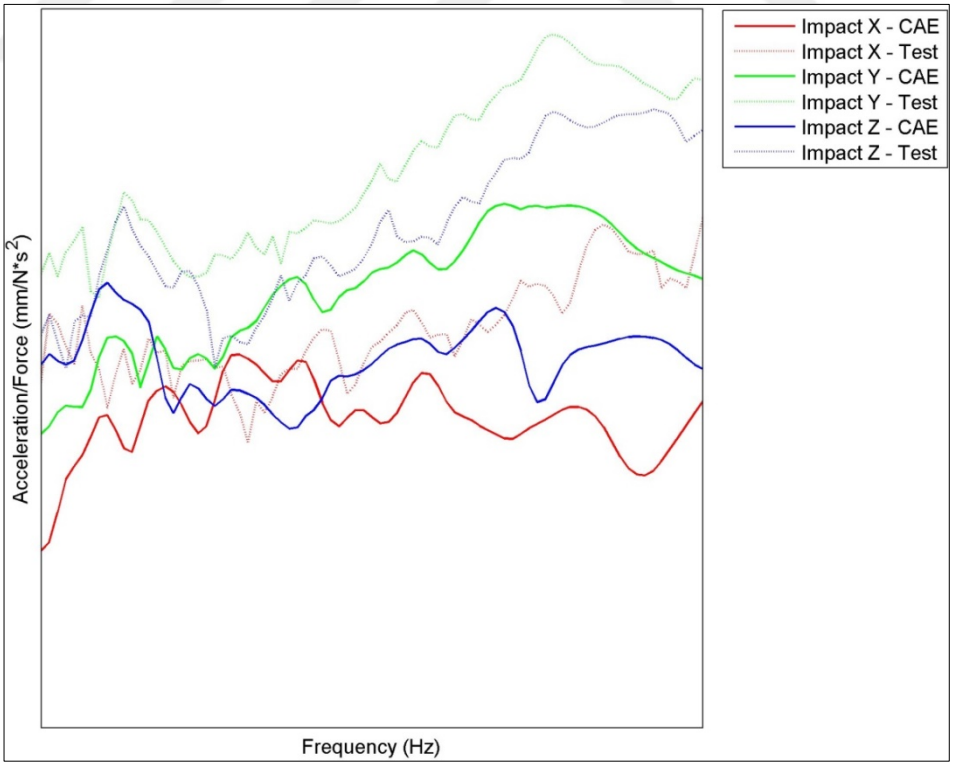

Figure 5.24: VTF correlation for transferpath4 response3.

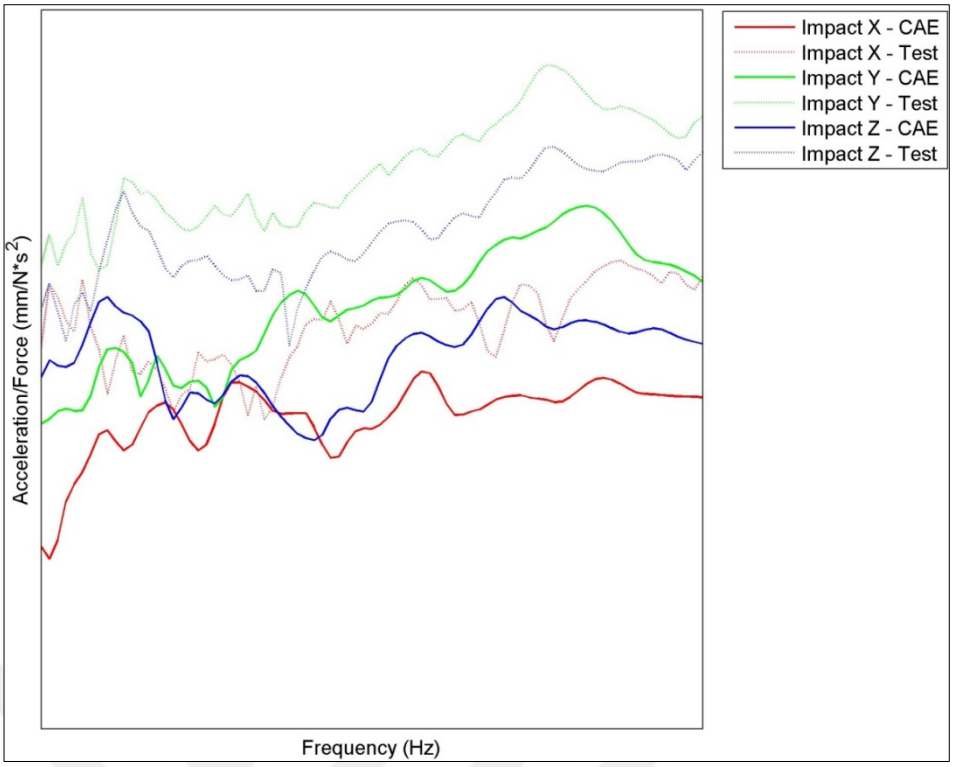

Figure 5.25: VTF correlation for transferpath4 response4.

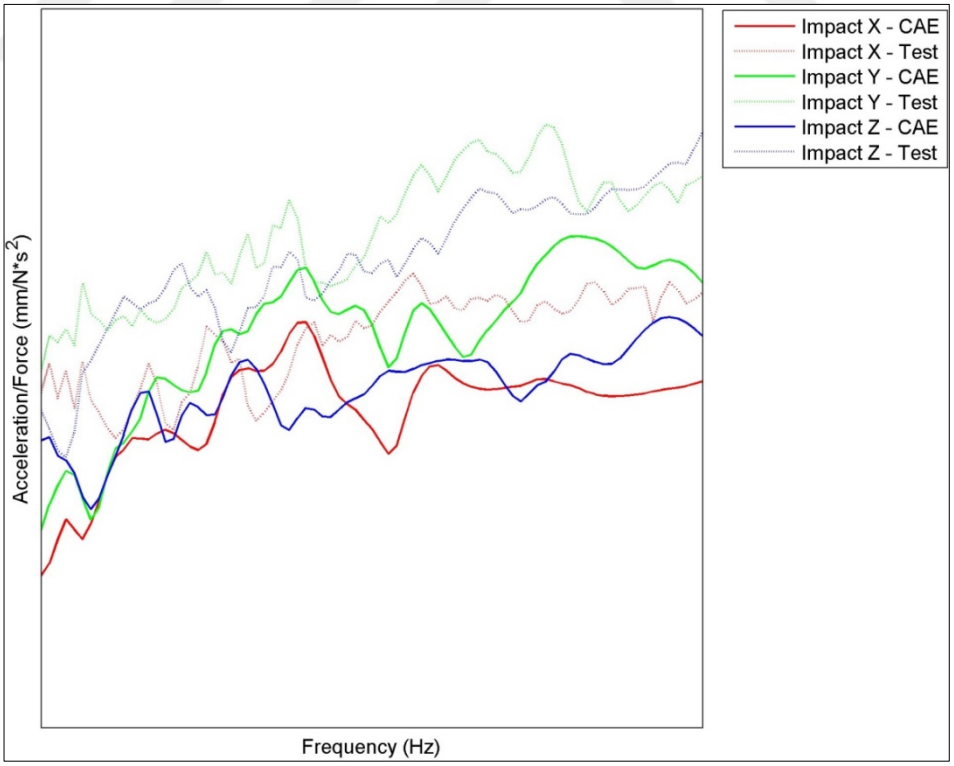

Figure 5.26: VTF correlation for transferpath4 response5.

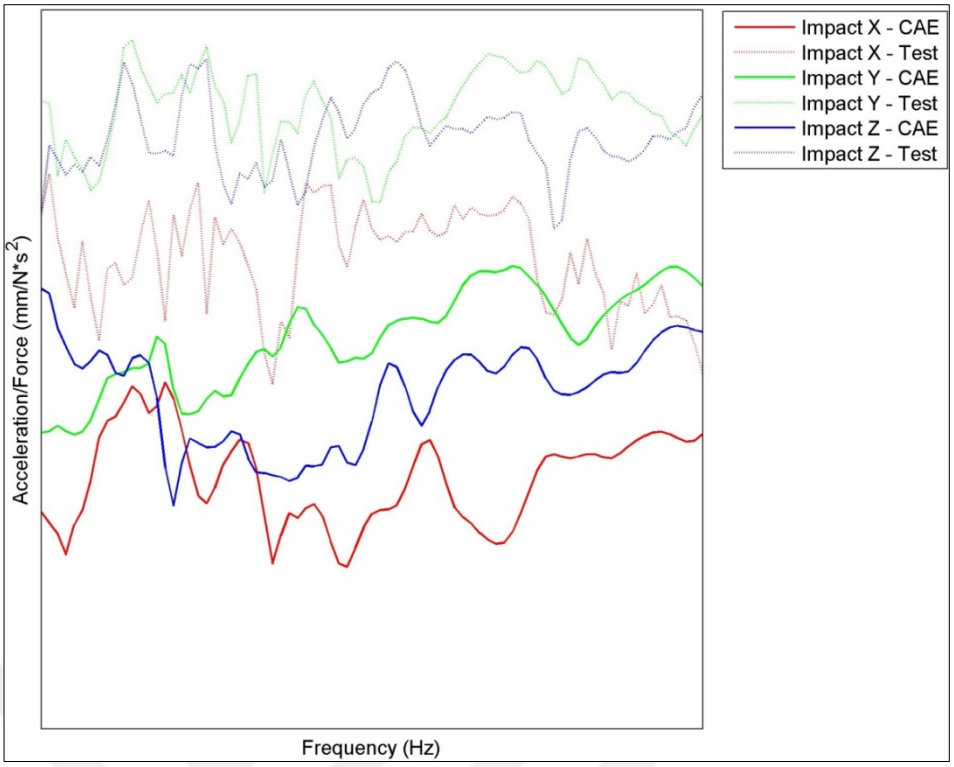

Figure 5.27: VTF correlation for transferpath4 response6.

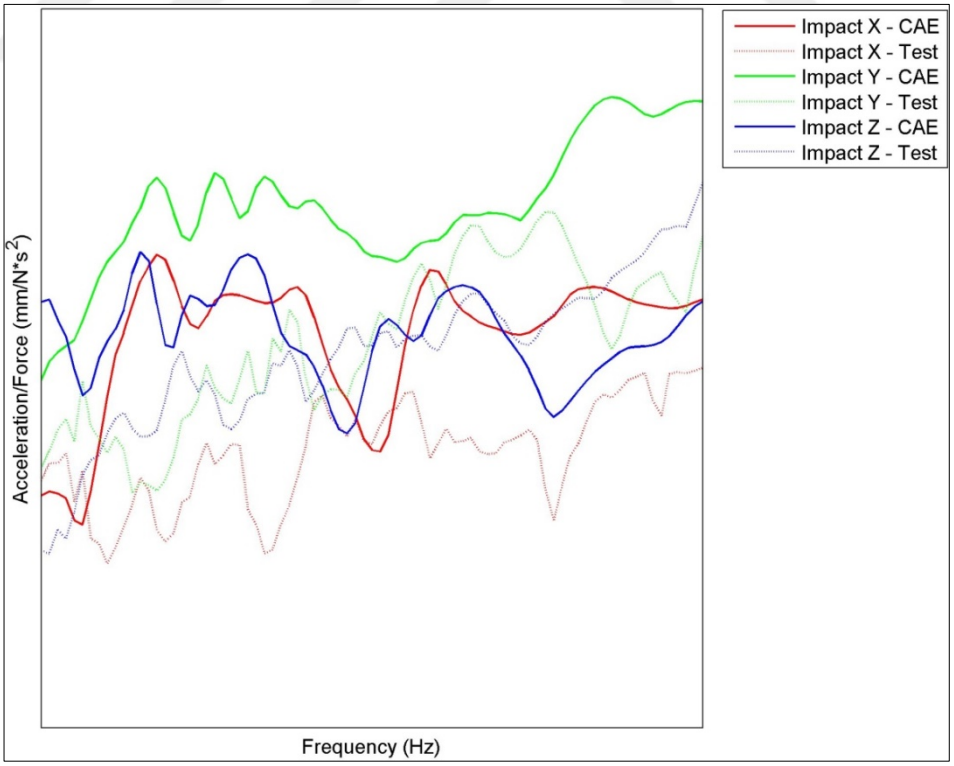

Figure 5.28: VTF correlation for transferpath4 response7.

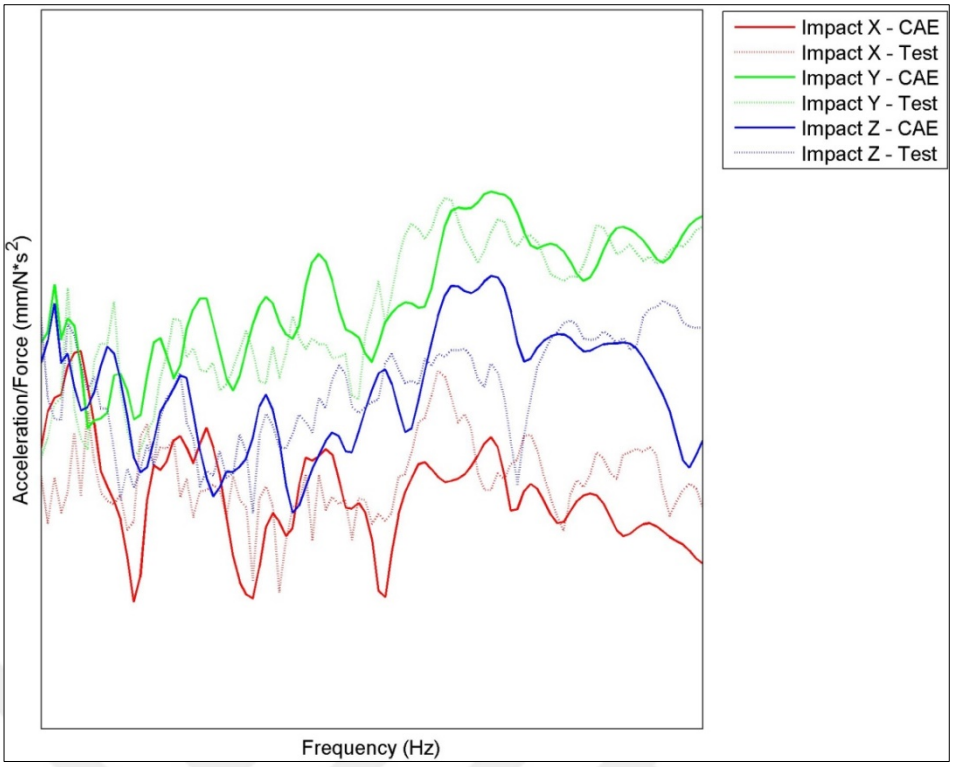

Figure 5.29: VTF correlation for transferpath5 response1.

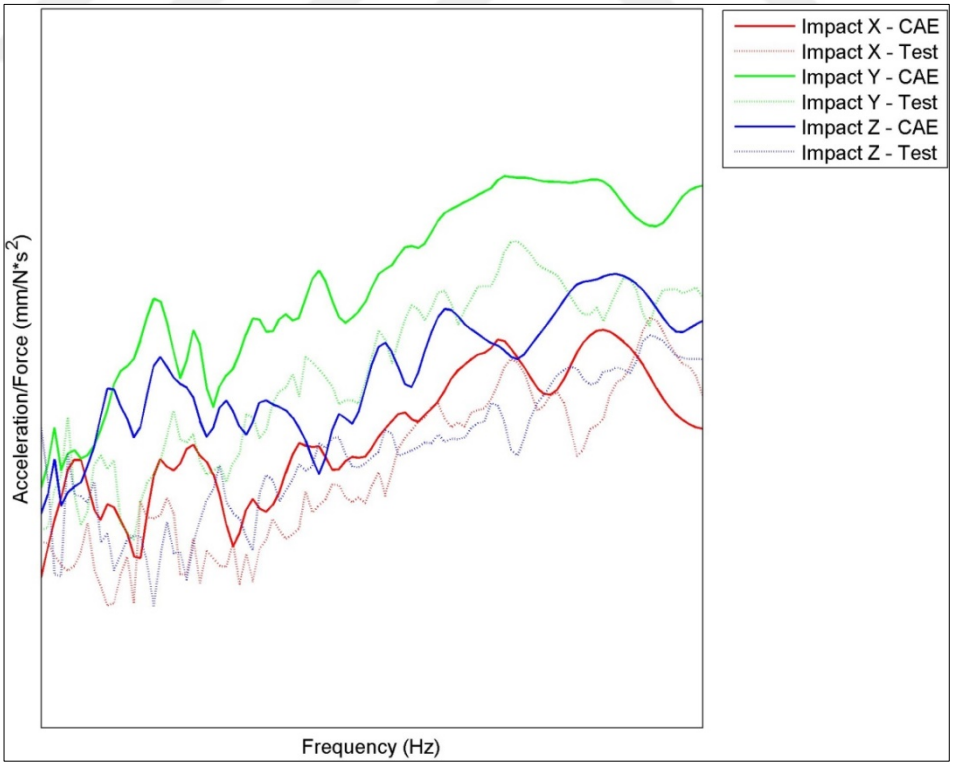

Figure 5.30: VTF correlation for transferpath5 response2.

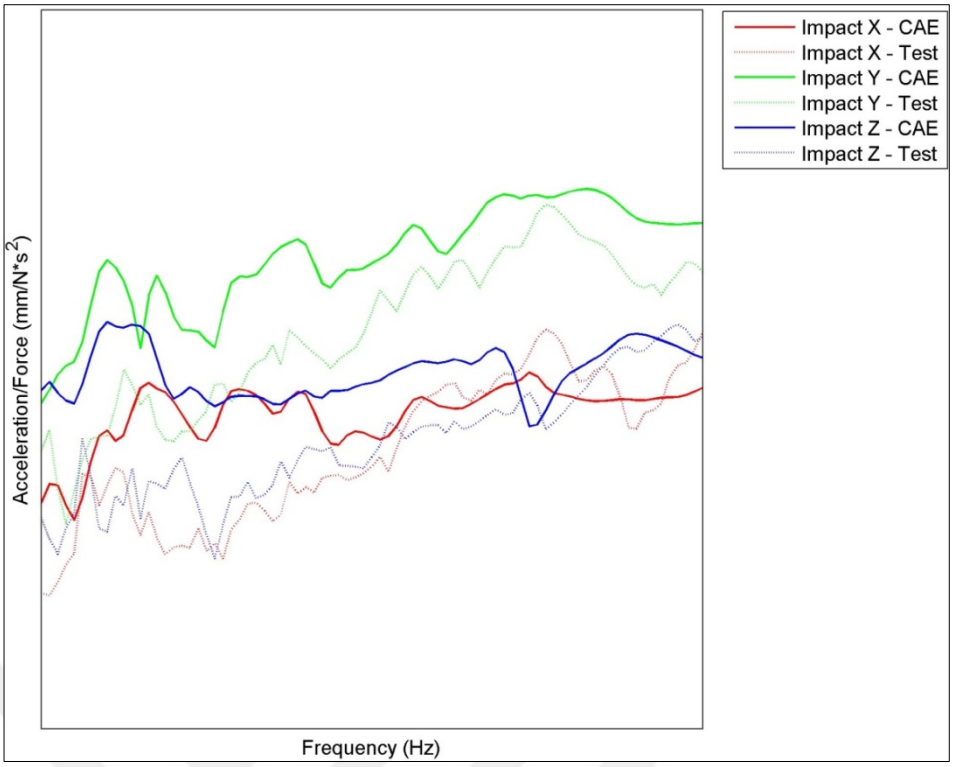

Figure 5.31: VTF correlation for transferpath5 response3.

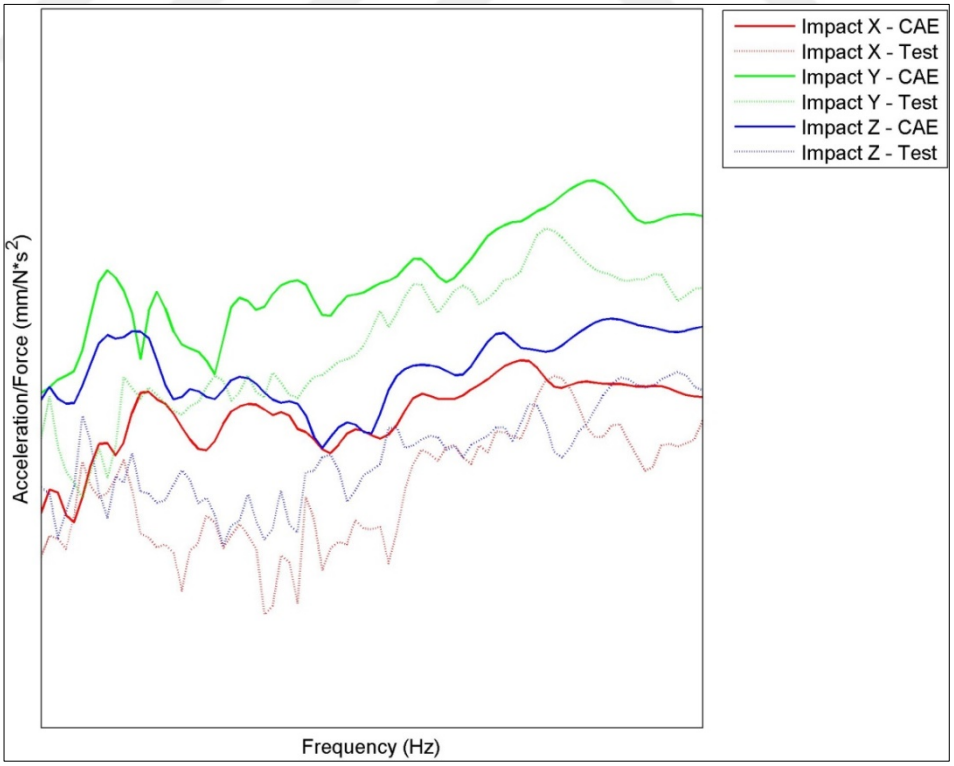

Figure 5.32: VTF correlation for transferpath5 response4.

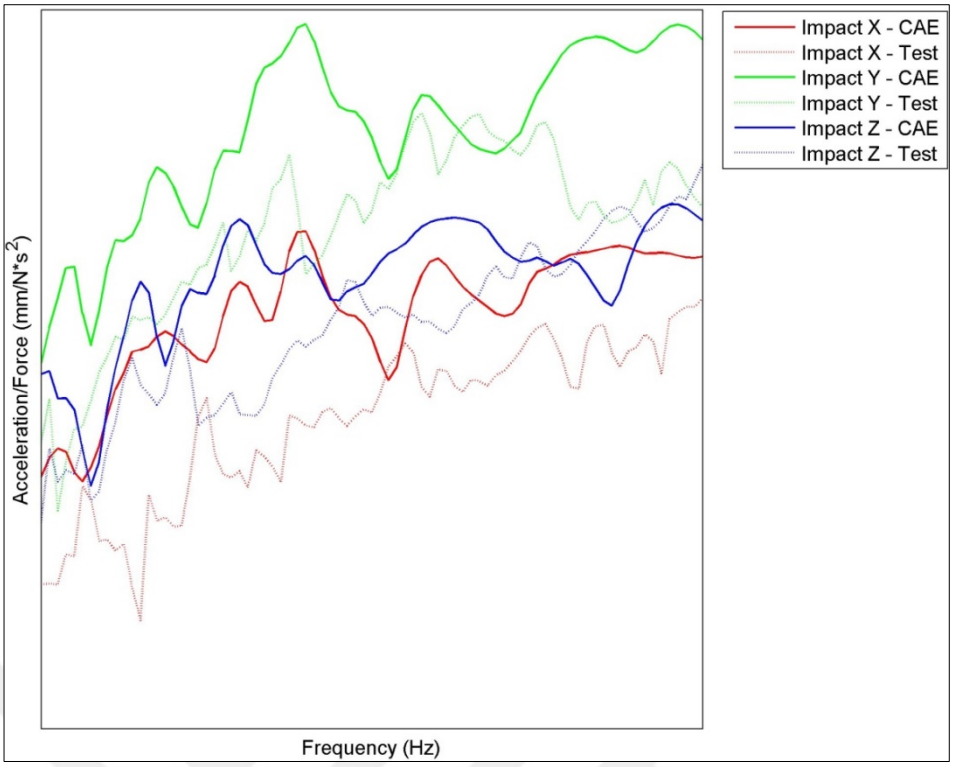

Figure 5.33: VTF correlation for transferpath5 response5.

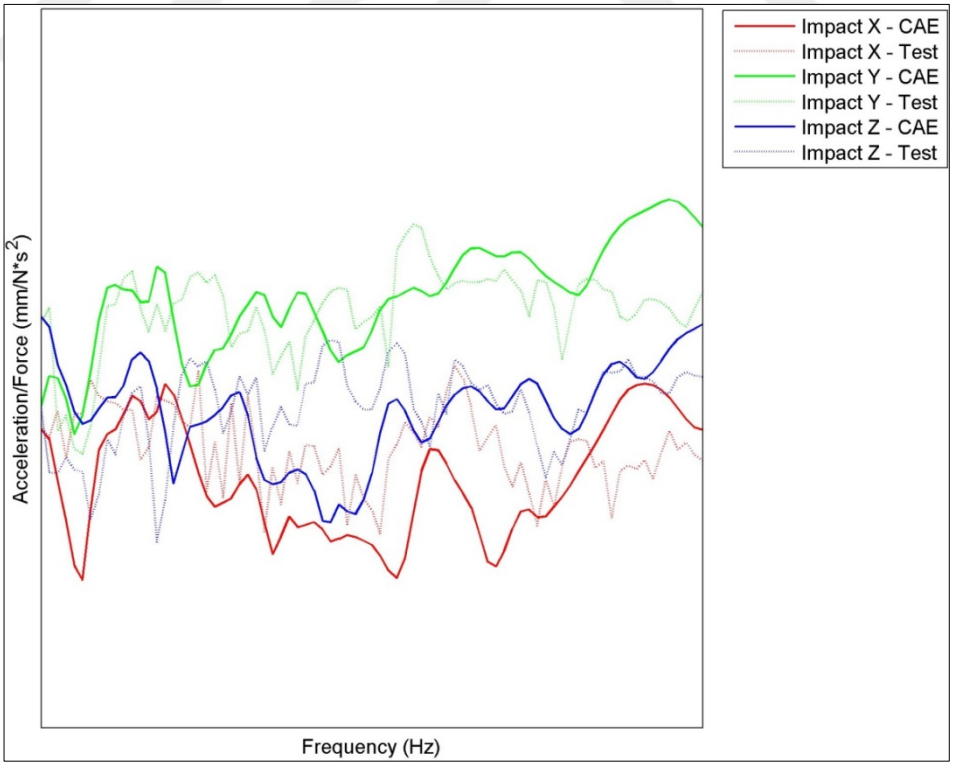

Figure 5.34: VTF correlation for transferpath5 response6.

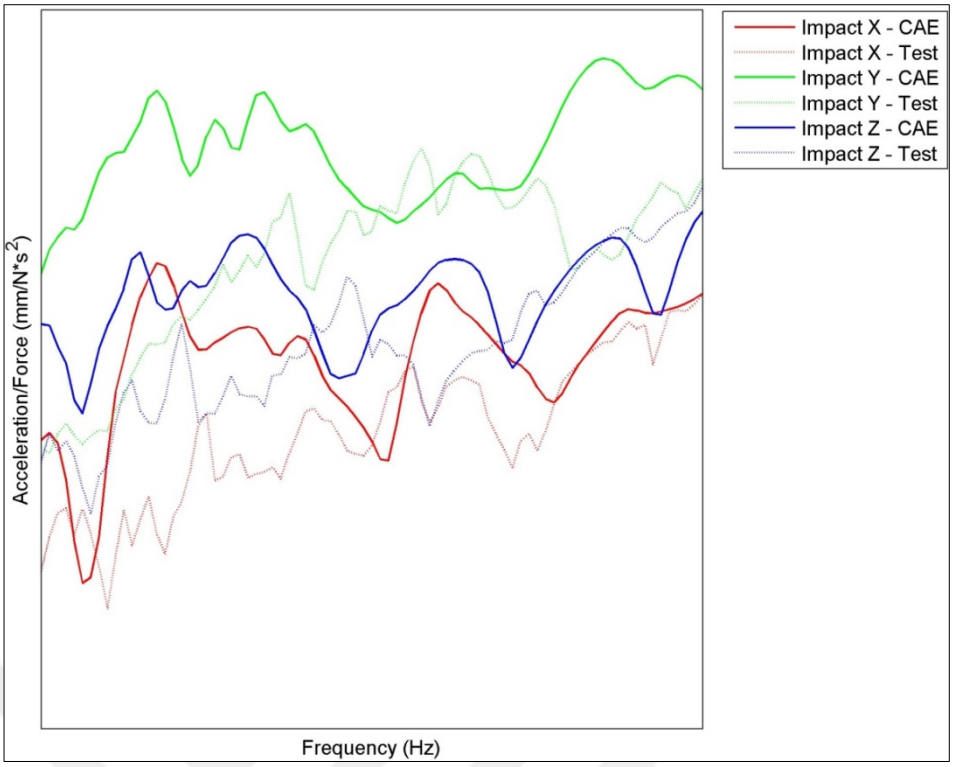

Figure 5.35: VTF correlation for transferpath5 response7.

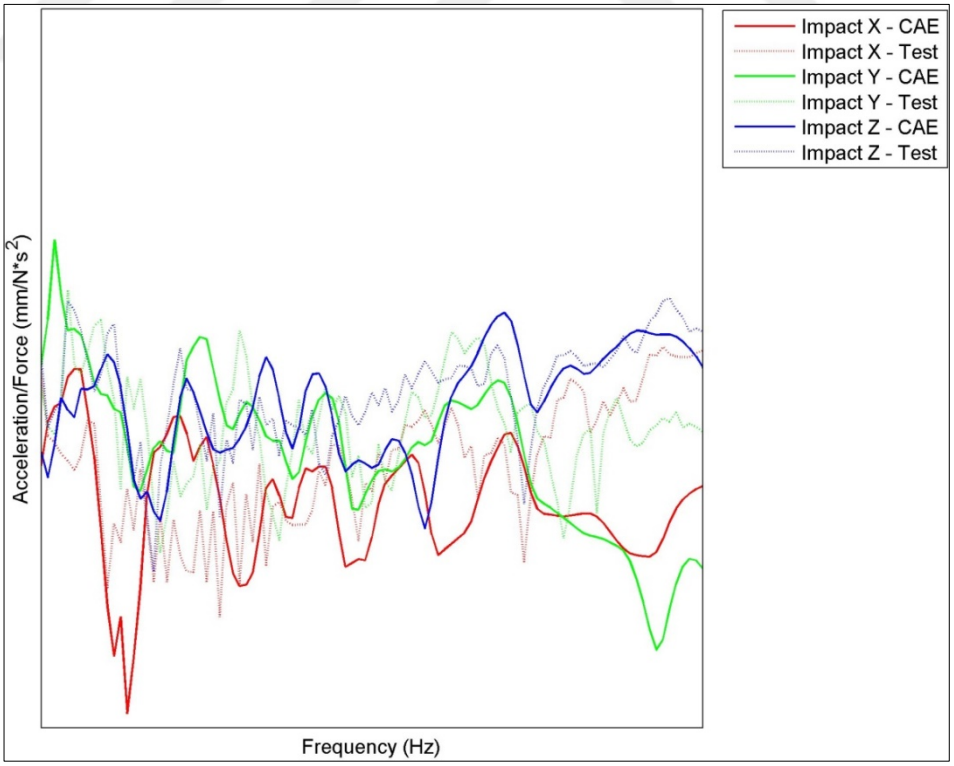

Figure 5.36: VTF correlation for transferpath6 response1.

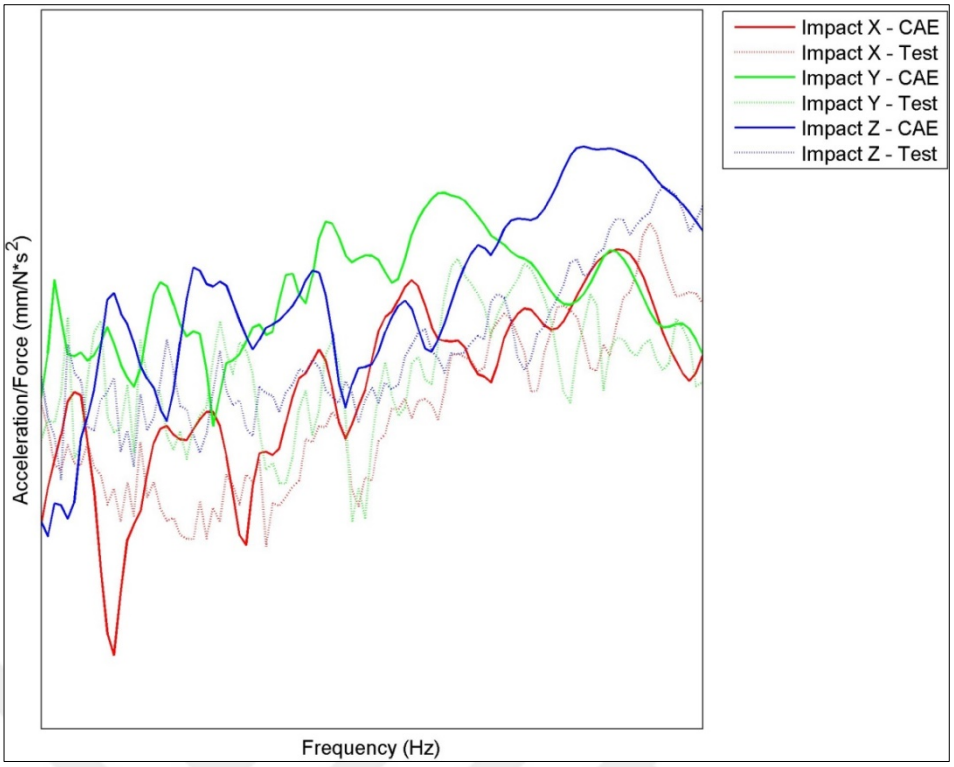

Figure 5.37: VTF correlation for transferpath6 response2.

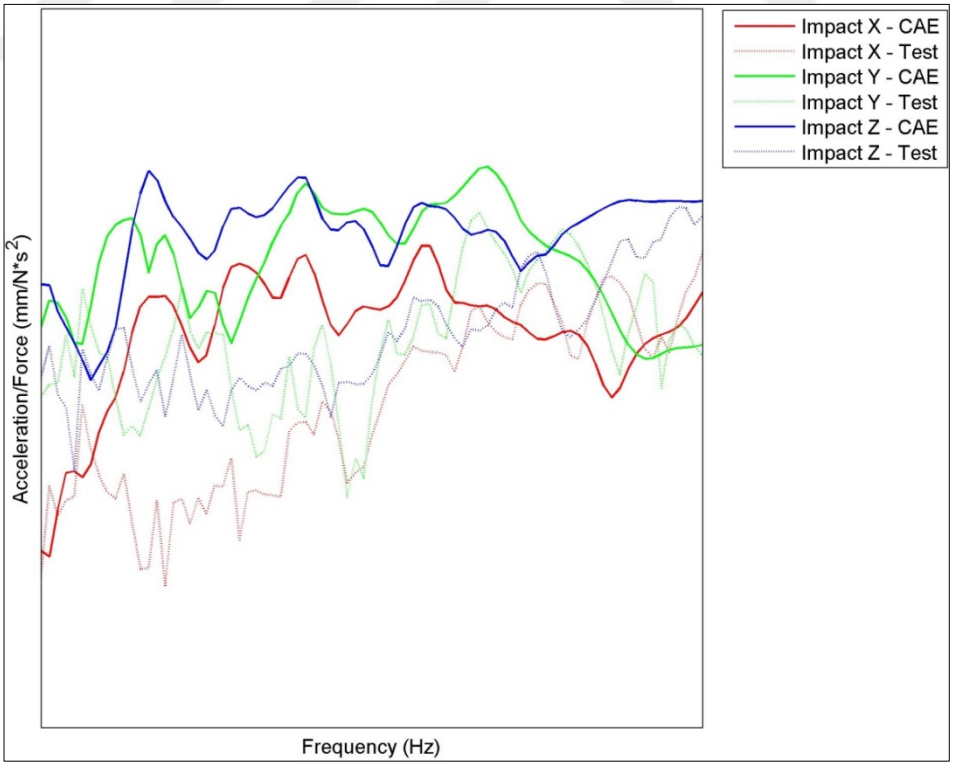

Figure 5.38: VTF correlation for transferpath6 response3.

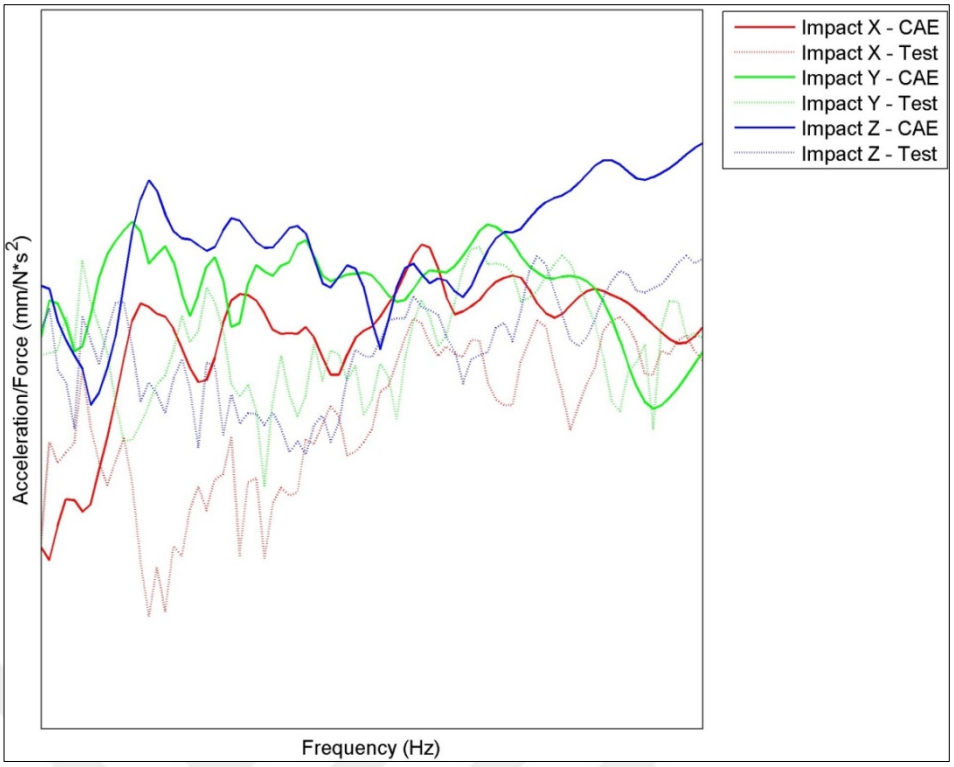

Figure 5.39: VTF correlation for transferpath6 response4.

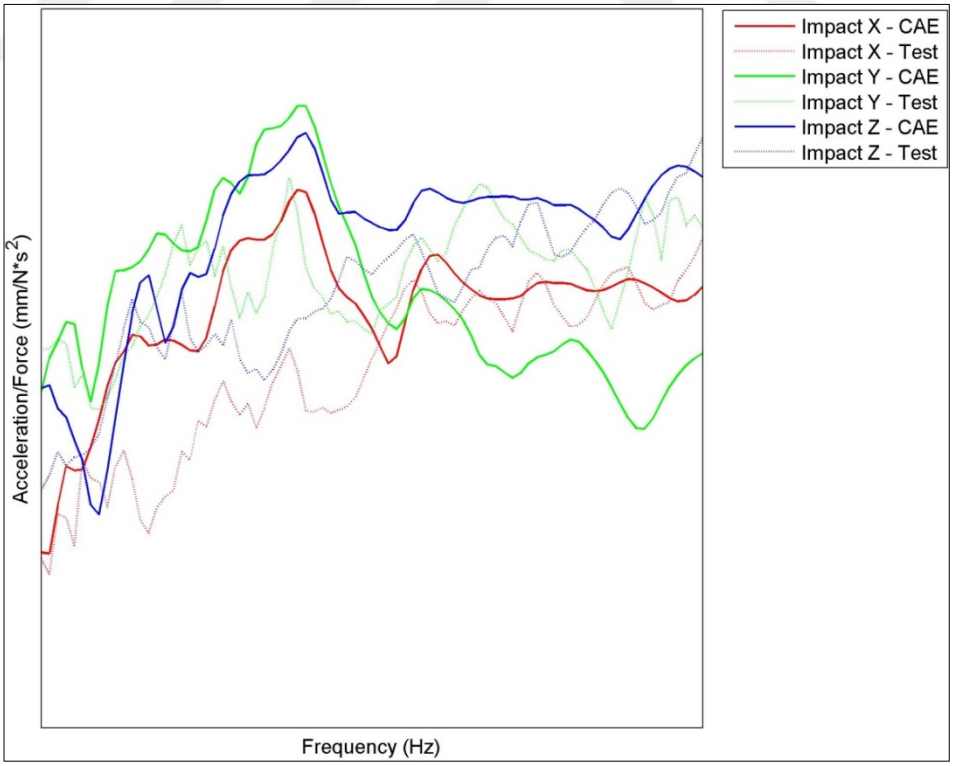

Figure 5.40: VTF correlation for transferpath6 response5.

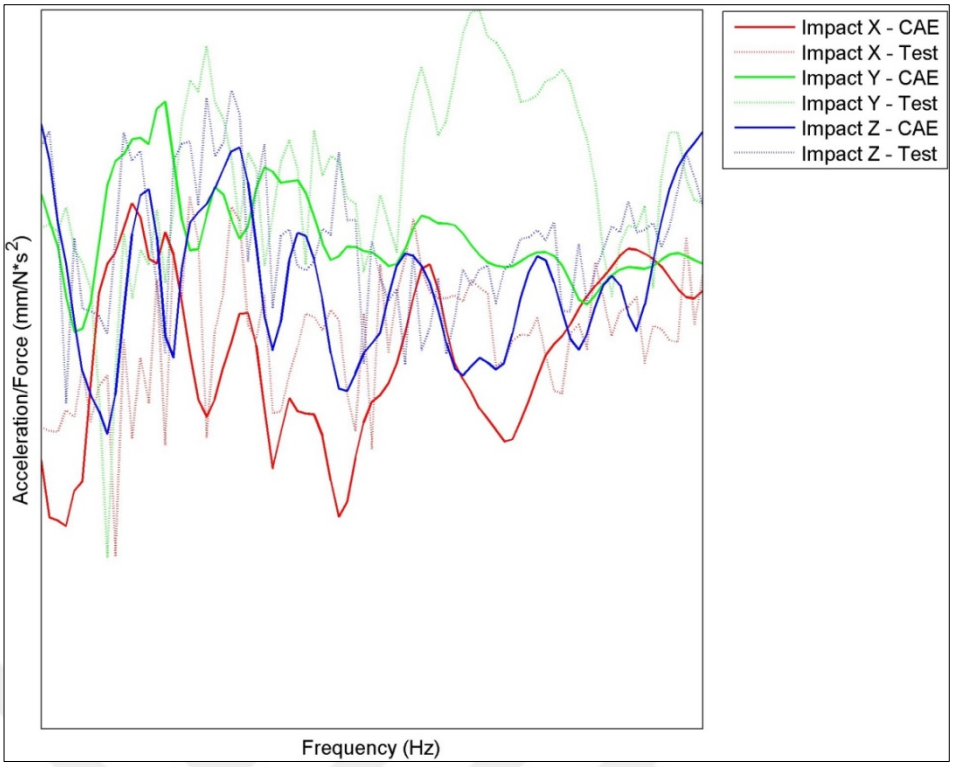

Figure 5.41: VTF correlation for transferpath6 response6.

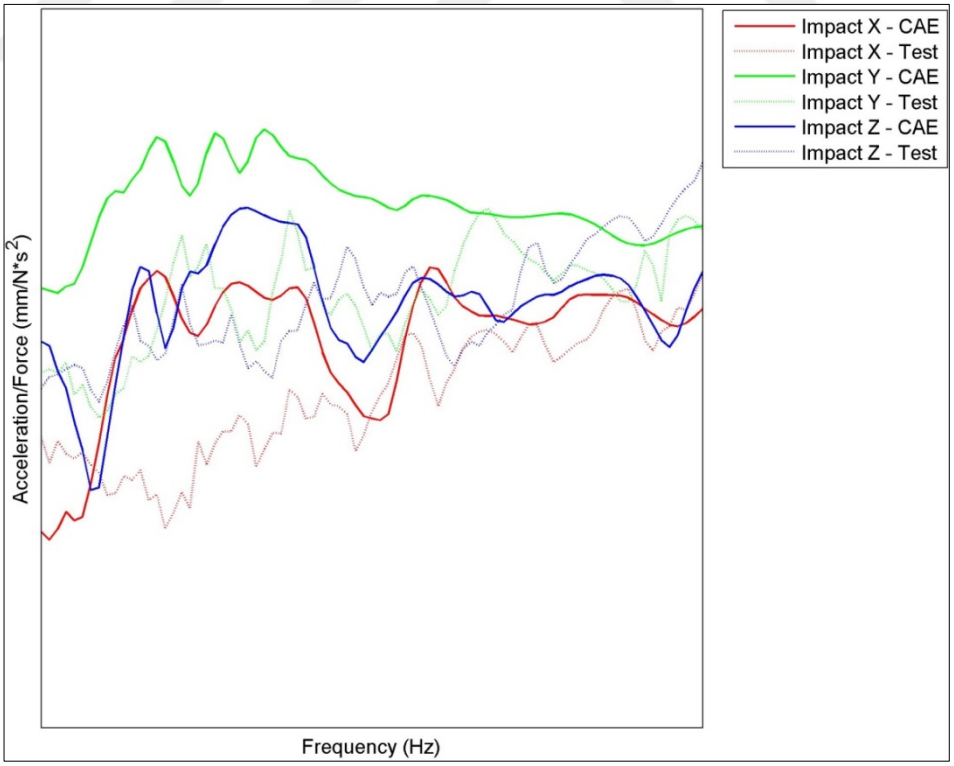

Figure 5.42: VTF correlation for transferpath6 response7.

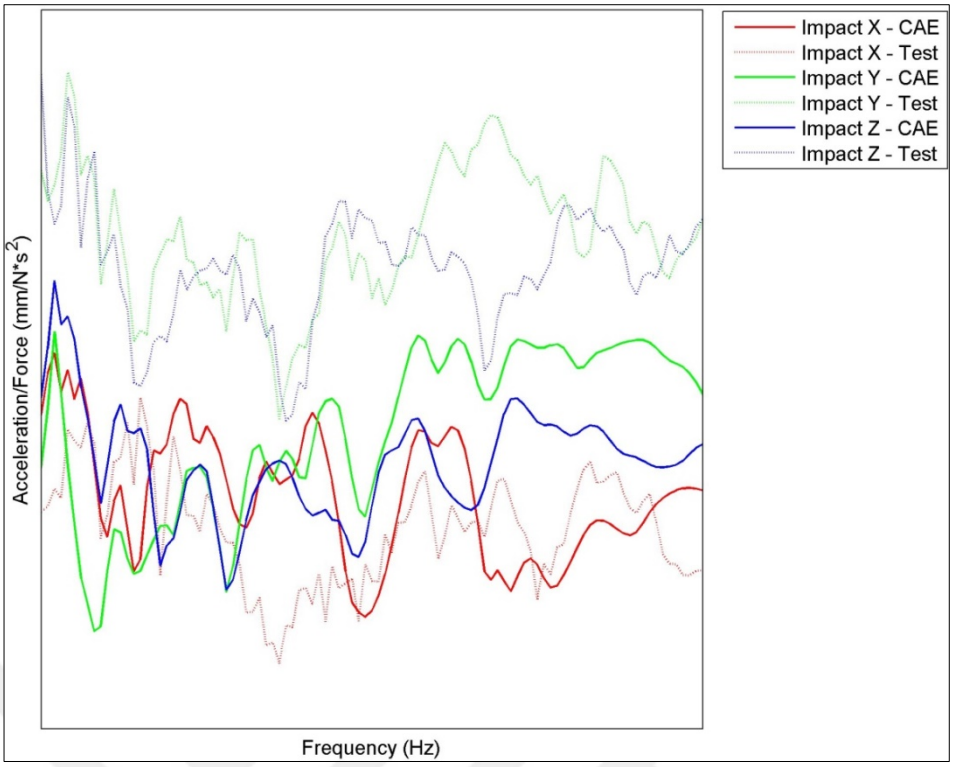

Figure 5.43: VTF correlation for transferpath7 response1.

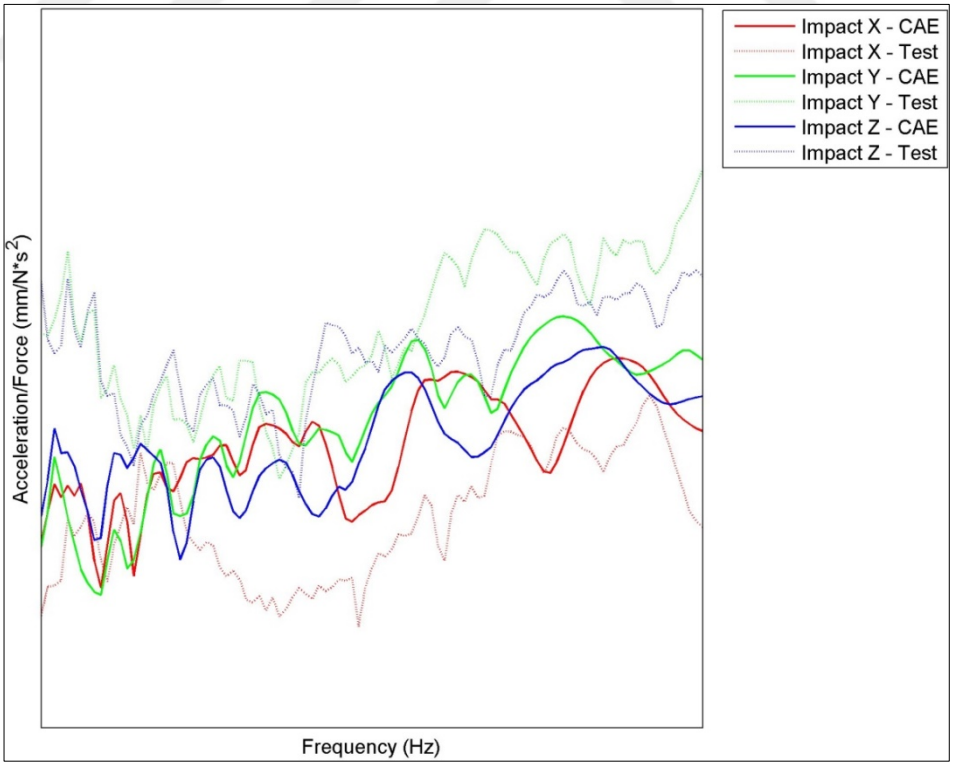

Figure 5.44: VTF correlation for transferpath7 response2.

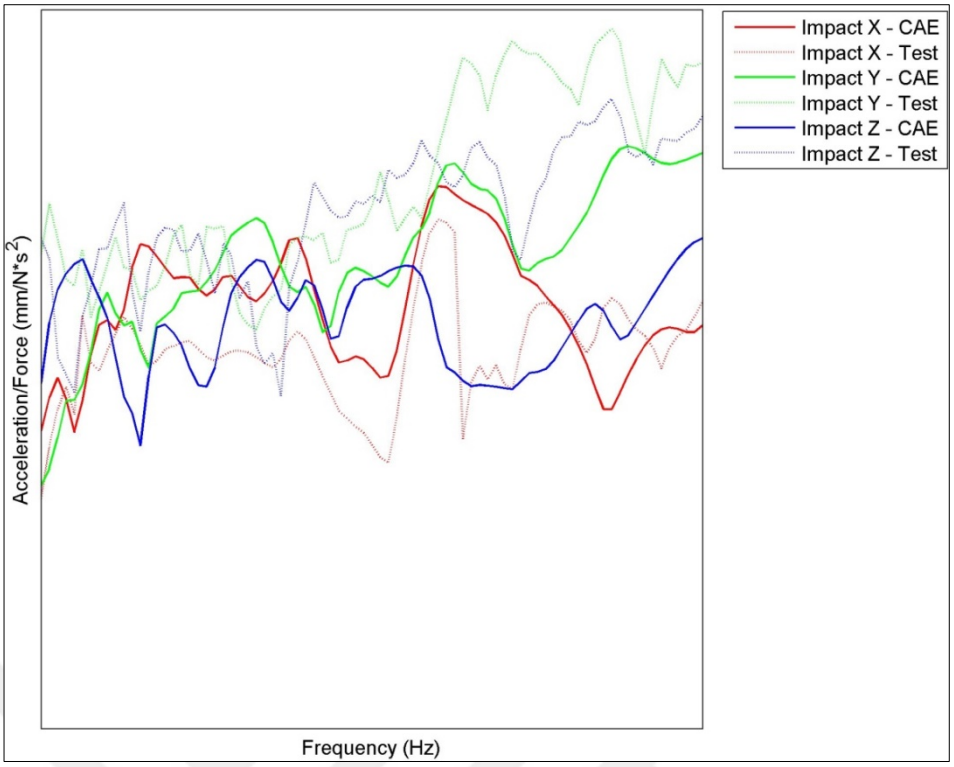

Figure 5.45: VTF correlation for transferpath7 response3.

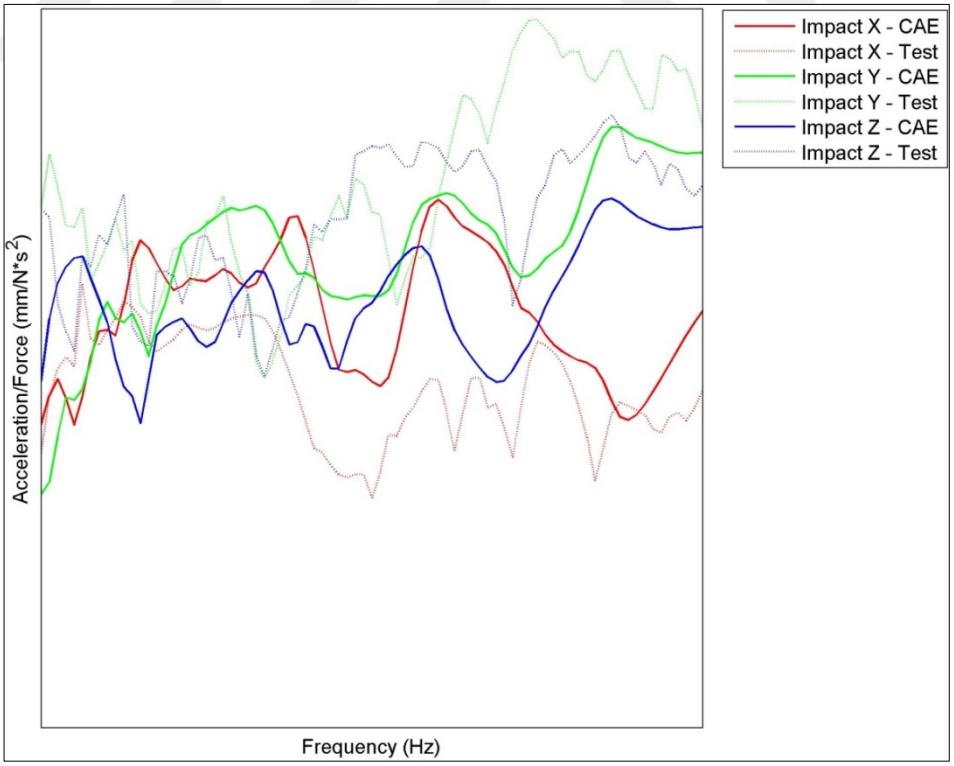

Figure 5.46: VTF correlation for transferpath7 response4.

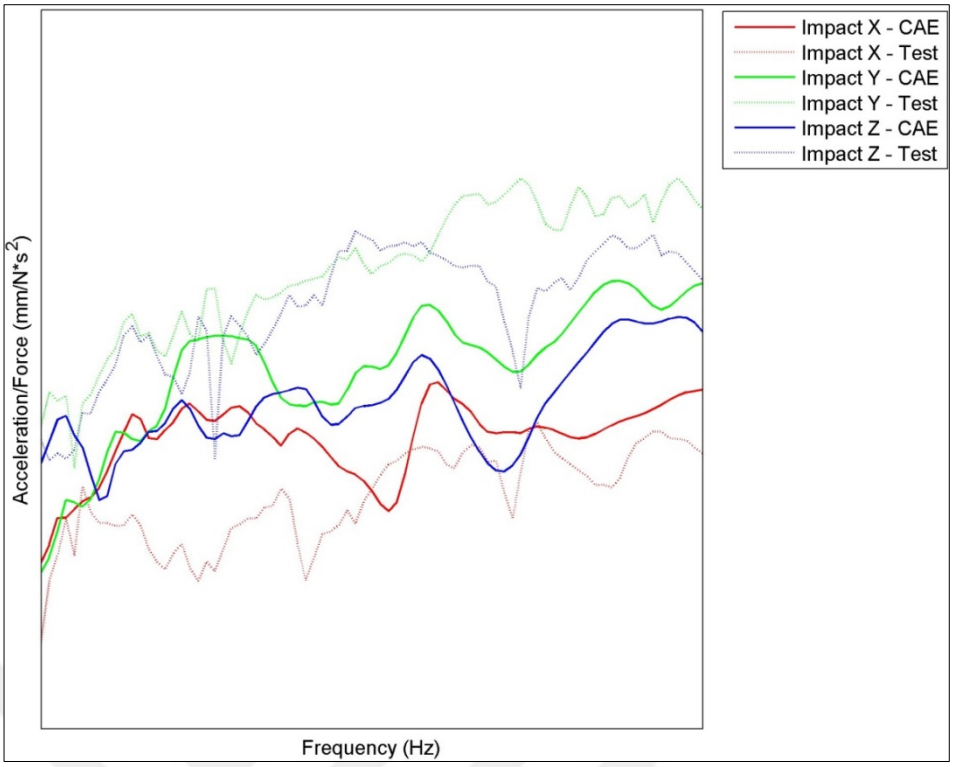

Figure 5.47: VTF correlation for transferpath7 response5.

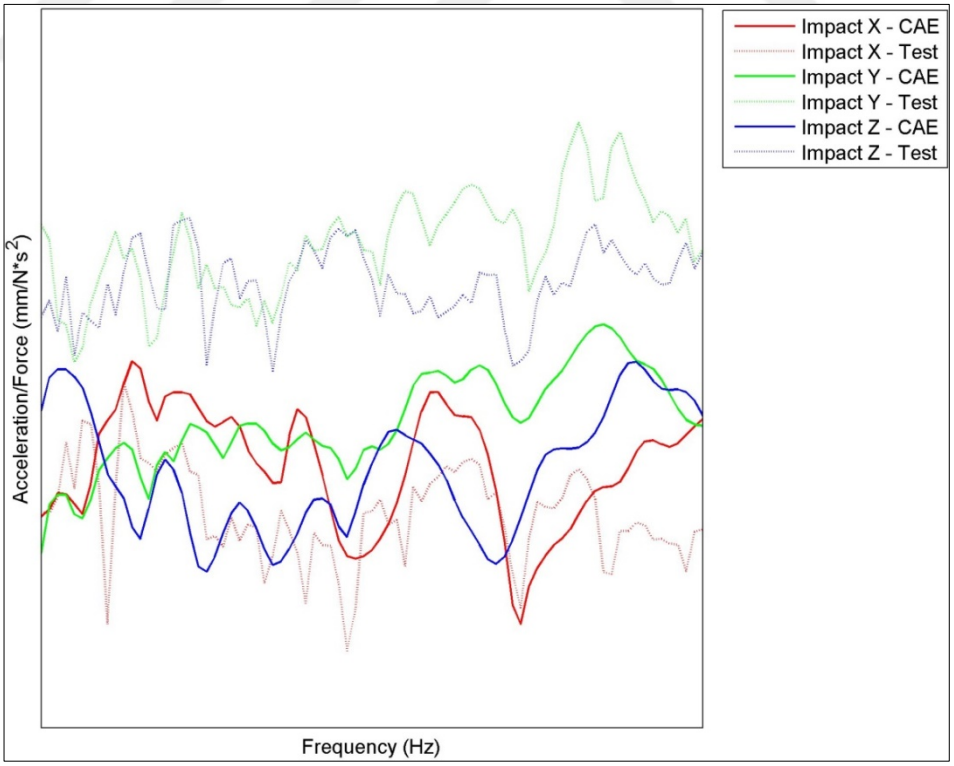

Figure 5.48: VTF correlation for transferpath7 response6.

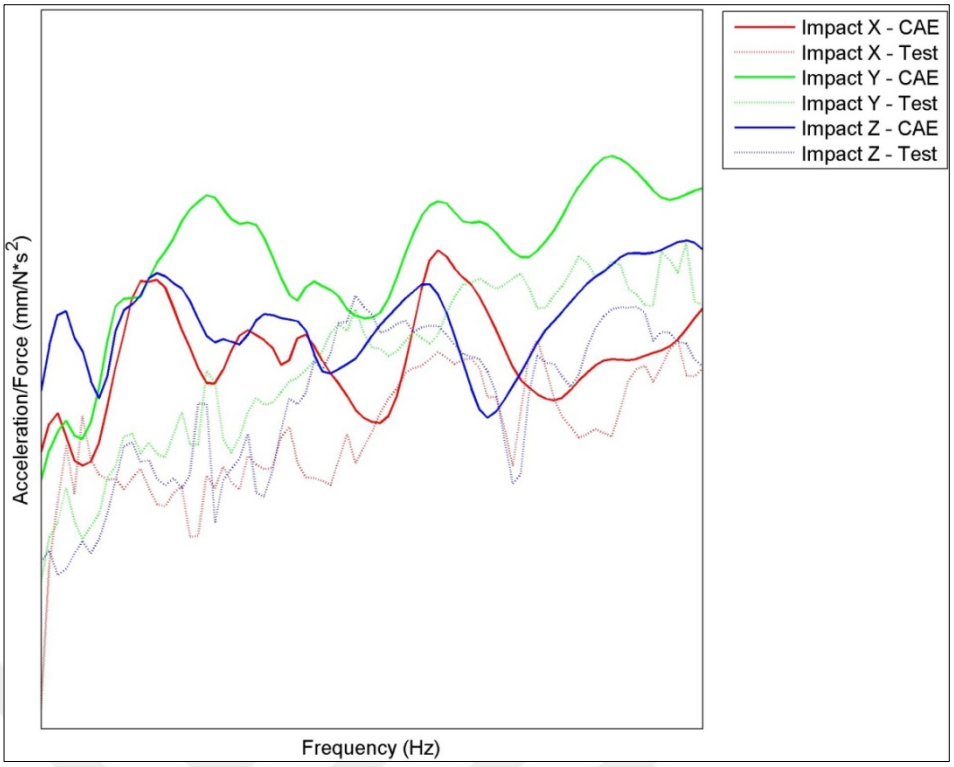

Figure 5.49: VTF correlation for transferpath7 response7.

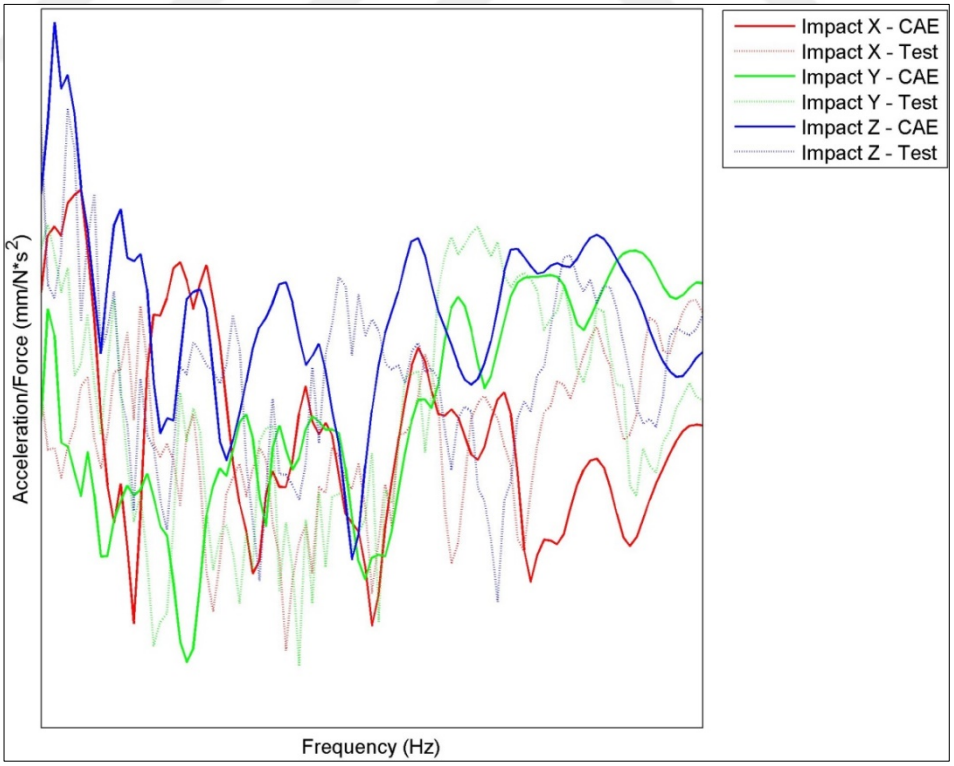

Figure 5.50: VTF correlation for transferpath8 response1.

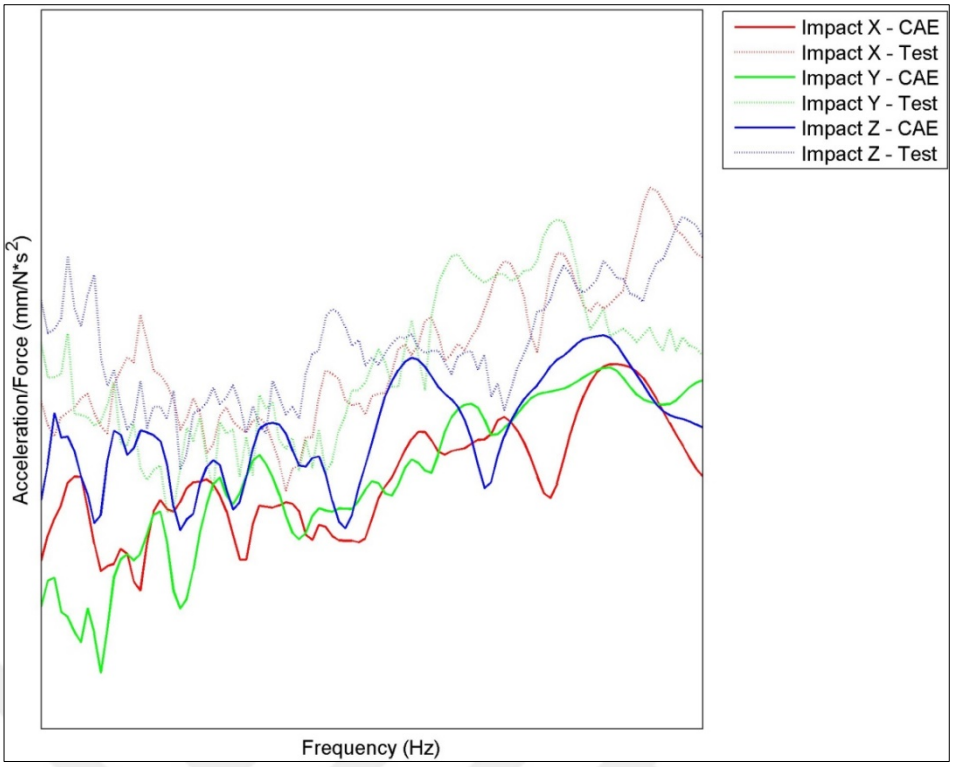

Figure 5.51: VTF correlation for transferpath8 response2.

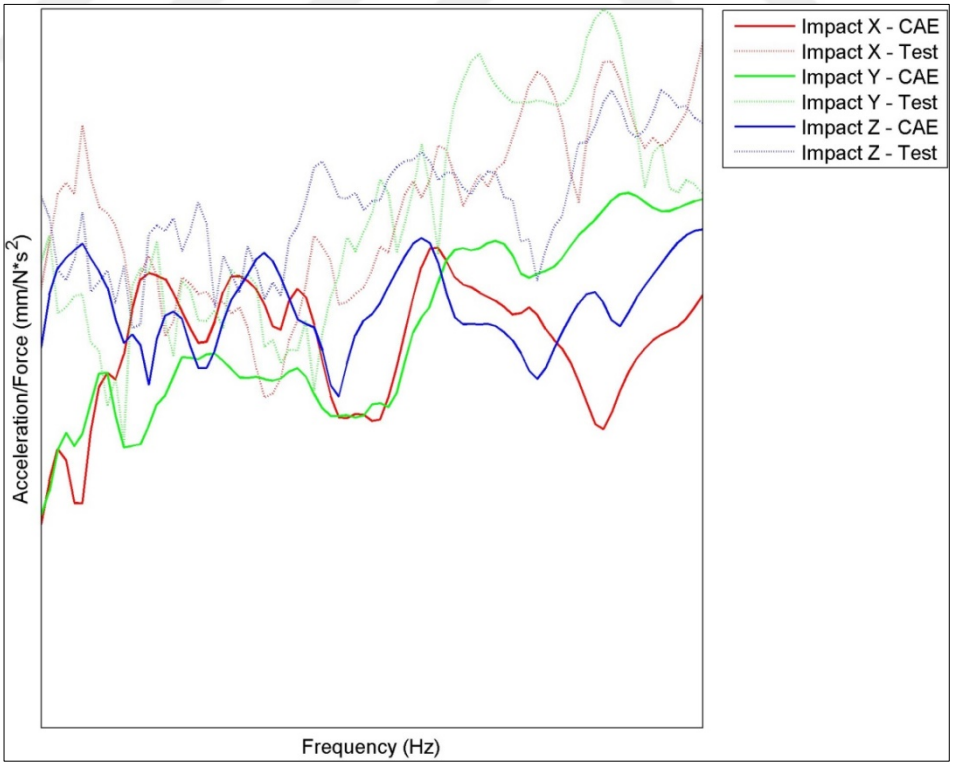

Figure 5.52: VTF correlation for transferpath8 response3.

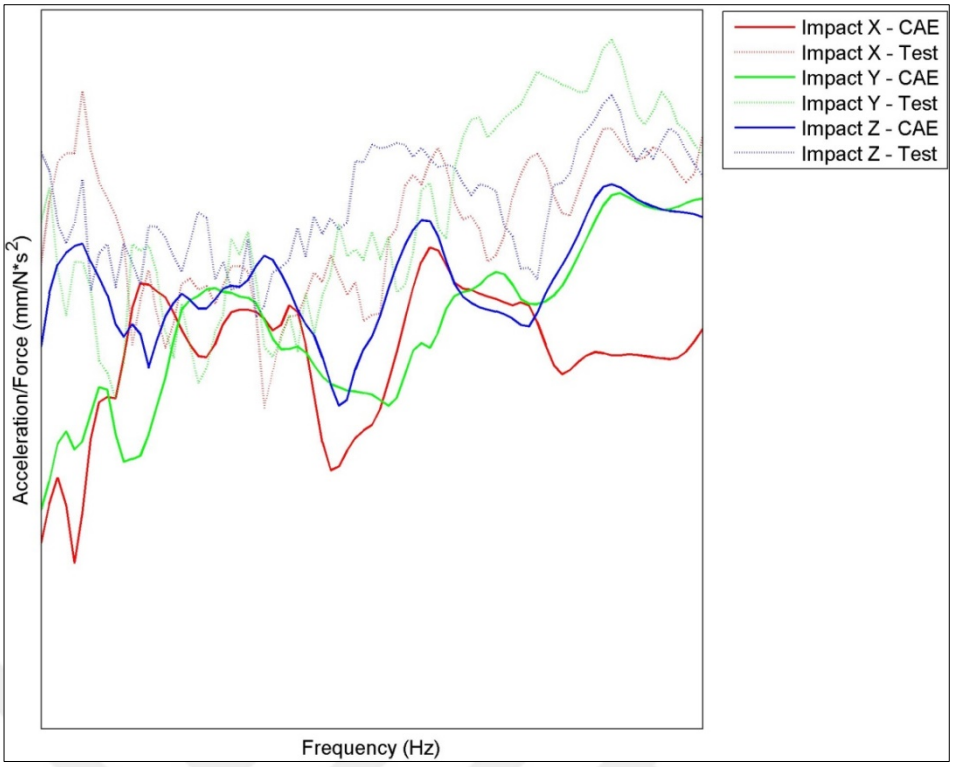

Figure 5.53: VTF correlation for transferpath8 response4.

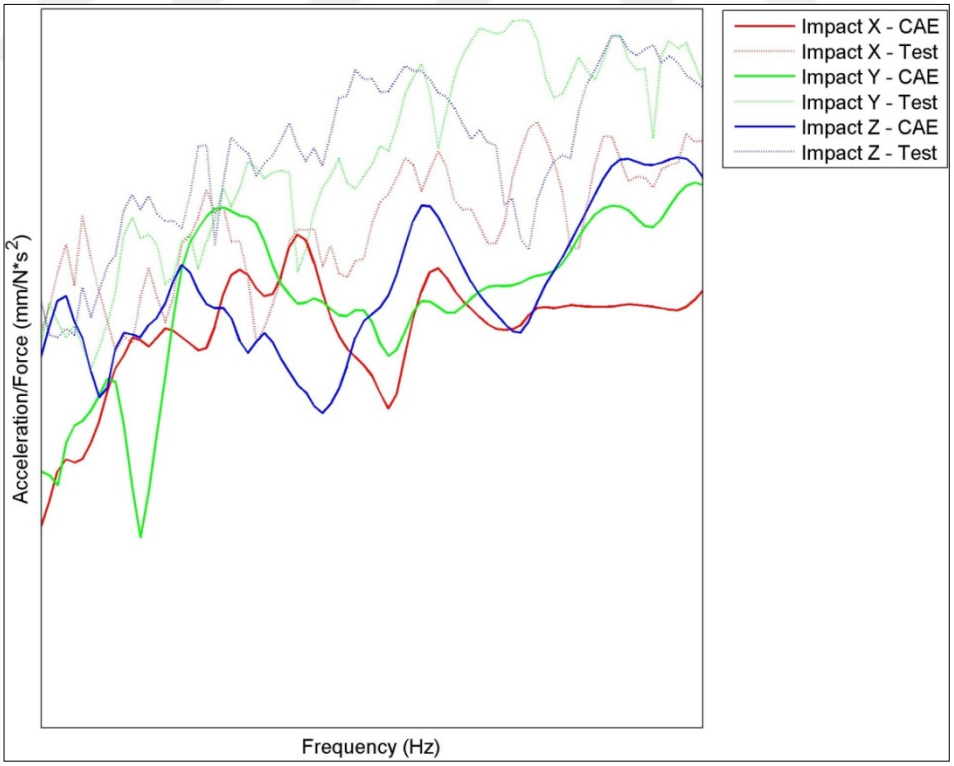

Figure 5.54: VTF correlation for transferpath8 response5.

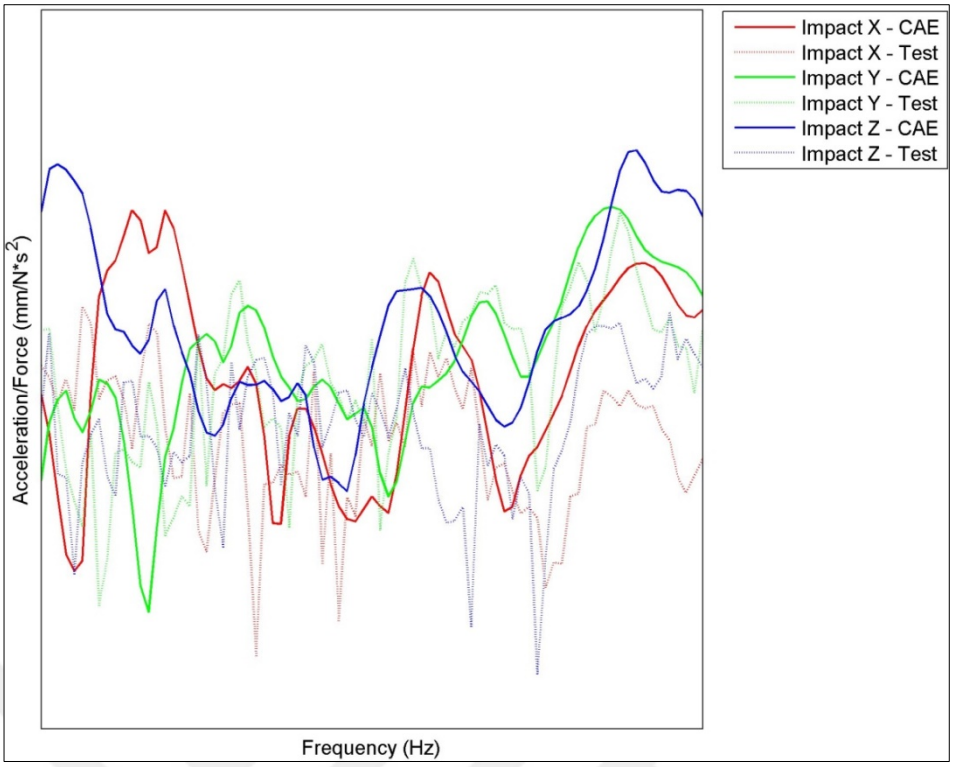

Figure 5.55: VTF correlation for transferpath8 response6.

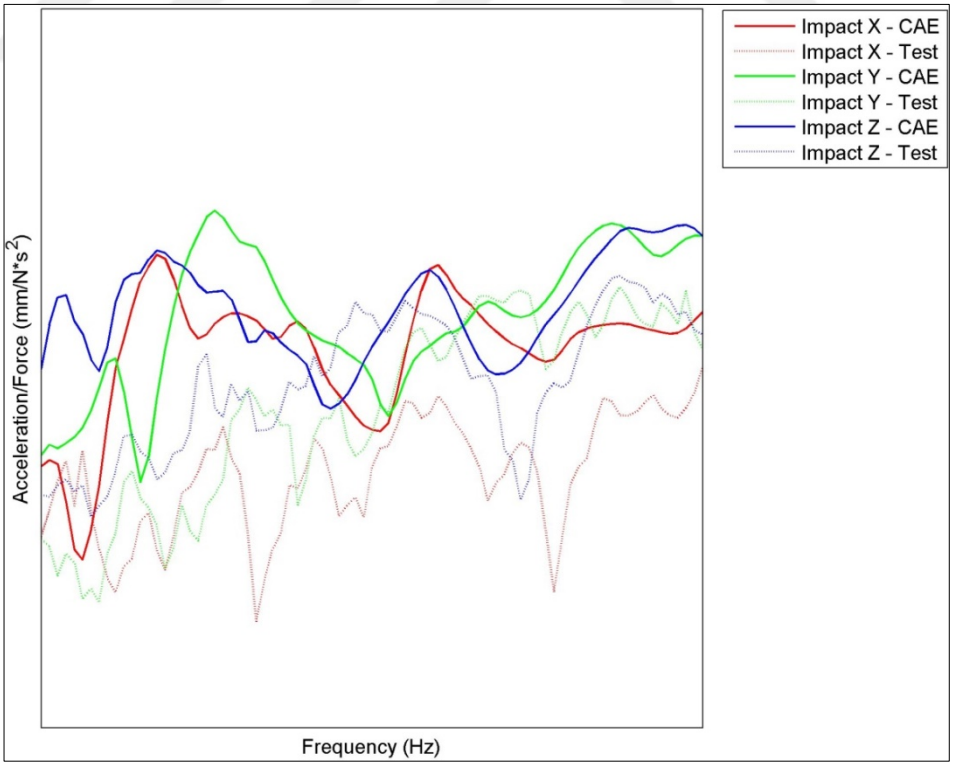

Figure 5.56: VTF correlation for transferpath8 response7.

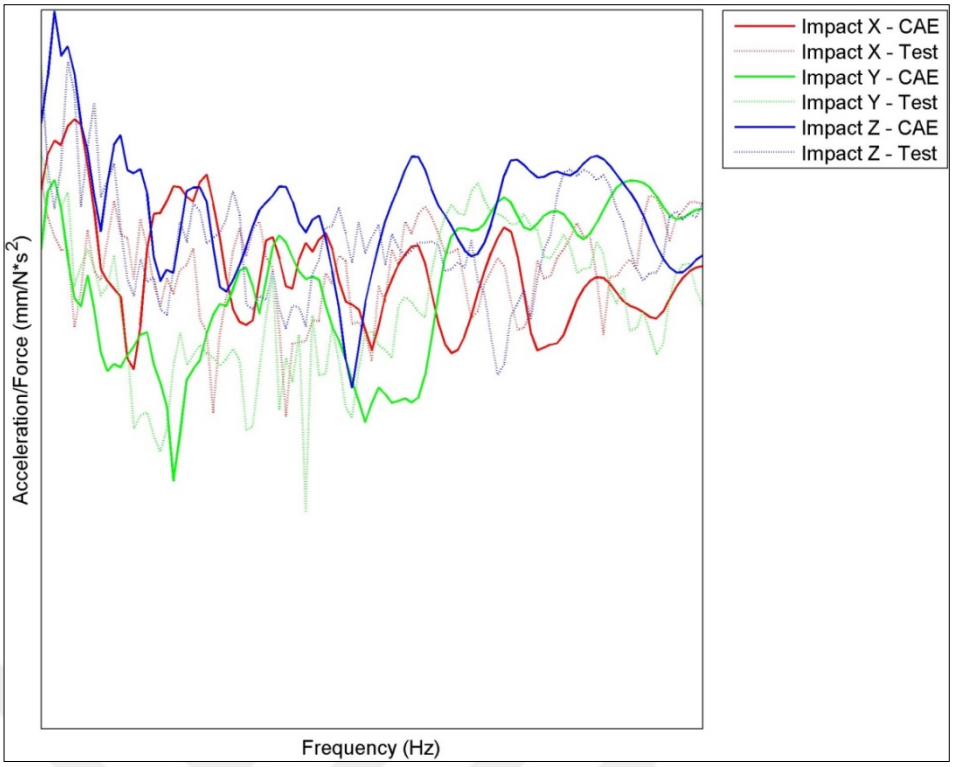

Figure 5.57: VTF correlation for transferpath9 response1.

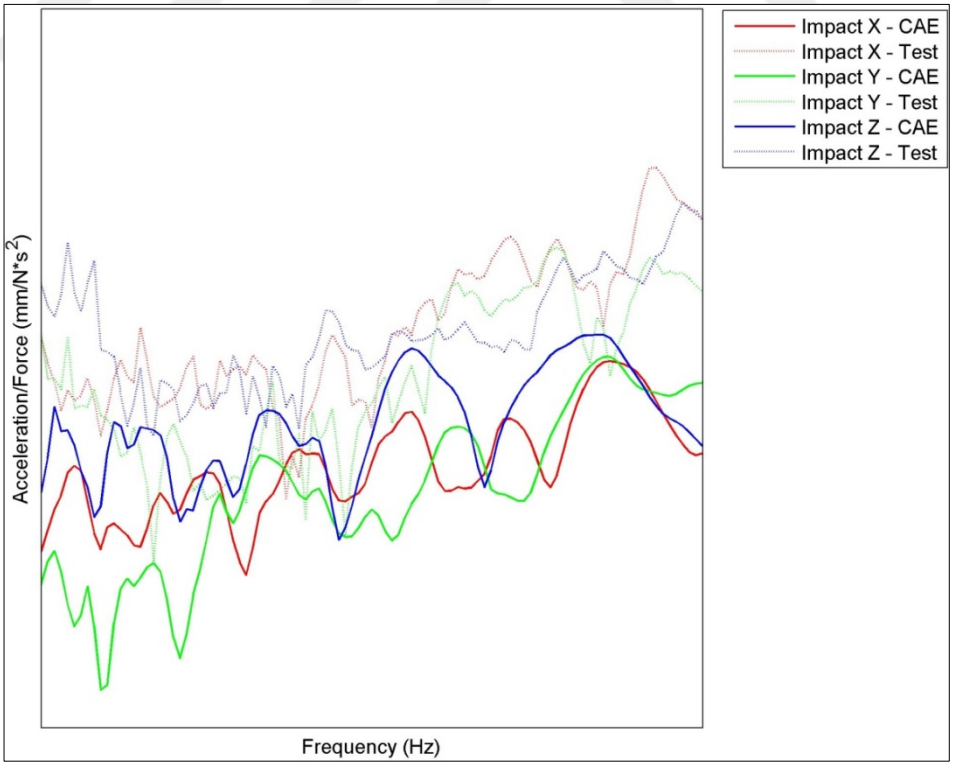

Figure 5.58: VTF correlation for transferpath9 response2.

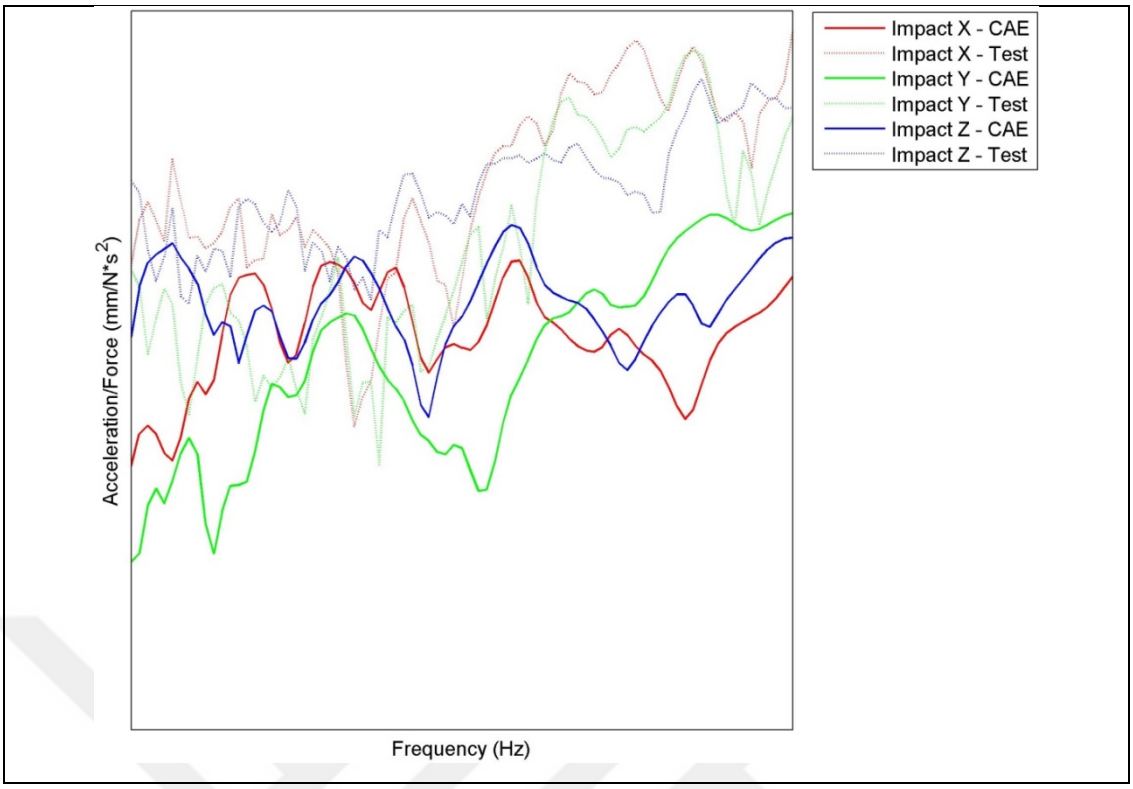

Figure 5.59: VTF correlation for transferpath9 response3.

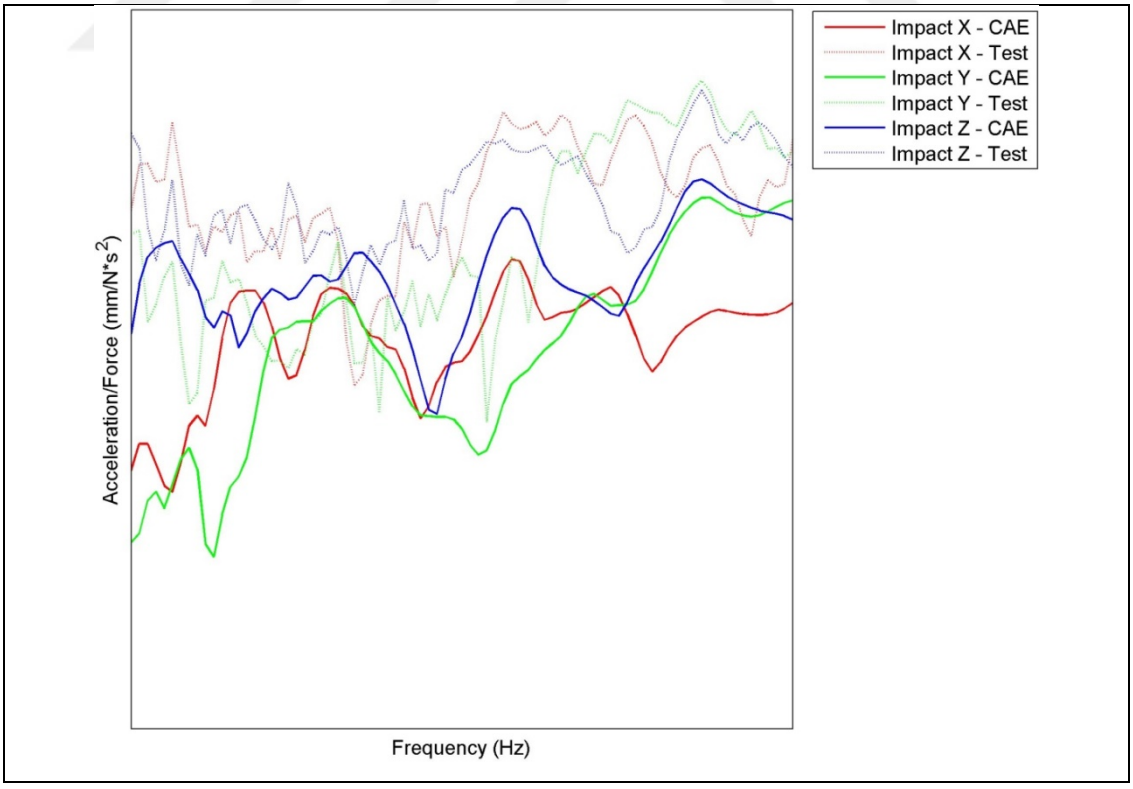

Figure 5.60: VTF correlation for transferpath9 response4.

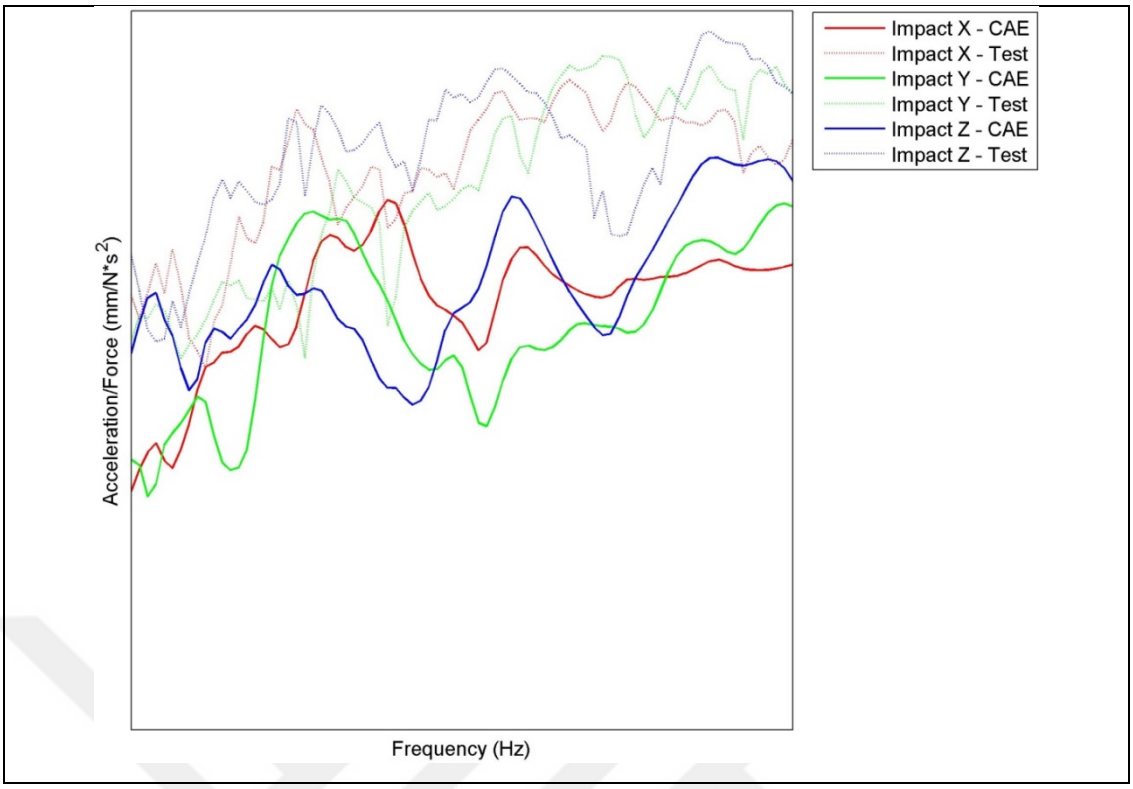

Figure 5.61: VTF correlation for transferpath9 response5.

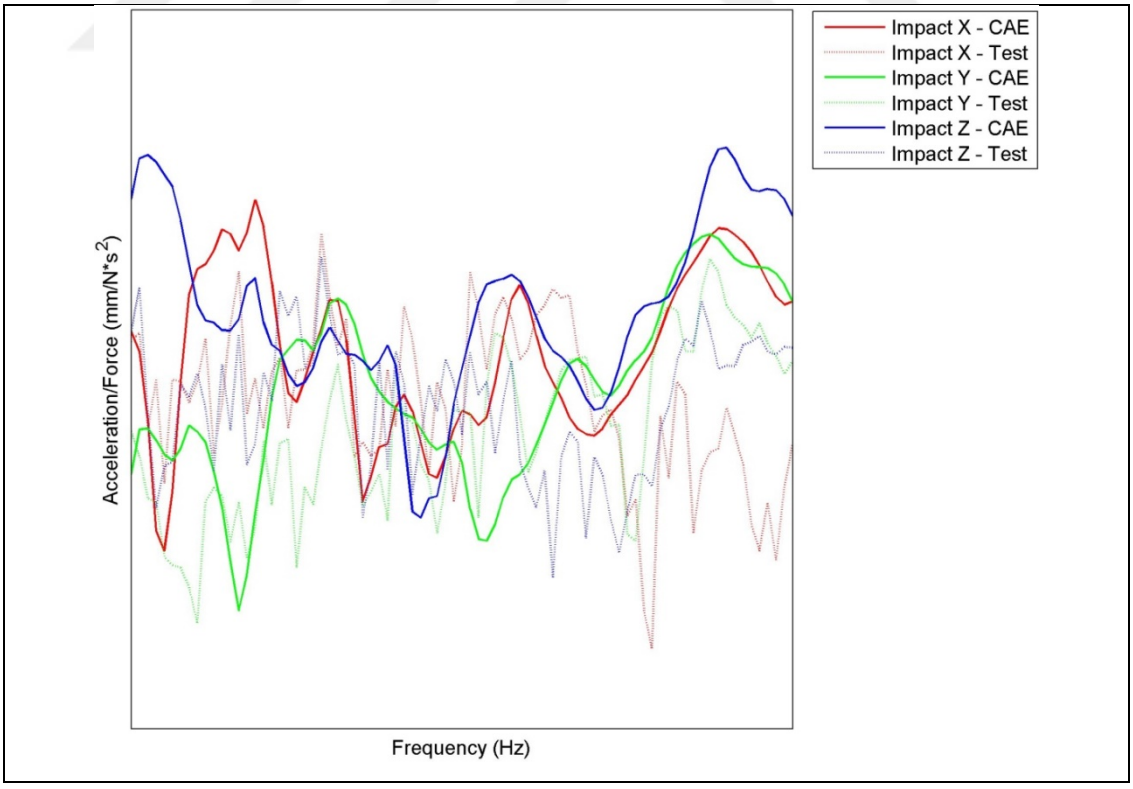

Figure 5.62: VTF correlation for transferpath9 response6.

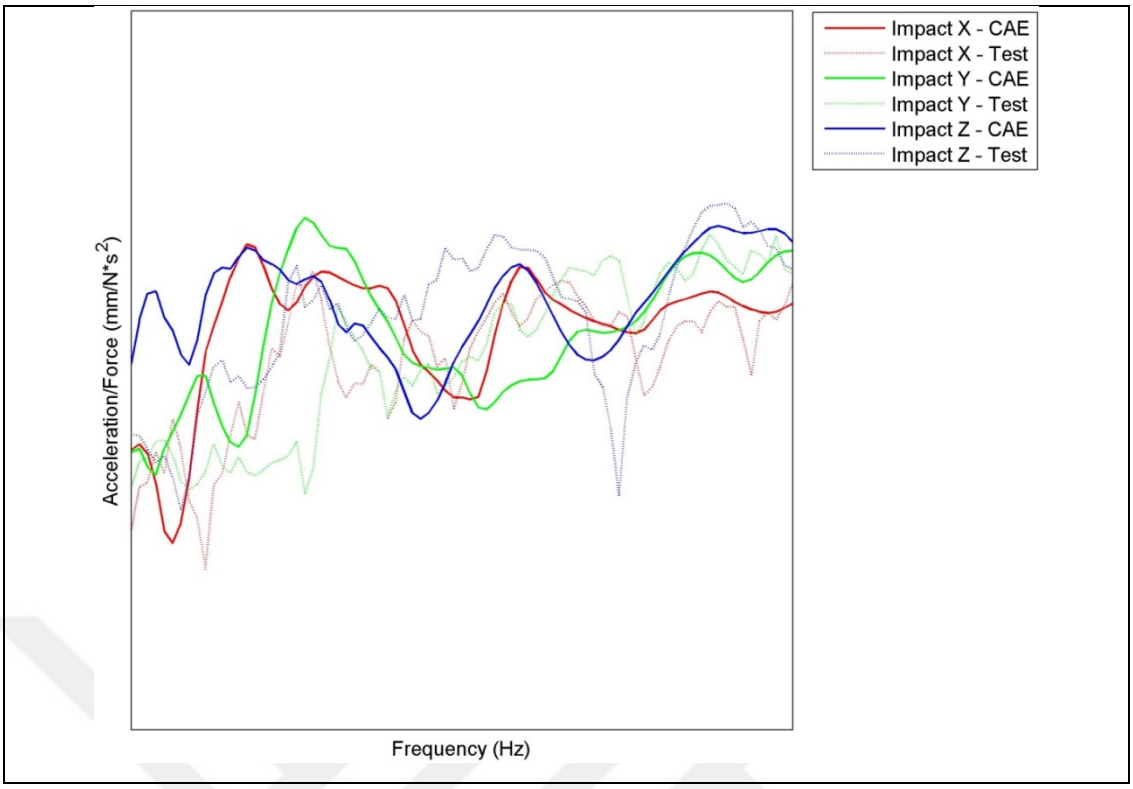

Figure 5.63: VTF correlation for transferpath9 response7.

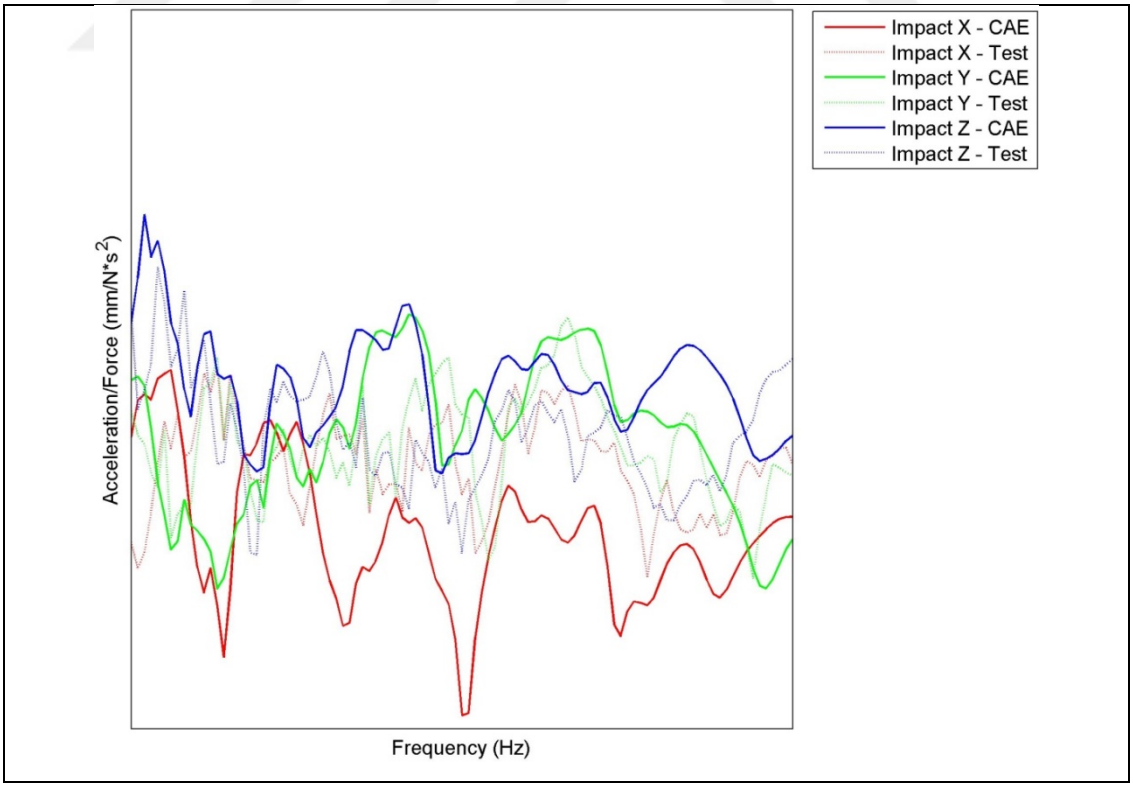

Figure 5.64: VTF correlation for transferpath10 response1.

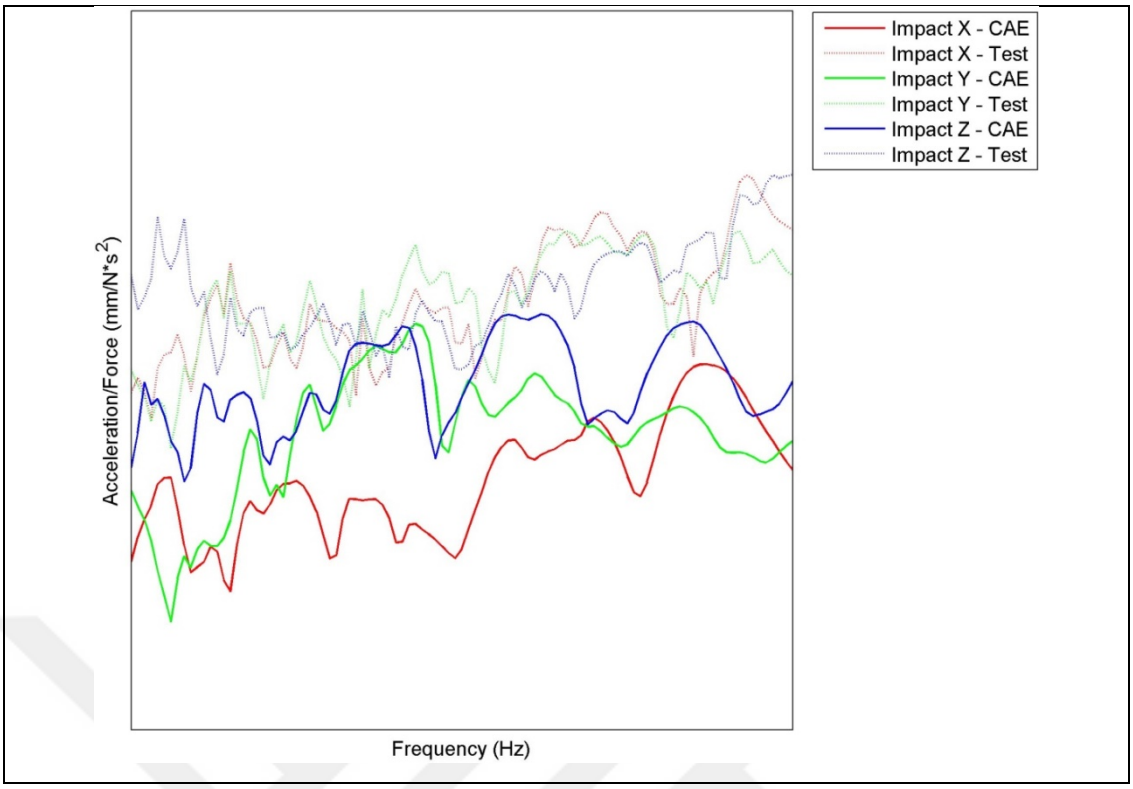

Figure 5.65: VTF correlation for transferpath10 response2.

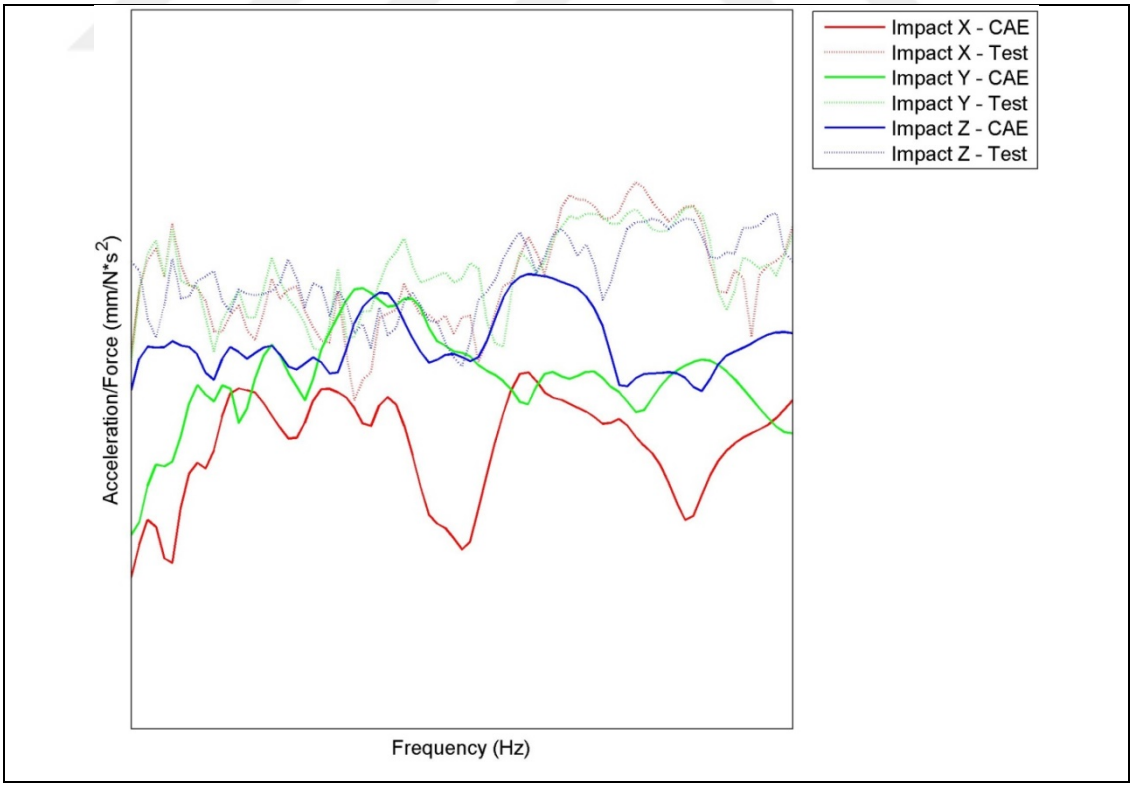

Figure 5.66: VTF correlation for transferpath10 response3.

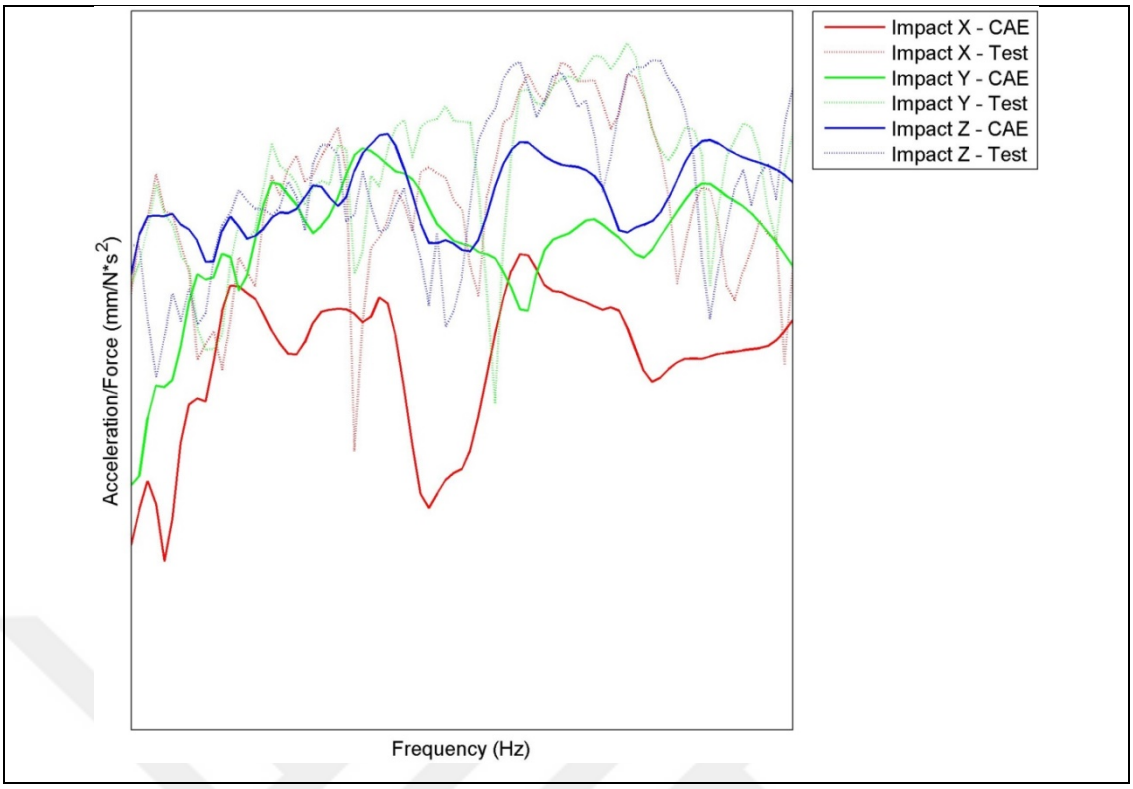

Figure 5.67: VTF correlation for transferpath10 response4.

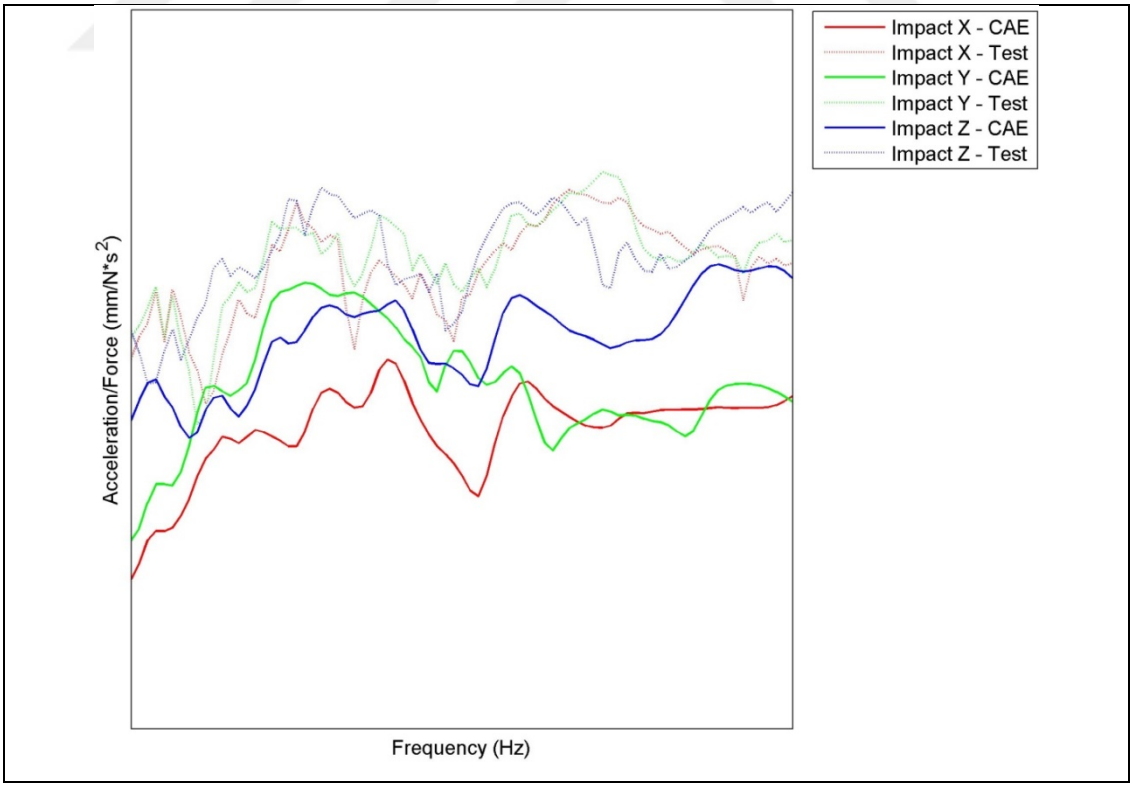

Figure 5.68: VTF correlation for transferpath10 response5.

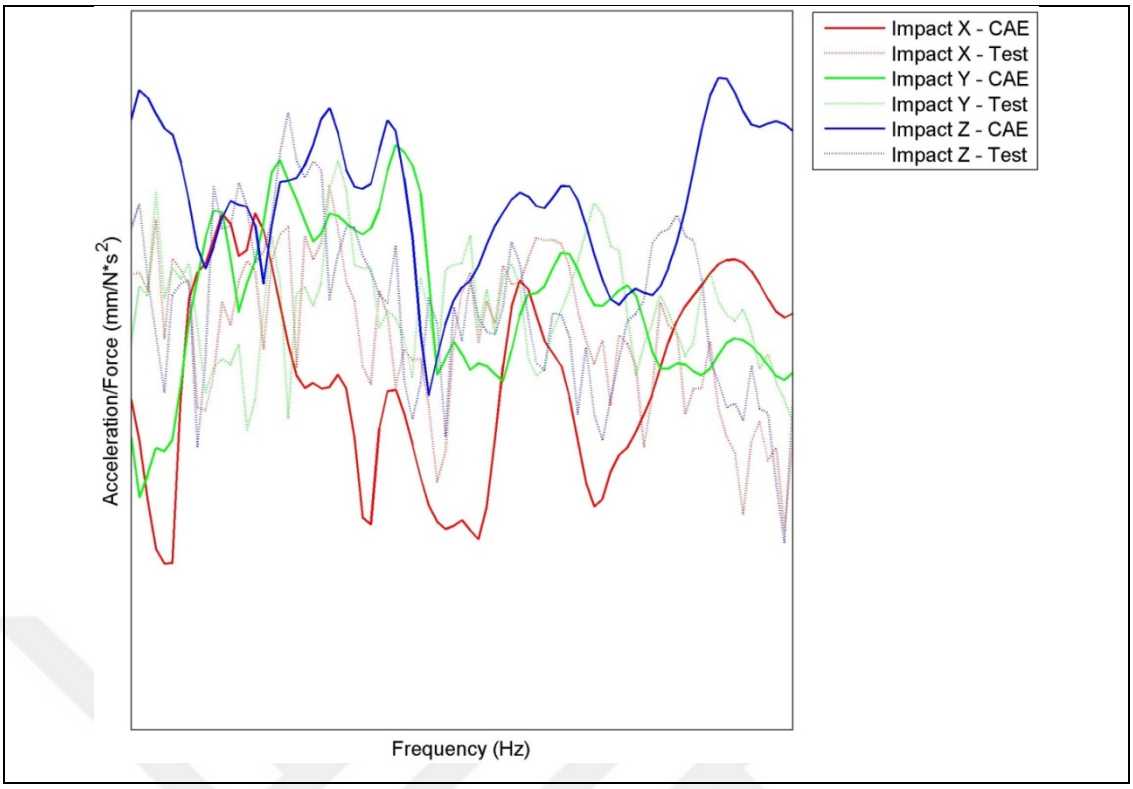

Figure 5.69: VTF correlation for transferpath10 response6.

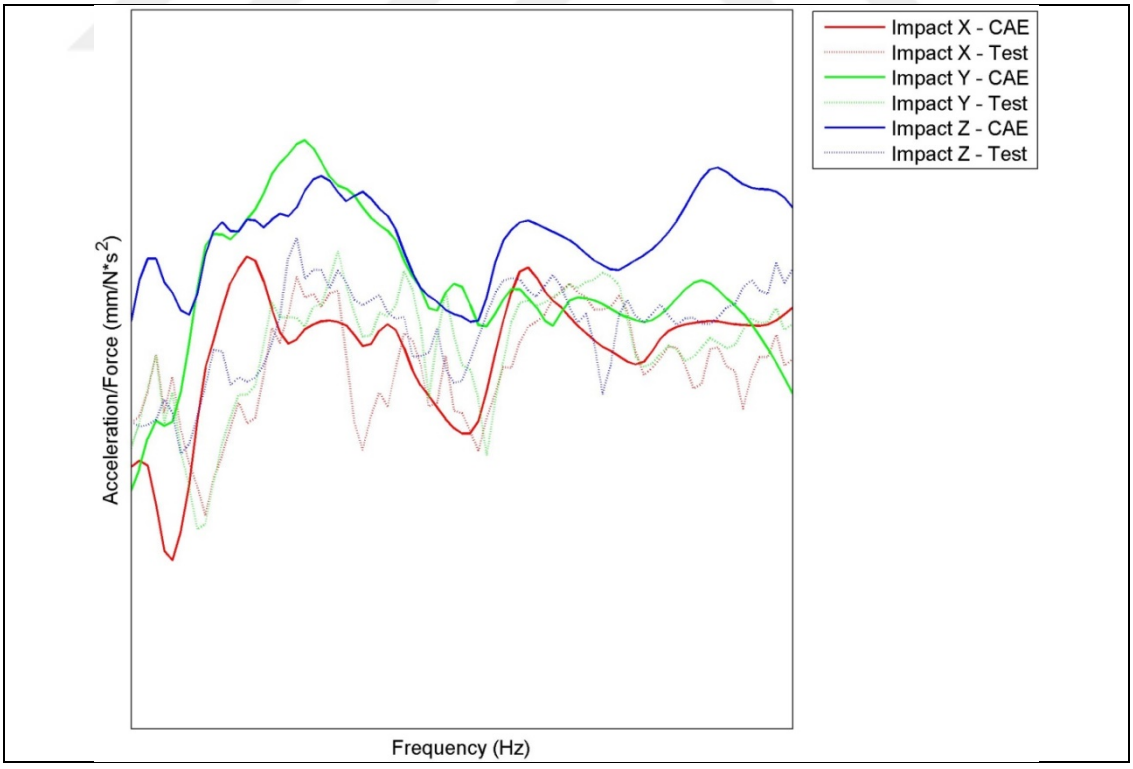

Figure 5.70: VTF correlation for transferpath10 response7.

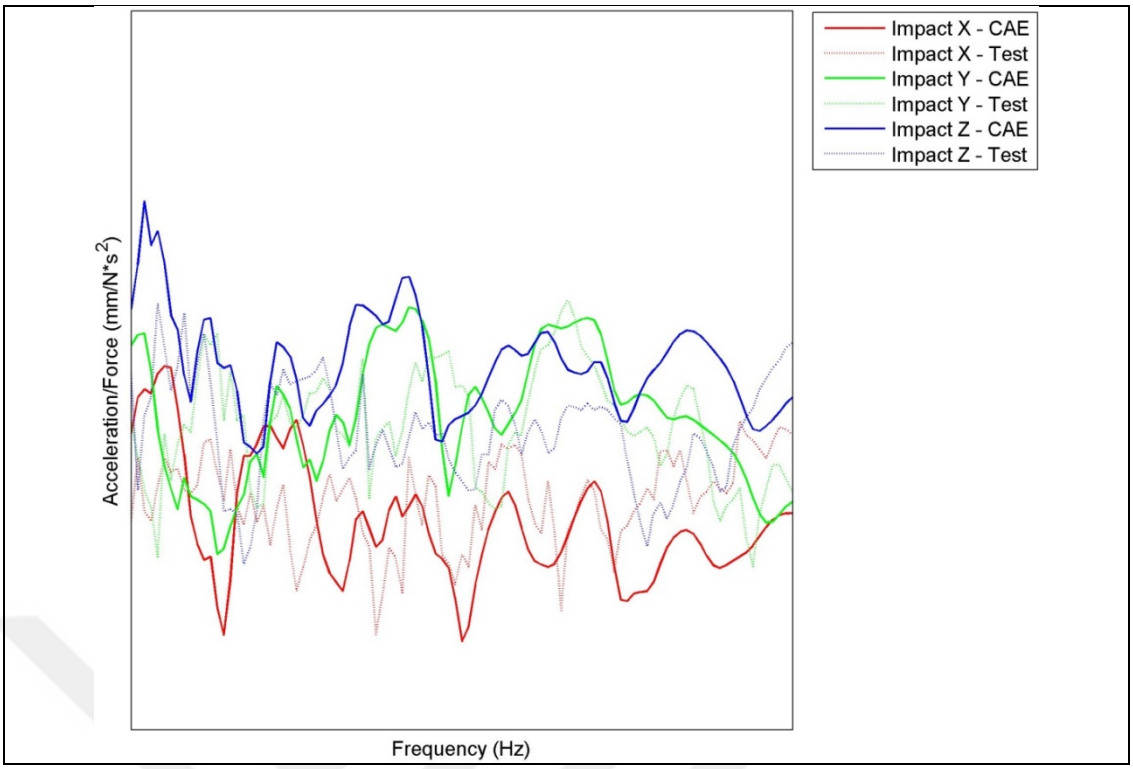

Figure 5.71: VTF correlation for transferpath11 response1.

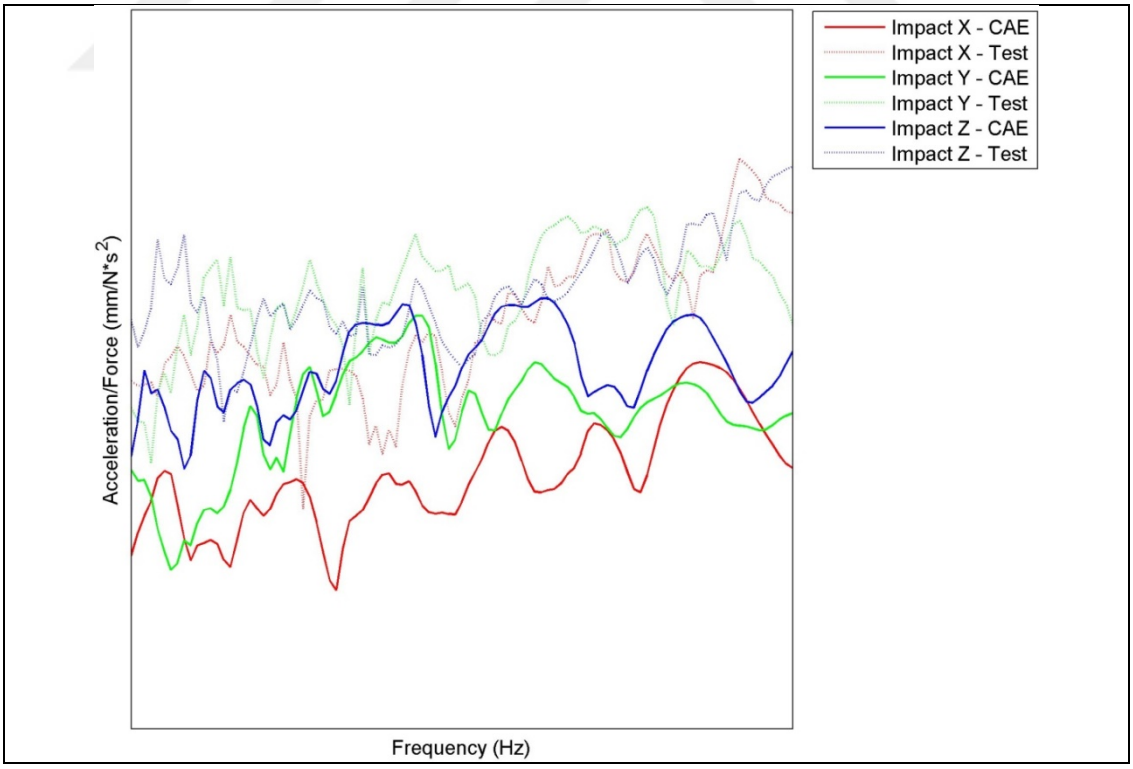

Figure 5.72: VTF correlation for transferpath11 response2.

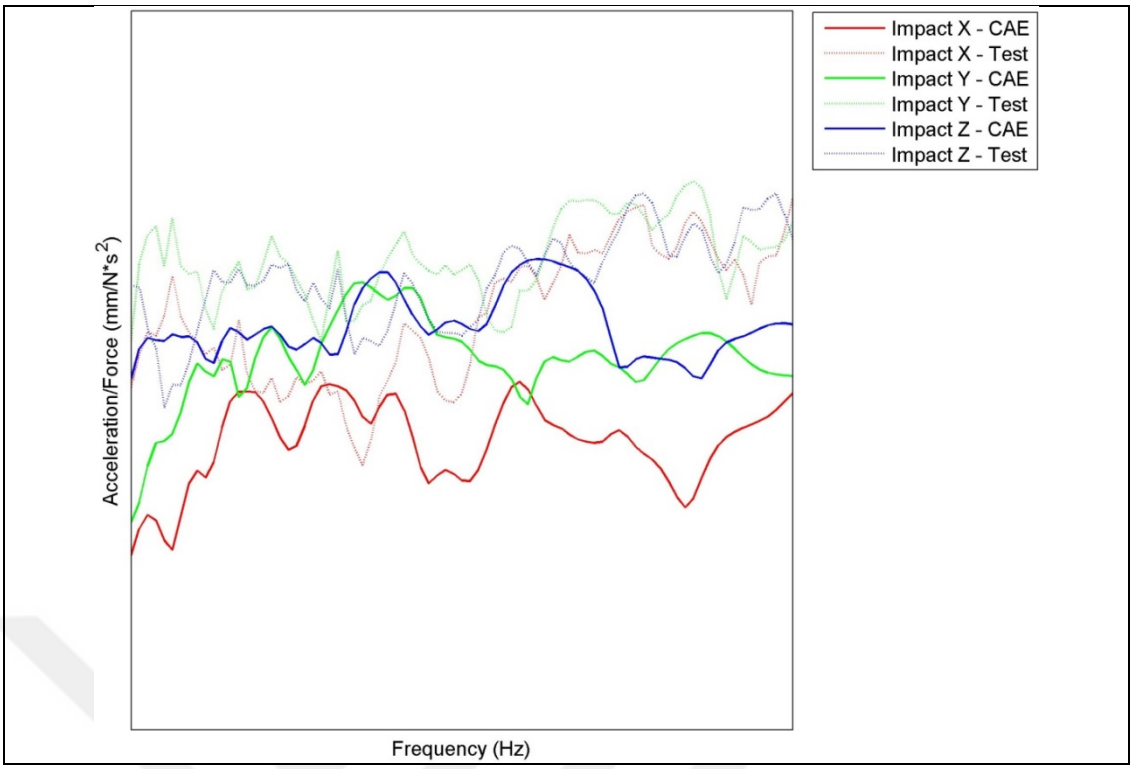

Figure 5.73: VTF correlation for transferpath11 response3.

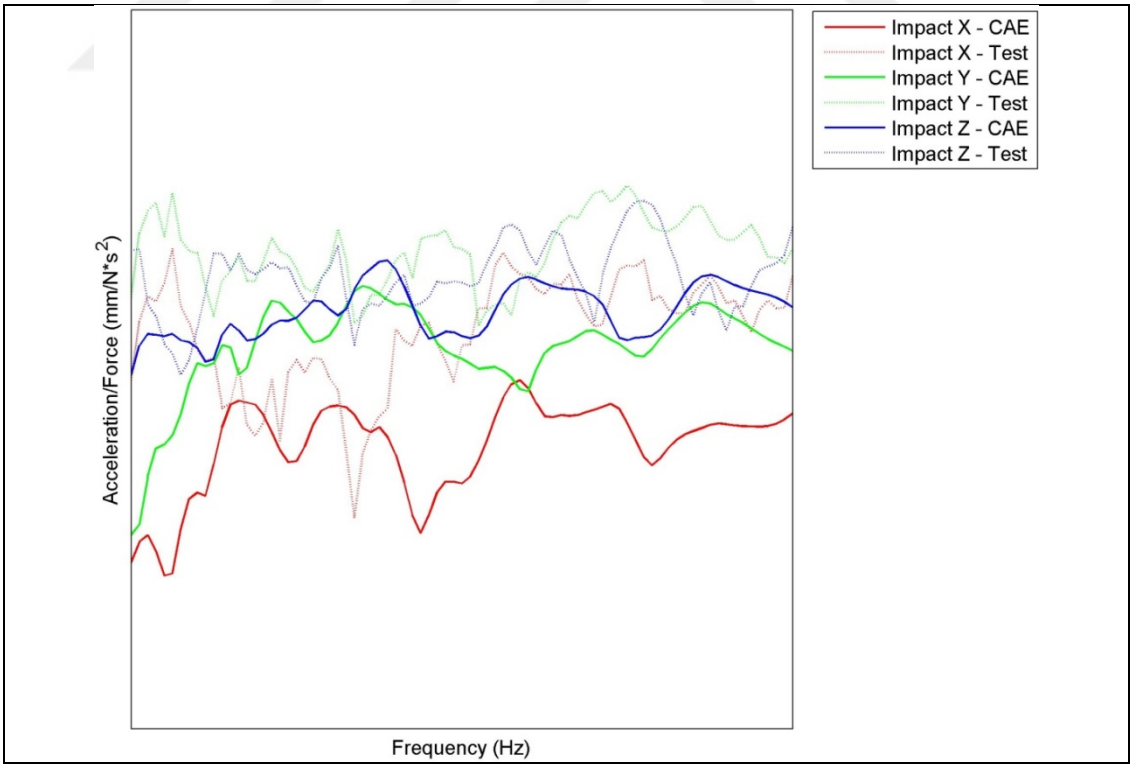

Figure 5.74: VTF correlation for transferpath11 response4.

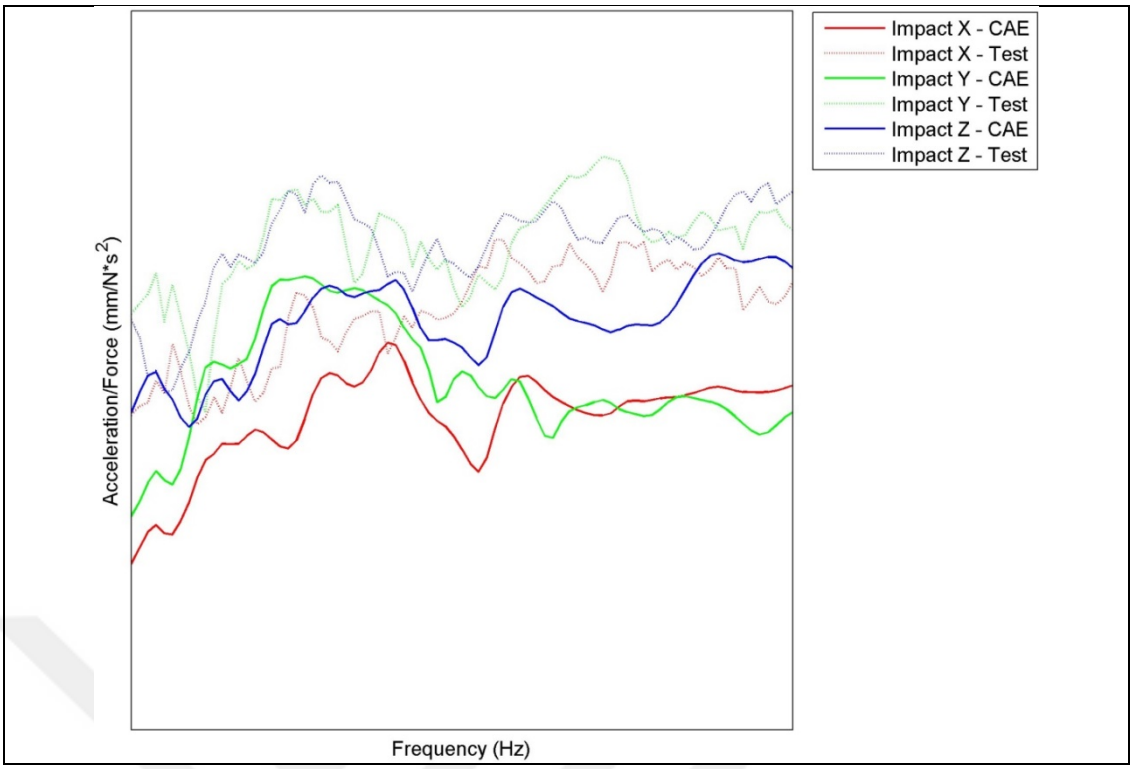

Figure 5.75: VTF correlation for transferpath11 response5.

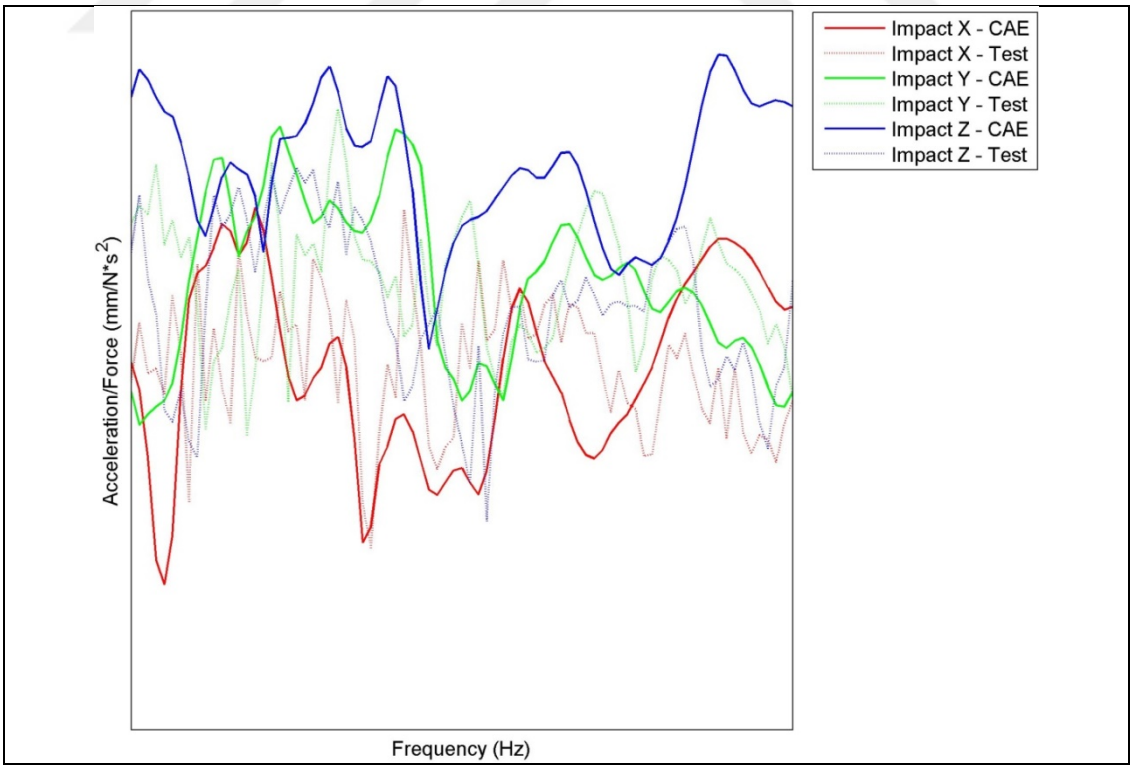

Figure 5.76: VTF correlation for transferpath11 response6.

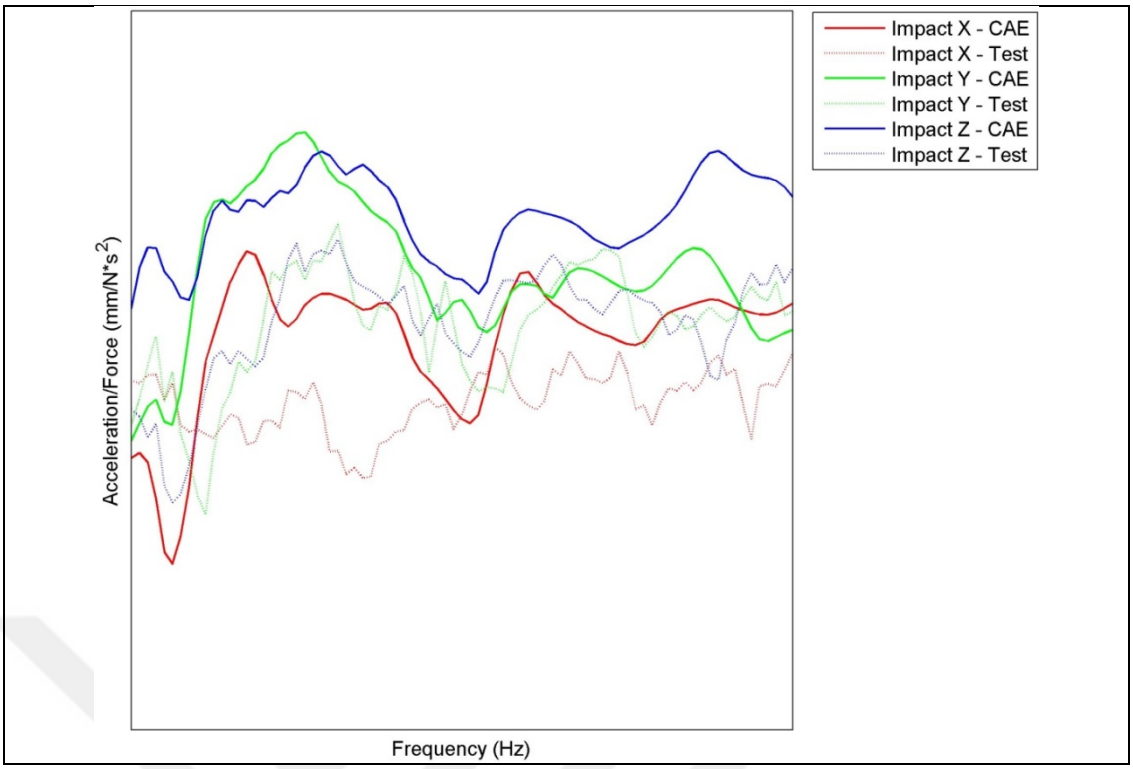

Figure 5.77: VTF correlation for transferpath11 response7.

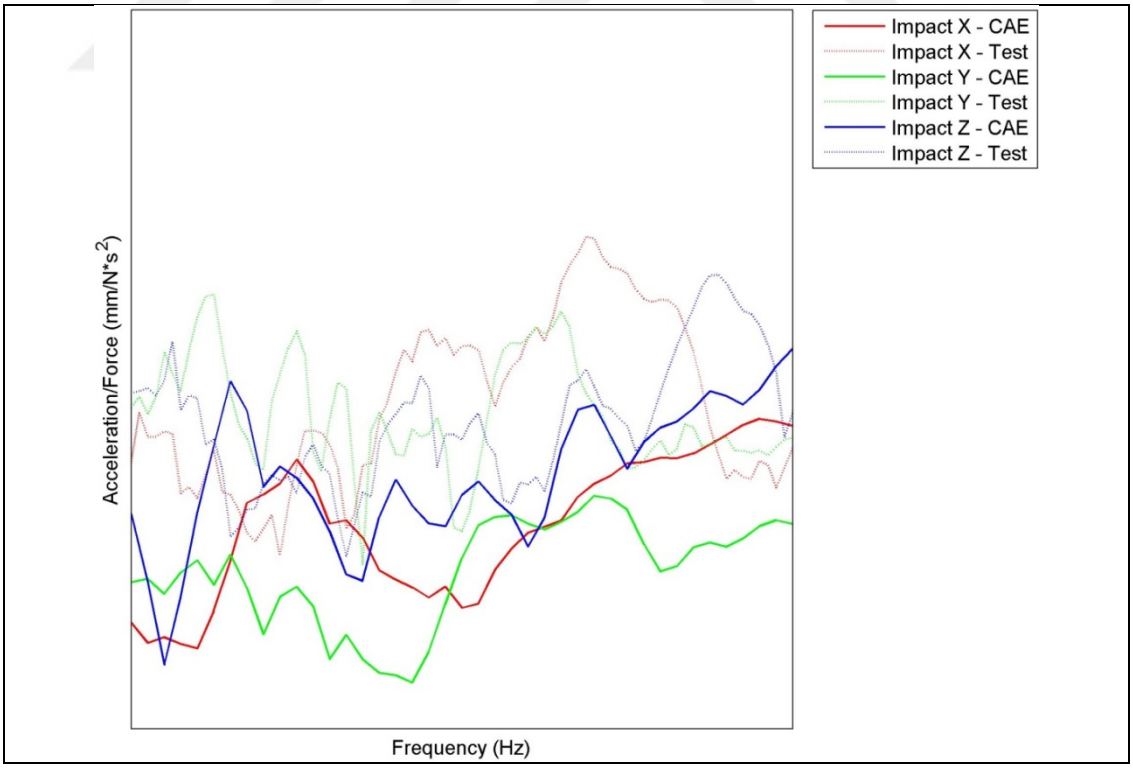

Figure 5.78: VTF correlation for transferpath12 response1.

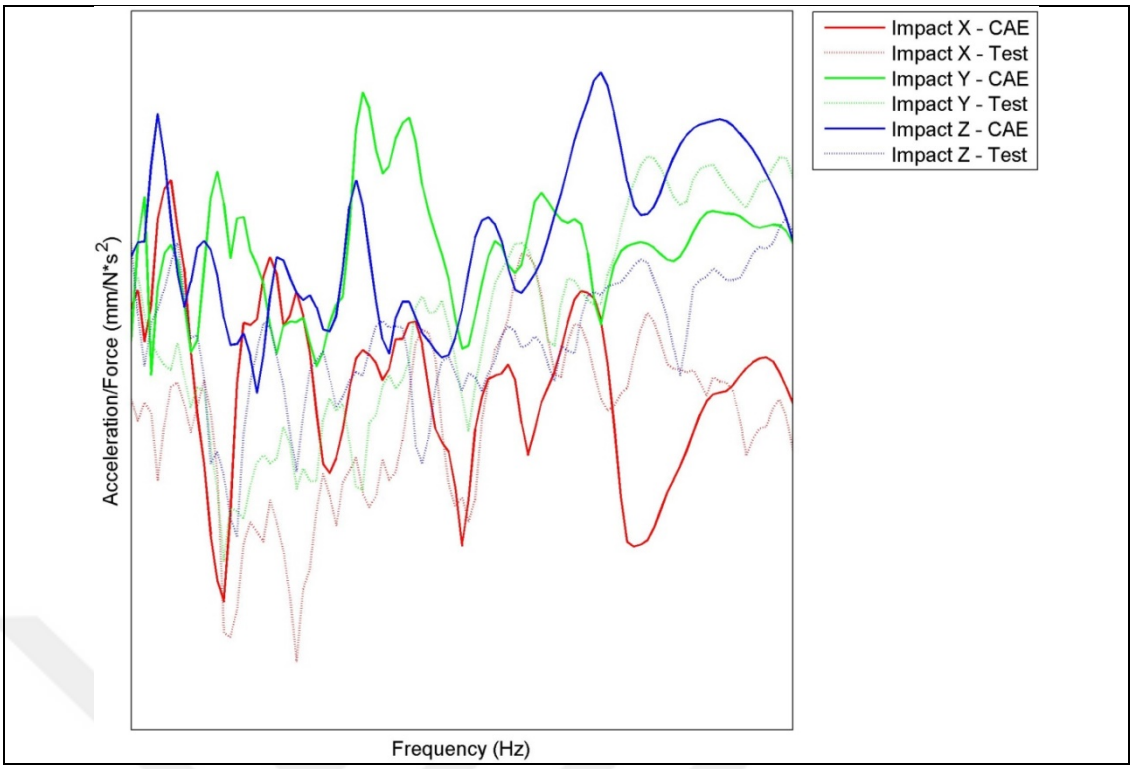

Figure 5.79: VTF correlation for transferpath13 response1.

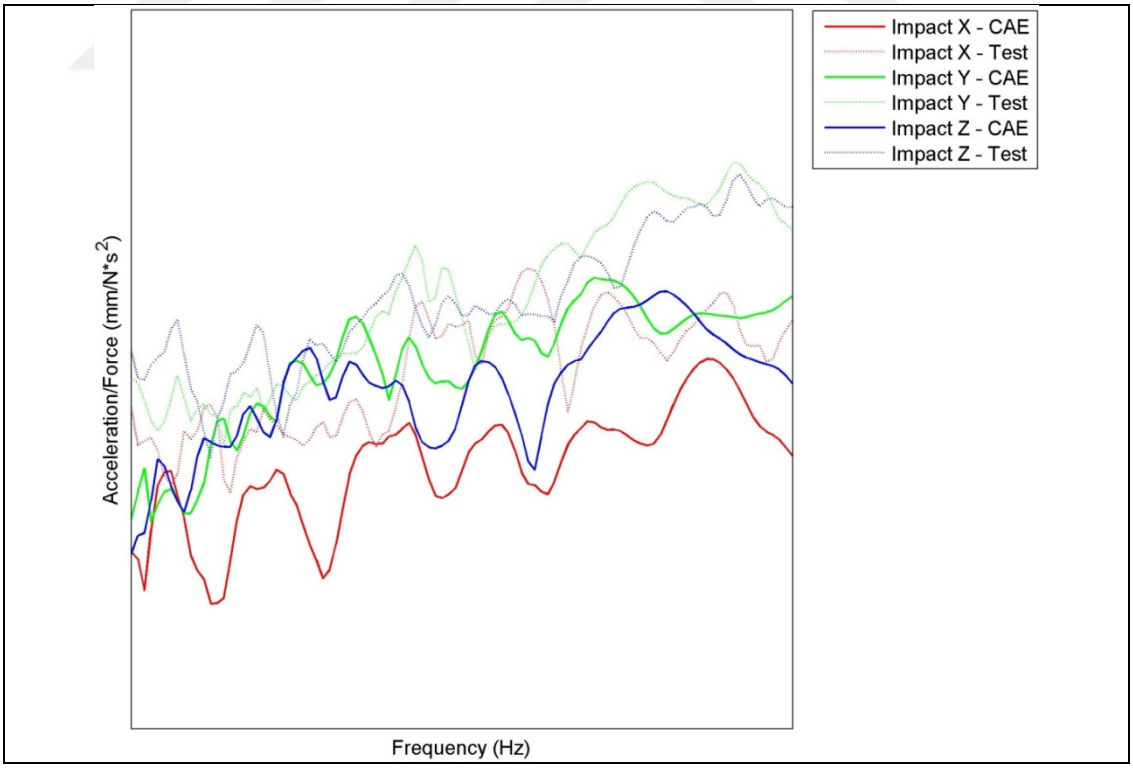

Figure 5.80: VTF correlation for transferpath13 response2.

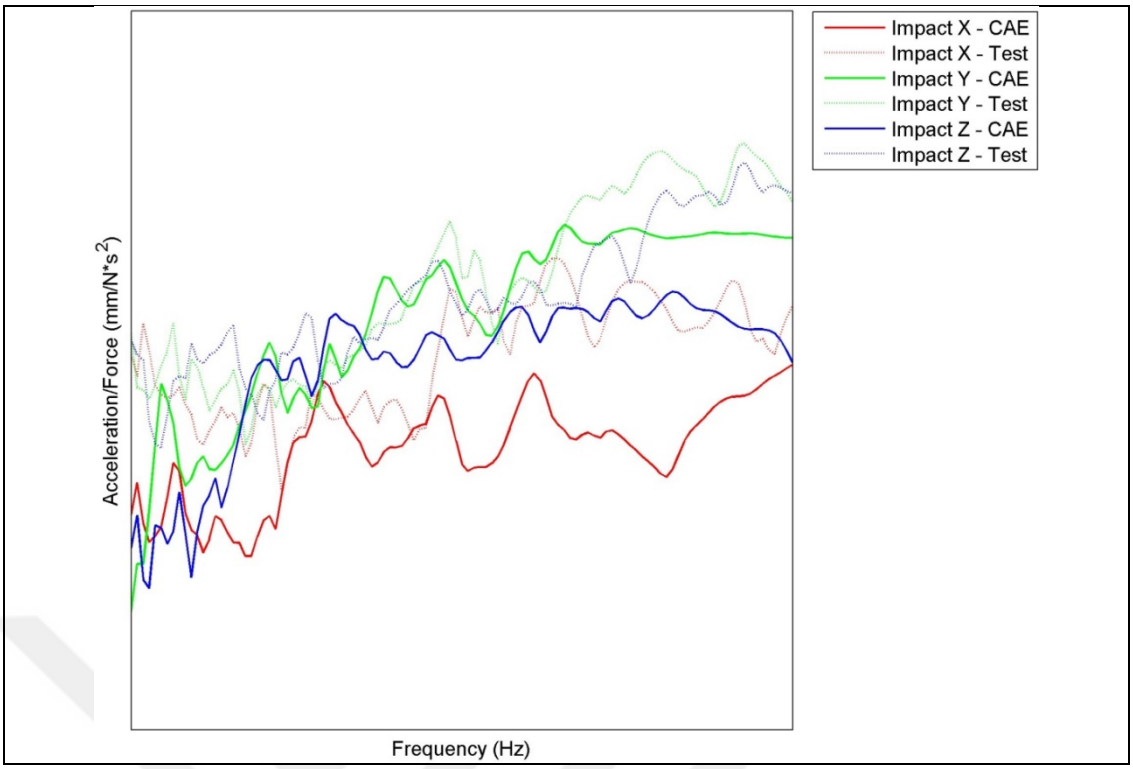

Figure 5.81: VTF correlation for transferpath13 response3.

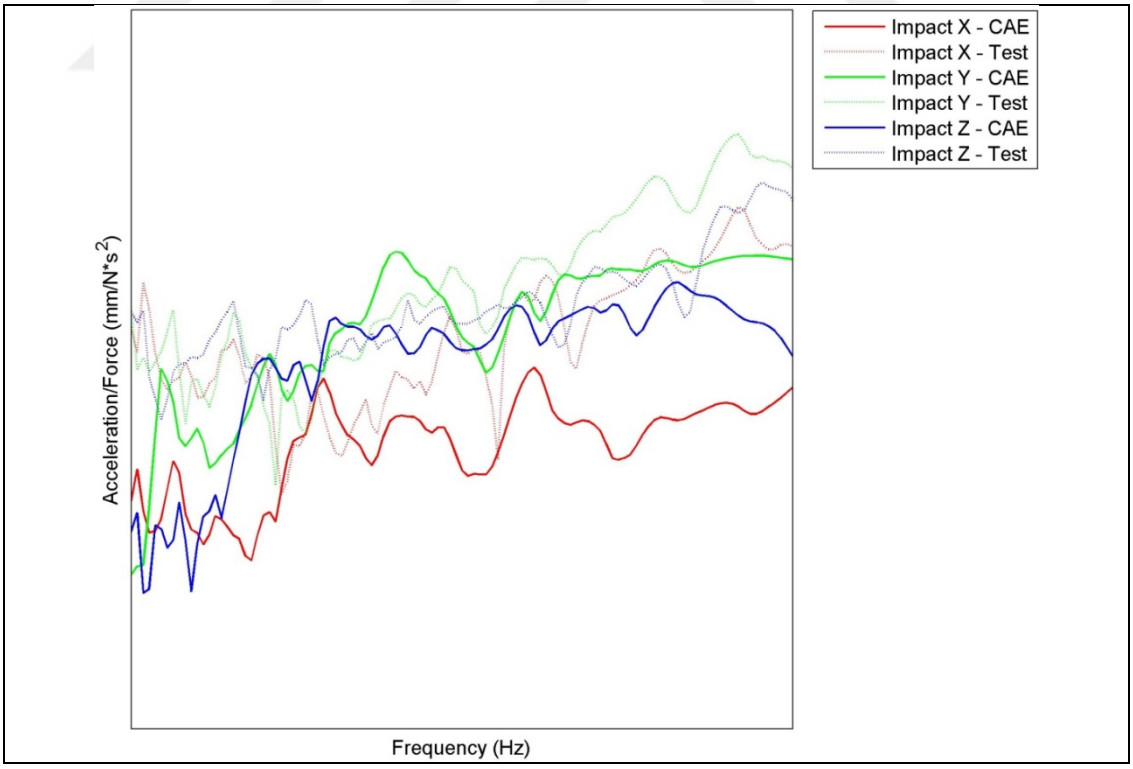

Figure 5.82: VTF correlation for transferpath13 response4.

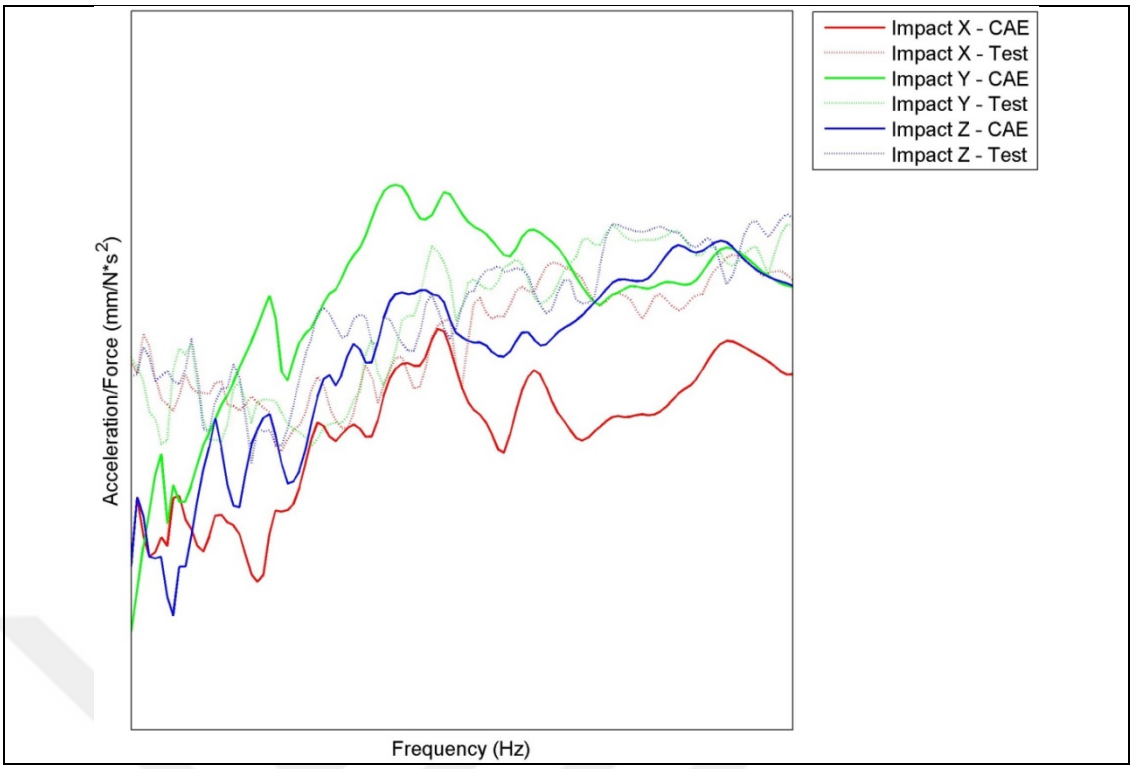

Figure 5.83: VTF correlation for transferpath13 response5.

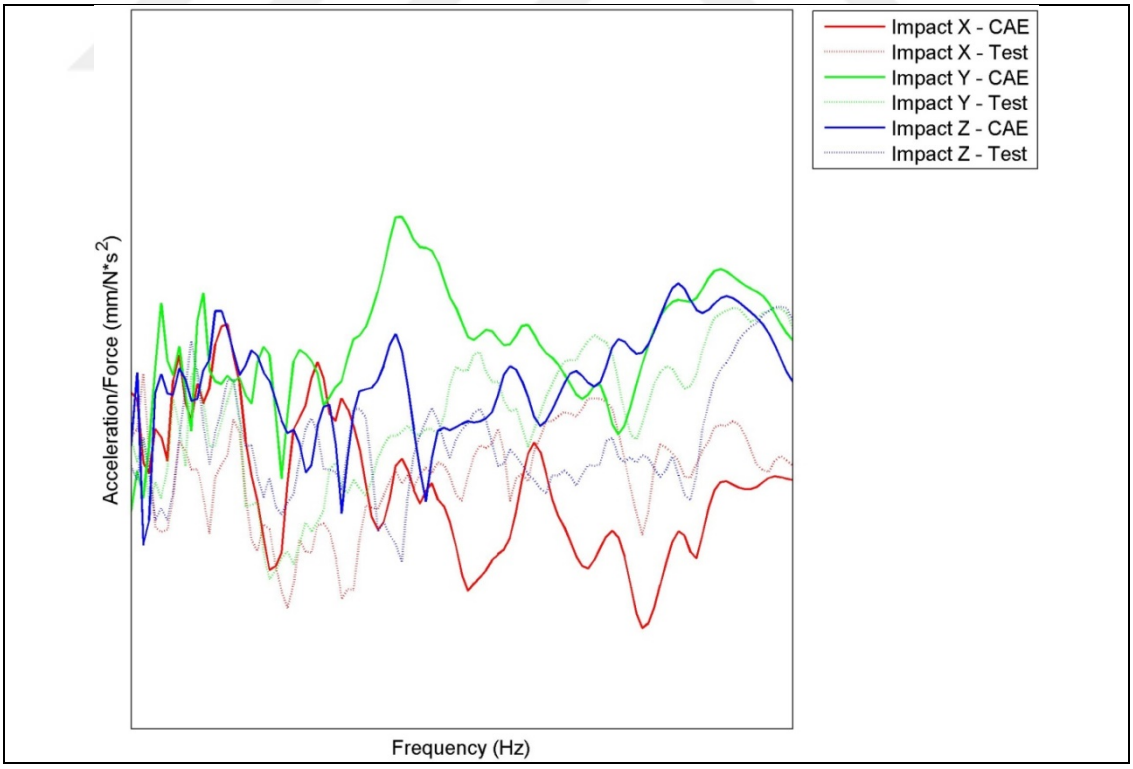

Figure 5.84: VTF correlation for transferpath13 response6.

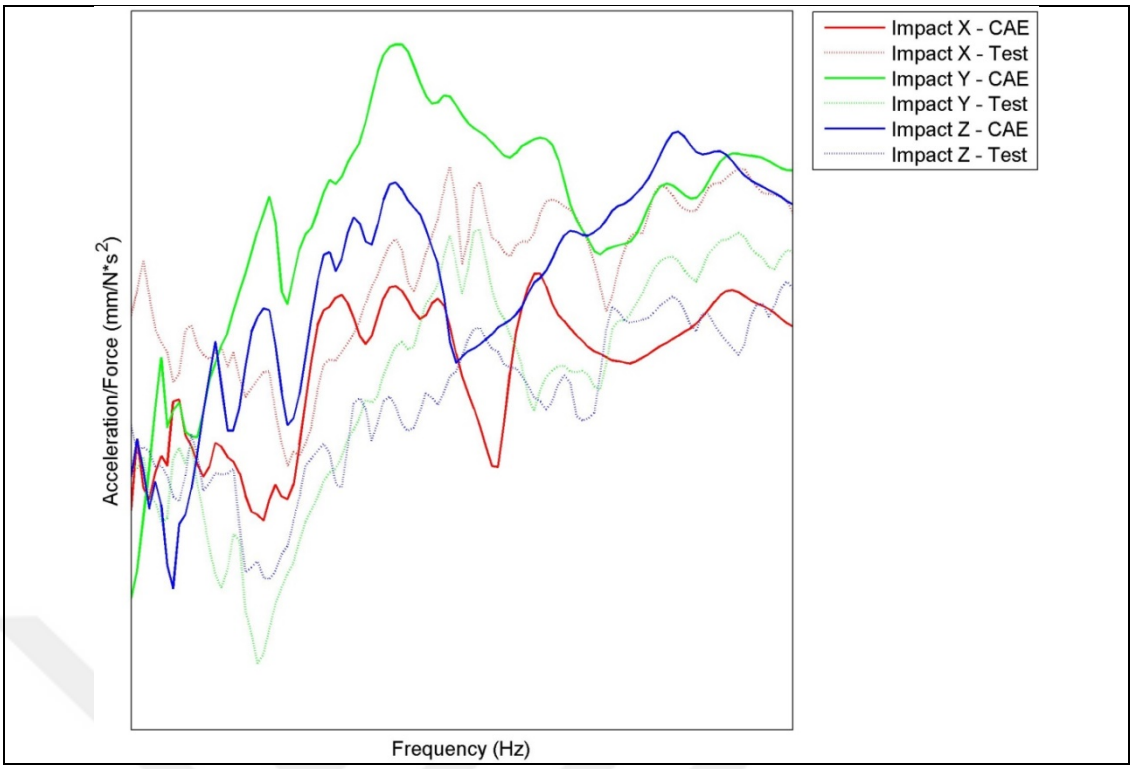

Figure 5.85: VTF correlation for transferpath13 response7.

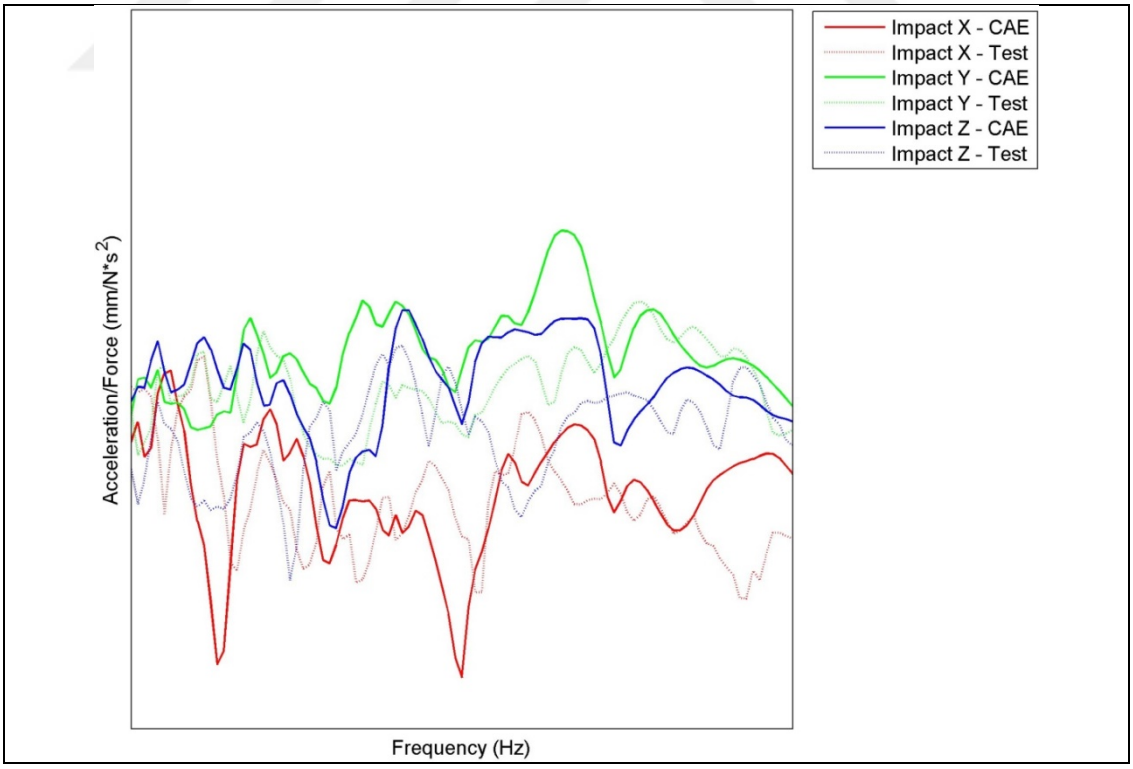

Figure 5.86: VTF correlation for transferpath14 response1.

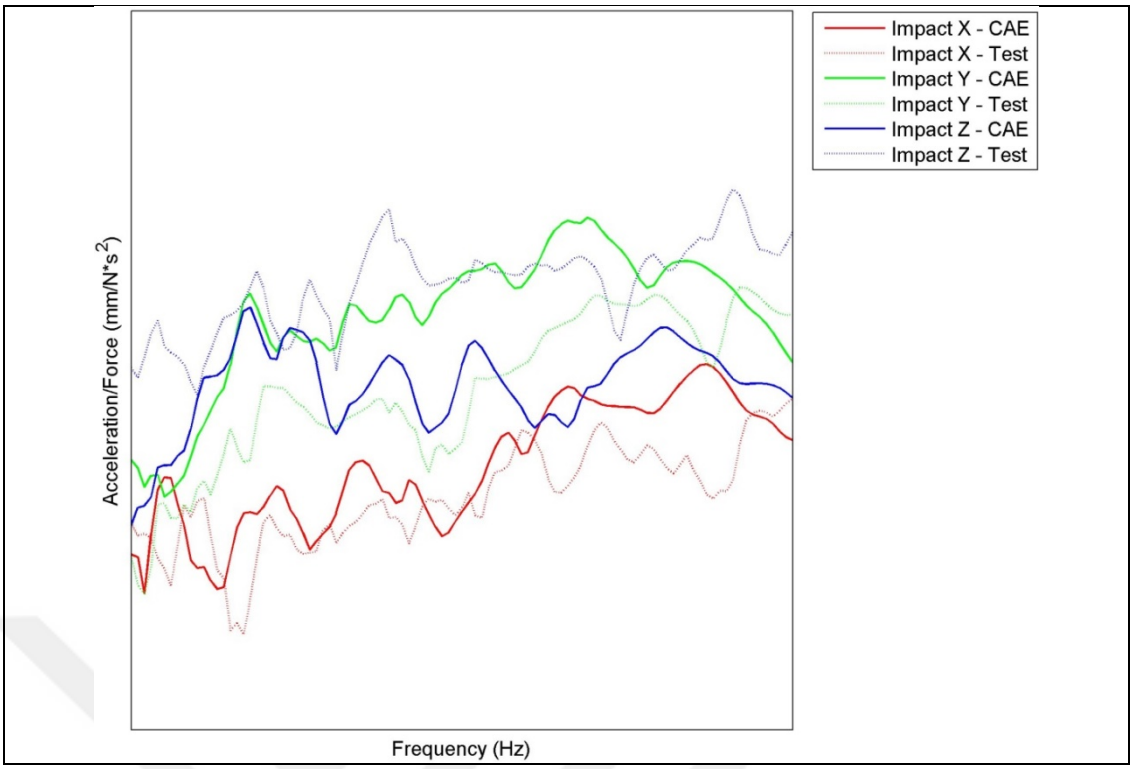

Figure 5.87: VTF correlation for transferpath14 response2.

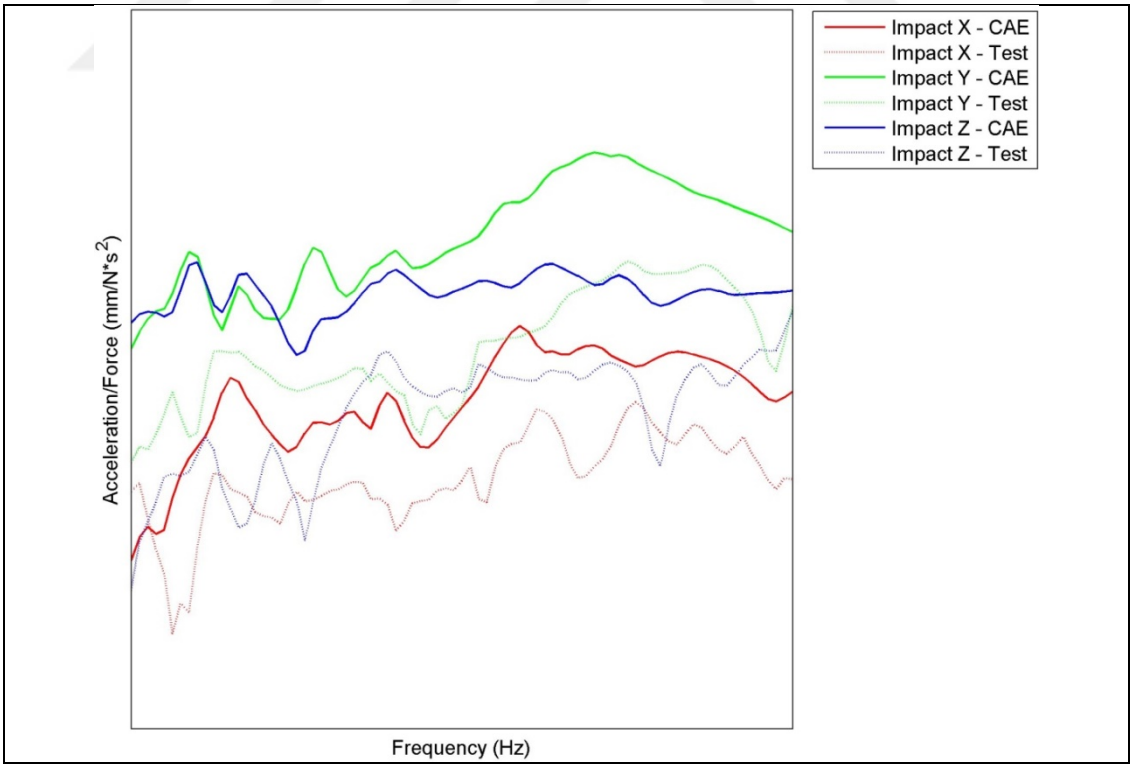

Figure 5.88: VTF correlation for transferpath14 response3.

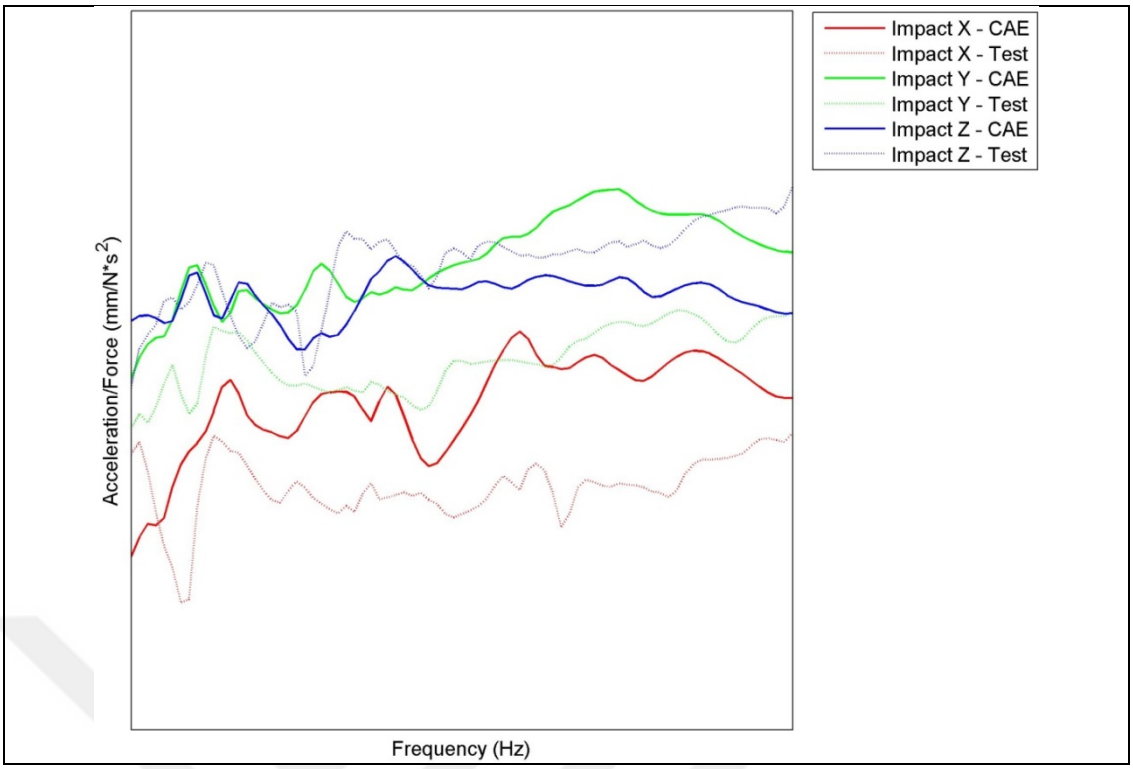

Figure 5.89: VTF correlation for transferpath14 response4.

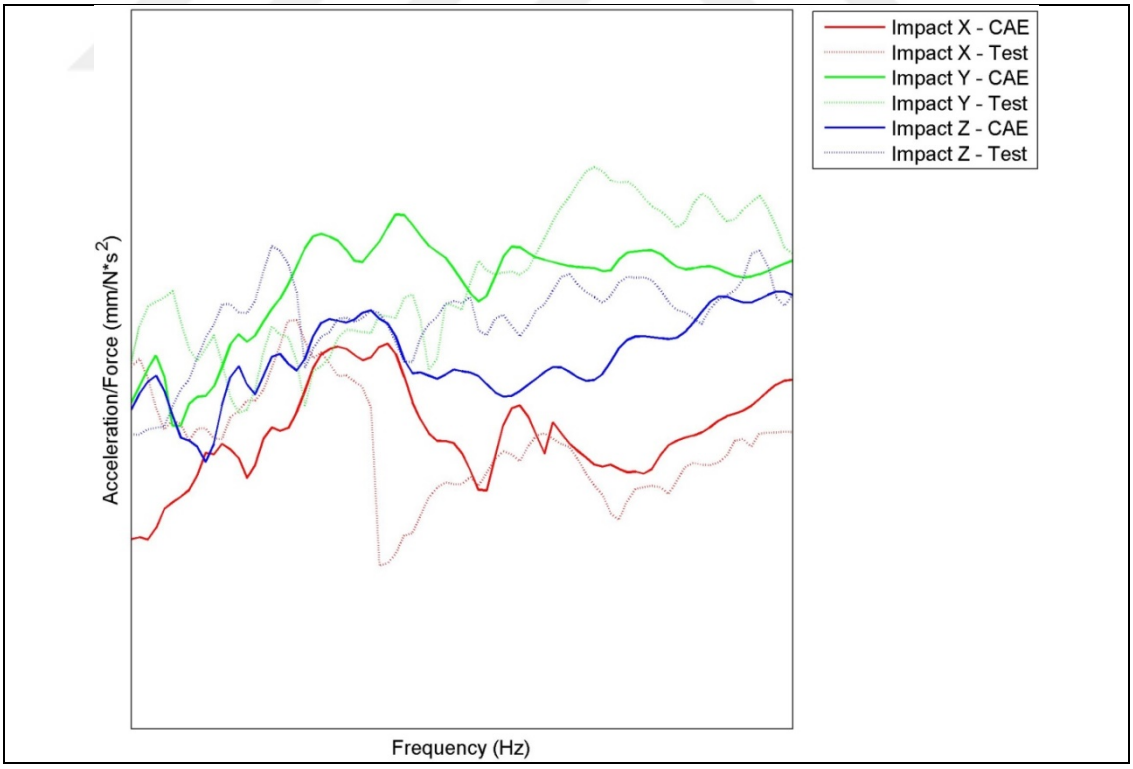

Figure 5.90: VTF correlation for transferpath14 response5.

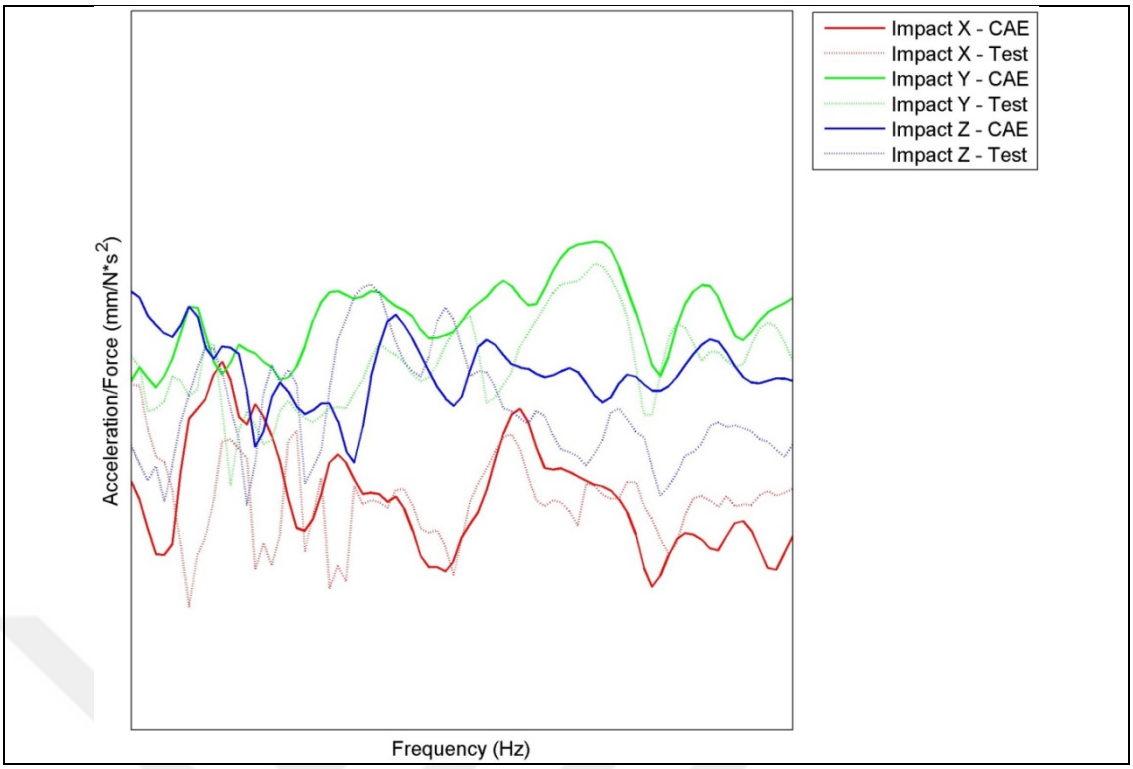

Figure 5.91: VTF correlation for transferpath14 response6.

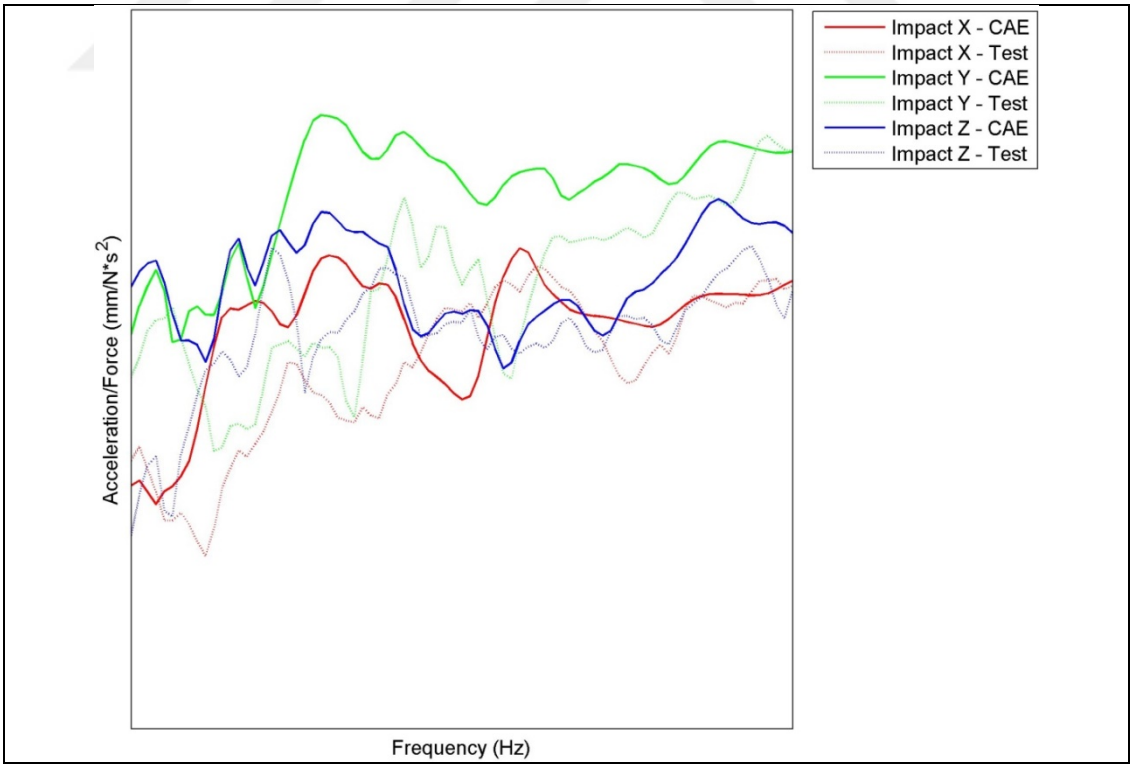

Figure 5.92: VTF correlation for transferpath14 response7.

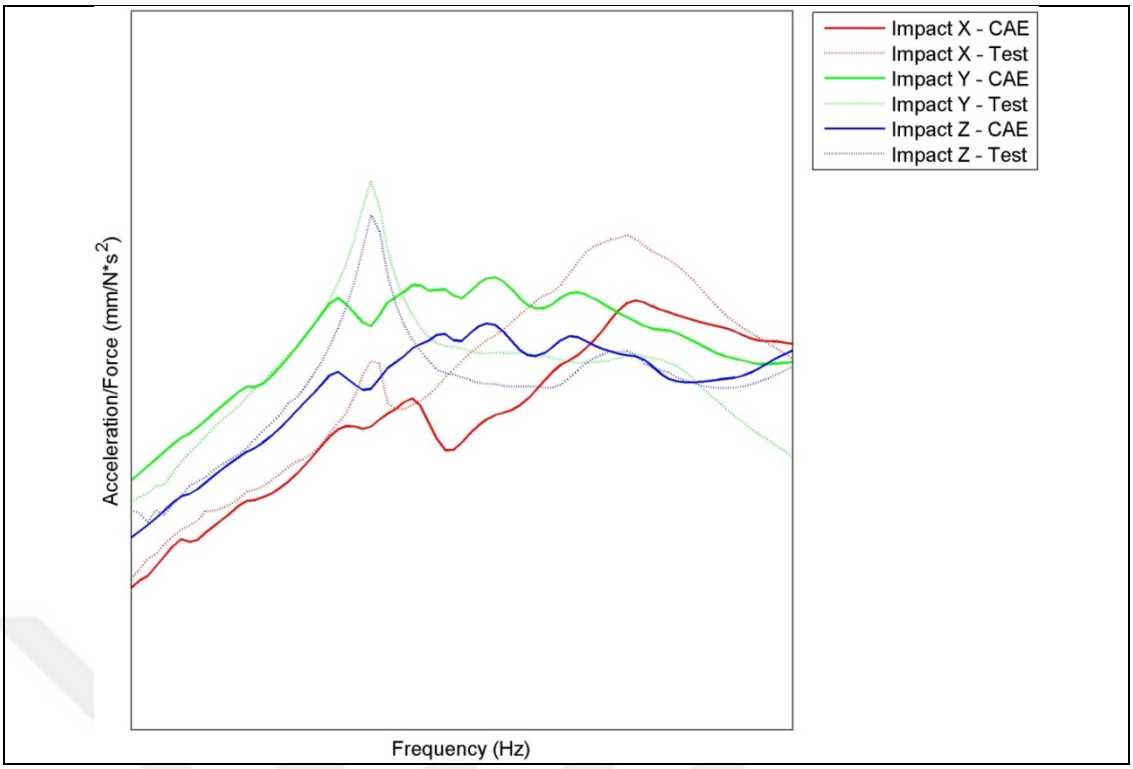

Figure 5.93: VTF correlation for transferpath15 response1.

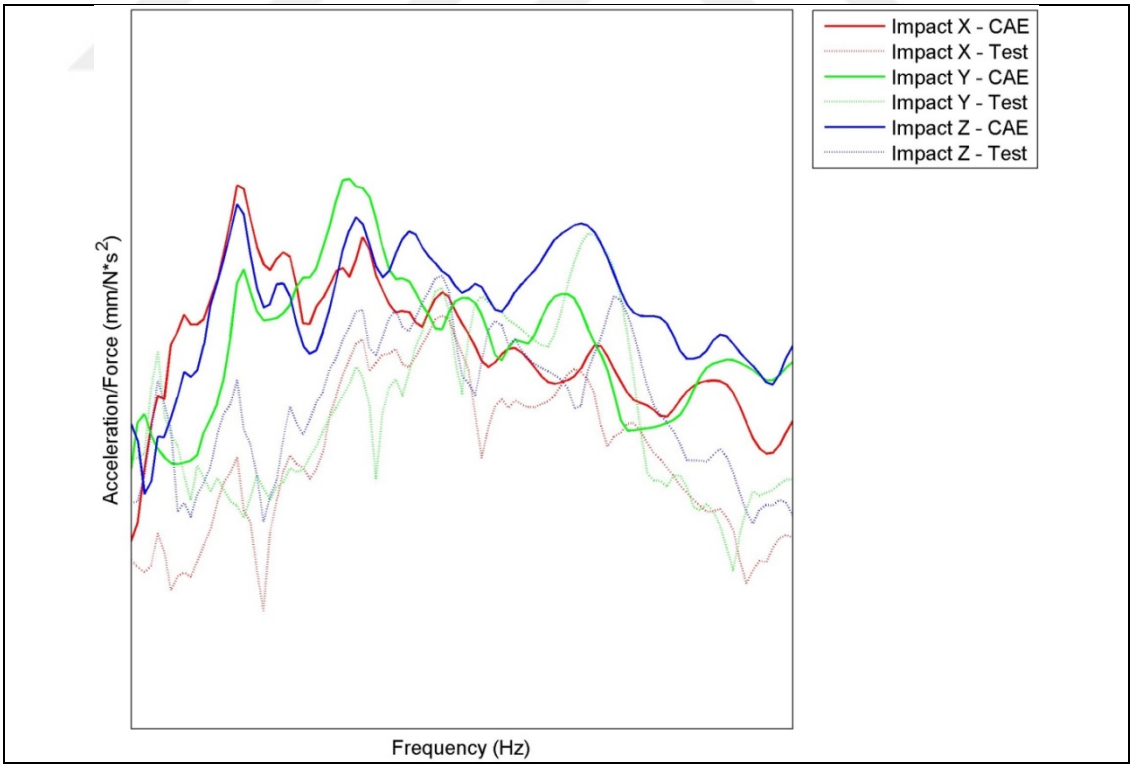

Figure 5.94: VTF correlation for transferpath16 response1.

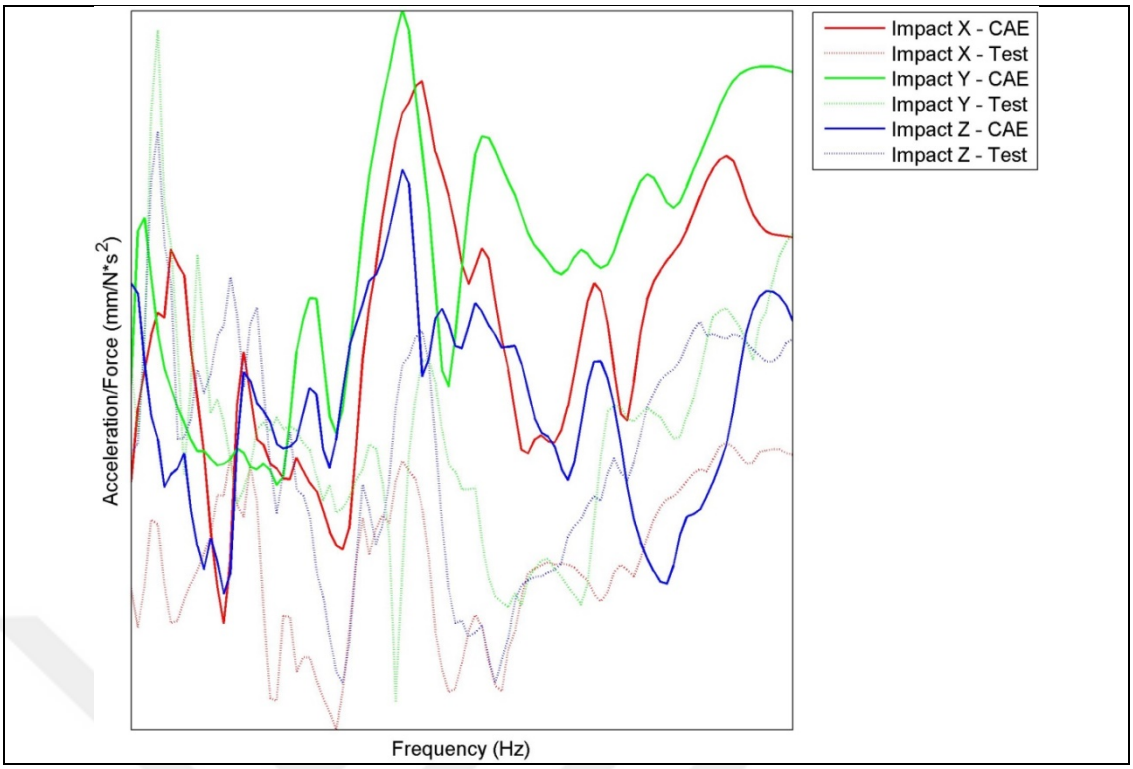

Figure 5.95: VTF correlation for transferpath16 response2.

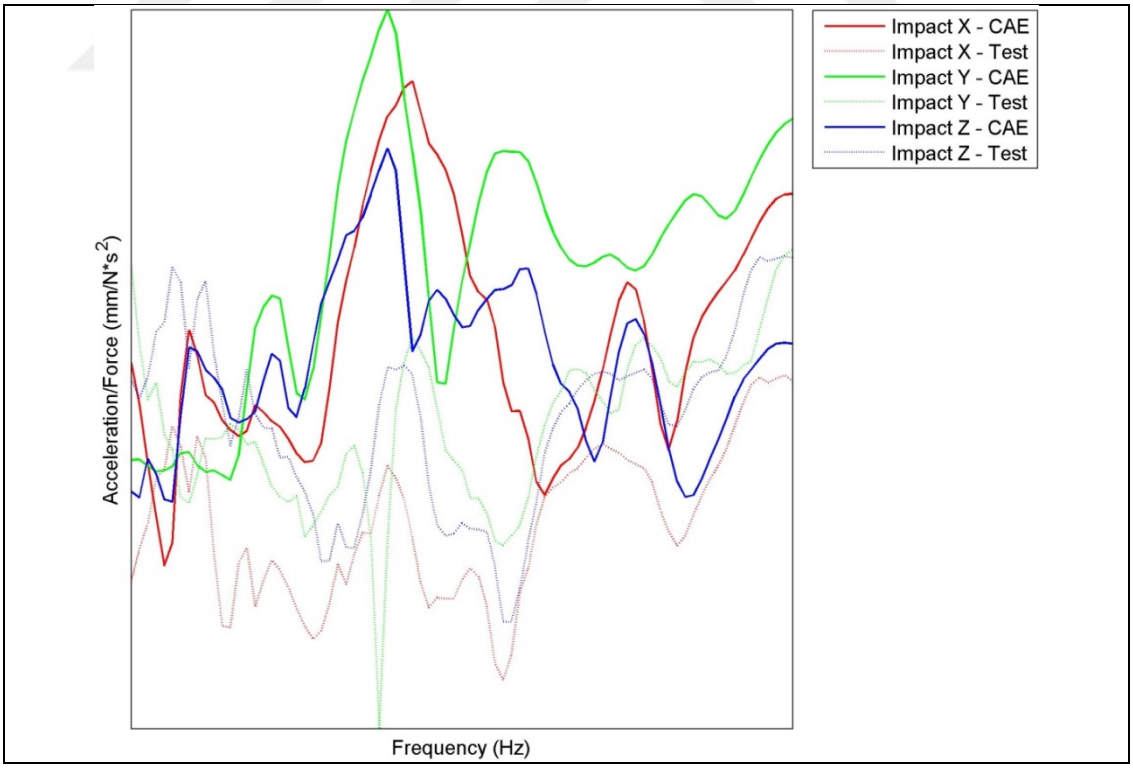

Figure 5.96: VTF correlation for transferpath16 response3.

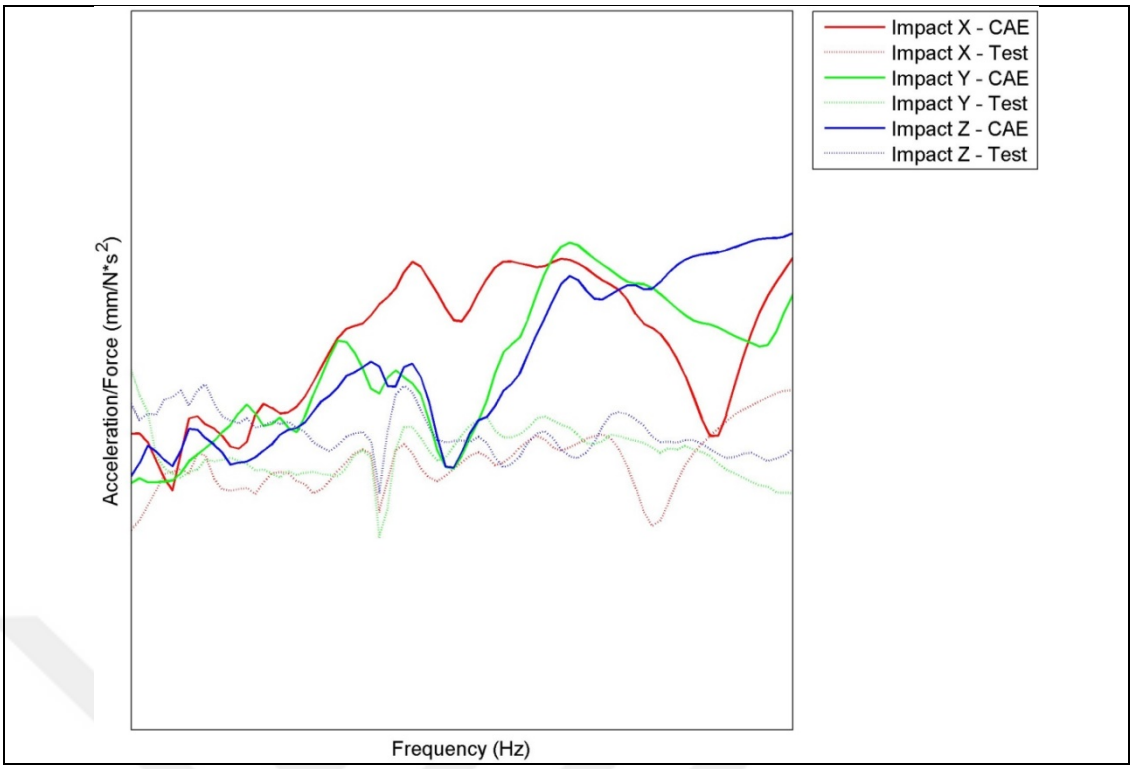

Figure 5.97: VTF correlation for transferpath16 response4.

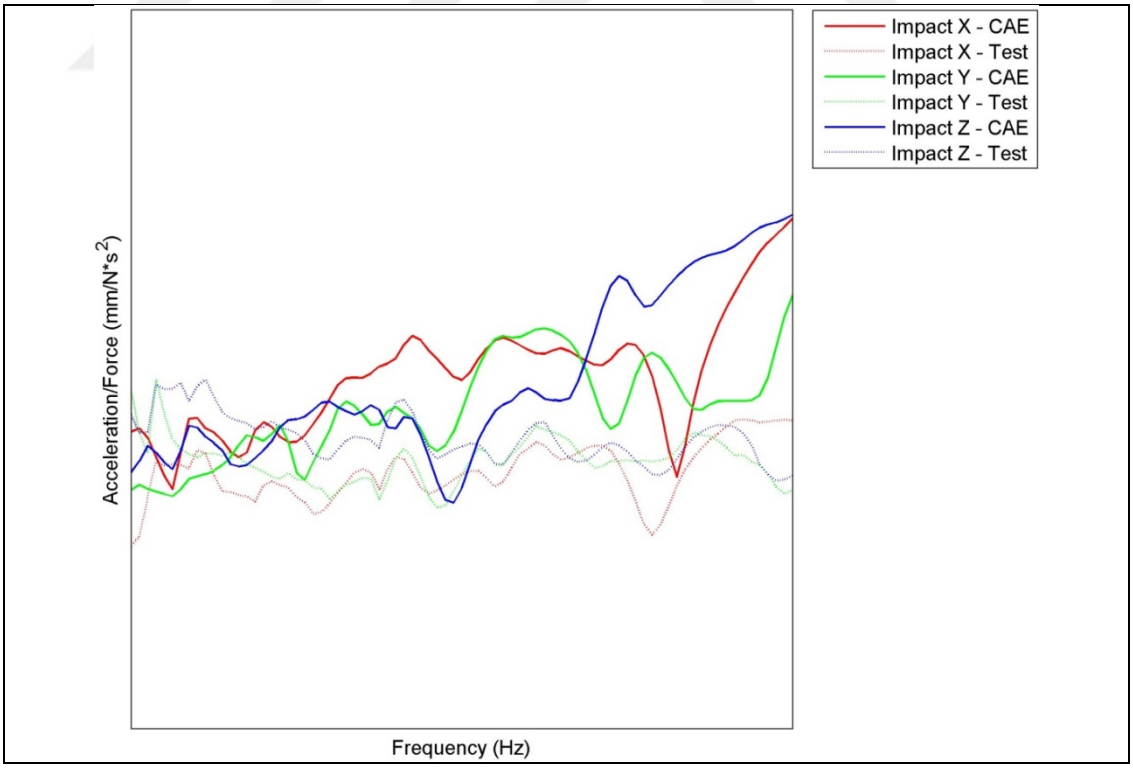

Figure 5.98: VTF correlation for transferpath16 response5.

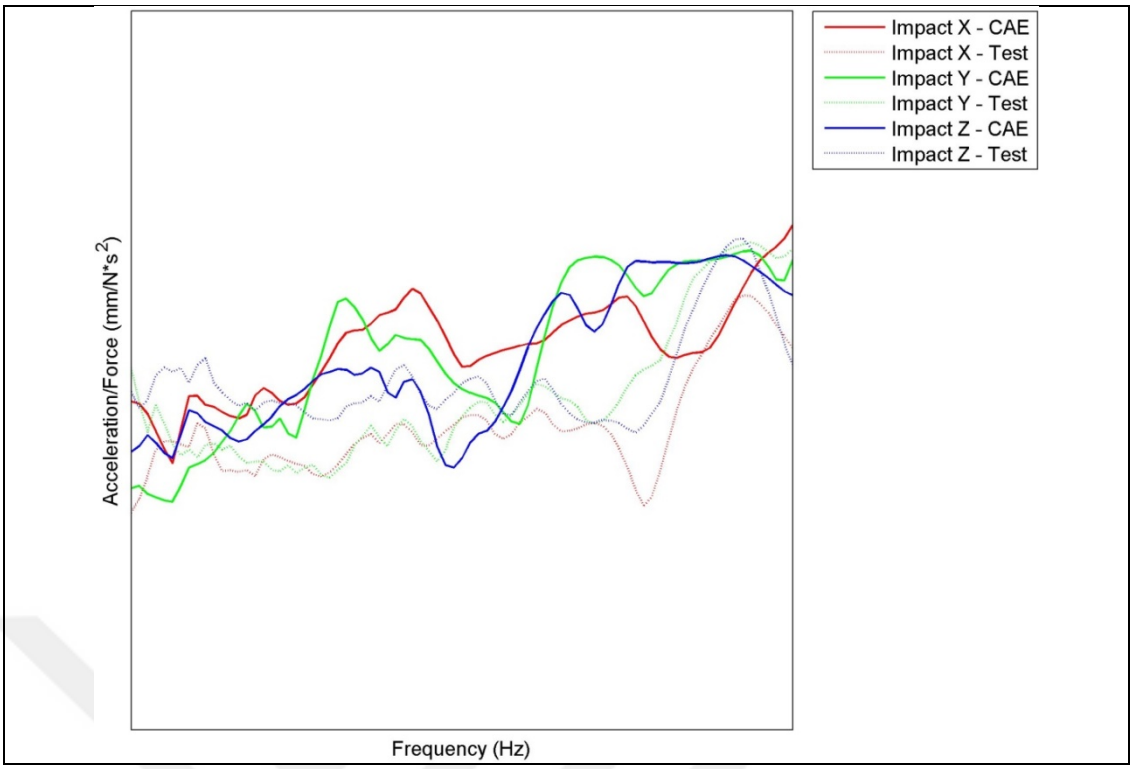

Figure 5.99: VTF correlation for transferpath16 response6.

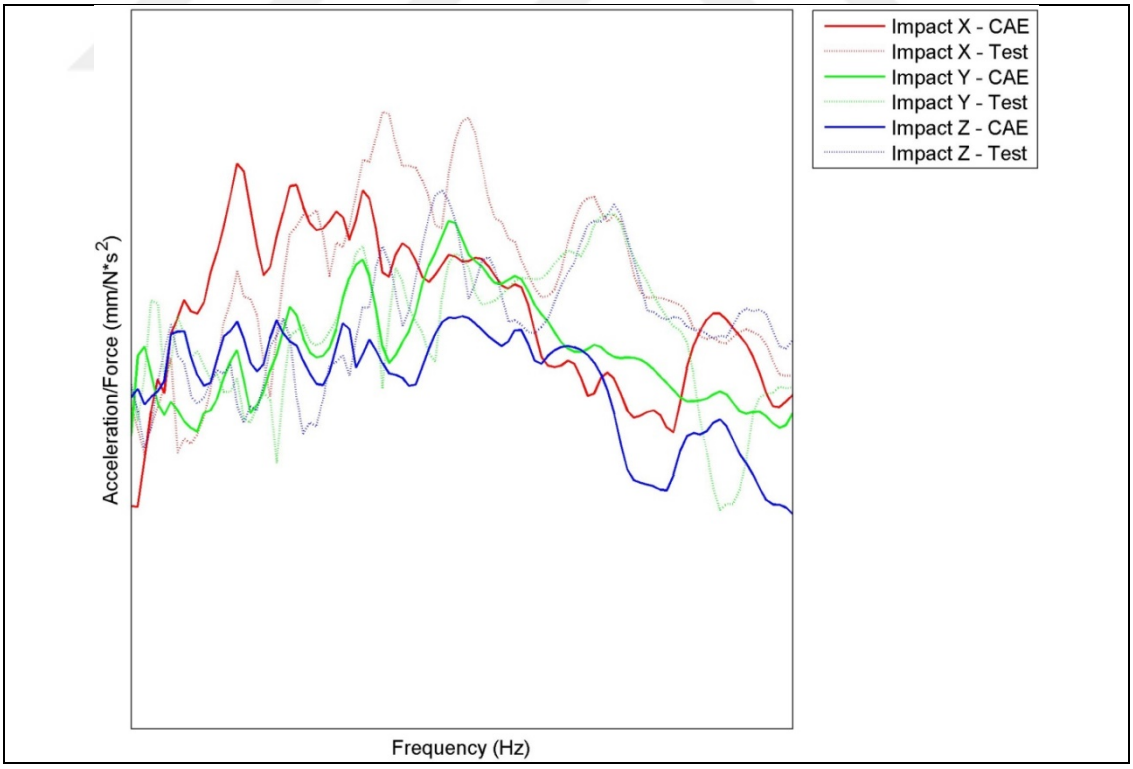

Figure 5.100: VTF correlation for transferpath17 response1.

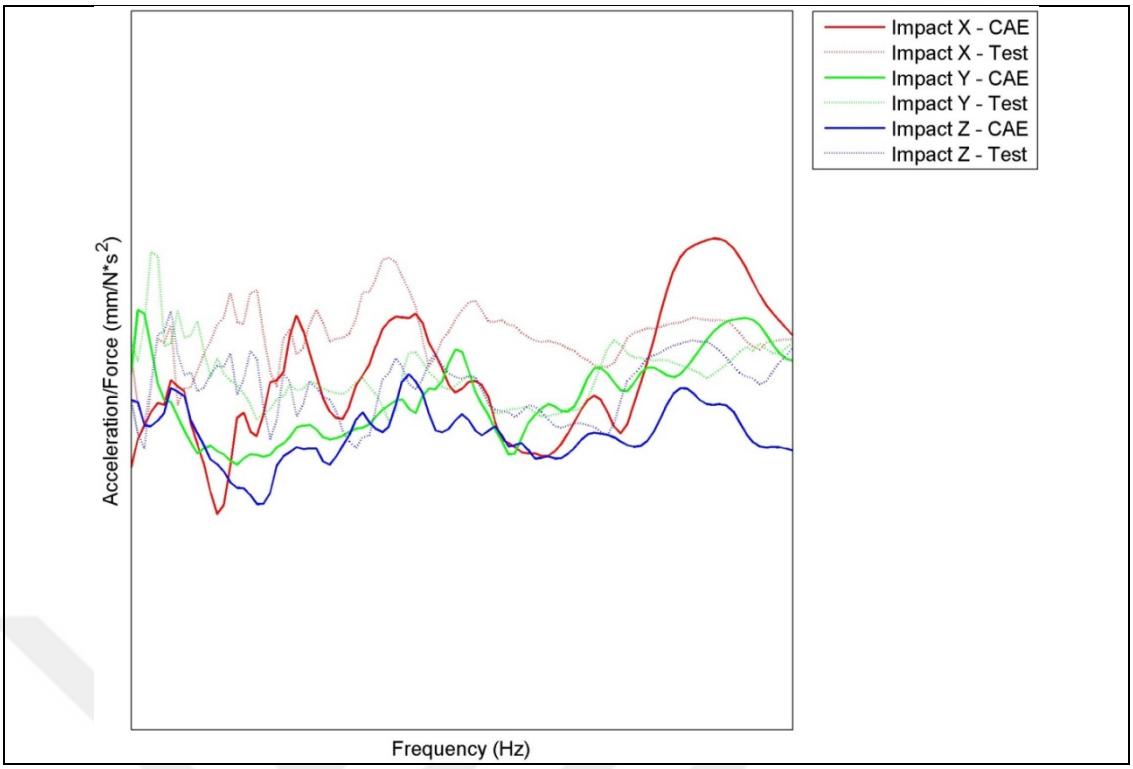

Figure 5.101: VTF correlation for transferpath17 response2.

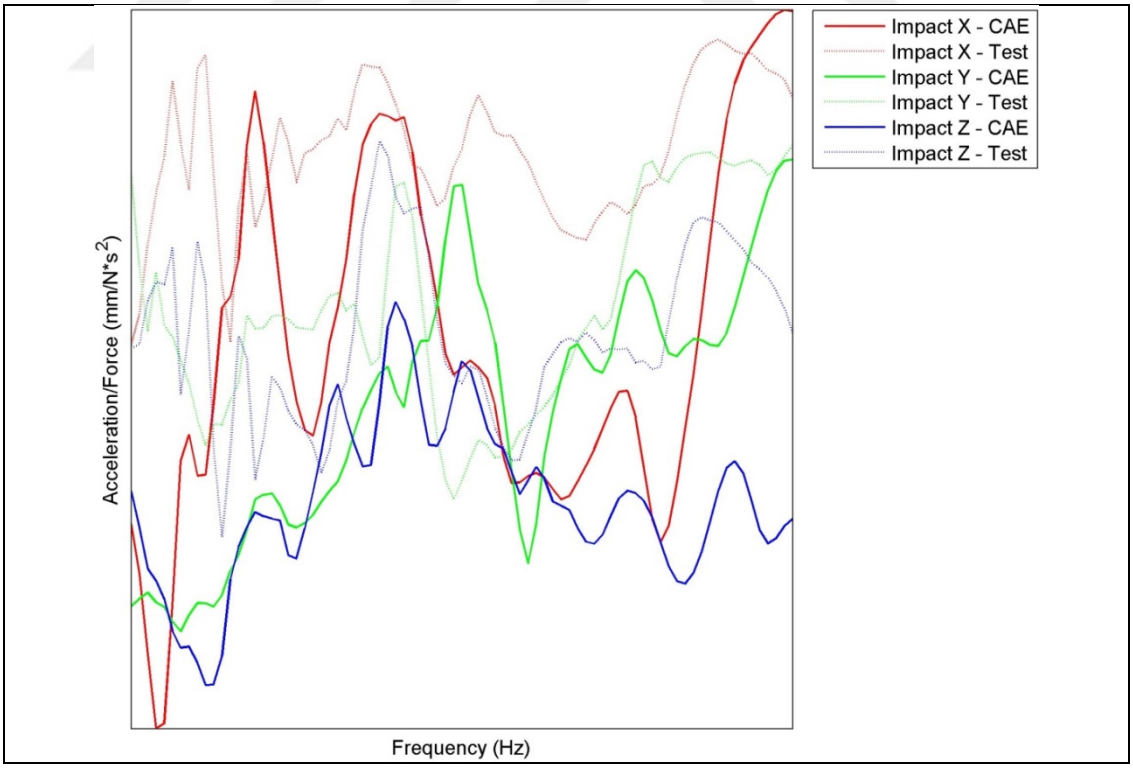

Figure 5.102: VTF correlation for transferpath17 response3.

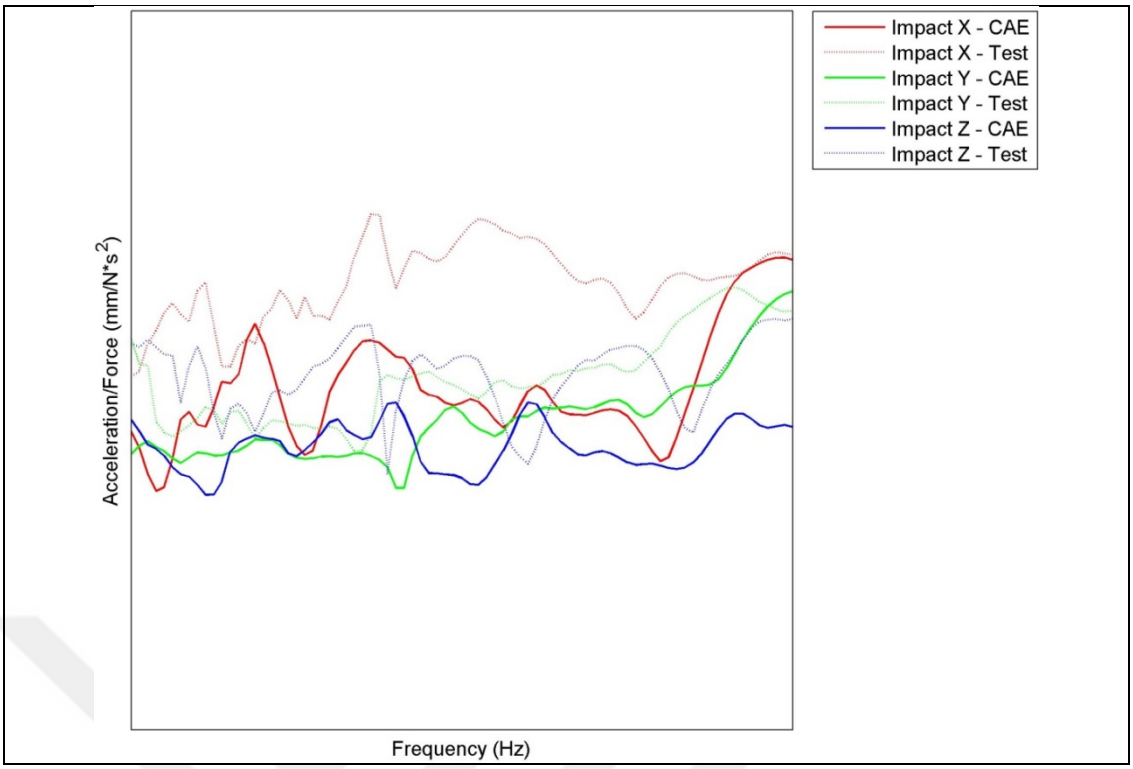

Figure 5.103: VTF correlation for transferpath17 response4.

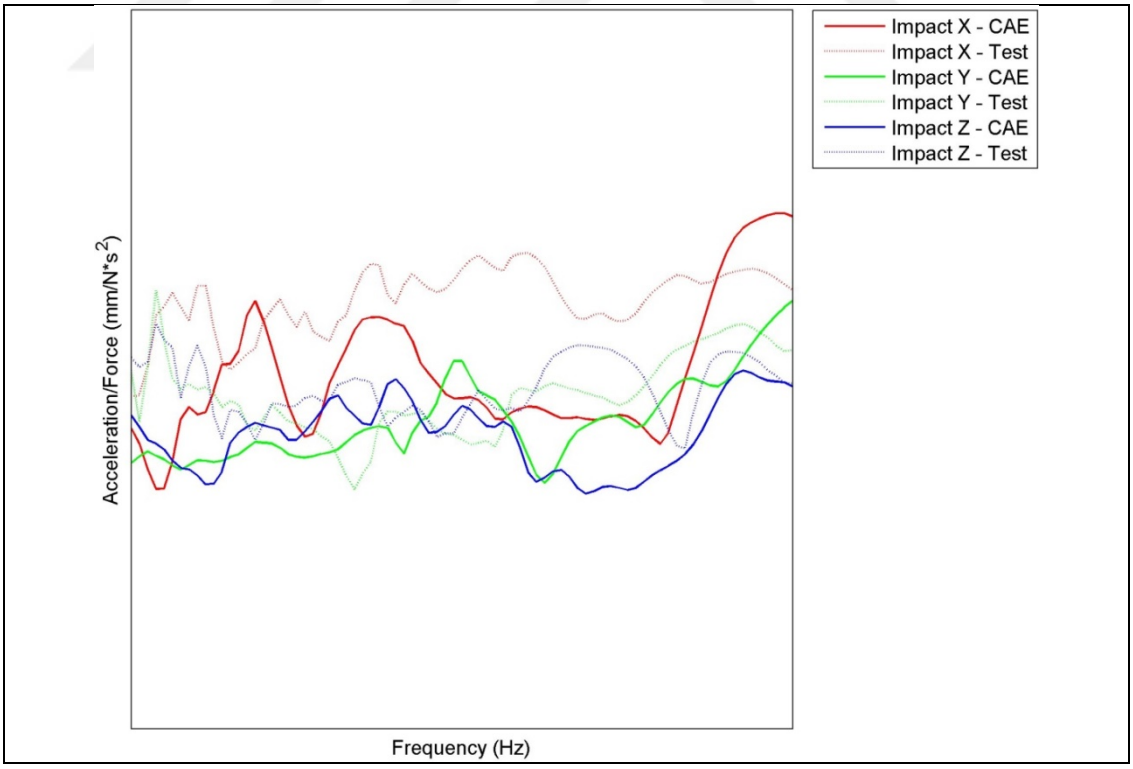

Figure 5.104: VTF correlation for transferpath17 response5.

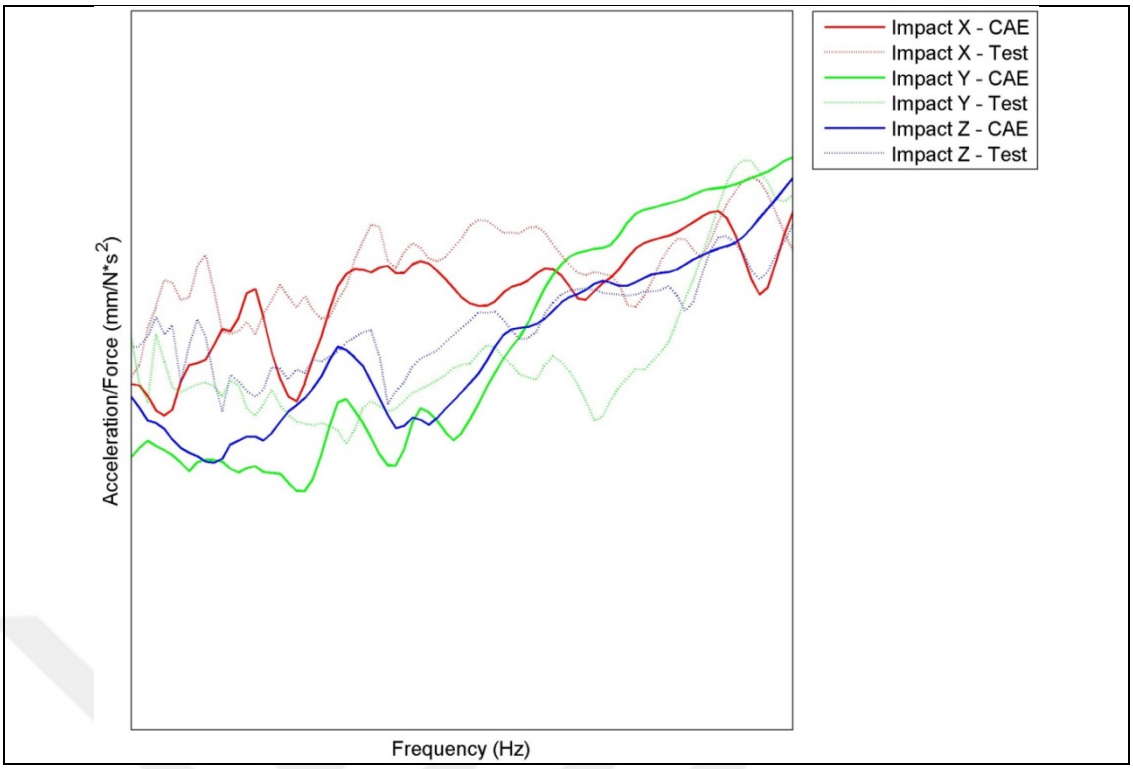

Figure 5.105: VTF correlation for transferpath17 response6.

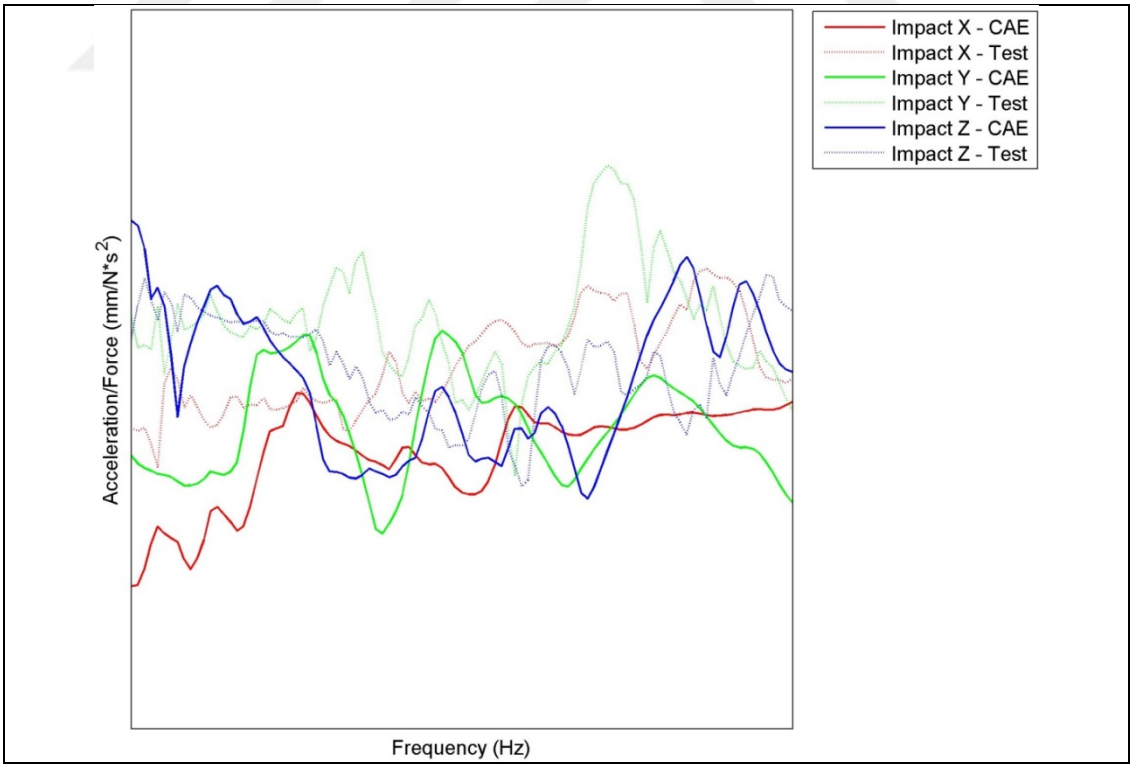

Figure 5.106: VTF correlation for transferpath18 response1.

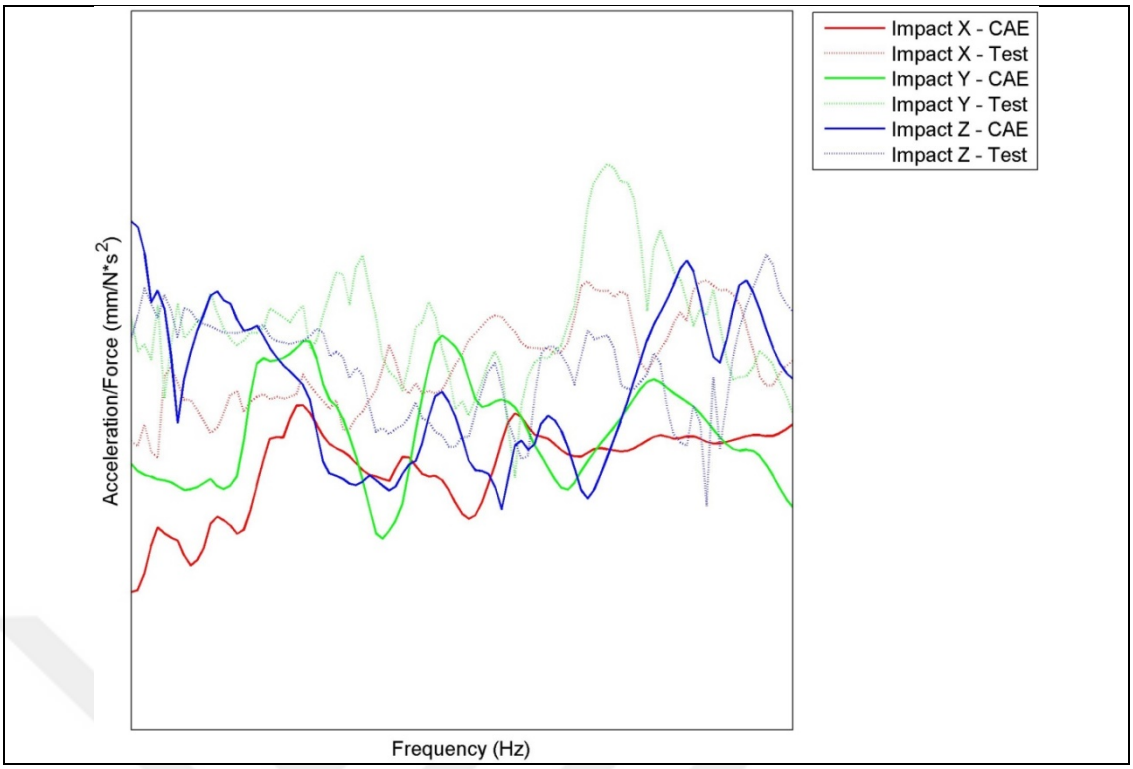

Figure 5.107: VTF correlation for transferpath18 response2.

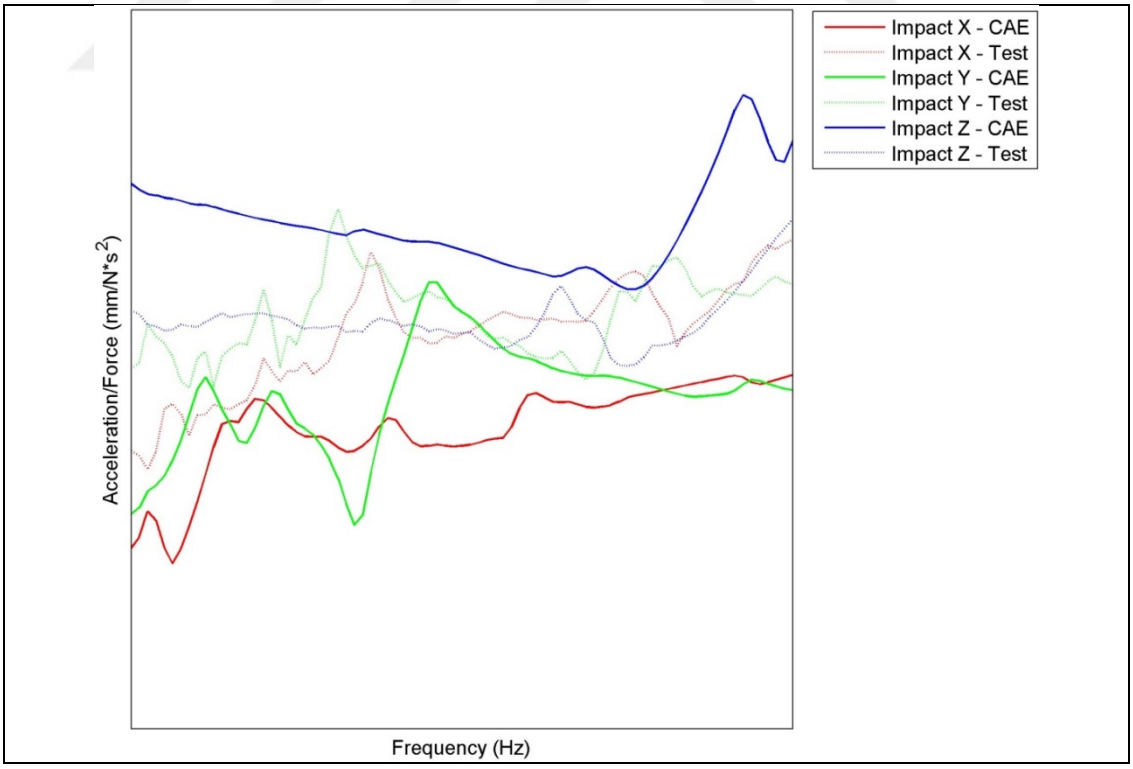

Figure 5.108: VTF correlation for transferpath18 response3.

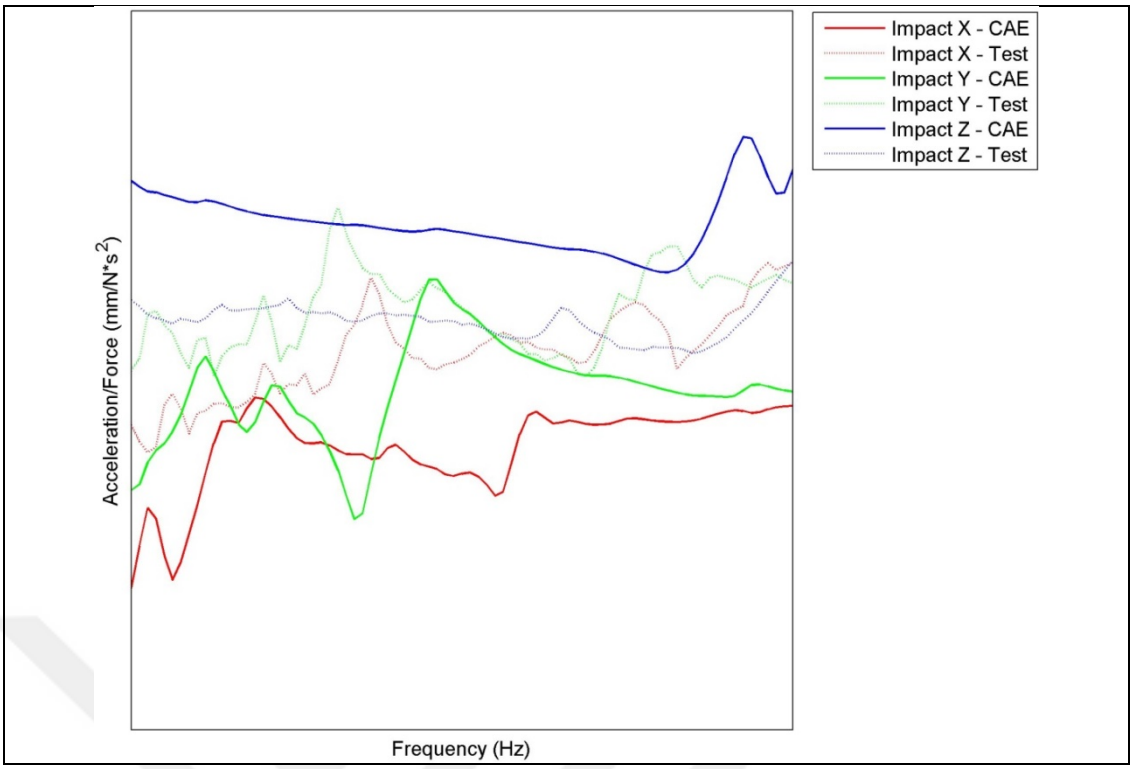

Figure 5.109: VTF correlation for transferpath18 response4.

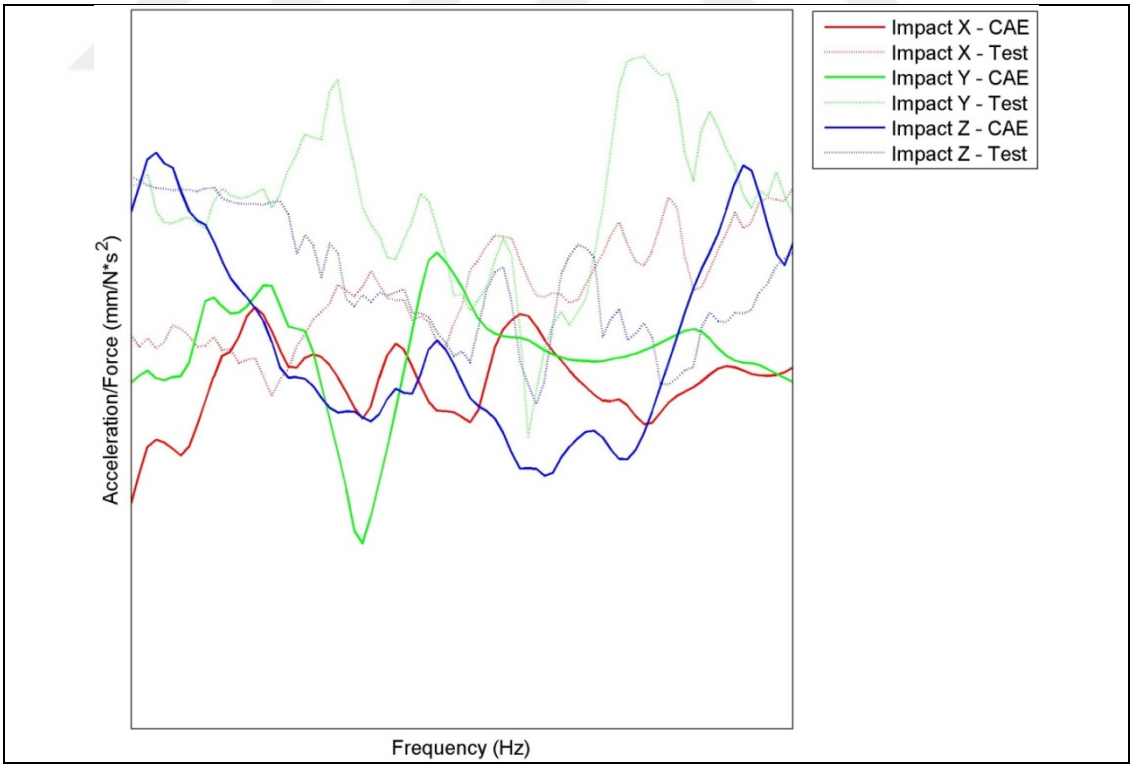

Figure 5.110: VTF correlation for transferpath18 response5.

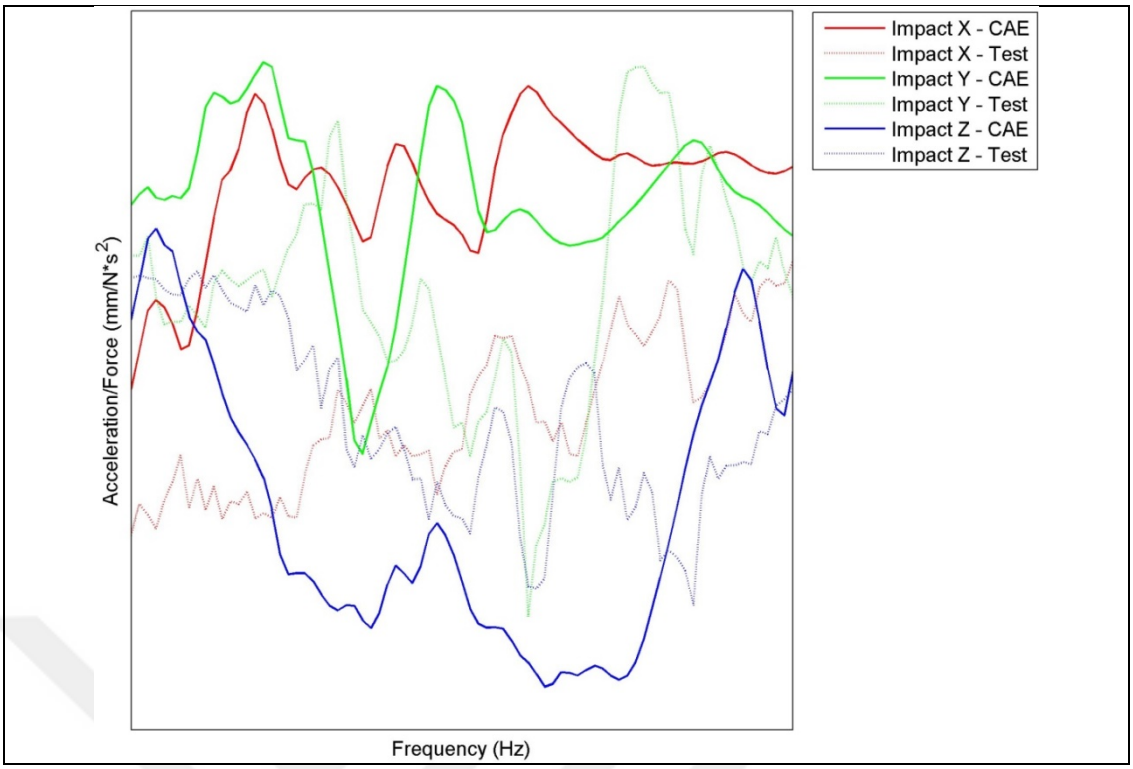

Figure 5.111: VTF correlation for transferpath18 response6.

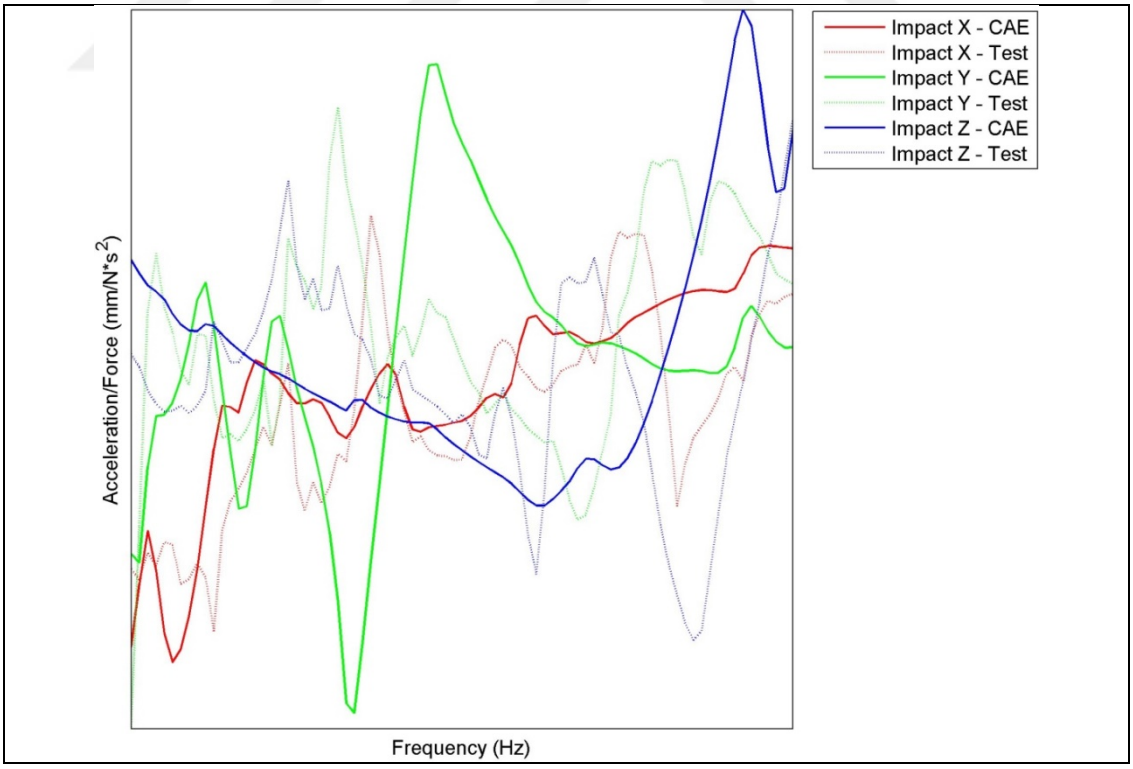

Figure 5.112: VTF correlation for transferpath18 response7.

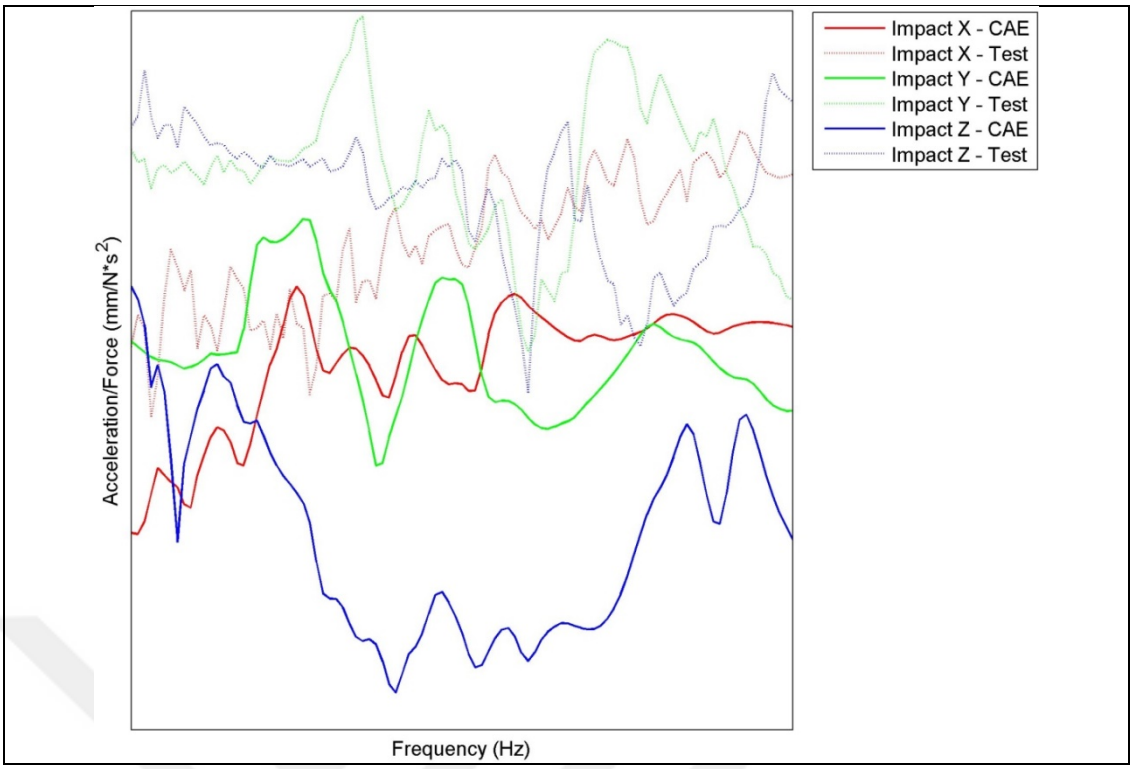

Figure 5.113: VTF correlation for transferpath19 response1.

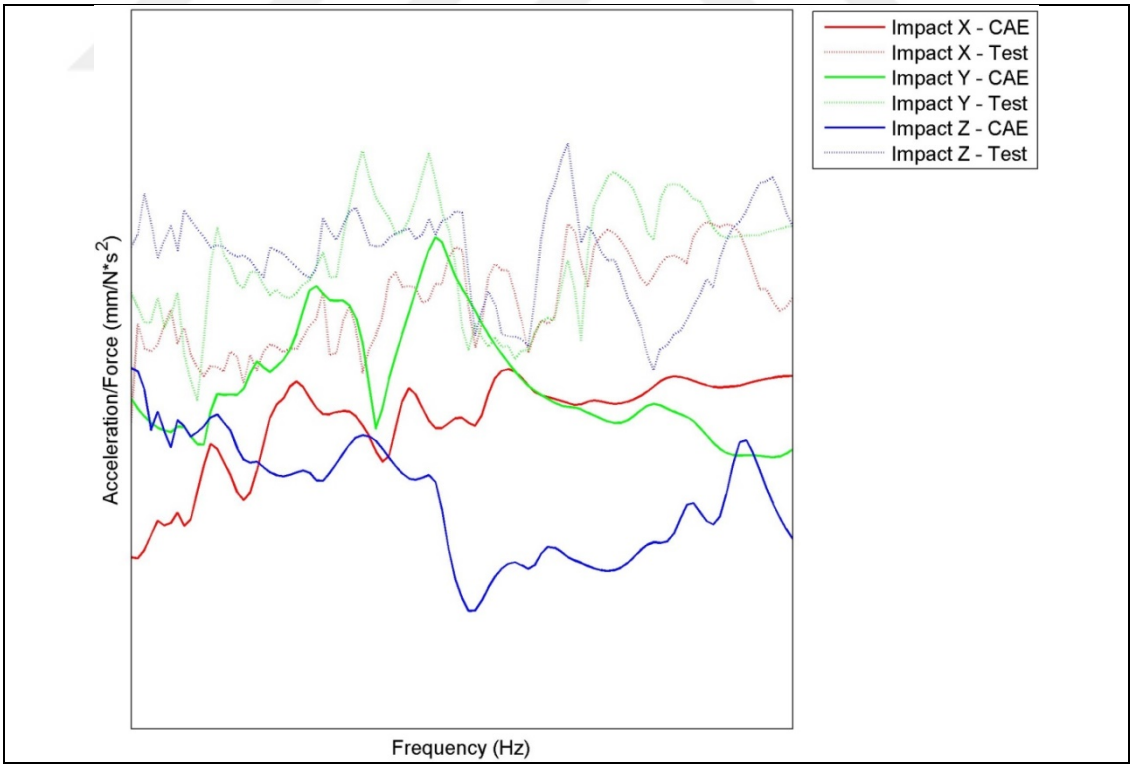

Figure 5.114: VTF correlation for transferpath19 response2.

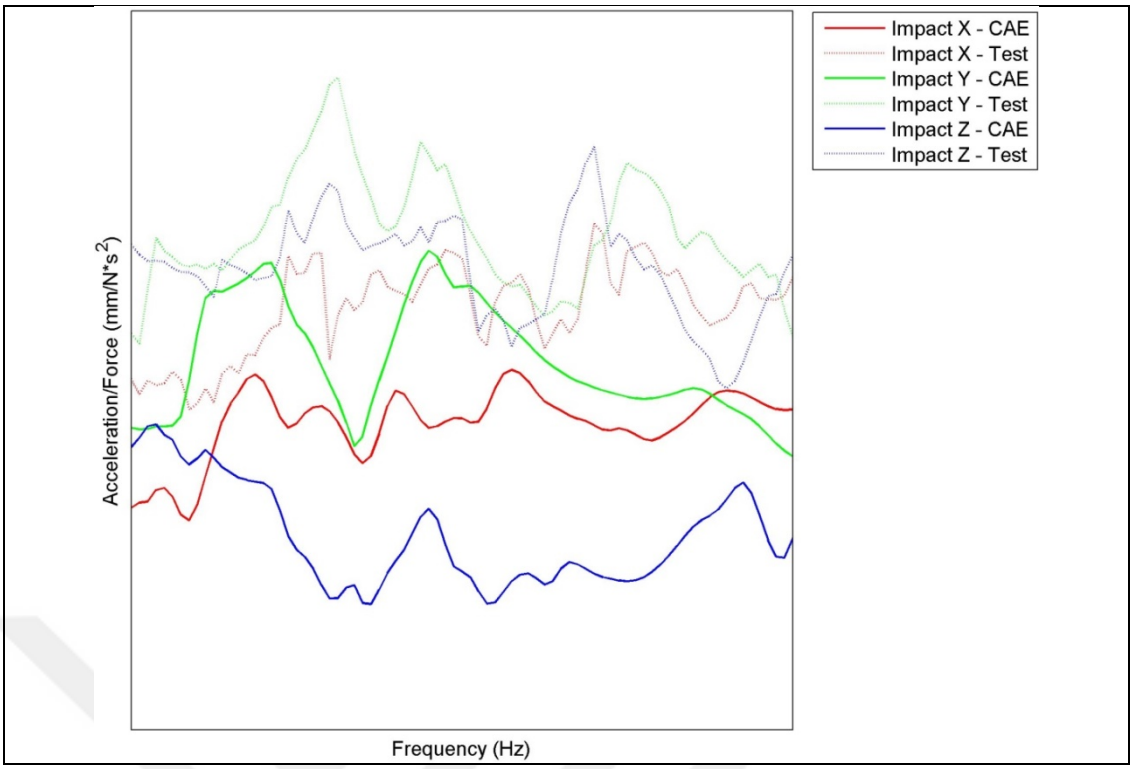

Figure 5.115: VTF correlation for transferpath19 response3.

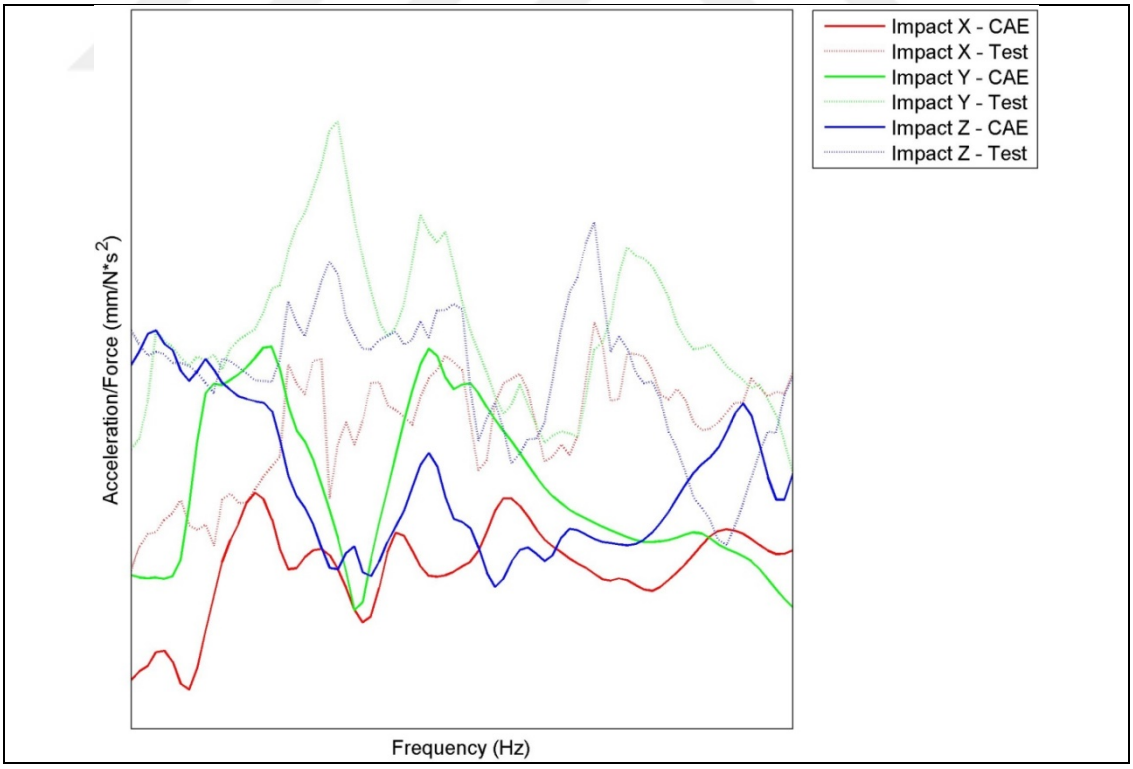

Figure 5.116: VTF correlation for transferpath19 response4.

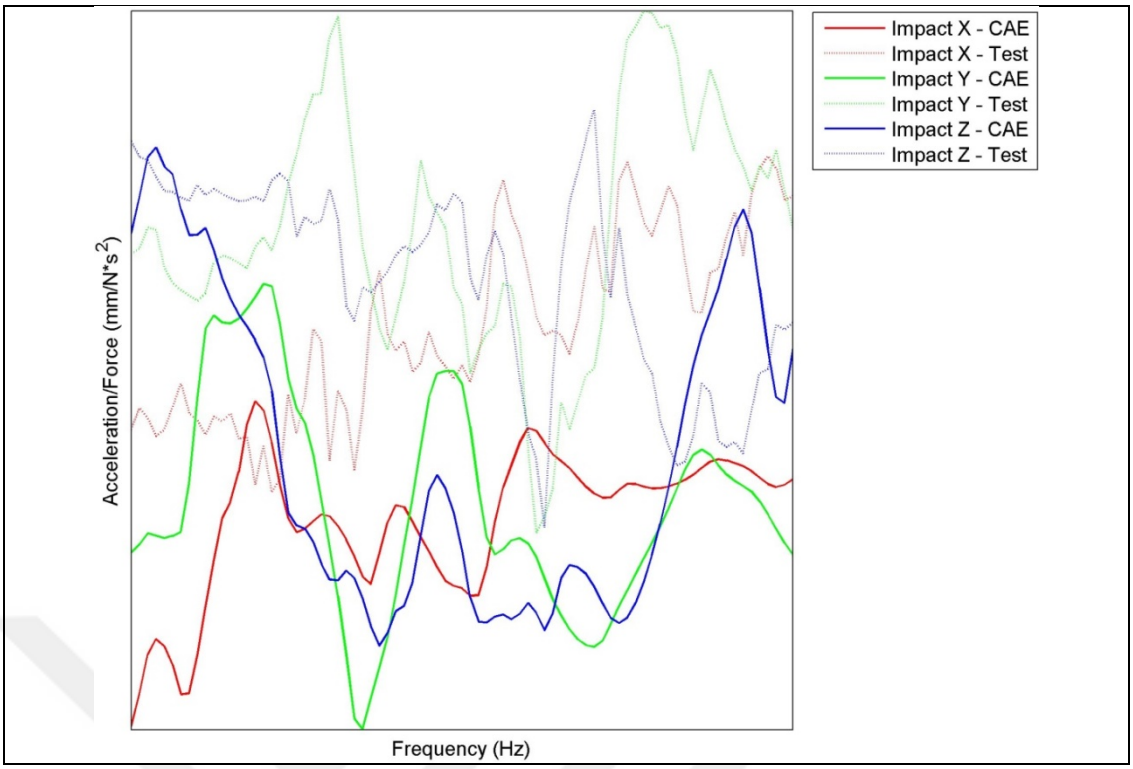

Figure 5.117: VTF correlation for transferpath19 response5.

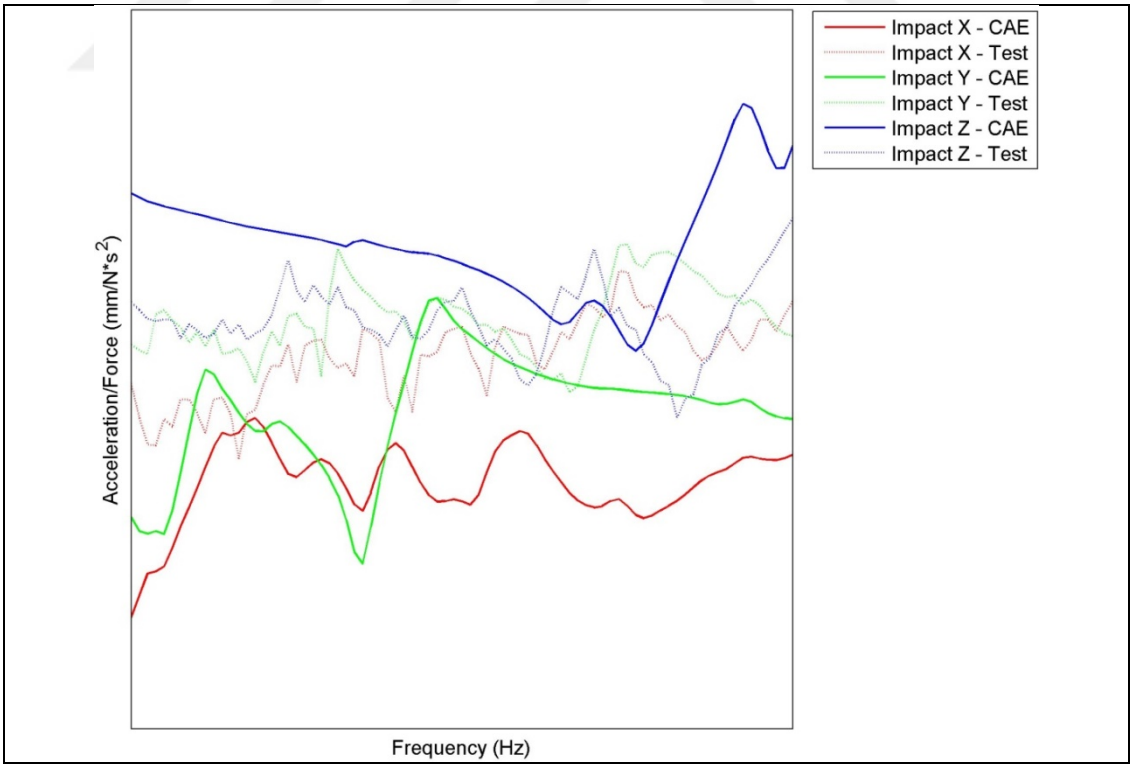

Figure 5.118: VTF correlation for transferpath19 response6.

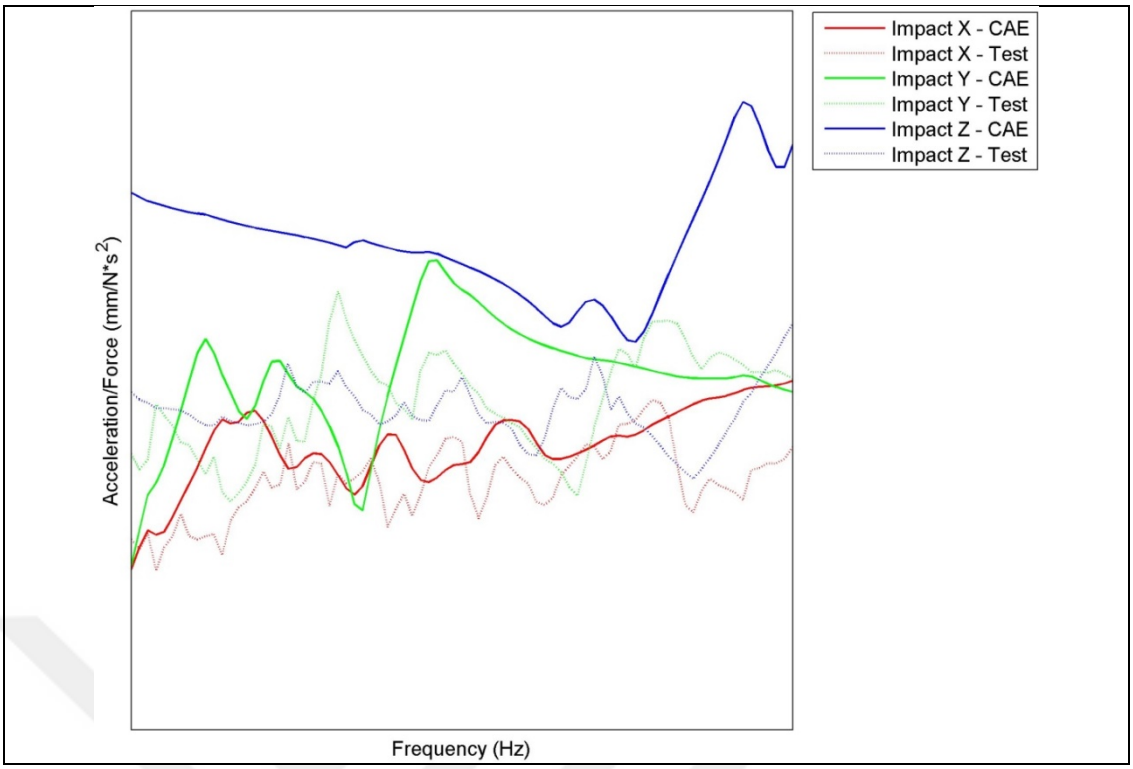

Figure 5.119: VTF correlation for transferpath19 response7.

5.2. NTF Correlation Results

In this section, NTF correlations are given. SPL (sound pressure level) measurements were performed in transfer paths 16 and 17. The dashed lines show the test results and the continuous lines show the CAE results. The red, green, and blue colors represent impacts in the x, y, and z directions, respectively.

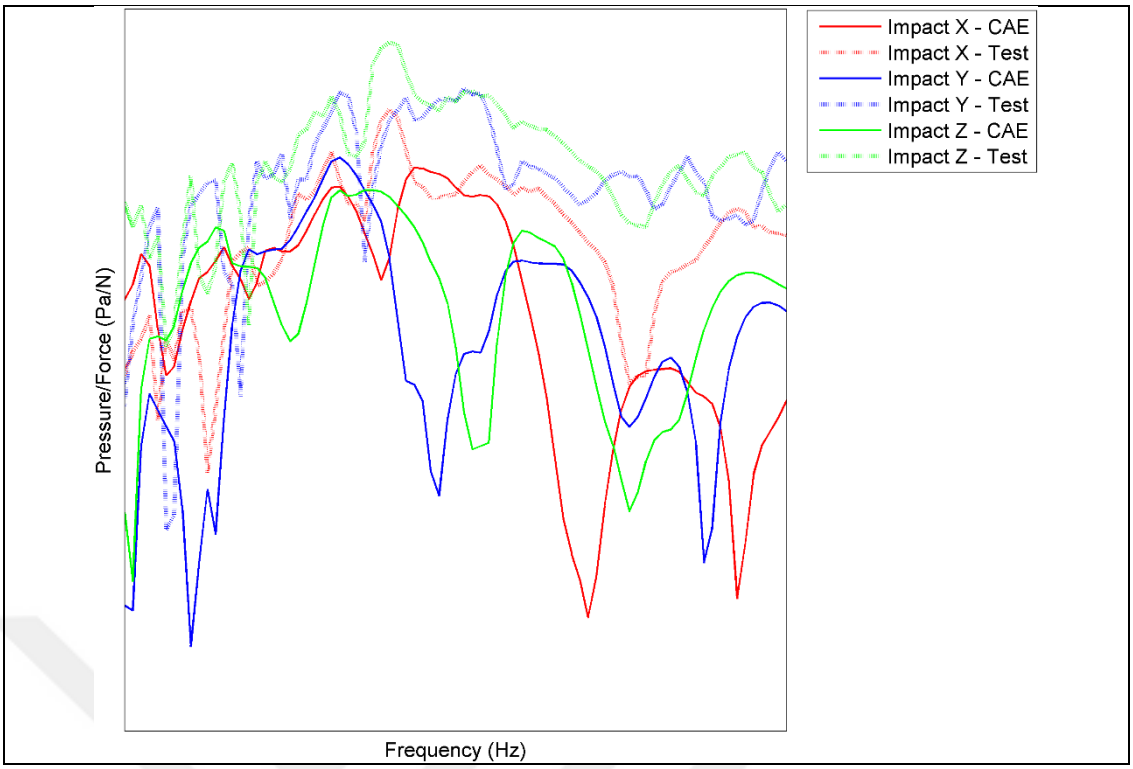

Figure 5.120: NTF correlation for transferpath16 response left passenger ear.

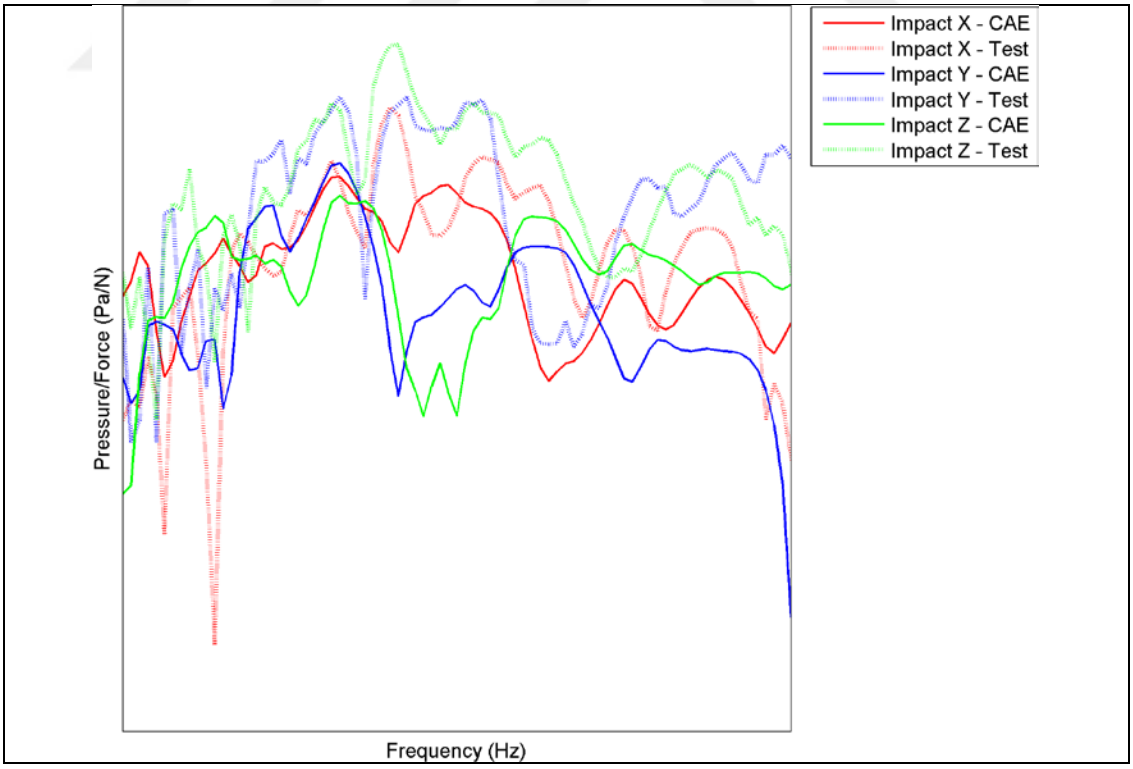

Figure 5.121: NTF correlation for transferpath16 response right passenger ear.

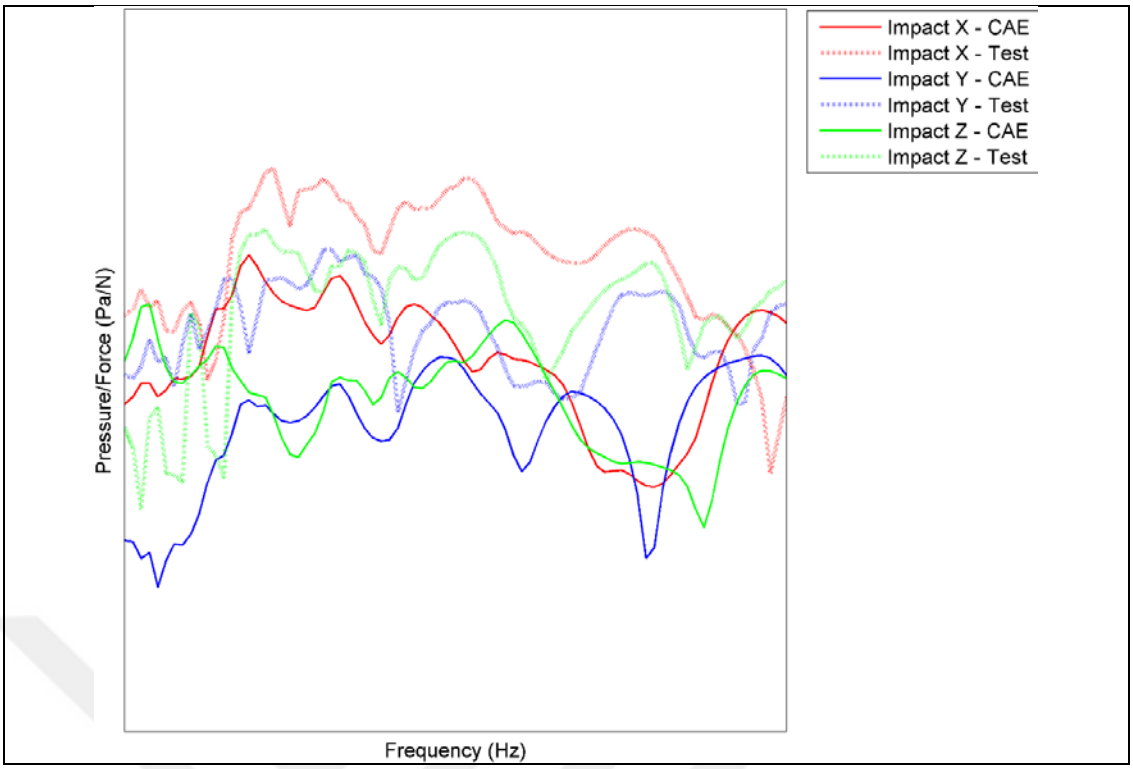

Figure 5.122: NTF correlation for transferpath17 response left passenger ear.

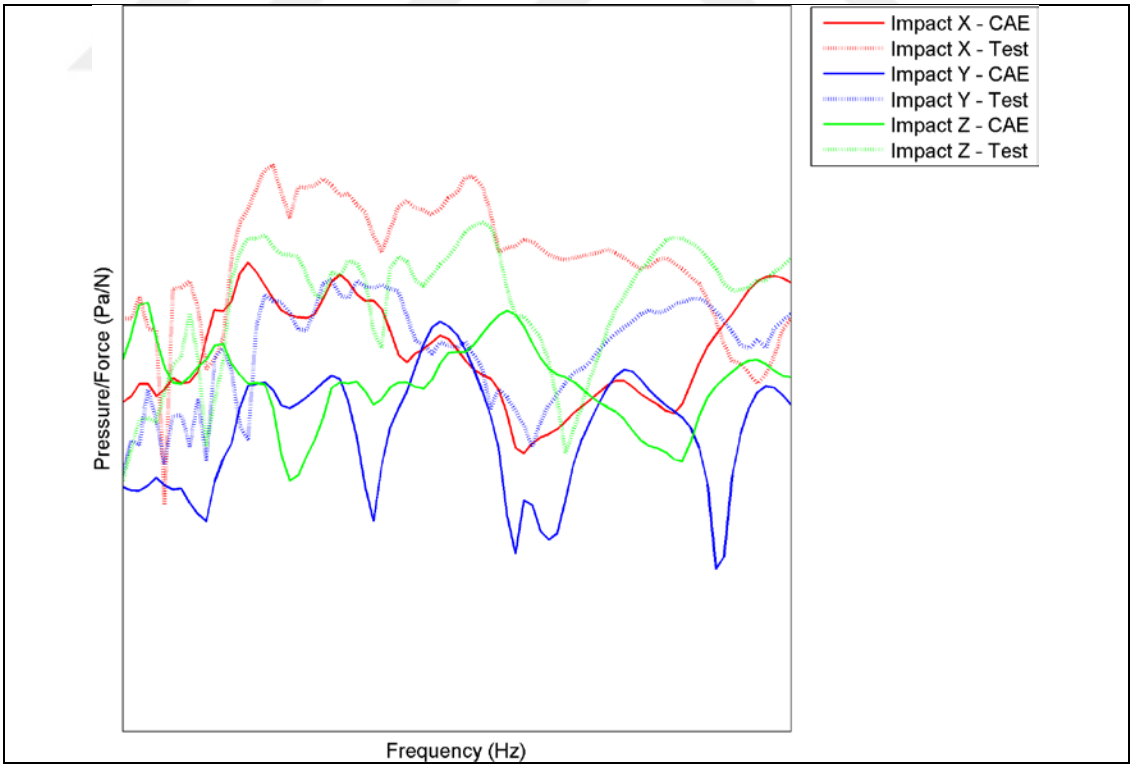

Figure 5.123: NTF correlation for transferpath17 response right passenger ear.

As shown in the NTF graphs, the frequency dependent fluctuation is higher than the fluctuations in the VTF graphs.

The discussion about graphics is presented in the next section.

6. DISCUSSION

In the previous chapter, the correlation plots are presented for each transfer path. In this chapter, results are discussed.

In this study, it is aimed to correlate the results obtained from the impact hammer test which is performed only once on the prototype vehicle, and the analytical results obtained by the numerous iterative variations on the CAE model. The results presented in the previous section are among the best results obtained at the full vehicle level during this study, among the many iterative results on the CAE model. But it should be noted that, a narrow frequency ranges of data are presented due to confidentiality and mostly problematic ranges are shown.

Initially, the effects of the iterative parameters were investigated with excessive changes (eg, changing the element size in the FE model, increasing the stiffness and hysteresis values 1000 times, and reducing it 1000 times). An iteration plan was created with the results of the effects of the parameters. It should be noted that the effects of the parameters are not linear, as are the different effects in different frequency ranges. This was one of the main challenges of this work. Again, non-linear effects of the parameters required very long computational time to make iterative changes on the model. This should be noted as another difficulty of working. Because there are so many iterations, the results of the iterations are not given here. Only the general interpretations obtained from the iterations are discussed here.

The iteration plan includes the following items:

- To correlate results at the amplitude level.
- To correlate results at the frequency level.
- To liken patterns (shape of the curves).

An example of a number of iterations for correlation at the level of amplitude is shown in Figure 6.1. In the figure, the dashed line represents the test result, and the continuous lines with different colors represent different CAE iterations. At the

beginning, the magenta color curve is away from the test result in the area indicated by the circle. Two of the different iterations (cyan and black lines) made a similar result to the downward pick in this region.

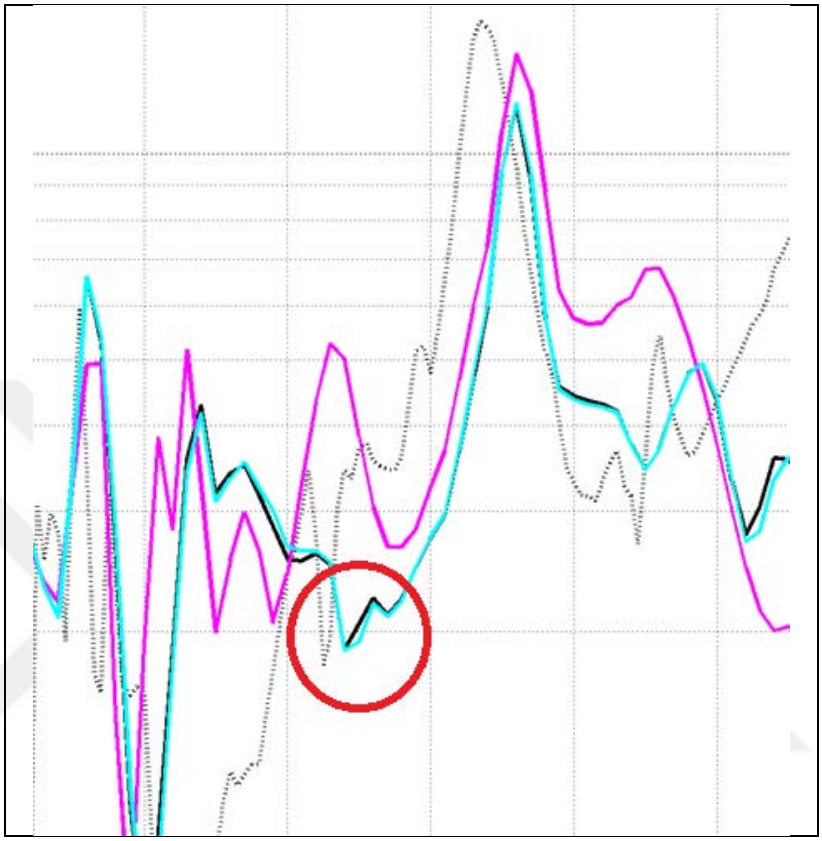

Figure 6.1: Iterations to correlate amplitude levels at a specific frequency.

Most generally, a change in the value of a bushing stiffness causes significant changes in FRF results. However, some bushings already have very high stiffness values, the increase in the stiffness of these bushings does not have an effect, nor does the small reductions have any effect. In this context, no iterative changes performed in stiffness and hysteresis in bushings with high stiffness values.

The first result that is examined not only to determine correlation on the amplitude level axis but also to check correlation on the frequency axis and the pattern context is the transfer path number 15 (see Figure 3.34). In transfer path 15, the impact was applied on the upper part of the exterior step and the acceleration data was collected from a very close place to impact point. For this transfer path, the amplitude values of the CAE analysis and the amplitude values of

the test are very close (see figure 5.93) but there is a problem with the patterns. This problem can be expressed as the peaks of the CAE result and the peaks of the test data being in opposite directions at certain frequency ranges. An example related this problem is shown in Figure 6.2. The inverse peaks is shown in the figure for impacts in Y and Z directions in transfer path 15.

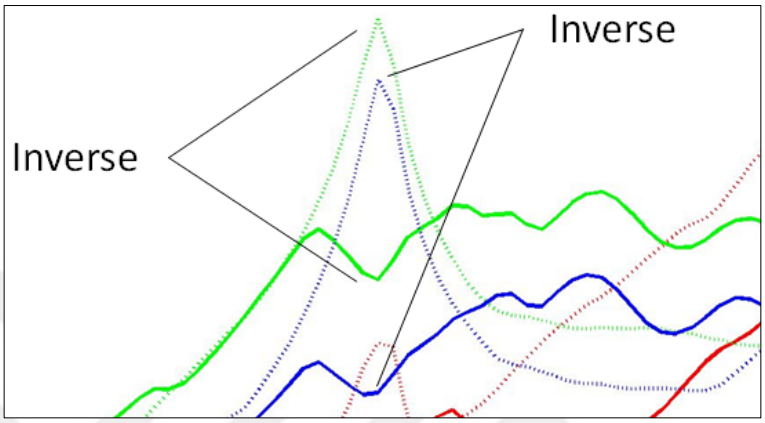

Figure 6.2: Inverse peaks problem at a specific frequency.

In the iterations, it was observed that the changes in the stiffness value could change the direction of the peaks, but this problem could not be solved because the changes were excessive and in other words the changes were far out of tolerance.

In figure 6.3, the dashed line represents the test result, and the continuous lines with different colors represent different CAE iterations. At the beginning, the peak in the black color curve is inverse of the peak on the test result curve in area indicated by the circle. Magenta color represent a useful iteration. By changing the stiffness parameter, the problem is solved. (But still amplitudes are not close).

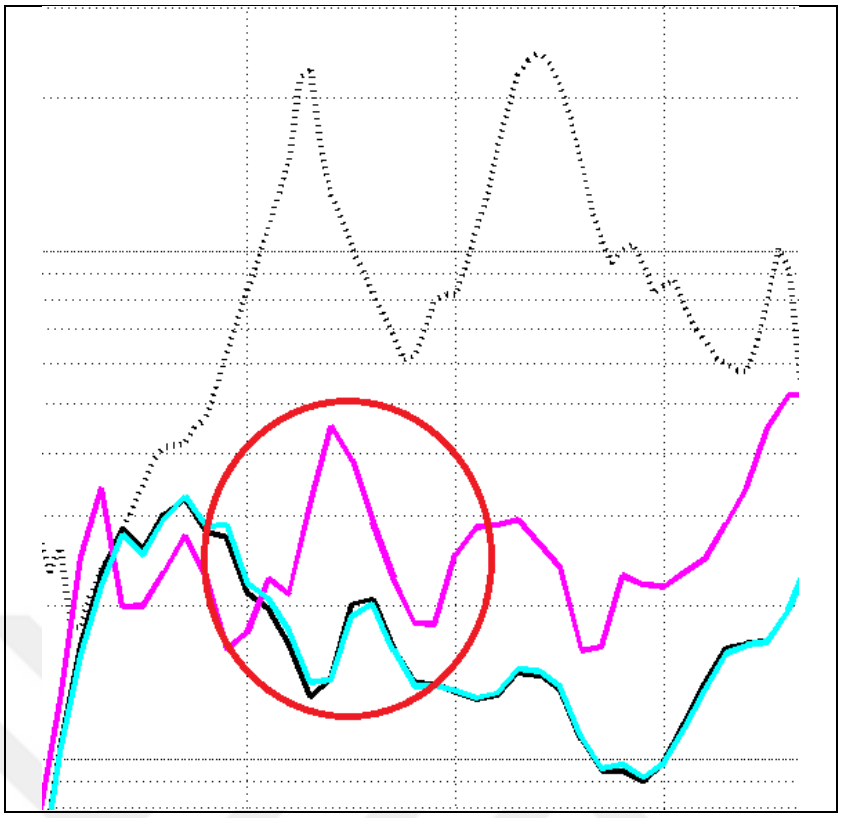

Figure 6.3: Iterations to change direction of a peak at a certain frequency.

Although the result from this iteration was successful, many iterations failed for most transfer paths. Because, as mentioned before, the effects of changes in parameters are not linear. In some transfer path iterations that solve the inverse peak problem in a certain frequency range failed the correlation in patterns or amplitude levels in other frequency ranges.

At this point, one of the biggest challenges of working with a complex model is that the parameters have different sensitivities and influences in different frequency ranges.

Additionaly, in some responses in CAE analysis (e.g. transferpath19 response6 impact Z, see Figure 5.118) a number of peaks couldn't be identified. The root cause of this problem is predicted as damping effect. Further investigation for this kind of problem is conducted for future correlation activities.

Last but not least, the problems seen in the VTF correlation were also seen in the NTF correlation. In particular, the inverse peaks in certain frequency ranges was also observed in four transfer function responses for NTF correlation.

7. DISCUSSION

In this study, the correlation of the transfer path analysis with the impact hammer test on the prototype of a heavy commercial vehicle and the transfer path analysis using the modal approach of the equivalent CAE model of the prototype vehicle were investigated.

Unlike many studies in the literature, the highly complex heavy commercial vehicle was modeled detailly with all hard and soft trimmings. Also unlike many other studies, instead of using direct FEM or BEM methods, FE models were created for each component (cabin, chassis, axles etc.) and modal analyzes were performed and the modal results were combined with an in-house software to create a full vehicle modal model. This approach (modal approach) reduces the FEM vehicle model with millions of DOF to a mass-spring system with thousands of DOF. This increases the computation speed and allows more iterations in the same time interval.

CAE-test correlation was investigated for previously defined 19 transfer paths by the FE model's mesh parameters, modeling techniques, and most importantly the iterations on bushing stiffness values (since they came with a large tolerance range from the manufacturer).

In this study, the correlation at the amplitude level is generally better than the correlation at the frequency axis. It should be emphasized that the CAE and test results can not be expected to be identical in a complex full vehicle model that is modeled with all trimmings. Both the results obtained from the CAE analysis and the results obtained from the test on the prototype vehicle have a specific error range. The initial assumptions made in the CAE model, the material properties described, and the modeling methods have implications on the outcome. Likewise, the test conditions on the prototype vehicle, the environmental conditions, the calibrations of the instrument used in the data (accelerometers and microphones) and the sensitivity ranges of the instrument bring together specific errors. All of the studies presented in the literature review argue that certain error rates occures in CAE model correlation. Again in this study, certain error rates are encountered. The

point to be contributed by this study is how to identify the source of these faults and how sensitive are the parameters and constraints that cause them.

In the context of this study, the physical test on the prototype vehicle was unfortunately performed once. Although the actions were taken to keep it at a minimum level, the effects of environmental conditions (ambient vibration and noise, floor attenuation etc.) are unknown.

To ensure higher correlation, tests can be done from the component level (cabin, chassis, axles etc.) to the full vehicle level. This approach is recommended for future researchers, ie the correlation is progressively progressed towards the full vehicle level at the component level. Also, multiple tests are recommended for future researches in order to meet reproducibility and repeatability.

REFERENCES

[1] Wang X., (2010), “Vehicle noise and vibration refinement”, 1st Edition, Woodhead Publishing.

[2] Gurgoze M., (1984), “A note on the vibrations of restrained beams and rods with point masses”, Journal of Sound and Vibration, 96 (4), 461-468.

[3] Suzuki S., Maruyama S., Ido H., (1989), “Boundary element analysis of cavity noise problems with complicated boundary conditions”, Journal of Sound and Vibration, 130 (1), 79-91.

[4] Pal C., Hagiwara I., (1993), “Dynamic analysis of a coupled structural-acoustic problem: Simultaneous multimodal reduction of vehicle interior noise level by combined optimization”, Finite Elements in Analysis Design, 14 (1), 225-234.

[5] Kamci G., Basdogan I., Koyuncu A., Yilmaz I., (2008), “Vibro-Acoustic modeling of a commercial vehicle to reduce the interior noise level”, InterNoise 2008, 5778-5787, Shanghai, China, 26-29 October.

[6] Freymann R., Stryczek R., Spannheimer H., (1995), “Dynamic response of coupled structural acoustic systems.” Journal of Low Frequency Noise, Vibration and Active Control, 14 (1), 11-32.

[7] Kim S. H., Lee J. M., Sung M. H., (1999), “Structural-acoustic model coupling analysis and application to noise prediction in a vehicle passenger compartment”, Journal of Sound and Vibration, 225 (5), 989-999.

[8] Ewins D. J., (1999), “Modal Analysis for Rotating Machinery”. In: M. Silva, M. Maia, Editors, “Modal Analysis and Testing”, Springer.

[9] Mohanty, A.R., Pierre, B.D., Narayanasami, P.S., (2000). “Structure-borne noise reduction in a truck cab interior using numerical techniques”, Applied Acoustics 59 (1), 1-17.

[10] Marburg S., Beer H. J., Gier J., Hardtke H. J., (2002), “Experimental verification of structuralacoustic modelling and design optimization” Journal of Sound and Vibration, 252 (4), 591-615.

[11] Marburg S., (2002), “Efficient optimization of a noise transfer function by modification of shell structure geometry – Part I: Theory”, Structural and Multidisciplinary Optimization, 24 (1), 51-59.

[12] Marburg S., Hardtke H. J., (2002), “Efficient optimization of a noise transfer function by modification of shell structure geometry – Part II: Application to a vehicle dashboard”, Structural and Multidisciplinary Optimization, 24 (1), 60-71.

[13] Herrin D. W., Martinus F., Seybert A. F., (2005), “Using Numerical Acoustics to Diagnose Noise Problems”, Technical Report No: 2005-01-2324, SAE, Warrendale, PA, USA.

[14] Plunt J., (2005), “Finding and fixing vehicle NVH problems with transfer path analysis”, Journal of Sound and Vibration, 39 (11), 12-16.

[15] Liu Z. S., Lu C., Wang Y. Y., Lee H. P., Koh Y. K., Lee K. S., (2006), “Prediction of noise inside tracked vehicle”, Journal of Applied Acoustics, 64 (1), 74-91.

[16] J. Plunt., (2005), “Finding and fixing vehicle NVH problems with transfer path analysis”, Journal of Sound and Vibration, 39 (11), 12-17.

[17] Slave R. B., Vianna E. P., Perseguim O. T., Andrade F., Fonseca F., Felicio J. A., Spada J. N, Comparini F., Berti O., Zambon H., (2008), “Vibration Mode Study of Steering Columns for Commercial Vehicles”, Technical Report No: 2008-36-0193, SAE, Warrendale, PA, USA.

[18] Shariyat M., Djamshidi P., (2009), “Minimizing the engine-induced harshness based on the DOE method and sensitivity analysis of the full vehicle NVH model”, International Journal of Automotive Technology, 10 (6), 687-696.

[19] Wolff O., Bree H., Tijs E., (2009), “A PU Probe Array Based Panel Noise Contribution Analysis Whilst Driving”, Technical Report No: 2009-01-2123, SAE, Warrendale, PA, USA.

[20] Han X., Guo Y.J., Yu H.D., Zhu P. ,(2009), “Interior sound field refinement of a passenger car using modified panel acoustic contribution analysis”, International Journal of Automotive Technology, 10(1), 79-85.

[21] Binxing W., Sifa Z., Lin Z., Shengqiang L., Xiaomin L., Keqiang L., (2010), “Acoustic modeling and analysis of vehicle interior noise based on numerical calculation”, 2010 International Conference on Intelligent Computation Technology and Automation, 404-407, Changsha, China, 11-12 May.

[22] Yuksel E., Kamci G., Basdogan I., (2010), “Vibro-acoustic analysis of a vehicle integrated with design of experiments methodology using three performance criteria”, Proceedings of 20th International Congress on Acoustics, 2190-2197, Sdyney, Australia, 23-27 August.

[23] Mansinh K., Miskin A., Chaudhari V., and Rajput A., (2011) "Simulations Based Approach for Vehicle Idle NVH Optimization at Early Stage of Product Development,", Technical Report No: 2011-01-1591, SAE, Warrendale, PA, USA.

[24] Guan J., Gruber H., (2012), “NVH Performance Optimization of Full Vehicles in Automotive”, Technical Report No: 2012-01-1525, SAE, Warrendale, PA, USA.

[25] Abreu R., Moura F., (2012) "Operational Modal Analysis Techniques Used for Global Modes Identification of Vehicle Body Excited from a Vehicle in Idle Engine", Technical Report No: 2012-36-0639, SAE, Warrendale, PA, USA.

[26] Xie R., Liu Z., Long S., Tian Z., (2012), “Test and simulation integrated transfer path analysis and optimization of the steering wheel vibration in idle”, Proceedings of the FISITA 2012 World Automotive Congress, 405-415, Beijing, China, 27-30 November.

[27] John B.V., Sivasankaran S., Loganathan E., Kupplili S.S., et al., (2013) "Commercial Vehicle NVH Refinement Through Test-CAE Development Approach", Technical Report No: 2013-01-1006, SAE, Warrendale, PA, USA.

[28] Akei M., Koizumi T., Tsujiuchi N., Yamauchi T., (2014), "Prediction of Vibration at Operator Position and Transfer Path Analysis Using Engine Multi Body Dynamics Model", Technical Report No: 2014-01-2316, SAE, Warrendale, PA, USA.

[29] Lu X., Ma J., (2015) "Development of an Optimization Process for Engine NVH Performance", Technical Report No: 2015-01-2292, SAE, Warrendale, PA, USA.

[30] Fard M., Liu Z., (2015), "Automotive Body Concept Modeling Method for the NVH Performance Optimization", Technical Report No: 2015-01-0012, SAE, Warrendale, PA, USA.

[31] Web 1, (2016), https://en.wikipedia.org/wiki/Vibration, (Date of Access: 30/10/2016).

[32] Web 2, (2016), http://www.colorado.edu/engineering/CAS/courses.d, (Date of Access: 10/10/2016).

[33] Rao S.S., (2010), “Mechanical Vibrations”, 5th Edition, Pearson.

[34] Soika E., Mankin R., Ainsaar A., (2010), “Resonant behavior of a fractional oscillator with fluctuating frequency” Physical Review E, 81 (1), 1-19.

[35] He G.T., Luo R.Z., Luo M.K., (2013), “Stochastic resonance in the overdamped fractional oscillator subject to multiplicative dichotomous noise”, Physica Scripta, 88 (6), 1-6.

[36] He G.T., Tian Y., Luo M.K., (2014), "Stochastic resonance in an underdamped fractional oscillator with signal-modulated noise", Journal of Statistical Mechanics: Theory and Experiment, 14 (5), 1-17.

[37] Web 3, (2016), http://www.vibrationdata.com/tutorials2/sforce.pdf, (Date of Access: 10/12/2016).

[38] Jacobsen F., Poulsen T., Rindel J.H., Gade A.C., Ohlrich M., (2011), "Fundamentals of Acoustics and Noise Control", Department of Electrical Engineering, 1st Edition, Technical University of Denmark.

[39] Web 4, (2016), https://www.nde-ed.org/EducationResources, (Date of Access: 10/12/2016).

[40] Web 5, (2016), https://en.wikipedia.org/wiki/Rarefaction, (Date of Access: 22/10/2016).

[41] Web 6, (2016), http://physics.tutorvista.com/waves/longitudinal-waves.html, (Date of Access: 01/12/2016).

[41] Web 7, (2016), https://en.wikipedia.org/wiki/Root_mean_square, (Date of Access: 01/12/2016).

[42] Stephen A.H., Shung H.S., Donald J.N., (2015), "Engineering Vibroacoustic Analysis: Methods and Applications", Noise and Vibration Series List, 1st Edition, Wiley.

[43] Web 8, (2016), http://empireacoustical.com, (Date of Access: 05/12/2016).

[44] Web 9, (2016), https://global.britannica.com, (Date of Access: 05/12/2016).

[45] Web 10, (2016), http://makina.deu.edu.tr, (Date of Access: 05/12/2016).

[46] Ford Motor Company, (2016), Internal CAE procedure documents, (Date of Access: 10/10/2016).

[47] Web 11, (2016), https://en.wikipedia.org/wiki/Computer-aided_engineering, (Date of Access: 05/09/2016).

[48] Bhatti M.A., (2005), "Fundamental Finite Element Analysis and Applications: with Mathematica and Matlab Computations", 1st Edition, Wiley.

[49] Web 12, (2016), https://en.wikipedia.org/wiki/Body_in_white, (Date of Access: 15/11/2016).

[50] Web 13, (2016), http://feaforall.com, (Date of Access: 05/12/2016).

[51] Web 14, (2016), http://manual.midasuser.com, (Date of Access: 05/12/2016).

[52] Huebner, K.H., Thornton, E.A., and Byrom, T.G., (1995), "The Finite Element Method for Engineers", 3rd Edition, New York: John Wiley and Sons Inc.

[53] Brüel P.V., Pope j., Zaveri H.K., (1997), "Introduction to Acoustical Measurement and Instrumentation", 1st Edition, John Wiley & Sons Inc.

[54] "Microphone Handbook", 1996, Brüel & Kjær, Nærum.

[55] Web 15, (2017), http://diyot.com, (Date of Access: 30/12/2016).

[56] Web 16, (2017), https://www.tekniksaat.com, (Date of Access: 30/12/2016).

[57] Web 17, (2017), http://www.elektrikport.com, (Date of Access: 30/12/2016).

BIOGRAPHY

Uğur Üresin (MSc.) was born in 1990. He received his bachelor degree from Dokuz Eylül University in mechanical engineering in 2014. He worked in an international company as a production engineer for a short time and continued to work in an engineering firm as a design engineer for more than 1 year. He received his first master's degree in the field of Engineering Management from Istanbul Technical University in 2016. Currently, he is working as a product development engineer at Ford Otosan R&D Center in Istanbul.